



Universidade de Aveiro Departamento de Física



Universidade do Porto Faculdade de Ciências



Universidade do Minho

Universidade do Minho Departamento de Física
2014

**David João da Silva
Carvalho**

**Simulação do recurso eólico em Portugal e futura
alteração de larga escala devido a alterações
climáticas de origem antropogénica**

**Wind energy resource modelling in Portugal and its
future large-scale alteration due to anthropogenic
induced climate changes**



David João da Silva
Carvalho

Wind energy resource modelling in Portugal and its future large-scale alteration due to anthropogenic induced climate changes

Simulação do recurso eólico em Portugal e respectivas futuras alterações de larga escala devido a alterações climáticas de origem antropogénica

Tese apresentada à Universidade de Aveiro para cumprimento dos requisitos necessários à obtenção do grau de Doutor em Física, realizada sob a orientação científica do Doutor Alfredo Rocha, Professor Associado com Agregação do Departamento de Física da Universidade de Aveiro, e co-orientação do Doutor Moncho Gómez-Gesteira, Professor do Departamento de Física da Universidade de Vigo, e do Doutor Carlos Silva Santos, Professor Adjunto convidado do Departamento de Engenharia Mecânica do Instituto Superior de Engenharia do Porto



universidade de aveiro
theoria poiesis praxis

FCT

Fundação para a Ciência e a Tecnologia
MINISTÉRIO DA EDUCAÇÃO E CIÊNCIA



PROGRAMA OPERACIONAL **POTENCIAL HUMANO**



Governo da República Portuguesa



QUADRO DE REFERÊNCIA ESTRATÉGICO NACIONAL
PORTUGAL 2007.2013



UNIÃO EUROPEIA
Fundo Social Europeu

Este trabalho teve apoio financeiro da Fundação para a Ciência e Tecnologia do Ministério da Educação e Ciência do Governo Português, através da bolsa de doutoramento com a referência SFRH/BD/73070/2010, financiada pelo Programa Operacional Potencial Humano do Quadro de Referência Estratégica Nacional (POPH-QREN) e participado pelo Fundo Social Europeu no âmbito do III Quadro Comunitário de Apoio.

This work had financial support from the Foundation for Science and Technology of the Portuguese Government Ministry of Education and Science, through a PhD grant with the reference SFRH/BD/73070/2010, funded by the Human Potential Operational Programme of the National Strategic Reference Framework and by the European Social Fund, in the scope of the III Community Support Framework.

To my parents for the constant and unconditional support, and to my wife Slavka and my son David for the joy and motivation.

o júri

presidente

Prof^ª. Dr.^ª Ana Isabel Couto Neto da Silva Miranda
professora catedrática da Universidade de Aveiro

Prof. Dr. Alfredo Moreira Caseiro Rocha
professor associado com agregação da Universidade de Aveiro

Prof. Dr. José Manuel Laginha Mestre da Palma
professor associado da Faculdade de Engenharia da Universidade do Porto

Prof. Dr. João Carlos Andrade dos Santos
professor auxiliar com agregação da Universidade de Trás-os-Montes e Alto Douro

Prof^ª. Dr.^ª Cristina Maria Mendes Andrade
professora adjunta do Instituto Politécnico de Tomar

Dr. Pedro Miguel Matos Soares
equiparado a professor adjunto do Instituto Superior de Engenharia de Lisboa

Dr.^ª. Maria Inés Álvarez Fernández
investigadora da Universidad de Vigo

Dr. Carlos Alberto Fernandes Marques
investigador de pós-doutoramento do CESAM - Centro de Estudos do Ambiente e do Mar da Universidade de Aveiro

acknowledgments

This work was supported by the Foundation for Science and Technology (FCT) through a PhD grant with the reference SFRH/BD/73070/2010. This work was also partially funded by the FCT and the European Union (COMPETE, QREN, FEDER) in the frame of the research projects PTDC/CTE-ATM/111508/2009: RESORT - High-resolution Rainfall EroSivity analysis and fORecasTing and EXCL/AAG-MAA/0383/2012: CLICURB - Urban atmospheric quality, climate change and resilience.

Firstly, I would like to thank to my supervisors Prof. Dr. Alfredo Rocha (Aveiro University), Prof. Dr. Moncho Gómez-Gesteira (Vigo University) and Prof. Dr. Carlos Silva Santos (Porto Superior Institute of Engineering) for all the valuable scientific support, availability and resources provided to me throughout this journey.

To the company Megajoule and Megajoule Inovação, namely to Eng. Rui Pereira, for providing me wind measurements vital to this work, and also for the valuable scientific knowledge, help and availability in solving technical problems and questions.

To EPhysLab (Environmental Physics Laboratory) research group of Vigo University, for all the help and constant availability.

To the following institutions that provided me essential data to perform this work, along with fruitful discussions about several technical and scientific issues and questions: European Centre for Medium-Range Weather Forecasts (ECMWF); National Centers for Environmental Prediction (NCEP), National Center for Atmospheric Research (NCAR) and National Oceanic and Atmospheric Administration (NOAA), particularly to Drs. Ross Hoffman, Wesley Ebisuzaki, Jeff Whiting, Jack Woollen and Bob Dattore; National Aeronautics and Space Administration (NASA), particularly to Drs. Michael Bosilovich and Eric Kemp.

To my colleagues of the Meteorology and Climatology Group of Aveiro University (Clim@UA) for all the help and companionship, particularly to Tiago Luna for the help in solving endless technical problems that arose throughout this work.

To my parents, my wife Slavka and my son David for all the support and motivation during my PhD. I dedicate this work to all of you.

palavras-chave

Energia eólica, WRF, Onshore, Offshore, Modelação, Recurso Eólico, Alterações Climáticas

resumo

A elevada dependência energética de Portugal face ao exterior em termos de combustíveis fósseis, aliada aos compromissos assumidos pelo País no contexto internacional e à estratégia nacional em termos de política energética bem como às temáticas da sustentabilidade dos recursos e alterações climáticas, inevitavelmente obrigam Portugal à necessidade de investir na sua auto-suficiência energética. A estratégia definida pela União Europeia, sob a forma da Estratégia 20/20/20, define que em 2020 60% do total da electricidade consumida seja proveniente de fontes de energia renováveis. A energia eólica constitui presentemente uma das principais fontes de produção de energia eléctrica em Portugal, produzindo em 2013 cerca de 23% do consumo total nacional de electricidade. A Estratégia Nacional para a Energia 2020 (ENE2020), que visa garantir o cumprimento da Estratégia Europeia 20/20/20, prevê que cerca de metade desta meta de 60% seja fornecida pela eólica.

O presente trabalho pretende aplicar e otimizar um modelo numérico de previsão do tempo na simulação e modelação do recurso eólico em Portugal, em zonas *offshore* e *onshore*. A optimização do modelo numérico baseou-se na determinação de quais as condições iniciais e de fronteira e opções de parametrizações físicas da camada limite planetária a usar no modelo que proporcionam simulações do fluxo de potência (ou densidade de energia), velocidade e direcção do vento mais próximas de dados medidos *in situ*. Especificamente para zonas *offshore* pretende-se também avaliar se o modelo numérico, uma vez optimizado, é capaz de produzir dados de vento e fluxo de potência mais concordantes com dados medidos *in situ* que dados de vento provenientes de satélites. Neste trabalho ambiciona-se ainda estudar e analisar possíveis impactos que alterações climáticas de origem antropogénica poderão ter no recurso eólico disponível sobre a Europa no futuro.

Os resultados deste trabalho revelaram que as reanálises do ECMWF ERA-Interim são aquelas que, entre todas as bases de dados de forçamento de modelos de previsão numérica presentemente disponíveis, permitem simulações do fluxo de potência, velocidade e direcção do vento mais concordantes com medições de vento *in situ*. Verificou-se também que as parametrizações da camada limite planetária Pleim-Xiu e ACM2 são as que permitem ao modelo usado neste trabalho obter os melhores resultados em termos de simulação do fluxo de potência, velocidade e direcção do vento. Esta optimização do modelo permitiu uma redução significativa dos erros de simulação do fluxo de potência, velocidade e direcção do vento e, para zonas *offshore*, a obtenção de simulações do fluxo de potência, velocidade e direcção do vento mais concordantes com medições de vento *in situ* do que dados provenientes de satélites, resultado este de grande valor e interesse. Este trabalho revela ainda que alterações climáticas de origem antropogénica poderão produzir impactos negativos no recurso eólico futuro na Europa, devido às tendências detectadas para uma futura diminuição das velocidades do vento especialmente na segunda metade do presente século e sob cenários de forte forçamento radiativo.

keywords

Wind Energy, WRF, Onshore, Offshore, Modelling, Wind Power Resource, Climate Change

abstract

The high dependence of Portugal from foreign energy sources (mainly fossil fuels), together with the international commitments assumed by Portugal and the national strategy in terms of energy policy, as well as resources sustainability and climate change issues, inevitably force Portugal to invest in its energetic self-sufficiency. The 20/20/20 Strategy defined by the European Union defines that in 2020 60% of the total electricity consumption must come from renewable energy sources. Wind energy is currently a major source of electricity generation in Portugal, producing about 23% of the national total electricity consumption in 2013. The National Energy Strategy 2020 (ENE2020), which aims to ensure the national compliance of the European Strategy 20/20/20, states that about half of this 60% target will be provided by wind energy.

This work aims to implement and optimise a numerical weather prediction model in the simulation and modelling of the wind energy resource in Portugal, both in offshore and onshore areas. The numerical model optimisation consisted in the determination of which initial and boundary conditions and planetary boundary layer physical parameterizations options provide wind power flux (or energy density), wind speed and direction simulations closest to *in situ* measured wind data. Specifically for offshore areas, it is also intended to evaluate if the numerical model, once optimised, is able to produce power flux, wind speed and direction simulations more consistent with *in situ* measured data than wind measurements collected by satellites. This work also aims to study and analyse possible impacts that anthropogenic climate changes may have on the future wind energetic resource in Europe.

The results show that the ECMWF reanalysis ERA-Interim are those that, among all the forcing databases currently available to drive numerical weather prediction models, allow wind power flux, wind speed and direction simulations more consistent with *in situ* wind measurements. It was also found that the Pleim-Xiu and ACM2 planetary boundary layer parameterizations are the ones that showed the best performance in terms of wind power flux, wind speed and direction simulations. This model optimisation allowed a significant reduction of the wind power flux, wind speed and direction simulations errors and, specifically for offshore areas, wind power flux, wind speed and direction simulations more consistent with *in situ* wind measurements than data obtained from satellites, which is a very valuable and interesting achievement. This work also revealed that future anthropogenic climate changes can negatively impact future European wind energy resource, due to tendencies towards a reduction in future wind speeds especially by the end of the current century and under stronger radiative forcing conditions.

Table of Contents

Chapter 1 - Introduction.....	1
1.1 - Motivation.....	1
1.2 – Objectives.....	11
1.3 – Structure of this work.....	13
Chapter 2 – Description of the NWP model.....	15
2.1 – General characteristics.....	15
2.2 –WRF-ARW modelling system architecture and operating chain.....	16
2.3 –WRF-ARW physical parameterizations.....	21
Chapter 3 – Optimisation of the WRF model wind simulation: testing of initial and boundary datasets.....	25
3.1 - Onshore.....	25
3.2 - Offshore.....	39
Chapter 4 – Optimisation of the NWP model wind simulation: testing of PBL parameterizations options.....	49
Chapter 5 – Comparison of NWP modelled and satellite-derived offshore wind data with in situ offshore wind measurements.....	63
5.1 – Determination of the best satellite offshore wind product.....	63
5.2 – Is the optimised WRF offshore wind simulation able to surpass satellite-derived and other alternative sources of offshore wind data?.....	76
Chapter 6 – Climate change impacts on future wind energy resource over Europe...90	90
Chapter 7 – Main conclusions.....	135
Chapter 8 – Future work.....	139
References.....	143

Chapter 1 - Introduction

1.1 - Motivation

In the last decades, the world population growth has escalated at an unprecedented pace. While in the 1950's the world population was around 2,500 million people, presently this number practically tripled to around 6,700 million. The United Nations project that in 2050 the world population will reach 9,200 million people. This increasing population means higher needs of food, water, transports, communications, infra-structures, etc. In short, more energy. Aside the well recognized fact that traditional energy sources based in fossil fuels are finite, increasingly scarce and, consequently, expensive, this growing global energy need must be faced bearing in mind the sustainability of the planet without aggravating global warming, climate changes, loss of biodiversity, geopolitical tensions and socio-economical unbalances.

The global warming and climate change issues are of paramount interest for the planet, and one of the main sources of uncertainty for future projections of the global political and socio-economical outlook. Presently, few (if any) doubts remain if the observed rises of global temperatures and changes in the global climatic system in recent decades are of anthropogenic sources or not. The latest report of the Intergovernmental Panel on Climate Change (IPCC), the IPCC Assessment Report 5 (IPCC AR5, 2013) confirms that it is virtually certain (>95%) that human activity has been the main cause of the observed increasing temperatures since the mid-20th century. Other possible factors, such as natural internal variability of the climate system and natural external forcings (variation of solar activity, activity of volcanoes, etc.), are considered to have a marginal contribution to this global warming. These climate changes are a consequence of the continuously increasing emissions of greenhouse gases (GHG), mainly CO₂, to the atmosphere, and several IPCC Assessment Reports are unanimous in stating that one of the main emission sources of GHG is the electricity generation from fossil fuels combustion (IPCC AR4, 2007; IPCC

AR5, 2013). It is worth mentioning some conclusions of IPCC AR5 that should be faced with the utmost attention and concern: the 1983-2012 period was likely the warmest 30-year period of the last 1400 years in the Northern Hemisphere, fact that was confirmed by the World Meteorological Organization (WMO) based on measured temperatures since 1850, stating that 13 of the 14 warmest years were observed in the last 14 years; global temperatures can rise 1 to 5°C over the next 100 years, depending on the amounts of GHG emitted and the sensitivity of the climate system; sea-level can rise 28 to 98 cm by the end of the current century, and to more than 3 meters by 2300; if no GHG emissions mitigation strategies are employed, in summer periods the Arctic Ocean will likely become virtually ice-free before 2050.

Thus, traditional energy sources like fossil fuels are, on the one hand, becoming increasingly scarce and costly due to their finite nature and, on the other hand, one of the main responsible for climate changes and the deterioration of the global environment. Thus, a revolution in the energy sector paradigm is unavoidable and alternative energy sources must be obtained. Renewable energy sources are a cornerstone in this revolution, and all efforts must be employed to support the penetration of renewable energy sources in energy production systems at a global scale.

Portugal can be seen as a good example in terms of support and investment in renewable energy sources, being the 4th country in Europe with higher penetration of renewable energy sources in the total electricity consumption. According to the Portuguese Association of Renewable Energies (APREN), in 2013 renewable energy sources (wind, biomass, solar and hydropower) supplied 58,3% of the total national electricity consumption that, according to the Portuguese Economy Ministry, allowed savings of 846 million EUR (ME) in fossil fuels imports and purchase of CO₂ emission licenses. Within all renewable energy sources presently used for electricity generation, wind is one of the global leaders in terms of installed generating capacity, fastest growth and technological maturing. In Portugal, wind-derived electricity production has grown in the last decade at a rate unbeaten by any other electricity generation source. According to the Portuguese Agency of Energy and Geology (DGEG) and the Portuguese Electrical Company (EDP), in 2003 Portuguese wind farms produced 494 GWh of electricity, corresponding to about 1%

of the total national electricity production. 2005 witnessed a turning point, when electricity produced from the wind reached 1.77 TWh, roughly 4% of the total national electricity consumption. From there on, this growth escalated. In 2008 wind-derived electricity reached more than 10% of the total national electricity production, and in 2012 the benchmark of 10 TWh of electricity production was reached by national wind farms. By half of 2013, DGEG announced that wind energy production already reached 11.5 TWh, more than 23 times what was produced in 2003. These figures clearly reflect the importance, impact and exponential growth of wind energy in Portugal witnessed in only one decade. Even at a global scale, and bearing in mind that is a relatively small country, Portugal is presently one of the world leading countries in terms of installed wind power, and this growth is still in progress. In 2011 and 2012, Portugal was ranked in 10th place worldwide and 5th place among European countries in terms of total wind energy installed capacity (Global Wind Energy Council 2011, 2012). This high wind energy installed power resulted that in the last years wind energy has been one of the main sources of national electricity production. Portugal is the 2nd country in the world where wind power contribution to the overall electricity consumption is higher, and growing each year: in 2010 Portugal was able to achieve an 18% quota of wind-derived energy in the total annual energy consumption, outranked worldwide only by Denmark (Global Wind Energy Council, 2010), and in 2012 this quota increased to 20%, again only outranked by Denmark (APREN, 2013). In 2013 Portuguese wind farms were able to produce 23% of the annual electricity consumption, supplying 84% of the instantaneous total electricity consumption at 2 AM October 23rd and 93% at 4:30 AM November 11th. According to the Portuguese Economy Ministry, the performances of national wind farms in 2013 resulted in a positive financial impact of 450 ME due to savings in fossil fuels imports and CO₂ emission licenses purchasing. As aforementioned, in 2013 Portugal saved 846 ME due to the use of renewable energy sources in its electricity production. As it can be seen, in this year wind power alone was responsible for half of this saving. The prospects for the current year of 2014 are even more encouraging: in January 2014, 35% of the total national electricity consumption was supplied by wind power (APREN, 2014).

Despite these recent promising figures, Portugal still has in average a strong dependency from foreign energy sources of about 70-80% in terms of primary energy sources (source:

Portuguese Economy Ministry), being that these imported primary energy sources are mainly constituted by fossil fuels. As an example, according to the Portuguese National Statistics Institute, the importation of fossil fuels in 2011 represented a deficit in the national trade balance of about 7,200 ME. The higher use of endogenous renewable energy sources witnessed in the last years allowed the foreign energy dependence to be reduced in about 7%. Thus, the path to further reduce this foreign energy dependence and increase national electricity production based in renewable energy sources is still long.

Since the late 1990's, Europe and the European Union (EU) have been leading the efforts to support and materialize the penetration of renewable energy sources in electricity production. These goals were reasserted in the 20/20/20 Energy and Climate Package (URL 1), approved by the EU in late 2008. This strategy binds all EU 27 state members to reduce GHG emissions in 20% by 2020 (relatively to 1990), increase to 20% the contribution of renewable energy sources to the total energy consumption (more than doubling the 2005 8.5% quota), and less 20% energy consumption by increasing energetic efficiency. At EU level, and considering the current wind energy growth rate, it is expected that wind can provide up to one third of this 20% of renewable energy sources contribution to the total energy consumption, with its electrical generating installed capacity increased up to fivefold in the upcoming decade (de Vries, 2008a and 2008b). These expectations reflect the central role of wind energy in the EU energetic strategy.

In order to comply with these EU targets, Portugal developed the National Energy Strategy 2020 (ENE2020), approved by the Portuguese Government in April 2010 (URL 2). The ENE2020 is more ambitious and went even further than the EU 20/20/20 Energy and Climate Package, aiming to achieve 31% of renewable energy sources contribution to the total energy consumption in 2020. Although these total energy consumption refers to transports, heating/cooling systems and electricity consumption all together, the latter is the one with the highest goal in terms of renewable energy sources contribution: in 2020, 60% of the total national electricity consumption must be produced by renewable energy sources (wind, solar, biomass, waves and hydropower). ENE2020 expects that about half of this 60% goal will be supplied by wind power alone, foreseeing that by 2020 the national wind energy installed capacity can double from the actual 4,724 MW (late 2013)

to 8,500 MW, which reinforces the extreme importance of wind power to Portugal energy strategy for the upcoming years.

Therefore, the high Portuguese foreign energy dependency, scarcity and high cost of imported fossil fuels, commitments to EU 20/20/20 Energy and Climate Package and goals defined by the ENE2020, together with the paradigms of sustainability and climate changes, inevitably bind Portugal to invest in its energetic self-sufficiency by taking advantage of its endogenous renewable energy sources. Considering the ENE2020 expectations on wind power contribution to total electricity consumption, it becomes clear the need for Portugal to further continue and even increase its investment in wind farms installation and/or optimisation. Although, and as previously mentioned, Portugal has already a considerable wind energy portfolio, its growing potential is still high: (i) upgrading the existing wind farm turbines by installing the latest models, more efficient and with higher energy production capabilities; (ii) installing new wind farms in areas until now considered as economically unattractive, but that future development on wind turbines technology might allow a profitable exploration; (iii) installing offshore wind farms. The latter has a huge growth potential since until the present moment Portugal does not have any offshore wind farm installed, mainly due to the fact that its continental shelf shows some unfavourable characteristics to the installation of offshore wind turbines (steep slopes and deep near-coast waters). However, future development and progress on offshore wind turbines technology are expected to overcome these limitations (for example, floating offshore wind turbines). Therefore, these national goals and expectations regarding the expansion of wind farms pose several and new challenges to the national wind power industry, mainly in mapping the most attractive sites for wind energy exploration and accurately assess the wind energy production potential of a given area. Also at an international level, the current and future expansion of the wind energy markets combined with the explosive growth of worldwide installed wind power over the last decade and the progressive liberalization of electricity markets support the need to accurately and efficiently perform these tasks.

Wind energy spatial mapping and production potential assessment at a given area are traditionally based on classical methods that rely on *in situ* wind measurements. These

methods are still the most reliable for an efficient and accurate spatial mapping of wind energy resource and/or wind energy production potential assessment at a given area, meaning higher certainty in the expected available wind resource and lower associated investment risks, key prerequisites for the successful development of wind energy projects (Carvalho et al., 2013). These *in situ* wind measurements, performed specifically for wind energy exploration purposes, are planned and conducted by wind farms promoters. These wind measuring campaigns are performed in candidate areas for wind farms installation, in which are installed one or more wind measuring masts that collect wind speed and direction observations for one or more years. However, these wind measurement campaigns have some constraints, namely their high costs (in particular for offshore areas, where the costs of installing wind measuring masts are exponentially higher when compared to onshore sites), data quality and/or availability and the need to perform measurements for a representative period, usually with a minimum duration of one year. Moreover, these time and money consuming measurement campaigns may reveal that the sites under analysis do not show an economically attractive wind energy potential, which will lead to an irreversible loss of a considerable amount of investment already materialized.

As an alternative to these tailored and “wind farm oriented” wind measuring campaigns, wind observations are usually available within national meteorological services measuring networks (although usually this data has restricted access). However, usually these meteorological stations are located in urban areas, which are not typically good candidates for wind farms installation due to construction restrictions and unattractive wind energetic potential caused by the fact that urban buildings tend to obstruct and dissipate low level winds. Adding to this, usually these meteorological stations measure the wind speed and direction at 10 meters (m) above ground level (a.g.l), and for wind energy spatial mapping and production potential assessment purposes higher altitudes are considered (80 to 120 m a.g.l.). Specifically for offshore winds, given that meteorological stations are not installed in ocean areas, there are other alternatives: wind measurements collected at buoys deployed in ocean, measurements collected onboard ships and vessels and satellite observations. However, these types of wind measurements are usually taken in a limited spatial and/or time window (in the case of buoys and vessels measurements), or at an

insufficient time and/or spatial resolution (typically for satellite derived wind data), thus making the data unrepresentative of the wind regime over a medium or large spatial area or temporal period. Moreover, usually these types of ocean wind measurements suffer from large data gaps due to instruments malfunctions and deterioration, related to the typical ocean harsh conditions. Furthermore, the increasing evolution of the wind energy industry is bringing the need to obtain a preliminary knowledge of the available wind resource at sites with few (or not at all) local measurements – wind resource mapping. In these sites, this preliminary knowledge of the local wind regimes is of the utmost importance, at least in a preliminary stage in order to help the wind production potential assessment process.

Considering these disadvantages of tailored wind measurement campaigns, together with the growing needs of the wind power industry, the value of an alternative way to obtain reliable wind data for wind energy spatial mapping and preliminary production potential assessment becomes obvious. Numerical weather prediction (NWP) models, which are atmospheric models that consider physical phenomena such as frictional, thermal and convective effects, are a very powerful and useful tool to simulate meteorological variables (Carvalho et al., 2012). In the recent past, NWP simulations have been used with interesting and promising results in several applications within the wind energy sector: building wind resource maps in spatially large areas, useful in large scale electrical grid planning and preliminary assessment of potential wind energy exploration sites; computing local long term climatologies to allow the assessment of the wind variability and the representativeness of measurement campaigns; and in the growing field of wind power production short term forecasting, due to the need to plan electrical grid balance. Therefore, due to the inexistence of wind observations for a given spatial area and/or time period or to the need of a high resolution representative mapping of the local wind resource over a determined area, NWP wind modelling might be unavoidable.

However, as with any numerical simulation, the limitations of this approach should be carefully considered on a case-by-case analysis. The use of NWP models as source of wind data offers, on the one hand, advantages when compared to wind measuring stations such as gap-free and fast data availability (depending on the available computational resources), low operational costs (most of the mesoscale models are freely available for download and

the costs involved in their use are residual), and higher sampling resolution (both horizontal and vertical, allowing the computation of virtual wind data sets for several sites at different heights). On the other hand, there are disadvantages due to the uncertainty associated to wind data derived from these types of models: NWP models do not represent the real state of the atmosphere like *in situ* observed measurements do, since atmospheric simulation models are, by definition, a simplified approximation of the real atmosphere. Thus, errors and deviations between modelled and real atmospheric variables will always occur. In order to minimize modelling errors, a detailed optimisation of the NWP model is a mandatory step, namely in testing the several NWP model running options and assessing which configuration produces the best modelling results.

Due to the chaotic nature of the atmosphere dynamics (Lorenz 1996), extremely small errors in defining the initial state of the atmosphere in NWP models will severely amplify and completely distort the simulated future atmospheric state. As stated by Edward Lorenz, “the approximate present does not approximately determine the future”. Therefore, one of the most critical issues regarding NWP modelling is the initial and boundary conditions used to force the model. Typically, these initial and boundary data are extracted from reanalysis datasets, which provide all the atmospheric information needed by NWP models to run their simulations. Reanalysis are gridded datasets that combine data obtained from global circulation models (GCMs) with meteorological measurements, providing a synthesis of the available worldwide observations in the context of a physical model (Trenberth et al., 2010). Currently, there are several freely available reanalyses datasets produced by leading meteorological agencies and research institutes (USA, Japan and Europe). Although all reanalyses share common features and are based in the same philosophy, they significantly differ from each other mainly in what is related to the GCM used, spatial and temporal resolutions, observed data assimilation methods, amount and sources of assimilated measurements, etc.. Therefore, it becomes relevant to test these several initial and boundary data available in order to assess if there are significant differences in using one instead of another and, if so, which one provides the most realistic initial and boundary data to drive wind modelling and thus allow a more accurate wind simulation by NWP models.

Aside the initial atmospheric state issue, wind modelling, and particularly the near-surface wind modelling, is still a major challenge to atmospheric modellers involved in meteorological research and applications mainly due to the strong interaction between these low-altitude atmospheric flows and the local terrain (topography, land use, roughness, etc.). Offshore winds, and particularly coastal/near-coast winds, constitute an even bigger modelling challenge when compared to open sea and onshore winds due to the fact that these winds are strongly influenced not only by the neighbour onshore topography but also by discontinuities between land and sea roughness and thermal gradients that result from land-sea temperature differences. Thus, the strong interaction between these low-level atmospheric flows and the surrounding topography and geographical characteristics makes that near-surface winds and its modelling results can vary according to the geographical area under study and its characteristics. This interaction, which influences the flow circulation patterns particularly for near-surface winds, is described by the atmospheric planetary boundary layer (PBL) theory. Since both onshore and offshore wind energy are extracted from near surface flows, the modelling results will strongly depend upon the ability of the NWP model to correctly represent and simulate PBL processes. Usually the majority of these occur at spatial scales smaller than the model grid resolution, making them sub-grid processes (thus, unresolved explicitly by the model) that require an implicit treatment. This is done using physical parameterization schemes, which use physical assumptions and empirical approximations to represent these processes. Typically, NWP models have available for the modeller several different choices regarding PBL processes parameterizations. Thus, another one of the main issues regarding NWP near-surface wind modelling is related to the choice of which PBL parameterization scheme produces the best wind modelling results for the desired geographical area.

Coming back to the climate changes issue, and although wind energy growth is a key part of the solution to reduce GHG emissions and consequently mitigate future climate change, this renewable energy source is highly sensitive to climate change itself due to possible changes in future atmospheric flow patterns. Regardless of what GHG mitigation policies and strategies will be effectively employed in the future (if any), climate changes are already on their way and will continue to occur in the upcoming decades due to irreversible consequences produced by past human actions. The typical lifetime of wind farms is

around 20 to 30 years (and can be more), and the question whether the energy yield expected when the wind farm is, or was, planned will change during its operation window due to ongoing climate changes can determine the success or failure of the wind farm to achieve its production goals, affecting their financial viability and economical attractiveness to investors. Given that the wind energetic potential varies with the wind speed cubed, even apparently small variations in future wind circulation patterns and characteristics can strongly impact the future wind energetic production potential. Moreover, it is important to evaluate if future wind power resource will change and quantify this hypothetical change, in order to assess if this renewable energy source will be able to continue to actively contribute to GHG emissions reduction in future times. On the one hand, if climate changes significantly impact future wind characteristics in a negative way (by decreasing wind speeds) the future wind energy resource will be lower. Thus, wind power will likely not be able to maintain an active and vital contribute to GHG emissions reduction, and other renewable energy sources should be encouraged. Therefore, the climate change itself will inherently diminish our ability to fight it, in a kind of “snow ball” effect, at least in what is related to the wind energy role in GHG emissions mitigation. On the other hand, if climate changes will originate stronger future winds, future prospects of wind energy growth are encouraging and a stronger support of new wind farms projects and technology should be actively materialized.

Aside the assessment of hypothetical wind energy resource changes due to anthropogenic climate changes, mainly translated by changes in the future mean wind speeds and their geographical distributions, other aspects can also strongly impact the future wind energy effective use. Changes in future inter and intra-annual variability of the wind resource can affect the reliability of the produced wind-derived electricity (Pryor and Barthelmie, 2010). The higher the intra-annual variability, more variable will be the injection of the produced energy into the electrical grid, causing offer-demand balancing problems and enhancing the need to perform short-term wind energy production forecasts. Inter-annual variability is a key issue for the economic feasibility of a wind farm: since the expected annual energy yield calculated for a wind farm in its planning stage is typically based in 1 to 3 years of wind measurements, if the years used as reference to compute the expected wind farm energy production are exceptionally higher or lower in terms of average wind speeds (this

is, abnormal years in terms of the mean wind climate) the obtained estimates of the wind farm energy yield will be significantly biased and not realistic for the entire wind farm lifetime. These biased wind farm energy production estimates can severely affect the wind farm economic and financial feasibility. Therefore, it is vital to investigate these issues, assessing if climate changes can alter future wind energy resources in a way that it becomes advisable for the wind energy industry sector to adapt their growth, operation, technological and business strategies.

Although Portugal has a high and growing wind energy installed productive capacity and high wind energy derived electricity quotas in its annual electricity consumptions, research about such critical issues regarding NWP wind modelling has not yet been done for Portuguese territory. Even for other areas of the globe, published research about these themes is scarce and not always objective. This work aims to fill these gaps and optimise a NWP model for wind simulation focused on national territory, by performing a thorough and complete testing of which initial/boundary datasets and PBL physical parameterizations produce more accurate wind speed and direction simulations for Portuguese territory, for both onshore and offshore areas. Furthermore, and due to the newest IPCC future climate projections presented in the recent IPCC AR5 and based in the recently completed Fifth Coupled Model Intercomparison Project (CMIP5), it becomes important to assess and quantify the impacts of the latest CMIP5 future climate projections on the wind energetic resource in Europe, one of the main areas in terms of installed wind-derived electricity generating capacity in the world. There is a lack of research that addresses this issue in the light of the new CMIP5 future climate projections for Europe, or for other areas of the globe, which this work also aims to cover.

1.2 – Objectives

The objectives of this thesis can be summarized as follows:

- 1.** To implement and optimise a NWP model in the simulation and modelling of the wind energy resource in Portugal, both for offshore and onshore areas. The NWP optimisation is

focused in the determination of which initial/boundary conditions and PBL physical parameterizations options provide wind power flux, wind speed and direction simulations closest to measured wind data.

2. Specifically for offshore areas, it is also intended to assess if the NWP model, once optimised, is able to provide power flux, wind speed and direction simulations more consistent with measured wind data than offshore wind measurements collected by satellites, a widely used alternative source of measured offshore wind data.

3. Finally, this work also aims to assess possible impacts that anthropogenic climate changes may have on the future wind energetic resource in Europe, one of the main areas in terms of installed wind-derived electricity generating capacity in the world, by analyzing the latest CMIP5 future climate projections.

By accomplishing the first two objectives, the present work has the ambition to objectively and decisively contribute to the progress of the wind energy penetration in Portugal, vital for Portugal to: reduce its foreign energy dependence; balance its commercial balance by saving financial resources in importing expensive fossil fuels and acquisition of CO₂ emission licenses; comply with its international commitments within the EU 20/20/20 Energy and Climate Package and with its internal goals defined by the national ENE2020; and follow a “greener” path regarding the climate changes and planet sustainability paradigms. The third objective aims to shed a new light in the issue of climate changes impacts on future wind energy resource and production, by analyzing the newest and state-of-the-art future wind climate projections offered by the CMIP5 project, with the ambition to assess if wind energy will continue to be a strong and active part of the solution to reduce GHG and mitigate future climate changes and also to offer more realism in the wind farms expected energy production estimates for its entire lifetime, vital for the success of the wind farms projects and for the wind energy stakeholders.

1.3 – Structure of this work

Due to the fact that all the work developed in this thesis was already published (or is currently submitted for publication) in international peer-reviewed scientific journals, this thesis was structured in the following way:

Chapter 2 presents a description of the NWP model used in this work, since this was not thoroughly done in the published articles.

Chapter 3 presents the research about the optimisation of the NWP model regarding which initial and boundary conditions used as forcing provide wind power flux, wind speed and direction simulations closest to *in situ* measured wind data. This chapter is composed by two research articles published in international peer-reviewed scientific journals, in its original published format: the first article focusing on onshore areas and the second article dedicated to offshore areas.

Chapter 4 presents the research about the optimisation of the NWP model regarding which PBL physical parameterization options provide wind power flux, wind speed and direction simulations closest to *in situ* measured wind data, both for offshore and onshore areas. This chapter is constituted by one research article published in an international peer-reviewed scientific journal in its original published format.

Chapter 5 assesses if the NWP model, once optimised, is able to provide power flux, wind speed and direction simulations more consistent with *in situ* measured offshore wind data than wind measurements collected by satellites and other alternative sources. This chapter is presented in the form of two research articles published in international peer-reviewed scientific journals, in its original published format.

Chapter 6 focuses in climate changes impacts of future wind energy resource in Europe. This research is presented in the form of an article presently submitted for publication to an international peer-reviewed scientific journal.

Chapters 3 to 6 include, in the published articles, introductory notes and literature surveys regarding the state-of-the-art of each topic under investigation.

Chapter 7 provides an integrated synthesis of the main conclusions derived from the research presented in Chapters 3 to 6.

Chapter 8 addresses the future work to be done in the issues focused in this thesis, suggesting possible research paths to develop and deepen the issues investigated in this thesis.

Chapter 2 – Description of the NWP model

The NWP model used in this work to perform the wind simulations was the Weather and Research Forecast (WRF) mesoscale model. Besides its numerical weather prediction applications, WRF is also an atmospheric simulation system designed for both research and operational applications. The WRF model is a state-of-the-art atmospheric modelling system, being the result of a continuous collaborative effort in which several institutions are involved: the National Centre for Atmospheric Research's (NCAR) Mesoscale and Microscale Meteorology (MMM) Division, the National Oceanic and Atmospheric Administration's (NOAA) National Centres for Environmental Prediction (NCEP) and Earth System Research Laboratory (ESRL), the Department of Defense's Air Force Weather Agency (AFWA) and Naval Research Laboratory (NRL), the Centre for Analysis and Prediction of Storms (CAPS) at the University of Oklahoma, and the Federal Aviation Administration (FAA), with the participation of university scientists.

2.1 – General characteristics

WRFs Advanced Research (ARW) dynamical core, version 3.4.1 (released in 2011), was the one used in this work. The summarized information regarding the WRF model presented in this section was taken from WRF-ARW Version 3 Modelling System User's Guide (NCAR, 2012) and from the WRF Version 3 NCAR Technical Note (Skamarock et al., 2008). Detailed information about all aspects of this modelling code can be found on these references. The ARW solver integrates the compressible, nonhydrostatic Euler equations and follows a conservative approach for scalar variables. Its prognostic variables are, among others: cartesian velocity U and V components, vertical velocity (W), perturbation potential temperature, perturbation geopotential and perturbation surface pressure of dry air, turbulent kinetic energy, water vapour mixing ratio, rain/snow mixing ratio, cloud water/ice mixing ratio, etc.. Its time integration is based in a 2nd or 3rd order Runge-Kutta scheme with smaller time step for acoustic and gravity-wave modes. The

spatial discretization uses 2nd to 6th order advective schemes. Full Coriolis terms are included to consider Earth rotation effects. WRF offers several nesting options (one-way, two-way interactive and moving nest), where higher resolution simulation meshes can be nested on lower resolution simulation grids. WRF also offers the capabilities of performing grid and observational nudging.

2.2 –WRF-ARW modelling system architecture and operating chain

An overview of WRF modelling system architecture is presented in Figure A, in the form of a flow chart that illustrates the several components of the model and the respective operating order.

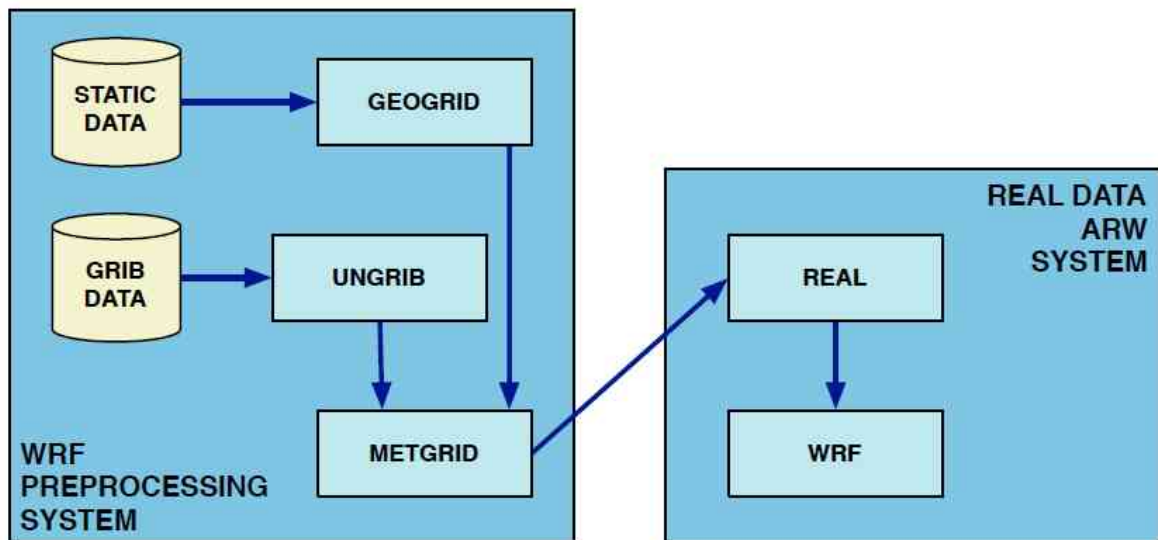


Figure A – WRF-ARW modelling system flow chart

The WRF Pre-Processing System (WPS) is a suite of programs that ingest terrestrial (static data) and meteorological data (in GRIB format) and processes them for input to the ARW real data system. The GEOGRID program is used to build a physical simulation grid by defining the projection type, location on the globe, size of the grid, nest locations, grid horizontal resolution (among other parameters) and incorporating terrestrial static data (topography, land-use, albedo, snow and vegetation cover, etc.) into that grid. The WRF-ARW supports grid nesting that allows increased resolution over a region of interest, by introducing additional grid(s) into the simulation. The option to add (or not) nested

simulation domains to the simulation is done in the GEOGRID program. Figure B presents two schematics of how nested domains can look like.

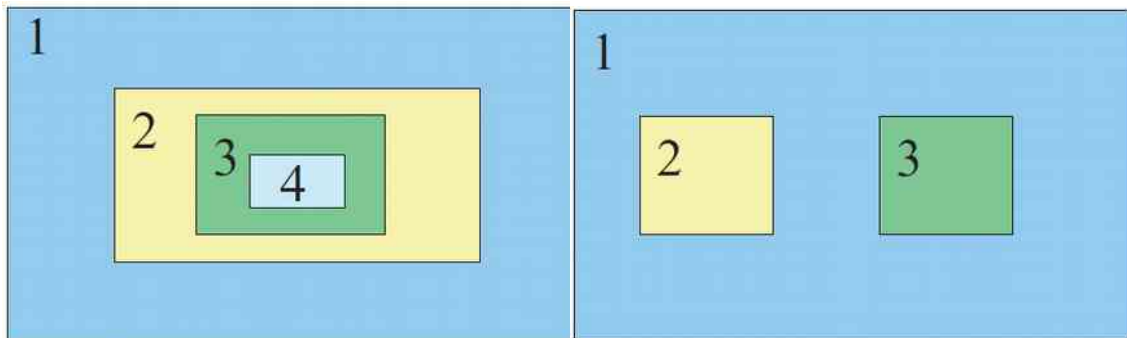


Figure B – Nested simulation grids

In Figure B, grid 1 is called the “parent domain” and grids 2 to 4 are the nested domains. As it can be seen, the nested domains can be nested in any of the other domains, as long as the grid where the domain is nested has a coarser resolution than the one to be used in the nested grid. The ability to use nested domains is of great utility since it allows high-resolution simulations maintaining model stability and accuracy. Interaction between the parent (coarser) and nested (finer) grids can be defined in two different ways: 1-way nesting, where information (lateral boundaries conditions) from the coarser (parent) grid is passed to the finer grid only; and 2-way nesting, where the finer grid solution replaces the coarser grid solution in grid points that lie inside the finest grid and this information exchange between the grids is in both directions (coarser-to-finer for the fine-grid lateral boundary computation and finer-to-coarser during the feedback at each coarse-grid time step).

The programs UNGRIB and METGRID are responsible for taking the meteorological data to be used as initial and boundary forcing conditions for the simulation and process them for incorporation in the simulation grid(s) provided by GEOGRID. While UNGRIB extracts the necessary data and reformats the GRIB meteorological data files into an internal binary format readable by WRF/WPS, METGRID horizontally interpolates this meteorological data onto the simulation grid(s). The output from the WPS package provides a complete 3-dimensional state of the atmosphere on the model grid(s) at the selected time instants, which is after used by the ARW real data system. This output

contains: 3-dimensional fields of temperature, relative humidity and horizontal components of momentum; 2-dimensional static terrestrial fields that include albedo, Coriolis parameters, terrain elevation, vegetation/land-use type, land/water mask, map scale factors, map rotation angle, soil texture category, vegetation greenness fraction and latitude/longitude; and 2-dimensional time-dependent fields which include surface pressure and sea-level pressure, layers of soil temperature and soil moisture, snow depth, skin temperature, sea surface temperature and a sea ice flags.

Each one of these resulting 3-D grids (one for each time instant and for each domain) consists in a staggered Arakawa-C type grid (Figure C), where the U and V components of horizontal velocity (wind) are normal to the respective faces of the grid cell, and the mass, thermodynamic, scalar and chemistry variables are located in the centre of the cell. The variable staggering has an additional column of U in the x-direction and an additional row of V in the y-direction since the normal velocity points define the grid boundaries. The horizontal momentum components reflect an average across each cell-face, while each mass, thermodynamic, scalar and chemistry variable is the representative mean value throughout the cell. Feedback is handled to preserve these mean values: the mass, thermodynamic, scalar and chemistry fields are fed back with an average from within the entire coarse grid point and the horizontal momentum variables are averaged along their respective normal coarse grid cell faces.

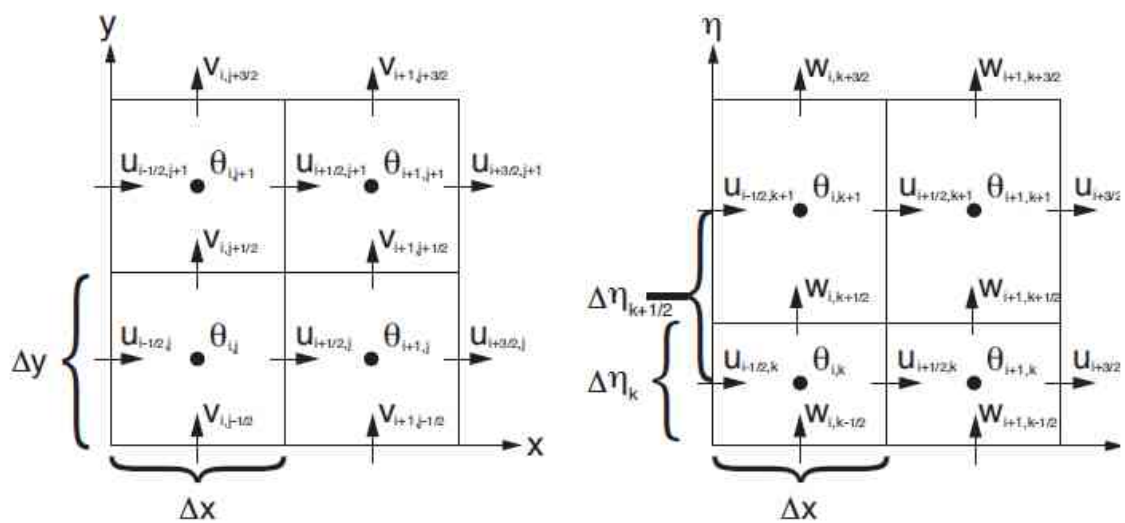


Figure C – WRF horizontal staggered grid

In the case of using nested domains, the staggered nested grids look like the ones shown in Figure D.

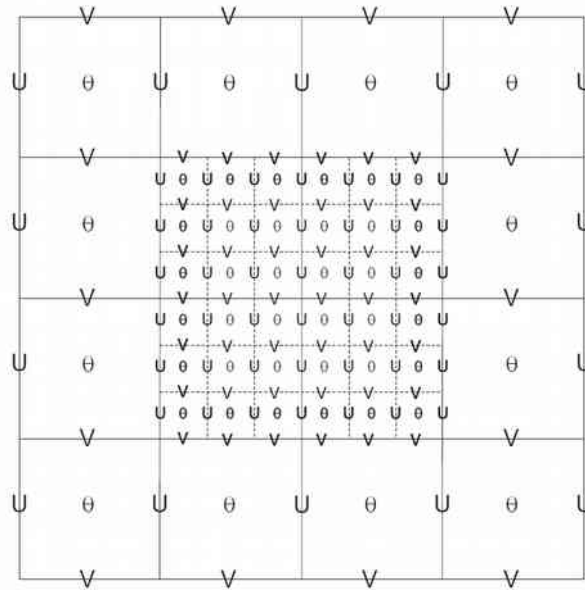


Figure D – Nested staggered horizontal grids

It should be borne in mind that although the WPS output consists in 3D grids, the vertical levels of these grids are the ones provided by the original forcing data (e.g., global models vertical levels). Thus, after running METGRID, which builds the initial and boundary data grids, the next step is to vertically interpolate the data onto the WRF model vertical levels. This is done by the REAL program (for simulations applied to real case studies, as is the case of this thesis). WRF vertical coordinates are terrain-following, dry hydrostatic-pressure, where the model top is a constant pressure surface (Figure E). These vertical coordinates, also called η (eta) levels, are defined by the following equation:

$$\eta = \frac{(P_h - P_{ht})}{(P_{hs} - P_{ht})}$$

Where P_h is the hydrostatic component of the pressure, P_{hs} is the hydrostatic pressure at the surface and P_{ht} is the hydrostatic pressure at the model domain top boundary. The coordinate definition is the traditional σ -coordinate used in many hydrostatic atmospheric models. η varies from a value of 1 at the surface to 0 at the upper boundary of the model domain. This vertical coordinate is also called a mass vertical coordinate.

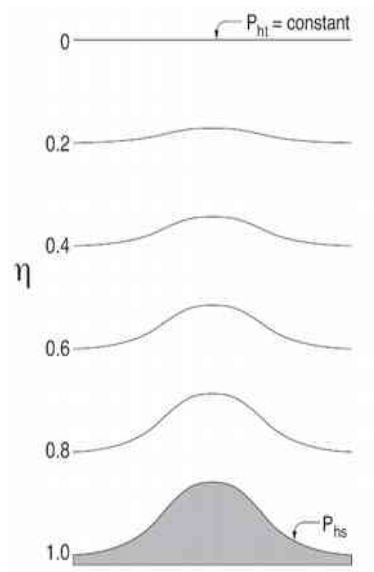


Figure E – WRF vertical coordinates

After building the input grids for the ARW real data system (WPS + REAL), which basically are the initial and boundary conditions of the simulation interpolated to the simulation domain(s), the next step will be to run the simulation. This is done by running the WRF program of the ARW real data system. The simulation configuration regarding all of its aspects is done in the configuration file of the WRF program. This configuration file defines, among other options, the temporal design of the simulation (starting and end dates, tie interval of the output, etc.), the domains configuration (nested or not, time steps, grid horizontal and vertical resolutions, etc.), the four dimensional data assimilation (FDDA) and the physical configuration of the simulations. The FDDA system, also known as nudging, consists in a method of maintaining the simulation close to reference datasets (considered as good representations of the atmospheric state, usually reanalysis/analyses and/or observations datasets) over the course of the simulation. This system supports two different types of FDDA, which can be used separately or in combination. Grid/analysis nudging forces the simulation towards a reanalyses/analyses dataset in all grid points. Observational nudging locally forces the simulation towards measured data in the vicinity of the measurement site. These FDDA methods are very useful to minimize the model divergence and accumulation of truncation errors in long simulations periods, in which the model typically is not often reinitialized. Since this work focuses on the physical parameterization schemes available in WRF, a brief description of the main characteristics

of the several groups of physical parameterization options available in WRF-ARW is presented.

2.3 –WRF-ARW physical parameterizations

WRF's physical parameterizations are employed to include the effects of sub-grid processes in the simulation grid. Sub-grid processes are usually defined as physical processes that occur at a spatial and/or temporal scale smaller than the model grid/time-step resolution and, therefore, cannot be explicitly solved by the model. In the impossibility of an explicit representation of such phenomena, an implicit representation of the sub-grid processes effects (and not the processes "*per se*") is included in the model grid variables (explicitly solved) through the use of parameterization schemes. These parameterization schemes are based on conceptual or empirical relationships to approximate the impact of sub-grid processes on the resolved scale dynamics and thermodynamics. WRF's physical parameterizations can be divided into different categories, each one containing several available choices. The physic parameterizations categories are: microphysics, cumulus, radiation, surface layer (SL), land-surface models (LSM) and planetary boundary layer (PBL).

Microphysics parameterization schemes deal with processes controlling formation of cloud droplets and ice crystals, their growth and fall-out as precipitation. These schemes include explicitly resolved water vapour, cloud, and precipitation processes.

Cumulus parameterization schemes are responsible for the sub-grid scale effects of convective and/or shallow clouds, and are designed to represent vertical fluxes due to unresolved updrafts/downdrafts and compensating motion outside the clouds, providing also vertical heating, moistening profiles and the convective component of surface rainfall. Cumulus parameterizations are theoretically only necessary to use in grid sizes greater than approx. 10 km, in order to properly release latent heat on a realistic time scale in the convective columns.

Radiation schemes handle the atmospheric heating due to radiative flux divergence and surface downward long- and short-wave radiation for the ground heat budget. Long-wave radiation includes infrared or thermal radiation absorbed and emitted by gases and surfaces. Upward long-wave radiative flux from the ground is determined by the surface emissivity, which depends on the land-use type and ground temperature. Short-wave radiation includes visible and neighbour wavelengths of the solar spectrum. Although the only source of short-wave radiation is the Sun, processes such as absorption, reflection, and scattering in the atmosphere and at surfaces are included. The upward short-wave radiation flux is the reflection due to surface albedo. In the atmosphere, radiation schemes respond to model-predicted cloud and water vapour distributions, as well as specified carbon dioxide, ozone, and (optionally) trace gas concentrations.

Surface layer schemes deal with the friction velocities and exchange coefficients that allow the calculation of surface heat and moisture fluxes by the land-surface models, and surface stress in the planetary boundary layer scheme. Over water surfaces, the surface layer scheme calculates the surface fluxes and diagnostic fields. These schemes provide the stability-dependent information about the surface layer for the land surface and PBL schemes.

The land surface models provide heat and moisture fluxes over land points and sea-ice points by combining information from the surface layer (atmospheric information), radiation (radiative forcing) microphysics and convective schemes (precipitation forcing), together with internal information on the land's state variables and land surface properties. These fluxes provide a lower boundary condition for the vertical transport done in the PBL schemes (or the vertical diffusion scheme in the case where a PBL scheme is not run, such as in large-eddy mode). Land surface models update the land's state variables which include the ground (skin) temperature, soil temperature profile, soil moisture profile, snow cover, and possibly canopy properties.

Planetary boundary layer schemes deal with the vertical sub-grid scale fluxes due to eddy transports in the entire atmospheric column, not just the boundary layer. Thus, when a PBL scheme is activated, explicit vertical diffusion is turned-off with the assumption that the

PBL scheme will handle this process. The surface fluxes are provided by the surface layer and land-surface model schemes. The PBL schemes determine the flux profiles within the well-mixed boundary layer and the stable layer, and thus provide atmospheric tendencies of temperature, moisture (including clouds), and horizontal momentum in the entire atmospheric column. The schemes are one-dimensional, and assume that there is a clear scale separation between sub-grid eddies and resolved eddies. This assumption will become less clear at grid sizes below a few hundred meters, where boundary layer eddies may start to be resolved, and in these situations the scheme should be replaced by a fully three-dimensional local sub-grid turbulence scheme such as the TKE diffusion scheme.

Although this categorization of model physics, there are many interactions between them through the model state variables (potential temperature, moisture, wind, etc.) and their tendencies, and through the surface fluxes (Figure F). All the physical parameterizations interact in some way with the surface physics (land-surface models, and, potentially, coupled ocean models). The surface physics, while not explicitly producing tendencies of atmospheric state variables, is responsible for updating the land-state variables. Although the microphysics schemes do not output tendencies, they do update the atmospheric state during the simulation.

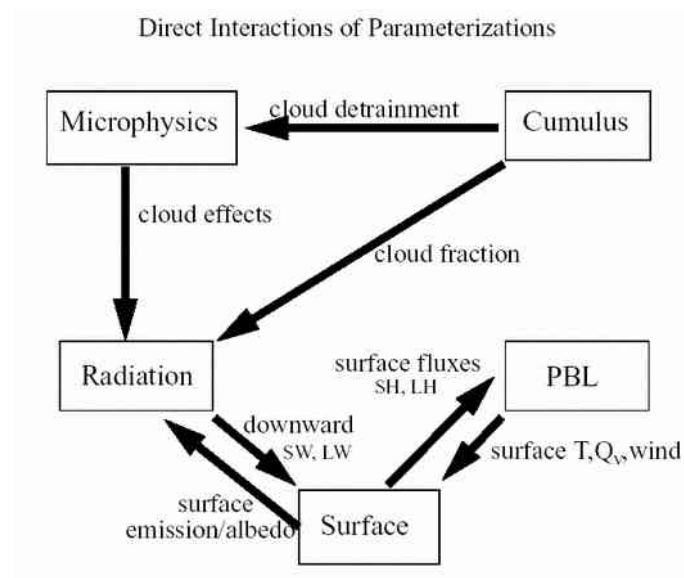


Figure F – Interactions between the several physical parameterizations (simplified)

Chapter 3 – Optimisation of the WRF model wind simulation: testing of initial and boundary datasets

This chapter presents the testing of which initial and boundary datasets used to force the WRF model produce the most accurate wind power flux, wind speed and direction simulation results. This chapter describes this research in the form of two published research articles, one for onshore areas and another one for offshore areas. In each of these articles it is detailed the methodology followed, area under study, initial/boundary datasets tested and *in situ* observed data used to compare the simulations driven by each initial and boundary dataset. Also introductory notes and state of the art are included.

3.1 - Onshore

The article presented below details the research about the testing of which initial and boundary datasets used to force the WRF model produce the most accurate wind power flux, wind speed and direction simulation results for onshore Portuguese continental territory. This article can be consulted in the link:

<http://www.sciencedirect.com/science/article/pii/S0306261913009847>



WRF wind simulation and wind energy production estimates forced by different reanalyses: Comparison with observed data for Portugal



D. Carvalho^{a,*}, A. Rocha^a, M. Gómez-Gesteira^b, C. Silva Santos^c

^a CESAM – Department of Physics, University of Aveiro, Campus Universitário de Santiago, 3810-193 Aveiro, Portugal

^b Environmental Physics Laboratory, EPHYSLAB, Facultad de Ciencias, Universidad de Vigo, 32004 Ourense, Spain

^c Instituto Superior de Engenharia do Porto, Rua Dr. António Bernardino de Almeida 341, 4200-072 Porto, Portugal

HIGHLIGHTS

- Simulated winds and wind energy estimates forced by different reanalysis were evaluated in Portugal.
- ERA-Interim reanalysis is the one that likely provides the most realistic initial and boundary data.
- NCEP-FNL and NCEP-GFS analyses showed better results than the other reanalyses datasets tested.
- New generation reanalysis provide considerable improvement in the near surface wind simulation.
- NCEP-FNL and NCEP-GFS analyses are the best alternatives to ERA-Interim.

ARTICLE INFO

Article history:

Received 6 May 2013

Received in revised form 11 November 2013

Accepted 2 December 2013

Available online 25 December 2013

Keywords:

WRF

Reanalyses

Analyses

Initial and boundary conditions

Wind modeling

Wind energy

ABSTRACT

The performance of the WRF mesoscale model in the wind simulation and wind energy estimates was assessed and evaluated under different initial and boundary forcing conditions. Due to the continuous evolution and progress in the development of reanalyses datasets, this work aims to compare an older, yet widely used, reanalysis (the NCEP-R2) with three recently released reanalyses datasets that represent the new generation of this type of data (ERA-Interim, NASA-MERRA and NCEP-CFSR). Due to its intensive use in wind energy assessment studies, the NCEP-GFS and NCEP-FNL analysis were also used to drive WRF and its results compared to those of the simulations driven by reanalyses.

Six different WRF simulations were conducted and their results compared to measured wind data collected at thirteen wind measuring stations located in Portugal in areas of high wind energy potential. Based on the analysis and results presented in this work, it can be concluded that the new generation reanalyses are able to provide a considerable improvement in wind simulation when compared to the older reanalyses. Among all the initial and boundary conditions datasets tested here, ERA-Interim reanalysis is the one that likely provides the most realistic initial and boundary data, providing the best estimates of the local wind regimes and potential wind energy production. The NCEP-GFS and NCEP-FNL analyses seem to be the best alternatives to ERA-Interim, showing better results than all the other reanalyses datasets here tested, and can therefore be considered as valid alternatives to ERA-Interim, in particular for cases where reliable forcing data is needed for real-time applications due to its fast availability.

© 2013 Elsevier Ltd. All rights reserved.

1. Introduction

Due to the current deterioration of the worldwide environment, together with the increasing scarcity and high cost of the conventional energy sources (mainly fossil fuels), renewable energies are currently one of the main areas of research and investment. One of the fastest growing renewable energy sources has been wind

* Corresponding author. Tel.: +351 234 370 356; fax: +351 234 378197.

E-mail addresses: david.carvalho@ua.pt (D. Carvalho), alfredo.rocha@ua.pt (A. Rocha), mgesteira@uvigo.es (M. Gómez-Gesteira), cmi@isep.ipp.pt (C. Silva Santos).

power, which is presently one of the main suppliers of electricity in European countries. Portugal has been one of the leading countries in terms of installed onshore wind generating power: in 2011, it ranked 10th worldwide and 5th among European countries in terms of total wind energy installed capacity [1]. In 2010, Portugal was able to achieve an 18% quota of wind-derived energy in the total annual energy consumption, only outranked worldwide by Denmark in this parameter [2]. The exponential growth of worldwide installed wind power, mainly over the last decade, together with the future expansion of the wind energy markets [3] brings new challenges to the wind power industry, namely in what is related to the identification of the most promising sites in terms

of wind energy potential. Although the use of this renewable energy source has been rapidly increasing worldwide, the lack of reliable measured wind data in several areas of the globe is still hampering the development of new wind energy projects, particularly in developing countries [4].

The wind energetic potential of one given area is traditionally assessed using locally acquired wind measurements and, in order to realistically represent the local wind climatology for wind energy assessment, a minimum of 1 year of measurements needs to be performed. However, the planning, installation and maintenance of wind measuring masts is an expensive endeavor, and if the wind measuring campaign reveals a poor wind energetic potential of the selected site, a considerable amount of investment is irreversibly lost. The need to obtain a preliminary knowledge of the available wind resource at sites with few or no local measurements becomes, therefore, of paramount importance. Due to these needs and limitations, alternative and reliable sources of wind data specifically designed to assess the wind energetic potential of one given area and/or to accurately forecast the wind constitute, nowadays, a very valuable service. One of the most used alternative sources of wind data are numerical weather prediction (NWP) models, capable of deriving wind climatologies at high resolution at the regional scale. In the recent past, mesoscale modeling using NWP codes has been used in several applications in the wind energy field: in the long-term wind climatology characterization of potential sites, in order to quantify the wind variability and representativeness of the local wind measurements to reduce uncertainty in annual energy production estimates; in short-term wind forecasting for wind farms already in operation, in order to correctly balance the electrical grid; and in mapping the average wind resource over large areas, very useful for large scale energy and/or electrical grid planning, to help promoters identify potential sites for wind energy exploitation, for greenfield or early-stage projects [5–13]. Despite the promising results obtained until now with NWP models, the wind simulation (and, particularly, the near-surface wind modeling) is still a major challenge to atmospheric modellers involved in meteorological research and applications, mainly due to the strong interaction between these low-altitude atmospheric flows and the local topography.

One of the most critical issues regarding mesoscale NWP modeling is the initial and boundary conditions that are fed into the model. Typically, for wind energy assessment and wind simulation studies, initial and boundary data are obtained through reanalysis datasets, which provide all the atmospheric information needed by the models to perform their simulations. Reanalysis are gridded datasets that combine data obtained from global circulation models (GCM's) with measured data, providing a synthesis of the available worldwide observations in the context of a physical model [14]. The first generation of reanalyses comprised three datasets: the NCEP-R1 [15], produced and released by the National Centres for Environmental Prediction (NCEP); the European Centre for Medium-Range Weather Forecasts (ECMWF) ERA-40 reanalysis [16]; and the Japanese Meteorological Agency JRA-25 reanalysis [17]. Due to several problems reported for the NCEP-R1, a second version known as the NCEP-R2 [18] was released by NCEP in order to correct the detected problems. NCEP-R2 is still processed up to the present in near real-time, which is a unique feature among these first generation reanalyses, considering that ERA-40 was discontinued in 2001 and the JRA-25 in 2004. Recently, a new generation of reanalyses has been produced and released, namely: the new ECMWF reanalysis (ERA Interim, described in [19]), the NCEP Climate Forecast System Reanalysis (NCEP-CFSR, described in [20]) and NASA's Modern Era Retrospective Analysis for Research and Applications (NASA-MERRA, described in [21]). This new generation of reanalyses is expected to provide a significant progress, due to advances in operational weather forecasting and also from

previous reanalyses improvement efforts [22]. However, in mesoscale wind modeling applied to wind energy potential assessment it is common to find studies which use two analyses datasets provided by NCEP: the NCEP Global Forecast System (NCEP-GFS) and the NCEP Final Analysis (NCEP-FNL). Although these two analyses datasets differ from the traditional reanalyses, as will be detailed further on, it was decided to include them in this work due to its use in the wind power industry.

In summary, NCEP-R2, ERA-Interim, NCEP-CFSR, NASA-MERRA, NCEP-FNL and NCEP-GFS are currently the only available initial and boundary conditions datasets that are freely and publicly available, continue up-to-date and include the geographical area under scope in this study. Summarized information about these datasets is shown in Table 1.

The main differences between them can be condensed as follows: NCEP-R2 has the coarsest horizontal and vertical resolutions of the six considered datasets, assimilating only a limited amount of satellite observations; ERA-Interim is the latest global reanalysis produced in Europe and, in opposition to the other considered reanalyses, they include a four-dimensional variational analysis, 4D-var [23,24] assimilation method; NCEP-CFSR is the only dataset that makes use of a coupled atmosphere–ocean–sea ice–land model and both in ERA-Interim and NCEP-CFSR a variational bias correction method is employed, which allows a significant improvement and correction of biases related to satellite radiances. Although NCEP-R2 and NCEP-CFSR were produced by the same institution, the last one brought significant improvements to the traditional NCEP-R2, namely a higher resolution model (actually, the highest resolution among the reanalyses used in this study) and increased use of satellite observations in its assimilation process. As for the NASA-MERRA reanalysis, the GEOS model (version 5) and data assimilation system are used [25]. Its 3D-Var data assimilation system includes the implementation of flow-dependent, anisotropic and inhomogeneous background error covariances, described in [26,27]. Another innovation in this product is the implementation of a nudging technique that allows a smooth transition from the model states toward the observed state, the Incremental Analysis Update [25,28]. As for the NCEP-FNL and NCEP-GFS, which consist in analyses and not reanalyses, the major differences between them and reanalysis data are: the amount of observational data assimilated, where the reanalyses datasets typically consider a higher volume of measured and observed data; the availability of the data, where the NCEP-FNL and NCEP-GFS data is available usually within a day (or even in the same day) of the present date while reanalysis datasets are available only a few days/months after; the homogeneity of the analyses, where the advantage of the reanalyses is that the same model physics, parameterizations, etc., are used for the entire dataset produced, while the NCEP-FNL and NCEP-GFS data are subject to whatever the operational configuration is at any given period that can cause some inconsistencies over time (to see an example of how the model setup has changed over time, please consult <http://www.emc.ncep.noaa.gov/gmb/STATS/html/model_changes.html>). NCEP-FNL and NCEP-GFS share practically all of their characteristics, including the atmospheric model and its configuration. The main differences between these two analyses are: NCEP-FNL assimilates a higher amount of measured data than NCEP-GFS, since it runs 3 h past synoptic time when more observational data is available; NCEP-GFS, although containing less observation data assimilated, it has a much finer spatial and vertical resolution (Table 1).

Considering that this new generation of reanalyses is recent, only the study performed by Carvalho et al. [6] compared the use of the reanalyses considered in this work in terms of their use as initial and boundary data in NWP models for wind simulation. However, that work was focused on offshore winds alone, and

Table 1
Main characteristics of the considered datasets.

Dataset	Type of dataset	Horizontal resolution	Vertical levels	Time coverage	Assimilation system
NCEP-R2	Reanalysis	2.5° lat/lon	28	1979–Present	3D-Var
ERA-Interim	Reanalysis	0.75° lat/lon	60	1979–Present	4D-Var
NCEP-CFSR	Reanalysis	0.5° lat/lon	64	1979–Present	3D-Var
NASA-MERRA	Reanalysis	0.5° lat – 2/3 lon	72	1979–Present	3D-Var
NCEP-FNL	Analysis	1° lat/lon	52	1999–Present	3D-Var
NCEP-GFS	Analysis	0.5° lat/lon	64	2004–Present	3D-Var

included only reanalyses datasets. The authors concluded that the simulation driven by ERA-Interim was the one that provided the highest overall accuracy, and also that the new generation reanalyses (ERA-Interim and NCEP-CFSR) are able to provide a considerable improvement in the ocean wind simulation when compared to the older reanalyses. Also Menéndez et al. [29] tested the use of several reanalyses in offshore wind simulation, but mainly using first generation reanalyses (NCEP-R1, JRA25, ERA-40 and ERA-Interim), concluding that simulations driven by ERA-Interim are the ones that present the best accuracy. A few studies were found that compare these and others sets of reanalyses, although not as initial and boundary conditions in NWP models but the datasets themselves [30–32]. These studies were unanimous in reporting significant improvements in the new generation reanalyses. This is consistent with the improvement in models, observations, and data assimilation, since more data (observations, scatterometer winds and improved microwave sounder) is being included through new data assimilation methods. In particular for ERA-Interim, it was suggested that its 4D-var assimilation system is a major advantage and produces better results when compared to the other reanalyses that use three-dimensional variational analysis. In particular for wind simulation, Tabata et al. [33] compared lower tropospheric horizontal winds from measurements and from global reanalyses over Indonesia, concluding that ERA-Interim showed the highest correlation coefficient and the lowest standard deviation when compared to measured winds. Specifically for wind energy assessment, Liléo and Petrik [34] compared the use of NCEP-R2, NASA-MERRA and NCEP-CFSR reanalyses for onshore wind resource assessment by comparing their data to locally acquired measurements, reaching the conclusion that the higher spatial and temporal resolutions of the new reanalyses allow a better representation of the local wind climate, representing a significant improvement in wind representation accuracy for energy production estimates.

In this study, the WRF mesoscale model is used to perform six simulations of near surface winds, each of them using as initial and boundary conditions a different dataset (reanalysis: NCEP-R2, ERA-Interim NCEP-CFSR and NASA-MERRA; analysis: NCEP-FNL and NCEP-GFS). Simulated winds are compared to the observed ones measured by 13 wind measuring stations scattered in Portuguese territory. These wind measuring stations are located in areas with an expected high wind energy potential, and the measurement campaigns were conducted specifically to assess the wind energetic potential of the sites. This study aims to compare the performance of this NWP model in simulating the local wind characteristics and potential wind energy production estimates, when forced by different initial and boundary conditions.

2. Methodology and data

2.1. Measured wind data

Wind data measured at thirteen wind measuring stations scattered around Portuguese territory (Fig. 1) was used in this work. These stations are concentrated in four main areas, where

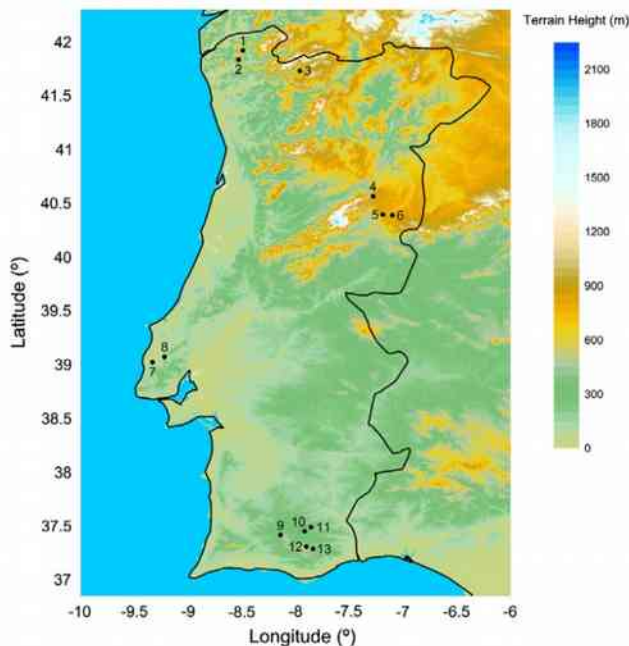


Fig. 1. Wind measuring stations locations.

several wind farms are currently in operation or planned to be built in the near future. It is important to mention that all of the wind data collected by these stations were measured before any wind farm was installed, therefore, this wind data is free from interferences and wake effects from wind turbines. The stations locations are depicted in Fig. 1, together with the terrain height extracted from the Shuttle Radar Topography Mission (SRTM) database, described in Farr et al. [35].

All stations measure the wind speed and direction with a temporal resolution of 10 min and at 60 m above ground level (a.g.l.), with the exception of stations 6, 7 and 8 that measure the flow at 80 m a.g.l. This study uses records corresponding to the time period January 1st to December 31st 2008.

2.2. Model and simulations design

The mesoscale meteorological model Weather Research and Forecast (WRF, version 3.4.1), a well known and widely used NWP model developed by the National Centre for Atmospheric Research (NCAR), was chosen to perform the simulations. A detailed description of the model is available in Skamarock et al. [36]. Information regarding the topography, land–water masks, land use/land cover classification, albedo, etc., was supplied to the WRF model using the GTOPO30 and the USGS data sets, made available by the US Geological Survey with a horizontal grid resolution of 0.0083° latitude/longitude. In addition, also daily sea surface temperatures (SST) were supplied to the model, being obtained from the real-time, global, sea surface temperature analyses database

from NCEP with a spatial resolution of 0.083° in latitude and longitude. The simulation domains followed a two-way nesting strategy. Due to the fact that the different datasets considered here have different spatial resolutions, it becomes necessary to build different simulation domains for each dataset (both in number of nested domains and spatial resolution of each one), in order to achieve a common size and resolution of the innermost domain. The main characteristics of the simulation domains for all simulations are presented in Table 2, and the vertical structure of the model is divided in 27 layers. Fig. 2 depicts the innermost simulation domain.

The complete year of 2008 was simulated, through 12 month-long independent simulations to avoid model divergence and the accumulation of truncation errors. Moreover, as suggested by Carvalho et al. [5], the grid nudging option of the WRF's Four-Dimensional Data Assimilation (FDDA) system was used in all the simulations. This grid nudging method is a specific three-dimensional analysis nudging, where the model is nudged towards the initial and boundary conditions (both in time and space) using a point by point relaxation term. To avoid possible interferences in the resolved mesoscale forcing mechanisms that are important to the boundary layer development [37], no nudging was applied inside the planetary boundary layer. A more detailed description of this technique can be found in [36,38]. WRF's physical configuration for all simulations considered the following schemes: Yonsei University for the planetary boundary layer, Monin–Obukhov MM5 for the surface layer, WRF Single-Moment 6-Class for the microphysics, Noah land surface model, RRTM scheme for the long-wave radiation, Dudhia parameterization for the short-wave radiation and the Kain–Fritsch scheme for cumulus parameterization.

Given this, six different simulations were performed, each one of them considering one of the four forcing datasets mentioned before. For each one of these simulations, wind speed and direction hourly time series were extracted at the same locations and measuring height of the 13 wind measuring stations by performing a horizontal and vertical bi-linear interpolation between the closest simulation grid points to the wind measuring sites.

2.3. Statistical and comparative analysis

The following statistical parameters were used to evaluate the simulations: the root mean squared error (RMSE),

$$RMSE = \left[\frac{1}{N} \sum_{i=1}^N (\theta'_i)^2 \right]^{1/2} \quad (1)$$

where

$$\theta' = \theta^{sim} - \theta^{obs} \quad (2)$$

is the deviation between the simulated wind speed (θ^{sim}) and the respective observed wind speed in the station (θ^{obs}), being N the total number of pairs of simulation/measured records. For the wind direction, which is a circular and nonlinear variable, θ takes a different expression due to the fact that the absolute deviation of

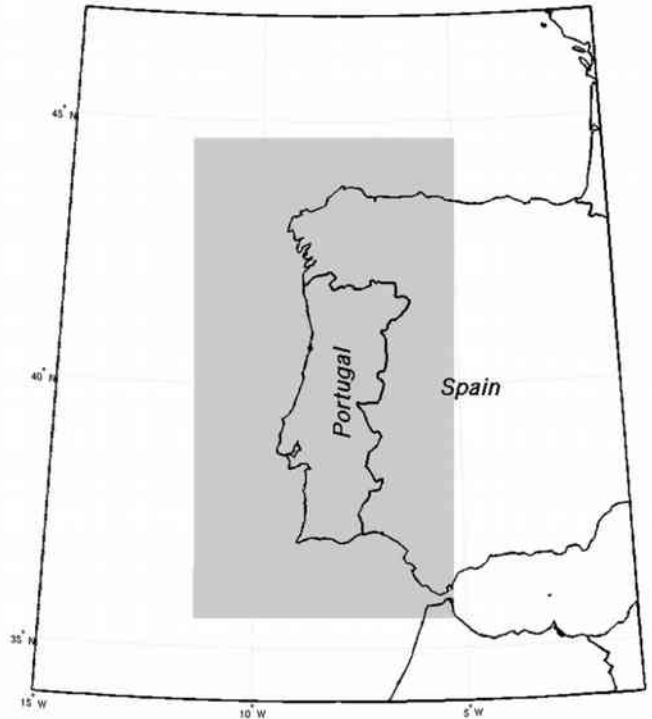


Fig. 2. Innermost simulation domain.

the wind direction cannot exceed 180° in module. For this case, θ is given by

$$\theta'_i = \left(\theta_i^{sim} - \theta_i^{obs} \right) * \left[1 - 360 / \left| \theta_i^{sim} - \theta_i^{obs} \right| \right], \quad \text{if } \left| \theta_i^{sim} - \theta_i^{obs} \right| > 180^\circ \quad (3)$$

The bias, defined as

$$Bias = \frac{1}{N} \sum_{i=1}^N \theta'_i \quad (4)$$

makes possible the evaluation of the data systematic errors. A positive (negative) bias means that the simulations overestimate (underestimate) the measured values. For the wind direction, a positive (negative) bias represents a clockwise (anti-clockwise) deviation. The Standard Deviation of the Error (STDE), which is useful to evaluate the dispersion of the error, is given by

$$STDE = \sigma(\theta'_i) = [RMSE^2 - Bias^2]^{1/2} \quad (5)$$

The STDE removes from the RMSE possible offsets (biases), and it shows if a given error is mainly due to a kind of offset (more easily corrected) or due to a more random component of the error. The correlation coefficients (R) for the wind speed and for the wind direction were computed to assess the correlation between the simulations and measured wind. In addition to the abovementioned statistical analysis, the Weibull probability density function (P.D.F.)

Table 2
Main characteristics of the domains for all simulations.

Simulation	Number of domains	Spatial resolutions (km)	Size of each domain (X–Y grid nodes)		
			D1	D2	D3
NCEP-R2	3	75, 15 and 5	60–70	96–111	112–205
ERA-Interim	2	15 and 5	95–110	112–205	–
NCEP-CFSR	2	15 and 5	95–110	112–205	–
NASA-MERRA	2	15 and 5	95–110	112–205	–
NCEP-FNL	2	25 and 5	65–75	112–205	–
NCEP-GFS	2	15 and 5	95–110	112–205	–

of the wind speed (U) was used to evaluate the simulated wind. The Weibull distribution is widely used to represent wind speed distributions for wind energy applications, not only due to its greater flexibility and simplicity but also because it accurately fits to experimental data [39–46]. The Weibull P.D.F. is given by

$$W_U = \frac{k}{A} \left(\frac{U}{A}\right)^{k-1} e^{-\left(\frac{U}{A}\right)^k} \quad (6)$$

The A (scale parameter) is mainly related to the mean state and mean value of the wind speed, while k (shape parameter) can be regarded as equivalent to the standard deviation. The most probable value of U (U_{prob}) can be calculated from the first derivative of following equation:

$$U_{prob} = A \left(\frac{k-1}{k}\right)^{1/k} \quad (7)$$

Finally, the potential wind energy production was estimated computing the power flux for all sites. The wind power flux ($W m^{-2}$) is a function of the wind speed, given by:

$$P_{flux} = \frac{1}{2} * \rho * U^3 \quad (8)$$

where U is the wind speed and ρ is the air density and the standard value of 1.225 kg m^{-3} was assumed. The mean wind power flux was computed at all sites for each simulated and measured wind speed record, adding all records power fluxes and then averaging this sum by the total number of records.

3. Results and discussion

3.1. Statistical analysis

The RMSE, Bias, STDE and correlation coefficients (R) between the stations and the wind data derived from the three simulations are presented in Table 3, considering only the number of simultaneous and valid pairs of records between the simulations and the respective station. Due to the high number of stations used in these comparisons, only the weighted average values are presented (average values weighted by the number of pairs of records used). The best error scores (lower errors and higher correlation coefficients) are highlighted in bold.

According to Table 3, the WRF simulations that used ERA-Interim reanalysis as initial and boundary conditions show the lowest overall errors in terms of RMSE, STDE and correlation coefficient, both for the wind speed and direction. For the Bias, again the simulation driven with ERA-Interim presents the lowest errors but now just for the wind direction. For the wind speed, the simulation driven with the NCEP-GFS analysis has the lowest bias but followed closely by the simulations forced with ERA-Interim and NCEP-FNL. The worst RMSE, STDE and R scores were obtained for the WRF simulations driven with NCEP-R2 reanalysis, while for the bias the simulation with the highest errors was the one driven

with NASA-MERRA and NCEP-R2 for the wind speed and NCEP-GFS driven simulation for the wind direction.

For all simulations, the overall wind speed bias is positive, indicating a tendency to overestimate the wind speed. For the wind direction, the weighted mean biases were positive for the simulation driven by NCEP-R2 reanalysis and negative for the simulations driven by the remaining input data. Therefore, NCEP-R2 driven simulations have a tendency to simulate the wind with a slight clockwise wind rotation relative to the measured wind, while ERA-Interim, NCEP-CFSR, NASA-MERRA, NCEP-FNL and NCEP-GFS simulated the wind direction with an anti-clockwise rotation. But, considering the magnitude of these obtained biases, the wind direction rotations are insignificant.

Although not shown in Table 3, all simulations underestimate the wind speed at two stations (stations 2 and 3) but overestimate it at all remaining ones, resulting in the weighted mean wind speed overestimation mentioned above. This fact may be surprising, because the application of mesoscale models for wind energy assessment studies typically shows wind speed underestimations at potential sites for installing wind farms (typically mountain ridges), and not overestimation. Although the aim of this study is not to analyze in detail the errors of the model but to conclude which one of these databases provides simulations closest to the measured wind data, it is worth looking in further detail to the possible reasons why the simulations tend to overestimate the wind speed.

Mesoscale errors for near surface winds may have multiple sources, from discrepancies in the atmospheric modeling at mesoscale level to incorrect representation of local terrain and roughness heights, leading to a misrepresentation of the local terrain complexity. Due to the limited resolution of the topography data supplied to the model, amplified by their own limited resolvable capacity, mesoscale models tend to smooth the real topography and its complexity in the simulation mesh. This leads to a two-pronged effect.

The first effect comes from the fact that this smoothing of the terrain complexity may have a speed-up effect in the simulated wind, since a flatter terrain means lower friction between the surface and the atmosphere, inducing higher surface wind speeds. The study [47] suggests that WRF exhibits a high wind speed bias over land due to the exclusion of sub-grid orographic drag in the formulation of roughness lengths. By formulating roughness length including these effects, they were able to significantly reduce the high wind speed bias in low-level winds. Moreover, this smoothing of the real topography will produce mountain peaks lower and valleys higher than in reality in its simulation mesh. Therefore, the mesoscale model will have a tendency to overestimate the wind speed in valleys and underestimate the wind speed in mountain peaks: the underestimation of the wind speed due to the underestimation of the site height is due, on the one hand, by the fact that places with lower elevation are typically characterized by lower mean wind speeds. As a consequence, if the model considers the simulation point lower than it is in reality, the computed wind

Table 3
Statistics of the comparison between observed and simulated wind data averaged for all stations.

Simulation	RMSE		Bias		STDE		R	
	Speed ($m s^{-1}$)	Direction ($^{\circ}$)	Speed ($m s^{-1}$)	Direction ($^{\circ}$)	Speed ($m s^{-1}$)	Direction ($^{\circ}$)	Speed ($m s^{-1}$)	Direction ($^{\circ}$)
NCEP-R2	2.49	43.77	0.49	0.46	2.41	43.55	0.69	0.68
ERA-Interim	2.10	35.02	0.34	-0.35	2.02	34.87	0.79	0.78
NCEP-CFSR	2.19	36.25	0.47	-0.89	2.07	36.10	0.78	0.76
NASA-MERRA	2.26	39.39	0.49	-1.21	2.15	39.19	0.76	0.75
NCEP-FNL	2.17	36.07	0.31	-0.87	2.09	35.89	0.77	0.75
NCEP-GFS	2.13	35.57	0.30	-2.14	2.05	35.38	0.78	0.75

speed may be lower than in reality also. On the other hand, typically mountain areas are characterized by wind speed-up effects due to the fact that the wind becomes compressed on the windy side of the mountain, and once the air reaches the ridge it can expand again as it soars down into the low pressure area on the lee side of the mountain. If the model considers the site lower than it is in reality, this speed-up effect will be lower and the simulated wind speeds will be underestimated [5]. The inverse situation is seen when the model overestimates the site height. The differences between the real heights of the 13 stations and its correspondent heights in WRF's simulation mesh were computed and, since all of the stations are located in mountain ridges (or points that are higher than the surrounding areas), WRF considers all stations with lower heights than in reality. Given this, the wind speed overestimation cannot be attributed to an overestimation of the stations heights. However, a wind speed overestimation effect by NWP models can arise in sites with high topographic elevations due to flow detachment phenomena: the flow regime in the vicinity of an orographic obstacle can be quantified in terms of the Froude number:

$$F_r = H * N / U \quad (9)$$

where H is the site height, N represents the moist Brunt-Väisälä frequency and U the wind speed. When $F_r < 1$, the atmospheric flow will tend to pass over the orographic obstacle and the aforementioned situation of wind speed underestimation by the model is most likely to occur. Oppositely, if $F_r > 1$ there will be a tendency for the atmospheric flow to be detached and a significant part of it to be diverted around the orographic obstacle instead of passing over it. For this case, since the NWP model topography is smoothed when compared to the real one, the model might not properly represent this flow detachment and simulate the flow as passing mainly over the orographic obstacle and not around it. In this case, an overestimation of the wind speed by the model is more likely to occur. Considering that the mountainous sites here considered are relatively low, together with a typical stability condition ($N \sim 10^{-2} \text{ s}^{-1}$) and wind speeds in average above 5 m s^{-1} , it is not expected that flow detachments can occur often. However, this can happen in localized areas and/or during particular synoptic/atmospheric conditions leading to the model to overestimate the wind speed. An example of these flow detachment phenomena can be seen in [48].

However, a second effect may occur since this simplification of the real topography and terrain complexity is not always straightforward and linear in terms of its impact in the modeling results, and may have other implications in the simulation performance. For example, if one station is located in the vicinity of a higher peak located North of the station, the real wind at the station will suffer an orographic blockage and winds coming from North will be slowed down due to the neighbor higher peak. If the mesoscale model smooths the topography to a state that the higher peak is much more smooth and low, this orographic blockage will not be properly captured by the model and it will overestimate wind speeds coming from North. If, in that station, the dominant wind direction is North the model will overestimate the wind speed on the majority of the wind occurrences, and the overall result is an overestimation of the wind speed at that site.

Therefore, and excluding errors that can arise from the misrepresentation of the synoptic conditions of the atmosphere, mesoscale models have limitations in their topography representation that can induce over or underestimation of the wind speed at one given site. The factors that can contribute to a wind speed overestimation are: smoothing of the surrounding topography and terrain complexity, meaning lower friction between the surface and the atmosphere, originating faster surface wind

speeds; overestimation of the site height, contributing to an overestimation of the wind speed (not applicable in the present case); the occurrence of flow detachment situations, contributing to the wind speed overestimation by the model due to its inability to capture this phenomena; and smoothing of the surrounding topography that can partially or completely misrepresent possible orographic blockages from certain wind direction sectors. Oppositely, the factor that can contribute to a wind speed underestimation is the underestimation of the site height, leading to an underestimation of the wind speed. The interaction and balance between these factors, together with the contribution of other sources of error related to the misrepresentation of the atmospheric synoptic conditions, can lead to an over or underestimation of the wind speed by the model. For example, the wind speed underestimation induced by the underestimation of the site height (typical in mountain peaks) can be partially/completely canceled and even surpassed due to low/high contribution of wind speed overestimation contributors, such as the terrain complexity smoothing and/or the misrepresentation of orographic blockages and flow detachments.

Although it is unrealistic to separate and quantify the contribution of each one of these factors, an example is depicted in Fig. 3, where it is clear the topography and terrain complexity smoothing of WRF's simulation mesh (mountain peaks lower and valleys higher than in reality), together with the occurrence of orographic blockage effects. Stations 1 and 2 were chosen as example, due to the fact that station 1 suffers from orographic blockages in its wind direction dominant sector (North-Northeast) and WRF overestimates the wind speed at this site, and station 2, located just 10 km away from station 1, does not suffer from orographic blockages and WRF underestimates the wind speed.

From Fig. 3 it is possible to see that the real topography induces an orographic blockage effect of the wind coming from the Northeast sector in station 1, while WRF's topography completely smooths the terrain and is not able to depict this feature. Therefore, in the mesoscale model the wind coming from the dominant sector is completely free from obstacles and an overestimation of the real wind speed arises. In other words, even though WRF significantly underestimates station 1 height, WRF's less complex and obstacle-free terrain will surpass this effect and induce an overestimation of the wind speed at this station. In opposition, in station 2 is not visible any significant orographic obstacle in the North-Northeast sector and WRF's less complex terrain contributor to the wind speed overestimation is not enough to surpass WRF's underestimation of station 2 height, resulting in the wind speed underestimation by the mesoscale model (typical mountain peak situation).

Moreover, from an analysis of the model errors in all stations versus the terrain complexity, quantified in the form of the RIX factor, there appears to be some correlation between the RIX values and WRF errors. The ruggedness index, or RIX [49], is defined as the percentage fraction of the terrain within a certain distance from a specific site which is steeper than some critical slope, typically considered of 0.3. This index can, therefore, be used as a site-specific measure of the terrain complexity, and can give indication of the effects of local topography and ruggedness on the accuracy of mesoscale near surface wind simulations. Stations located in more complex terrain (high RIX values) have a tendency to show higher errors. This is not wholly surprising, and it is a feature common to almost any type of model, due to their low mesh resolution that cannot properly represent terrain-induced circulations. In other words, RIX values can be seen as crude indications of the terrain oscillations, with the highest values suggesting a poor characterization by the coarse mesoscale grid.

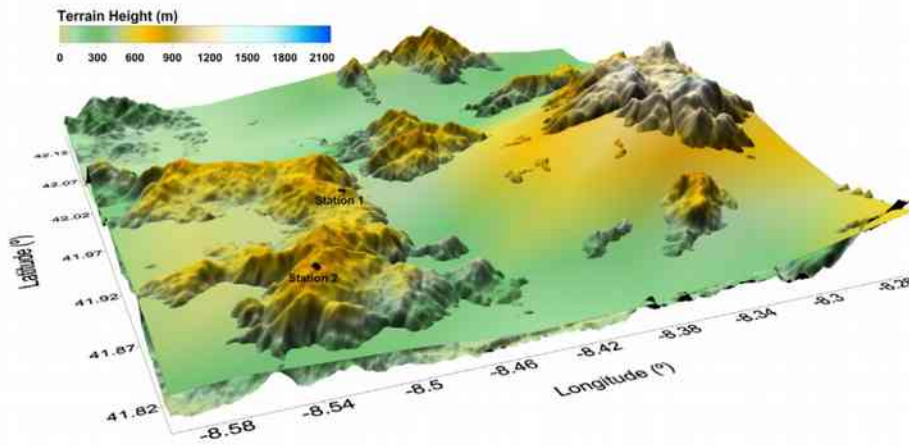


Fig. 3. Overlay of real (SRTM derived) and WRF topography.

3.2. Simulations error dependence on measured wind speed and direction

In this section, the variation of the simulated wind speed and direction error with the observed wind speed and direction is assessed. To this end, the measured wind speed and direction were binned into four categories and the RMSE and Bias computed and analyzed. Table 4 shows the results for the first comparison, in which four measured wind speed bins were considered: wind speeds below 4 m s^{-1} , between 4 and 8 m s^{-1} , between 8 and 12 m s^{-1} and above 12 m s^{-1} . Again, due to the high number of stations used in these comparisons only the weighted average values are presented for each wind speed bin.

According to the weighted average results for all stations, the most striking feature is that all simulations show a better performance in the presence of intermediate wind speeds (between 4 and 12 m s^{-1}) while for weak and strong wind speeds the simulated wind speed errors are higher, with significant higher errors when strong wind speeds are observed (both for the RMSE and Bias). Another remarkable feature is that all simulations tend to overestimate wind speeds below 8 m s^{-1} and underestimate wind speeds above this value. There seems to be a somewhat linear variation of the Bias with the measured wind speed: for low wind speeds the bias tends to be positive and high, gradually diminishing with increasing measured wind speed and for strong wind speeds the biases are now negative and again high in value.

Among the different simulations, the one driven with ERA-Interim shows again the lowest error scores for all the wind speed bins, being the exception the bias for the second and fourth wind speed bins. Table 5 shows the same comparison but now for the simulated wind direction.

Table 5 clearly shows that, for all simulations, the wind direction RMSE rapidly decreases with increasing wind speed. The opposite tendency is seen for the Bias, but for the latter the differences in its scores among the wind speed bins are negligible, when

compared to the RMSE differences among the wind speed bins. This fact is to be expected, since in the presence of low wind speeds the wind direction measurement/simulation is subjected to higher errors. Moreover, from the bias values it is possible to see that the errors in wind direction are mainly on the same side with respect to the real wind vector for intense wind speeds, while for low wind speeds they are distributed more uniformly on both sides. Again, ERA-Interim driven simulation is the one with the best results, with the exceptions of the Bias for wind speeds above 8 m s^{-1} . Table 6 (7) depicts the second comparison, in which the simulated wind speed (direction) error variation with the measured wind direction is assessed. Four wind direction bins were considered: North (angles between 315° and 45°), East (angles between 45° and 135°), South (angles between 135° and 225°) and West (angles between 225° and 315°).

Table 6 shows that the wind speed errors do not show any particular dependence with the measured wind direction. Table 7 shows a remarkable issue: the South sector shows the highest errors when compared to the remaining ones, which is particularly visible in the RMSE scores. This can be related to the fact that in the Atlantic coast of the Iberian Peninsula southerly winds are usually associated to a very unstable atmosphere with a weak synoptic forcing, originating very changeable winds that mesoscale models are not able to accurately detect, mainly due to its limited resolute capacity [50].

3.3. Weibull P.D.F. comparison and AEP estimates

The Weibull P.D.F.'s of the measured and simulated wind data are analyzed and depicted in Fig. 4. Only 2 stations are shown, due to the fact that all the Weibull P.D.F.'s are similar for all the stations. They only differ if the model under or overestimates the wind speed. Therefore, one example of each is shown in Fig. 4 (stations 1 and 2).

Table 4
Simulated wind speed RMSE and Bias per measured wind speed bin averaged for all stations.

Simulation	<4 m s ⁻¹		4–8 m s ⁻¹		8–12 m s ⁻¹		>12 m s ⁻¹	
	RMSE (m s ⁻¹)	Bias (m s ⁻¹)	RMSE (m s ⁻¹)	Bias (m s ⁻¹)	RMSE (m s ⁻¹)	Bias (m s ⁻¹)	RMSE (m s ⁻¹)	Bias (m s ⁻¹)
NCEP-R2	2.72	1.61	2.29	0.52	2.34	-0.27	3.55	-2.07
ERA-Interim	2.12	0.93	2.00	0.41	2.01	-0.03	3.01	-1.77
NCEP-CFSR	2.24	1.07	2.09	0.54	2.07	0.11	3.02	-1.69
NASA-MERRA	2.40	1.26	2.14	0.53	2.08	0.05	3.11	-1.83
NCEP-FNL	2.22	1.01	2.06	0.36	2.06	-0.14	3.12	-1.80
NCEP-GFS	2.13	0.94	2.04	0.35	2.03	-0.08	3.03	-1.76

Table 5
Simulated wind direction RMSE and Bias per measured wind speed bin averaged for all stations.

Simulation	<4 m s ⁻¹		4–8 m s ⁻¹		8–12 m s ⁻¹		>12 m s ⁻¹	
	RMSE (°)	Bias (°)	RMSE (°)	Bias (°)	RMSE (°)	Bias (°)	RMSE (°)	Bias (°)
NCEP-R2	69.03	0.83	37.86	1.21	19.10	-1.09	16.20	-2.68
ERA-Interim	60.02	-0.12	26.72	0.31	14.51	-1.54	13.64	-3.49
NCEP-CFSR	62.28	0.39	27.29	-0.60	15.29	-2.31	14.17	-4.00
NASA-MERRA	65.26	0.71	31.52	-1.17	16.14	-2.71	15.03	-3.76
NCEP-FNL	61.61	0.22	27.75	-0.76	14.88	-1.74	13.71	-3.71
NCEP-GFS	60.65	-1.13	26.95	-2.12	15.09	-2.70	13.88	-4.37

Table 6
Simulated wind speed RMSE and Bias per measured wind direction bin averaged for all stations.

Simulation	North		East		South		West	
	RMSE (m s ⁻¹)	Bias (m s ⁻¹)	RMSE (m s ⁻¹)	Bias (m s ⁻¹)	RMSE (m s ⁻¹)	Bias (m s ⁻¹)	RMSE (m s ⁻¹)	Bias (m s ⁻¹)
NCEP-R2	2.33	0.38	2.78	0.69	2.62	0.26	2.41	0.67
ERA-Interim	1.98	0.28	2.46	0.54	2.10	0.29	1.98	0.32
NCEP-CFSR	2.06	0.42	2.51	0.61	2.26	0.51	2.06	0.43
NASA-MERRA	2.12	0.51	2.60	0.51	2.31	0.34	2.16	0.54
NCEP-FNL	2.01	0.13	2.59	0.53	2.21	0.53	2.02	0.31
NCEP-GFS	1.99	0.19	2.48	0.50	2.20	0.46	2.00	0.24

Table 7
Simulated wind direction RMSE and Bias per measured wind direction bin averaged for all stations.

Simulation	North		East		South		West	
	RMSE (°)	Bias (°)	RMSE (°)	Bias (°)	RMSE (°)	Bias (°)	RMSE (°)	Bias (°)
NCEP-R2	36.35	-1.81	45.59	-3.80	57.55	3.08	41.70	5.68
ERA-Interim	29.50	-0.27	37.82	-3.58	43.87	-0.14	34.33	1.66
NCEP-CFSR	31.19	-1.10	39.97	-4.66	44.80	0.10	34.81	1.54
NASA-MERRA	35.35	-4.21	44.70	-2.98	46.12	4.17	35.28	1.85
NCEP-FNL	32.12	-0.59	40.10	-2.40	41.48	-0.58	34.27	-0.47
NCEP-GFS	30.53	-1.84	39.48	-5.31	42.50	-1.56	34.24	-0.66

Fig. 4 shows that the simulations driven with ERA-Interim, NCEP-FNL and NCEP-GFS are the ones with a Weibull P.D.F. closer to the ones derived from measured data, and this was seen for all stations. This fact was expected, since the simulations driven with these datasets were the ones with the lowest biases scores for the wind speed. Because Weibull P.D.F.'s are merely cumulative and do not take into account the temporal simultaneity of the measured and simulated records, the simulations with lower errors related to the mean state of the wind speed tend to be the best candidate to show the Weibull P.D.F. curve closest to the observed one. The worst P.D.F.'s were obtained with NCEP-R2 reanalysis. In all stations where the simulations overestimated the wind speed (here represented by station 1), it is visible a shifting of the simulated P.D.F.'s to the right side of the wind speed axis (relatively to the observed P.D.F.). This shifting means that low wind speed frequencies are underestimated by the model while strong wind speed frequencies are overestimated by the simulations. This conjugation of the overestimation of strong winds frequencies and the underestimation of low winds frequencies originates the overall wind speed overestimation tendency detected. Oppositely, in the stations where the model underestimated the wind speed (station 2), the model underestimates the frequency of strong wind speeds and overestimates the frequency of intermediate wind speeds.

Table 8 depicts the Weibull P.D.F.'s A and k parameters, most probable wind speed (U_{prob}), mean wind speed (U_m) and wind energy estimates (P_{flux}) estimates percentual deviations when compared to the observed data.

Table 8 shows that NCEP-GFS simulations are the ones with the lowest errors in all the parameters, with the exception of the power flux where NCEP-FNL driven simulation shows the best

estimates. In fact, ERA-Interim, NCEP-FNL and NCEP-GFS driven simulations show very similar results. The worst results are obtained with NCEP-R2 driven simulations, except for the power flux estimates where the simulation driven with NCEP-CFSR reanalysis is the one with the highest deviation. Also visible is that all simulations depict the mean and the most probable wind speed higher than the measured values, in particular for the latter. Due to this fact, the wind energy fluxes estimates deviations show an overestimation of the expected energy output.

From the results shown in this and the previous sections, it becomes clear that the new generation reanalyses (ERA-Interim, NCEP-CFSR and NASA-MERRA) brought significant improvement, providing simulations with overall lower errors when compared to simulations driven with NCEP-R2 reanalysis both in terms of wind speed and direction. This improvement is more pronounced in what is related to wind temporal variability accuracy. This is consistent with the improvement in models, observations, and data assimilation, since more data (observations, satellites and improved microwave sounders) is being included through new data assimilation methods. Among these two new generation reanalyses, it is clear that ERA-Interim is the one with the best performance when compared to measured winds, using the current mesoscale model and configuration. One of ERA-Interim characteristics that can be related to these results is that, in opposition to the other considered reanalyses that make use of three-dimensional variational analyses, the European database includes a four-dimensional variational analysis assimilation method. This feature has been reported as a major advantage, producing better results when compared to the other reanalyses that use three-dimensional variational analysis. Furthermore, the higher errors

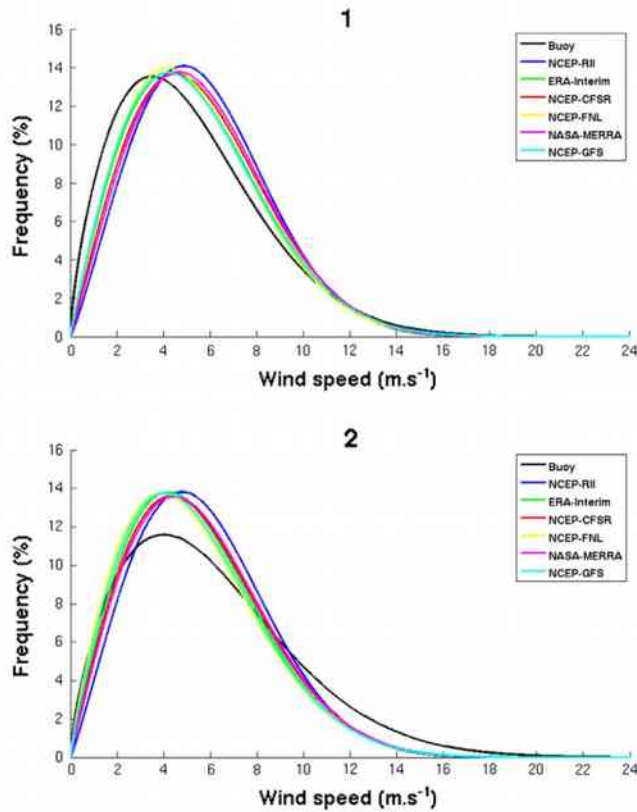


Fig. 4. Weibull P.D.F. curves for stations 1 and 2.

Table 8

Weibull P.D.F.'s parameters, mean and most probable wind speed together with wind energy flux deviations averaged for all stations.

Simulation	A (%)	k (%)	U_m (%)	U_{prob} (%)	P_{flux} (%)
NCEP-R2	7.8	6.1	7.8	13.7	15.9
ERA-Interim	5.3	1.4	5.3	7.4	14.5
NCEP-CFSR	7.5	3.1	7.4	11.0	19.4
NASA-MERRA	7.8	5.1	7.8	12.5	18.2
NCEP-FNL	4.9	1.4	4.8	7.0	14.3
NCEP-GFS	4.8	0.7	4.7	6.6	14.7

of NCEP-R2 driven simulations, particularly visible for the temporal variability errors, are also attributable to the poorer resolution of reanalysis, which will introduce these temporal variability lags when the NCEP-R2 data is interpolated to the model simulation grid points.

The simulations driven with analysis datasets (and particularly the one driven by NCEP-GFS) showed the best results in what concerns wind speed mean state errors (which include the Bias), Weibull wind speed probability distribution and wind energy fluxes estimates accuracy. Even for the other error metrics here employed, they were the simulations with the best results after ERA-Interim driven simulation. This was not expected, since traditionally reanalyses are considered as the best representations of the local meteorological parameters due to the fact that they assimilate a higher amount of observed data. Therefore, it would be expected that the simulations driven with the remaining reanalyses would provide better results than the ones driven by analyses. However, there are some relevant differences between reanalyses and analyses, mainly related to differences in the methodologies and techniques employed in their building processes, that can explain this good performance: the analyses use the most up-to-date operational model (which include the most recent improvements

and updates), observed data assimilation methods and schemes, which might not have been used when the reanalyses were produced. Due to the fact that the reanalyses are an attempt to ensure continuous datasets (that is, changes in the assimilation schemes and/or operational model configuration configurations are slow and conservative in approach to minimize discontinuities which might cause unrealistic time trends), the continuous improvements and updates in the operational model and observed data assimilation schemes are not necessarily included in the reanalyses. Moreover, the spatial resolution of the models used for reanalyses may be different than the underlying model that generates the analyses product (GFS model). Finally, the analyses, while obviously not using as many observations as the reanalyses products, use an assimilation model that runs at much higher resolution than the ones used in the reanalyses. Therefore, if the area under study is rich in terms of operational observational data (as is the present case), the potential added benefit for using reanalyses may not be apparent.

4. Conclusions

This study aimed to evaluate and compare the performance of the WRF mesoscale model near surface wind simulation and wind energy estimates when forced by different initial and boundary conditions. Six datasets were used to drive wind simulations for Portuguese territory, and its results were compared with measured wind data collected from thirteen wind measuring stations scattered along Portuguese mainland. The objective was to determine which one of these forcing datasets produces more accurate wind simulations and wind energy estimates at typical hub height levels. The main conclusions to be drawn from this study can be summarized as follows:

- The new generation reanalyses ERA-Interim, NASA-MERRA and NCEP-CFSR were able to offer improvements and progress in terms of reanalyses, providing simulations with lower errors when compared to simulations driven by NCEP-R2 reanalysis, both in terms of wind speed and direction, but mainly in terms of RMSE, STDE and correlation coefficients (which translate the simulations accuracy in terms of representing the wind temporal variability). The simulations which used ERA-Interim were the ones with the best results, except for the wind speed mean state errors, where the simulations driven by NCEP-FNL and NCEP-GFS analyses yielded the best scores. However, even for these error metrics the simulation driven with ERA-Interim followed very closely the NCEP-FNL and NCEP-GFS performance.
- For the wind speed, all simulations showed better results in simulating intermediate wind speeds (between 4 and 12 m s⁻¹), while for weak and strong wind speeds the model errors are somewhat higher. Moreover, all simulations show a tendency to globally overestimate the wind intensity. This overestimation tendency is a result of smoothing and over-simplification of the terrain characteristics by the mesoscale model. When analyzing this issue per wind speed bin all simulations tend to overestimate wind speeds below 8 m s⁻¹ and underestimate wind speeds above this value. There seems to be a somewhat linear variation of the Bias with the measured wind speed: for low wind speeds the bias tends to be positive and high, gradually diminishing with increasing measured wind speed and for strong wind speeds the biases are now negative and again high in value.
- For the wind direction, NCEP-R2 driven simulations showed a tendency to simulate the wind with a slight clockwise rotation while the remaining simulations showed the opposite, with a tendency to simulate the wind with a slight anti-clockwise

rotation. However, the magnitudes of these rotations are not significant. Furthermore, in the presence of low wind speeds the errors associated to the wind direction are clearly higher, and the errors rapidly decrease when the measured wind speed becomes higher.

- In terms of wind energy estimates, the NCEP-FNL and NCEP-GFS driven simulations were the ones with the wind speed distributions and wind energy fluxes estimates closest to the ones obtained with measured wind data. Although the analyses-driven simulations showed the lowest errors for these metrics, ERA-Interim driven simulation showed results very similar to the ones obtained with NCEP-FNL and NCEP-GFS.

The results presented in this study suggest that the choice of the initial and boundary data supplied to the model constitute a significant error source for the WRF model wind simulation. Due to the continuous progress in the models, measurements and data assimilation used in the reanalyses, the new generation datasets are able to provide a considerable improvement in the mesoscale wind simulation when compared to the older sets. The higher spatial resolutions, amount of measured and observed data assimilated together with the improvements of data assimilation and correction techniques of the new generation reanalyses allow a more accurate and realistic representation of the local wind regime. Based on the analysis and results presented in this work, ERA-Interim reanalysis is the one that likely provides the most realistic initial and boundary data, which will produce wind and wind energy estimates closer to real winds. Although the simulations driven with analyses datasets showed the lowest wind energy estimates errors, ERA-Interim driven simulation showed very similar error values and for the wind temporal variability it was the dataset that clearly provided the best results. Therefore, ERA-Interim should be considered as the best choice in terms of initial and boundary data for mesoscale wind simulations. Nevertheless, the analyses products NCEP-FNL and NCEP-GFS seem to be the best alternatives to ERA-Interim, showing better results than all the other reanalyses datasets here tested.

Acknowledgements

D. Carvalho was supported by the Portuguese Foundation for Science and Technology (F.C.T.) Ph.D grant SFRH/BD/73070/2010. The authors would like to express their gratitude to all the climate and meteorological institutions referred in the text and also to Megajoule S.A. for providing the atmospheric data used in this work.

References

- [1] Global Wind Energy Council. Global Wind Report. Annual market update: 2011. <http://www.gwec.net/fileadmin/documents/NewsDocuments/Annual_report_2011_lowres.pdf>.
- [2] Global Wind Energy Council. Global Wind Energy Report 2010. <http://www.gwec.net/fileadmin/images/Publications/GWEC_annual_market_update_2010_-_2nd_edition_April_2011.pdf>.
- [3] Gallego C, Pinson P, Madsen H, Costa A, Cuerva A. Influence of local wind speed and direction on wind power dynamics – application to offshore very short-term forecasting. *Appl Energy* 2011;88(11):4087–96.
- [4] Ucar A, Balo F. Investigation of wind characteristics and assessment of wind-generation potentiality in Uludağ-Bursa, Turkey. *Appl Energy* 2009;86(3):333–9.
- [5] Carvalho D, Rocha A, Gómez-Gesteira M, Santos C. A sensitivity study of the WRF model in wind simulation for an area of high wind energy. *Environ Modell Softw* 2012;33:23–34.
- [6] Carvalho D, Rocha A, Gómez-Gesteira M. WRF model ocean surface wind simulation forced by different reanalysis: comparison with observed data along the Iberian Peninsula coast. *Ocean Model*. 2012;56:31–42.
- [7] Carvalho D, Rocha A, Silva Santos C, Pereira R. Wind resource modeling in complex terrain using different mesoscale–microscale coupling techniques. *Appl Energy* 2013;108:493–504.
- [8] Foley AM, Leahy PG, Marvuglia A, McKeough EJ. Current methods and advances in forecasting of wind power generation. *Renew Energy* 2012;37(1):1–8.
- [9] Al-Yahyai S, Charabi Y, Gastli A. Review of the use of Numerical Weather Prediction (NWP) Models for wind energy assessment. *Renew Sust Energy Rev* 2010;14(9):3192–8.
- [10] Byrkjedal O, Berge E. The Use of WRF for wind resource mapping in Norway. In: 9th WRF users' workshop; 2008.
- [11] Shimada S, Ohsawa T. Accuracy and characteristics of offshore wind speeds simulated by WRF. *SOLA* 2011;7:21–4.
- [12] Gastion M, Pascal E, Frias L, Marti I, Irigoyen U, Cantero E, et al. Wind resources map of Spain at mesoscale: methodology and validation. In: European wind energy conference (EWEC); 2008.
- [13] Chagas G, Guedes RA, Manso MDO. Estimating wind resource using mesoscale modelling. In: European wind energy conference (EWEC); 2009.
- [14] Trenberth K, et al. Atmospheric reanalyses: a major resource for ocean product development and modeling. Proceedings of OceanObs'09: Sustained Ocean Observations and Information for Society (Vol. 2) 2010, Venice, Italy.
- [15] Kalnay E et al. The NCEP/NCAR 40-year reanalysis project. *Bull Amer Meteor Soc* 1996;77:437–70.
- [16] Uppala SM et al. The ERA-40 re-analysis. *Quart J R Meteorol Soc* 2005;131:2961–3012.
- [17] Onogi K et al. The JRA-25 reanalysis. *J Meteor Soc Jpn* 2007;85:369–432.
- [18] Kanamitsu M et al. NCEP-DOE AMIP-II Reanalysis (R-2). *Bull Amer Meteor Soc* 2002;83:1631–43.
- [19] Simmons A, et al. ERA-Interim: New ECMWF reanalysis products from 1989 onwards. ECMWF Newsletter, No. 110 2007, ECMWF, Reading, United Kingdom, p. 25–35.
- [20] Saha S et al. The NCEP climate forecast system reanalysis. *Bull Amer Meteor Soc* 2010;91:1015–57.
- [21] Rienecker MM et al. MERRA: NASA's modern-era retrospective analysis for research and applications. *J Climate* 2011;24:3624–48.
- [22] Bengtsson L et al. The need for a dynamical climate reanalysis. *Bull Amer Meteor Soc* 2007;88:495–501.
- [23] Dee DP, Uppala S. Variational bias correction of satellite radiance data in the ERA-interim reanalysis. *Quart J R Meteorol Soc* 2009;135:1830–41.
- [24] Dee DP et al. The ERA-Interim reanalysis: configuration and performance of the data assimilation system. *Quart J R Meteorol Soc* 2011;137(656):553–97.
- [25] Rienecker MM, et al. The GEOS-5 Data Assimilation System—Documentation of versions 5.0.1 and 5.1.0. NASA GSFC Tech. Rep. Series on Global Modeling and Data Assimilation, NASA/TM-2007-104606;2008: 27.
- [26] Purser RJ, Wu W-S, Parrish DF, Roberts NM. Numerical aspects of the application of recursive filters to variational statistical analysis. Part I: Spatially homogeneous and isotropic Gaussian covariances. *Mon Wea Rev* 2003;131: 1524–35.
- [27] Purser RJ, Wu W-S, Parrish DF, Roberts NM. Numerical aspects of the application of recursive filters to variational statistical analysis. Part II: Spatially inhomogeneous and anisotropic general covariances. *Mon Wea Rev* 2003;131:1536–48.
- [28] Cullather RI, Bosilovich MG. The moisture budget of the polar atmosphere in MERRA. *J Climate* 2011;24:2861–79.
- [29] Menéndez M, et al. A methodology to evaluate regional-scale offshore wind energy resources. *OCEANS 2011 IEEE*, p. 1–8.
- [30] Hodges KI et al. A comparison of extratropical cyclones in recent reanalyses ERA-Interim, NASA MERRA, NCEP CFSR, and JRA-25. *J Climate* 2011;24:4888–906.
- [31] Bromwich DH et al. An assessment of precipitation changes over Antarctica and the Southern Ocean since 1989 in contemporary global reanalyses. *J Climate* 2011;24:4189–209.
- [32] Bao X, Fuqing Z. Evaluation of NCEP-CFSR, NCEP-NCAR, ERA-Interim, and ERA-40 Reanalysis Datasets against Independent Sounding Observations over the Tibetan Plateau. *J Climate* 2013;26:206–14.
- [33] Tabata Y et al. Lower tropospheric horizontal wind over Indonesia: a comparison of wind profiler network observations with global reanalyses. *J Atmos Sol-Terr Phys* 2011;73(9):986–95.
- [34] Liléo S, Petrik O. Investigation on the use of NCEP/NCAR, MERRA and NCEP/CFSR reanalysis data in wind resource analysis. In: Proceedings of EWEC 2010, Warsaw, Poland.
- [35] Farr TG, Rosen PA, Caro E, Crippen R, Duren R, Hensley S, et al. The shuttle radar topography mission. *Rev. Geophys.* 2007;45(2):1–33.
- [36] Skamarock WC, Klemp JB, Dudhia J, Gill DO, Barker DM, Huang XY et al. A Description of the Advanced Research WRF Version 3. NCAR Technical Note, Mesoscale and Microscale Meteorology Division of NCAR; 2008.
- [37] Borge R et al. A comprehensive sensitivity analysis of the WRF model for air quality applications over the Iberian Peninsula. *Atmos Environ* 2008;42:8560–74.
- [38] Stauffer DR, et al. Use of four-dimensional data assimilation in a limited-area mesoscale model. Part II: effects of data assimilation within the planetary boundary layer. *Mon Wea Rev* 1991;119:734–54.
- [39] Corotis RB, Sigl AB, Klein J. Probability models of wind velocity magnitude and persistence. *Sol Energy* 1978;20:481–93.
- [40] García A, Torres JL, Prieto E, De Francisco A. Fitting wind speed distributions: a case study. *Sol Energy* 1998;62:139–44.
- [41] Gupta BK. Weibull parameters for annual and monthly wind speed distributions for five locations in India. *Sol Energy* 1986;37:469–71.

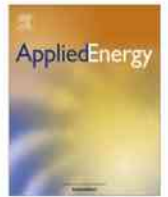
- [42] Hennessey Jr JP. A comparison of the Weibull and Rayleigh distributions for estimating wind power potential. *Wind Eng* 1978;2(3):156–64.
- [43] Justus CG, Hargraves WR, Mikhail A, Graber D. Methods for estimating wind speed frequency distributions. *J Appl Meteorol* 1978;17(3):350–3.
- [44] Rehman S, Halawani TO, Husain T. Weibull parameters for wind speed distribution in Saudi Arabia. *Sol Energy* 1994;53(6):473–9.
- [45] Stevens MJM, Smulders PT. The estimation of the parameters of the Weibull wind speed distribution for wind energy utilization purposes. *Wind Eng* 1979;3(2):132–45.
- [46] Takle ES, Brown JM. Note on the use of Weibull statistics to characterize wind-speed data. *J Appl Meteorol* 1991;30:823–33.
- [47] Mass CF, Ovens D. Fixing WRF high speed wind bias: a new subgrid scale drag parameterization and the role of detailed verification. In: *WRF Users Workshop*; 2011.
- [48] Miglietta MM, Buzzi A. A numerical study of moist stratified flows over isolated topography. *Tellus* 2011;53A:481–99.
- [49] Bowen AJ, Mortensen NG. Exploring the limits of WASP: the wind atlas analysis and application program. In: *Proceedings of the European Union wind energy conference*; 1996. p. 584–7.
- [50] Penabad E et al. Comparative analysis between operational weather prediction models and QuikSCAT wind data near the Galician coast. *J Mar Syst* 2008;72:256–70.

3.2 - Offshore

This article details the research about the testing of which initial and boundary datasets used to force the WRF model produce the most accurate wind power flux, wind speed and direction simulation results for offshore areas.

Until the recent past Portugal did not have any sources of *in situ* offshore measured winds, due to the inexistence of buoys that measure the wind speed and direction moored offshore the Portuguese continental coast. In 2009-2010 three buoys equipped with wind measuring instruments were moored offshore the Portuguese continental coast, one near Leixões harbour and two located in the Nazaré Canyon. However, at the time that this research was performed these buoys did not have one complete year of measurements available (due to several intermittences in their operation) and were not, therefore, considered in this study as sources of *in situ* offshore measured wind data. Due to this lack of offshore measured wind data along the Portuguese continental coast, and as detailed in the article, offshore wind measurements collected by buoys equipped with wind measuring instruments moored offshore the Galician coast and the Gulf of Cádiz (the nearest areas to the Portuguese continental coast) were used as offshore wind measurements. This article is available in the following link:

<http://www.sciencedirect.com/science/article/pii/S0306261914008216>



Offshore wind energy resource simulation forced by different reanalyses: Comparison with observed data in the Iberian Peninsula



D. Carvalho^{a,*}, A. Rocha^a, M. Gómez-Gesteira^b, C. Silva Santos^{c,d}

^a CESAM – Department of Physics, University of Aveiro, Campus Universitário de Santiago, 3810-193 Aveiro, Portugal

^b Grupo de Física de la Atmósfera y del Océano, Facultad de Ciencias, Universidad de Vigo, 32004 Ourense, Spain

^c Instituto Superior de Engenharia do Porto, Rua Dr. António Bernardino de Almeida 341, 4200-072 Porto, Portugal

^d MEGAJOLE Inovação, Rua Eng. Frederico Ulrich 2650, 4470-605 Moreira da Maia, Portugal

HIGHLIGHTS

- Simulated offshore winds were forced by different reanalysis and analysis.
- New generation reanalysis are able to improve offshore wind simulation.
- ERA-Interim driven simulation showed the lowest wind temporal variability errors.
- NCEP-R2 provide the most accurate offshore wind energy production estimates.
- NCEP-FNL and NCEP-GFS can be seen as valid alternatives to traditional reanalyses.

ARTICLE INFO

Article history:

Received 12 February 2014

Received in revised form 30 July 2014

Accepted 4 August 2014

Keywords:

NCEP-R2
ERA-Interim
NCEP-CFSR
NCEP-FNL
GFS
Offshore winds

ABSTRACT

Due to the increasing interest in the prospection of potential sites for the installation of offshore wind farms, it becomes important to extend the tests presented on Carvalho et al. (2014) to offshore areas. For that, the WRF model was used to conduct ocean surface wind simulations forced by different initial and boundary conditions (NCEP-R2, ERA-Interim, NCEP-CFSR, NASA-MERRA, NCEP-FNL and NCEP-GFS) aiming to assess which one of these datasets provides the most accurate ocean surface wind simulation and offshore wind energy estimates. Six near surface wind simulations were performed, each one of them forced by a different initial and boundary dataset. Results were evaluated using data collected at five buoys that measure the wind in the Iberian Peninsula region (Galician coast and Gulf of Cádiz).

The results show that the simulation driven with ERA-Interim reanalysis provided the lowest errors in terms of offshore wind temporal variability. NCEP-R2 driven simulation showed the lowest offshore wind speed bias, mean wind speed and offshore wind energy production estimates. However, it was the one with the highest errors related to the wind temporal variability. The simulations driven with the NCEP-FNL and NCEP-GFS analyses products also showed interesting results, better than the NCEP-CFSR and NASA-MERRA reanalyses.

Based on the results presented in this work and in Carvalho et al. (2014), ERA-Interim reanalysis likely provide the most accurate initial and boundary data to force near-surface wind simulations for the offshore and onshore areas. However, for offshore sites the NCEP-R2 reanalysis seem to provide the most accurate estimation of the potential wind energy production, fact that is of great importance for the wind energy industry. Furthermore, the NCEP-GFS and NCEP-FNL analyses can be considered as valid alternatives to ERA-Interim and NCEP-R2, in particular for cases where reliable forcing data is needed for real-time applications due to their fast availability.

© 2014 Elsevier Ltd. All rights reserved.

1. Introduction

The present study is based on the previous work of [1], in which the performance of the WRF mesoscale model in the wind and potential wind energy production simulation was assessed and evaluated under different initial and boundary forcing conditions:

* Corresponding author. Tel.: +351 234 370 356; fax: +351 234 378 197.

E-mail addresses: david.carvalho@ua.pt (D. Carvalho), alfredo.rocha@ua.pt (A. Rocha), mggesteira@uvigo.es (M. Gómez-Gesteira), cmi@isep.ipp.pt, carlos.santos@megajoule.pt (C. Silva Santos).

Table 1
Main characteristics of the several reanalyses and analyses used to force the WRF model.

Dataset	Type of dataset	Horizontal resolution	Vertical levels	Vintage
NCEP-R2	Reanalysis	2.5° lat/lon	28	1979–Present
ERA-Interim	Reanalysis	0.75° lat/lon	60	1979–Present
NCEP-CFSR	Reanalysis	0.5° lat/lon	64	1979–Present
NASA-MERRA	Reanalysis	0.5° lat – 2/3 lon	72	1979–Present
NCEP-FNL	Analysis	1° lat/lon	52	1999–Present
NCEP-GFS	Analysis	0.5° lat/lon	64	2004–Present

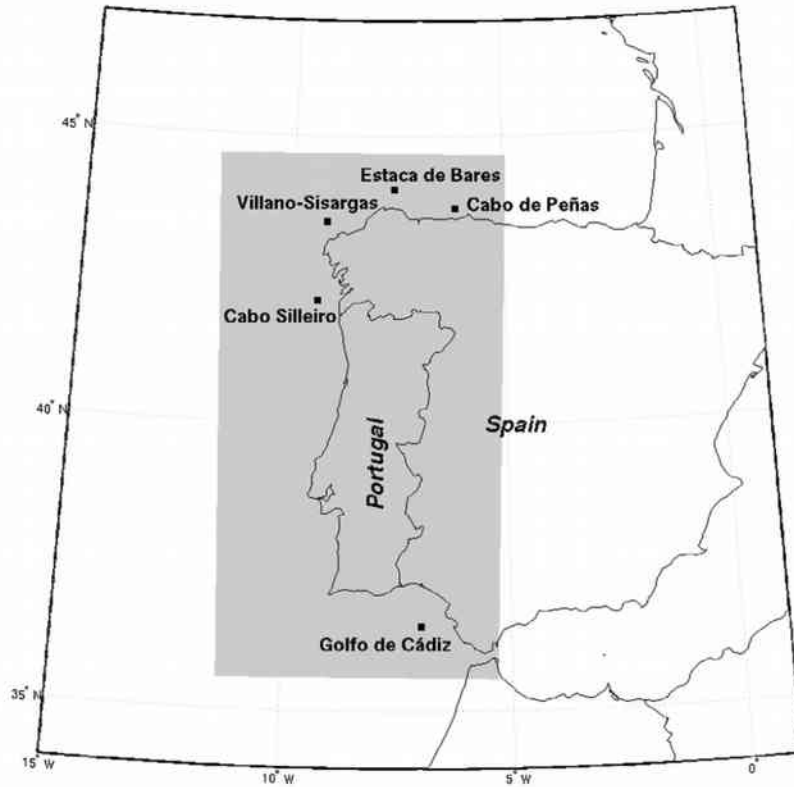


Fig. 1. The study area and the simulation domain with the considered buoys from Puertos del Estado Spanish Agency.

Table 2
Main characteristics of the considered buoys from Puertos del Estado Spanish Agency.

Buoy	Latitude	Longitude	Distance to the coast
Cabo de Peñas	43°45'N	6°9'36"W	~20 km
Estaca de Bares	44°3'54"N	7°37'5"W	~32 km
Villano–Sisargas	43°30'N	9°12'36"W	~30 km
Cabo Silleiro	42°7'48"N	9°23'24"W	~40 km
Golfo de Cádiz	36°28'37"N	6°57'47"W	~55 km

extrapolate their wind data to 10 m a.s.l. Real winds depend on the atmospheric stability, and to extrapolate winds taking into account this atmospheric stability methods such as the Monin–Obukhov theory [33] should be used. To apply this method information about the friction velocity, temperature and surface heat fluxes are necessary. Since this data is not available from the buoys considered in this work, methods that assume a neutrally stable atmosphere (that is, do not consider the atmospheric stability) have to be considered, being a widely used one the method described in [34]. However, this algorithm also requires information that is not collected by the buoys here considered, such as air and sea surface temperatures, pressure and relative humidity. Therefore, in the absence of such data, the logarithmic wind profile expression

(1) will be here used as alternative method to extrapolate the measured winds from 3 to 10 m a.s.l.:

$$U_z = (U_{z_m}) * \ln\left(\frac{z}{z_0}\right) / \ln\left(\frac{z_m}{z_0}\right) \quad (1)$$

U_z refers to the wind speed at a height z , z_m is the measurement height and U_{z_m} is the wind speed at the measurement height. z_0 is the local roughness length, and [35] suggest the value of 1.52×10^{-4} m as a typical one for the ocean surface. Using the logarithmic wind profile, that extrapolates the wind considering an atmosphere with neutral stability, it becomes pertinent to analyze what are the possible differences between the neutrally stable winds obtained from this law and real ones, which depend on the atmospheric stability. Several studies [36–39] focused on these differences between real (stability-dependant) and neutrally stable winds, concluding that these differences are usually low over the global ocean. According to these studies, neutrally stable winds are slightly than real winds (about 0.2 m s^{-1}) in terms of monthly winds, but can reach a maximum of 0.5 m s^{-1} in terms of hourly winds, due to the fact that over most of the global ocean the planetary boundary layer is slightly unstable. Besides this fact, the extrapolation here performed is made for a relatively low height difference (3–10 m) over an ocean surface that typically shows

Table 3
Statistics of the comparison between observed and simulated wind data.

Station	Simulation	RMSE		Bias		STDE		R	
		Speed (m s ⁻¹)	Direction (°)	Speed (m s ⁻¹)	Direction (°)	Speed (m s ⁻¹)	Direction (°)	Speed (-)	Direction (-)
Cabo de Peñas	NCEP-R2	2.53	54.66	0.63	9.65	2.45	53.80	0.76	0.76
	ERA-Interim	2.14	49.95	0.69	7.15	2.03	49.44	0.84	0.81
	NCEP-CFSR	2.27	51.49	0.75	4.53	2.15	51.29	0.83	0.78
	NASA-MERRA	2.39	53.26	0.90	3.00	2.21	53.18	0.81	0.78
	NCEP-FNL	2.24	50.04	0.82	8.14	2.09	49.37	0.83	0.80
	NCEP-GFS	2.24	50.17	0.73	7.11	2.12	49.66	0.83	0.80
Estaca de Bares	NCEP-R2	2.28	39.32	-0.05	3.32	2.28	39.18	0.81	0.86
	ERA-Interim	1.67	30.94	0.25	-2.02	1.65	30.87	0.91	0.89
	NCEP-CFSR	1.70	31.69	0.29	-2.34	1.67	31.61	0.90	0.89
	NASA-MERRA	1.76	34.64	0.16	-1.99	1.75	34.58	0.89	0.83
	NCEP-FNL	1.70	30.72	0.24	-2.02	1.68	30.66	0.90	0.90
	NCEP-GFS	1.73	31.50	0.30	-2.44	1.70	31.41	0.90	0.88
Villano-Sisargas	NCEP-R2	2.31	41.95	0.30	5.01	2.29	41.65	0.82	0.83
	ERA-Interim	1.73	32.67	0.57	2.83	1.64	32.55	0.91	0.91
	NCEP-CFSR	1.84	33.93	0.65	4.14	1.72	33.68	0.90	0.89
	NASA-MERRA	1.90	36.13	0.67	4.28	1.78	35.87	0.89	0.89
	NCEP-FNL	1.79	32.79	0.59	3.66	1.69	32.58	0.90	0.90
	NCEP-GFS	1.80	33.47	0.66	3.67	1.68	33.27	0.91	0.90
Cabo Silleiro	NCEP-R2	2.52	49.97	0.32	4.69	2.50	49.75	0.74	0.69
	ERA-Interim	1.84	41.79	0.49	4.48	1.77	41.55	0.88	0.72
	NCEP-CFSR	1.87	42.95	0.62	5.92	1.76	42.54	0.88	0.70
	NASA-MERRA	1.91	43.17	0.69	2.82	1.79	43.08	0.87	0.75
	NCEP-FNL	1.91	44.80	0.55	5.69	1.83	44.43	0.87	0.69
	NCEP-GFS	1.85	42.67	0.54	5.21	1.77	42.35	0.88	0.71
Golfo de Cádiz	NCEP-R2	2.52	48.62	0.51	7.52	2.46	48.03	0.70	0.77
	ERA-Interim	1.87	39.07	0.41	4.64	1.83	38.79	0.86	0.84
	NCEP-CFSR	2.03	37.73	0.66	6.27	1.92	37.20	0.85	0.85
	NASA-MERRA	2.10	42.08	0.56	0.69	2.03	42.07	0.83	0.70
	NCEP-FNL	1.87	37.48	0.45	4.49	1.81	37.21	0.86	0.86
	NCEP-GFS	1.88	35.94	0.57	4.68	1.79	35.63	0.87	0.86
Weighted mean	NCEP-R2	2.43	46.74	<u>0.34</u>	6.01	2.40	46.33	0.76	0.78
	ERA-Interim	<u>1.85</u>	38.59	0.48	3.41	<u>1.78</u>	38.36	<u>0.88</u>	<u>0.83</u>
	NCEP-CFSR	1.94	39.22	0.60	3.81	1.84	38.91	0.87	<u>0.83</u>
	NASA-MERRA	2.01	41.57	0.59	<u>1.80</u>	1.91	41.47	0.86	0.79
	NCEP-FNL	1.89	38.83	0.53	3.96	1.81	38.53	0.87	<u>0.83</u>
	NCEP-GFS	1.89	<u>38.40</u>	0.56	3.66	1.80	<u>38.12</u>	<u>0.88</u>	<u>0.83</u>

low roughness values. Considering all these factors, it is expected that the difference between measured and extrapolated winds is negligible. Additionally, by considering a whole year of observed data, it can be assumed that the average atmospheric stability will be close to neutral, in particular for onshore areas.

Details about the numerical mesoscale model used in this work (the WRF model), together with a full description regarding the simulations and their configurations can be found in [1]. Also in that work is available a full description of the statistical metrics employed in the simulated wind data evaluation. It is important to highlight that, both in this work and in [1], the computation of the wind power flux was performed considering only the wind speed records comprised between 3.5 and 25 m s⁻¹, in accordance with the typical wind turbines cut-in and cut-off speeds.

3. Results and discussion

3.1. Statistical analysis

In this section, the statistical metrics Root Mean Square Error (RMSE), Bias, Standard Deviation of the Error (STDE) and the correlation coefficients for the wind speed and direction between modelled and observed data are presented in Table 3. The lowest error scores in the weighted mean values are underlined for guidance.

For the wind speed, ERA-Interim driven simulation is the one closest to the measurements in terms of RMSE, STDE and R (NCEP-GFS shows the same correlation coefficient for the wind

speed). The lowest Bias is obtained with NCEP-R2 reanalysis, although this simulation shows the highest RMSE and STDE together with the worst correlation coefficients. For the wind direction, NCEP-GFS driven simulation shows the lowest RMSE and STDE, but closely followed by ERA-Interim driven simulation. The lowest bias for the wind direction is obtained with NASA-MERRA reanalysis. The worse overall results (both for the wind speed and direction) are seen for the NCEP-R2 driven simulation, with the aforementioned exception of the wind speed Bias. Due to its poorer horizontal resolution, when NCEP-R2 data are interpolated to the model simulation grid points some phase lags can be introduced affecting its temporal variability accuracy. In opposition, for the Bias the NCEP-R2 driven simulation was the one with the lowest error scores for the wind speed, but with the highest bias for the wind direction.

The wind speed and direction biases are positive for all simulations, indicating a tendency for the model to overestimate the wind speed and simulate the wind with a slight clockwise wind rotation relative to the measured wind, for all of the considered input data. This overestimation of the wind speed for offshore sites might be explained by the fact the WRF model does not include an ocean model, considering the ocean as a constant flat surface, while the real ocean has higher and variable roughness lengths as a consequence of variations in the ocean surface height (tides, swells, etc.). Therefore, the lower roughness lengths simulated by the model over the ocean will originate higher winds, due to the lower friction between atmosphere and ocean surface.

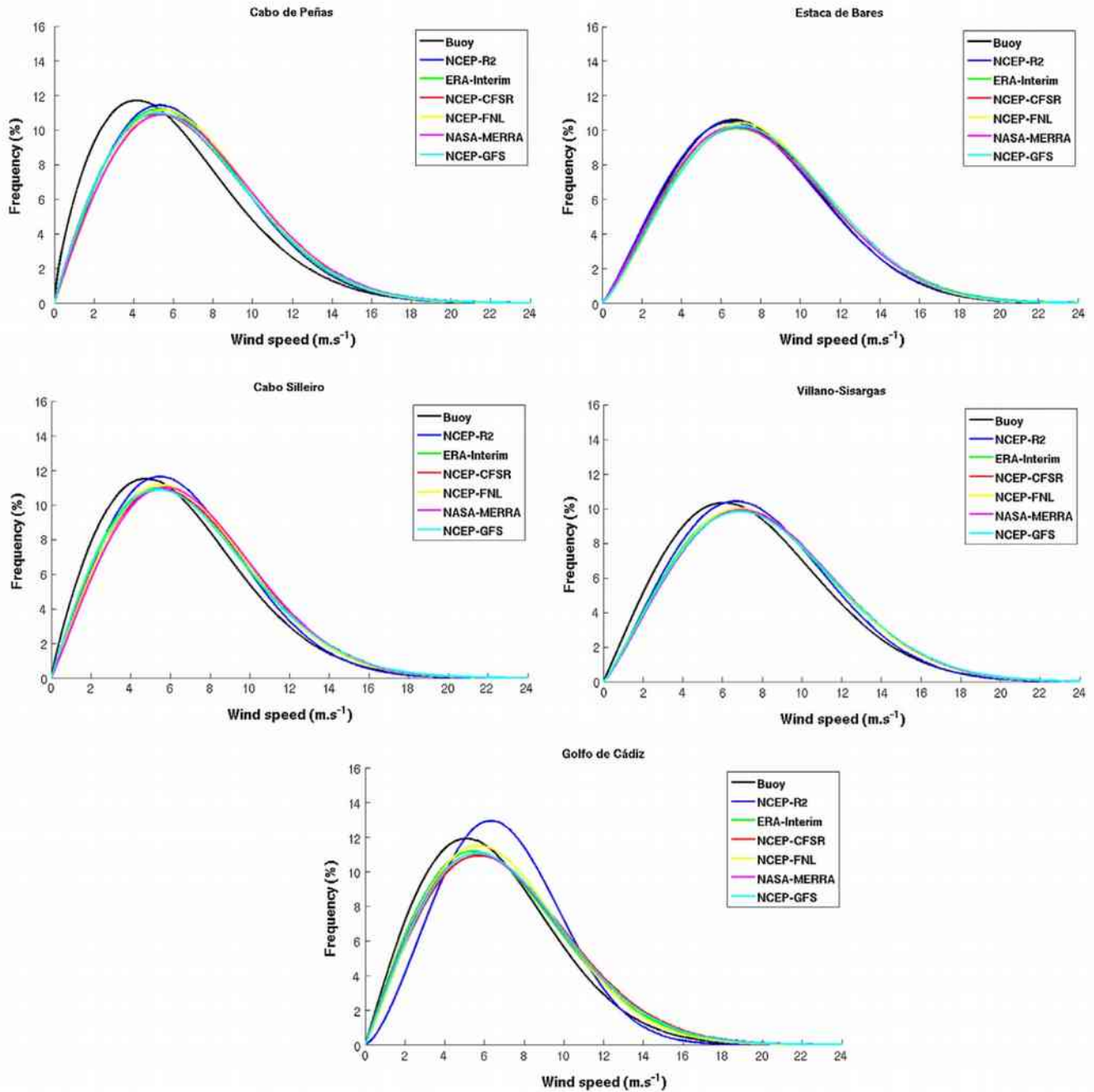


Fig. 2. Weibull distribution PDF curves for all buoys.

The worst results are observed for Cabo de Peñas buoy, mainly in terms of RMSE. The Cape of Peñas is located close to a mountain range with very complex topography, where the model is not able to accurately represent terrain-induced circulations due to its limited resolution. Moreover, this buoy is the one closest to the coast and land-sea circulations might not be properly solved by the model. Following Cabo de Peñas, also Golfo de Cádiz buoy shows higher errors when compared to the remaining sites. Golfo de Cádiz buoy is located in a gulf with very complex coastal topography that favors topography-induced atmospheric flows, making this site more subject to model errors due to its limited resolution. More details regarding these issues can be found in [9].

Comparing these statistical error scores with the ones for onshore sites presented in [1], the model shows slightly lower errors for offshore sites mainly in the wind speed RMSE, STDE

and correlation coefficients both for the wind speed and direction. Since in ocean areas these terrain topography/complexity model limitations are attenuated, the model is able to show lower errors.

3.2. Weibull PDF comparison

In this section, the Weibull PDF's for all the buoys considering simulated and measured winds are depicted in Fig. 2.

According to Fig. 2, there are not significant differences among the several simulated PDF's, with the exception of NCEP-R2. For Villano-Sisargas, Estaca de Bares and Cabo Silleiro buoys, all the simulated PDF's are close to the measured ones, in particular for Bares. For Peñas and Cádiz the results are somewhat worse, in similarity to what was seen in the results presented in Table 1. These simulated PDF's also show the tendency for the model to overestimate the

Table 4
Weibull PDF's parameters, mean and most probable wind speed together with wind energy flux deviations.

Buoy	Simulation	A (m s ⁻¹)	Error (%)	k (-)	Error (%)	U _m (m s ⁻¹)	Error (%)	U _{prob} (m s ⁻¹)	Error (%)	P _{flux} (W s ⁻¹)	Error (%)
Cabo de Peñas	Buoy	6.76	–	1.74	–	6.03	–	4.14	–	404	–
	NCEP-R2	7.51	11.1	2.00	14.7	6.65	10.3	5.31	28.1	427	5.6
	ERA-Interim	7.59	12.2	1.97	13.2	6.71	11.3	5.30	27.9	456	12.9
	NCEP-CFSR	7.65	13.0	1.92	10.1	6.77	12.3	5.21	25.7	482	19.3
	NASA-MERRA	7.82	15.6	1.98	13.5	6.93	14.9	5.48	32.2	488	20.9
	NCEP-FNL	7.73	14.3	2.01	15.5	6.84	13.4	5.50	32.6	460	13.9
Estaca de Bares	NCEP-GFS	7.63	12.8	1.93	10.8	6.75	12.0	5.22	26.1	475	17.5
	Buoy	8.70	–	2.22	–	7.74	–	6.65	–	551	–
	NCEP-R2	8.67	–0.3	2.17	–2.0	7.68	–0.8	6.54	–1.7	554	0.5
	ERA-Interim	9.01	3.5	2.18	–1.9	7.98	3.1	6.80	2.2	624	13.4
	NCEP-CFSR	9.06	4.1	2.23	0.3	8.03	3.7	6.94	4.4	616	11.9
	NASA-MERRA	8.92	2.4	2.17	–2.0	7.90	2.0	6.72	1.1	610	10.8
Villano–Sisargas	NCEP-FNL	9.01	3.5	2.27	2.4	7.97	3.0	6.98	5.0	593	7.6
	NCEP-GFS	9.07	4.2	2.24	1.0	8.03	3.8	6.97	4.8	617	12.1
	Buoy	8.43	–	2.05	–	7.49	–	6.08	–	556	–
	NCEP-R2	8.79	4.3	2.20	7.4	7.78	3.8	6.67	9.8	574	3.4
	ERA-Interim	9.09	7.8	2.15	5.0	8.05	7.5	6.80	11.8	651	17.2
	NCEP-CFSR	9.18	8.9	2.18	6.4	8.14	8.5	6.92	13.9	660	18.8
Cabo Silleiro	NASA-MERRA	9.20	9.1	2.18	6.7	8.16	8.8	6.95	14.4	656	18.1
	NCEP-FNL	9.11	8.1	2.19	6.7	8.08	7.8	6.89	13.4	641	15.4
	NCEP-GFS	9.18	8.9	2.15	5.2	8.15	8.7	6.87	13.1	665	19.7
	Buoy	7.16	–	1.88	–	6.35	–	4.77	–	421	–
	NCEP-R2	7.53	5.2	2.06	10.1	6.66	4.9	5.46	14.5	411	–2.3
	ERA-Interim	7.72	7.8	1.96	4.2	6.84	7.7	5.35	12.2	479	13.8
Golfo de Cádiz	NCEP-CFSR	7.86	9.8	2.00	6.4	6.96	9.6	5.54	16.2	486	15.5
	NASA-MERRA	7.94	10.9	2.06	9.6	7.03	10.7	5.74	20.4	473	12.4
	NCEP-FNL	7.78	8.7	2.04	8.5	6.89	8.5	5.58	17.1	457	8.6
	NCEP-GFS	7.77	8.5	1.96	4.4	6.88	8.3	5.39	13.0	486	15.5
	Buoy	7.21	–	2.00	–	6.39	–	5.10	–	384	–
	NCEP-R2	7.78	7.9	2.49	24.3	6.90	7.9	6.32	24.0	361	–5.9
Weighted mean	ERA-Interim	7.68	6.6	2.00	0.2	6.80	6.4	5.44	6.8	452	17.9
	NCEP-CFSR	7.96	10.4	2.04	2.1	7.05	10.3	5.72	12.3	481	25.5
	NASA-MERRA	7.84	8.7	2.02	1.1	6.94	8.7	5.59	9.7	474	23.4
	NCEP-FNL	7.72	7.2	2.11	5.3	6.83	6.9	5.69	11.6	430	12.0
	NCEP-GFS	7.87	9.1	2.04	2.1	6.96	8.9	5.66	11.0	468	22.0
	NCEP-R2	–	<u>5.7</u>	–	11.9	–	<u>5.5</u>	–	15.6	–	<u>3.6</u>
ERA-Interim	–	7.5	–	4.7	–	7.1	–	11.8	–	15.0	
NCEP-CFSR	–	9.2	–	5.0	–	8.9	–	14.3	–	18.2	
NASA-MERRA	–	9.3	–	6.4	–	8.9	–	15.2	–	17.1	
NCEP-FNL	–	8.2	–	7.5	–	7.8	–	15.5	–	11.5	
NCEP-GFS	–	8.7	–	<u>4.6</u>	–	8.3	–	13.4	–	17.3	

wind speed, due to their shift to the right side of the wind speed axis when compared to the PDF's derived from measured data. This shifting translates a model underestimation (overestimation) of low (strong) wind speed frequencies, which will have as a consequence the detected model wind speed overestimation tendency.

Comparing the several simulations NCEP-R2 driven simulation is the one with the PDF's closest to the measured ones in all sites, with the exception of Golfo de Cádiz where the ERA-Interim provides the best results and clearly NCEP-R2 shows the worst PDF when compared to the measured one. For all sites (except Golfo de Cádiz), the simulations driven with ERA-Interim and NCEP-GFS seem to show PDF's closer to the measured wind speed distributions, after NCEP-R2 driven simulation. These results translate the fact that NCEP-R2 driven simulation was the one with the lowest biases for the wind speed, and since PDF's are purely cumulative they do not take into account the temporal simultaneity of the observed and simulated data, the simulation with lower wind speed biases will most likely be the one with the PDF closest to the measured one [1].

Table 4 shows the Weibull distribution scale (A) and shape (k) parameters, the mean (U_m) and most probable (U_{prob}) wind speed together with the wind energy flux (P_{flux}) estimates percentual deviations when compared to the observed data. The lowest error scores in the weighted mean values are underlined for guidance.

Table 4 shows that NCEP-R2 driven simulation has the lowest errors for the Weibull A parameter, mean wind speed wind power flux estimations. For the most probable wind speed ERA-Interim driven simulation is the one with the lowest weighted mean deviations, and for the Weibull k parameter the simulation driven with NCEP-GFS is the one with the best performance. However, the ERA-Interim driven simulation is the one with the second best performance for all parameters with the exception of the wind power flux, where the simulation driven with NCEP-FNL shows the best performance after the simulation driven with NCEP-R2. Although the good performance of NCEP-R2 driven simulation, it shows the worst results for the most probable wind speed and k parameter. Again it is visible the wind speed overestimation tendency both for the mean but especially for the most probable wind speed, which is also translated in the overestimation of the wind power flux estimations by the model.

Considering the results presented in Table 4, NCEP-R2 reanalysis is able to provide the best wind energy flux estimations, the most relevant factor for wind energy resource assessment studies. However, the results depicted in Table 3 showed that the simulation forced with ERA-Interim is the one with the lowest errors in terms of accurately representing the wind temporal variability (RMSE and STDE). This better accuracy in terms of wind temporal variability is also relevant for other wind energy related aspects,

such as wind turbines installation and preliminary assessment of the variability of wind energy injection in the electrical grid. The latter is a paramount issue for the electrical grid balancing, which must at all times balance the amount of electricity injected in the grid with one being consumed. Since electricity derived from wind farms is very variable in time (due to the inherent temporal variability of the wind), it is important for electrical grid operators to possess a preliminary estimate of the typical local wind temporal variability. Moreover, accurate wind data in terms of temporal variability is a key factor to drive ocean wave energy models, as wind is the main energy source of ocean waves [40,41]. Inaccuracies in the local wind fields can have a strong impact in wave energy modelling results, due to distortions of the model forcing mechanisms.

The results presented in this work show that, in accordance to what was concluded for onshore sites in [1], the new generation reanalyses are able to offer significant improvements in the near-surface wind simulation, providing simulations with lower errors especially in what is related to the wind temporal variability accuracy. ERA-Interim is, among the new generation reanalyses, the one with the best overall performance when compared to measured winds, both for onshore and offshore sites. However, for offshore sites NCEP-R2 provides the simulation with the lowest errors in terms of the mean wind speed (bias, mean wind speed and wind power flux deviations), while for onshore areas the NCEP-FNL and NCEP-GFS showed the lowest errors for these metrics [1]. Combining these results for onshore and offshore sites, it becomes clear that although the new generation reanalyses are able to improve the wind temporal variability simulation, they do not show similar improvement for the wind speed mean state. These higher wind speed biases of the new generation reanalyses can be related to the fact that, although the new variational bias correction techniques applied to the new generation reanalyses allow smoother transitions between different satellites observations, it also produces a potential drift toward the model bias [42], which is poorly assessed in areas with strong data scarcity such as ocean areas [9].

Furthermore, and as seen for onshore sites in [1], the simulations driven with analysis datasets (NCEP-FNL and NCEP-GFS) show lower errors when compared to the other new generation reanalyses (NCEP-CFSR and NASA-MERRA). This can be explained by the fact that, unlike reanalyses products, analyses use the most recent and up-to-date operational model, improvements and updates, together with observed data assimilation methods and schemes [1]. However, for offshore sites the use of these analyses products apparently do not provide such better results (when compared with the use of reanalyses) as for onshore sites because, despite these potential advantages, ocean areas such as the ones under study here are typically characterized by a strong scarcity of measured data, which can favor the use of reanalyses products: most of the measured data in such areas is not directly assimilated into operational models such as the GFS model (in which NCEP-FNL and NCEP-GFS are based), being instead assimilated in a later stage during the construction of reanalyses datasets. Therefore, in areas poorly covered in terms of operational measurements (as is the present case), it is expected that analyses products are not able to show results as good as the ones provided for onshore sites (which are richer in operational measured data), and reanalyses datasets can provide better performances (as seen for ERA-Interim and NCEP-R2, but not the case of NCEP-CFSR and NASA-MERRA).

4. Conclusions

The present work arises as an extension of the previous study of [1], in which the WRF model was forced by different initial and boundary conditions (NCEP-R2, ERA-Interim, NCEP-CFSR and NASA-MERRA reanalyses, and also the NCEP-FNL and NCEP-GFS

analyses) aiming to assess which one of the tested reanalyses datasets provides the most accurate near-surface wind simulations for onshore sites. Due to the fact that offshore areas are characterized by considerably higher wind-derived energy potential production than onshore sites (due to stronger near-surface wind speeds), there has been an increasing interest of the wind power industry in the prospection of potential sites for the installation of offshore wind farms. Therefore, it becomes paramount to analyze which one of these initial and boundary data products offers the most accurate wind simulation also for offshore sites. For this, six reanalyses/analyses products were used to drive ocean near-surface wind simulations and its results compared with measured wind data collected in five buoys located offshore of the Iberian Peninsula (Galician coast and Gulf of Cádiz). The main conclusions can be summarized as follows:

ERA-Interim driven simulation is globally the one closest to the measured winds, with the best performance in terms of the wind temporal variability (RMSE, STDE and R). NCEP-R2 driven simulation was the one with the best performance related to the mean wind speed, showing the lowest bias, mean speed and wind power flux deviations. However, it was the one with the highest errors related to the wind temporal variability.

All the simulations tend to overestimate the wind speed and consequently the available wind power flux, due to the underestimation of low wind speed frequencies and overestimation of strong wind speed occurrences.

The model, in all simulations, showed poorer results for the Cabo de Peñas and Golfo de Cádiz buoys, as a consequence of the complex orography and coastal topography of these locations. These terrain characteristics produce terrain-induced atmospheric flows that are not properly represented by the mesoscale model, due to its limited resolving capacity and low-resolution terrain data.

This work and the previous study [1] constitute a complete and solid analysis and testing on the use of the main reanalyses and analyses datasets in the near-surface wind modelling, both for onshore and offshore sites. Based on the results and findings of these studies, ERA-Interim reanalysis will likely provide the most accurate initial and boundary data to force near-surface wind simulations, both for onshore and offshore sites. Although for offshore sites the NCEP-R2 reanalysis provided the most accurate simulation of the potential wind power flux, fact that is of great importance for the wind energy industry, ERA-Interim reanalysis showed the best accuracy in terms of wind temporal variability, which can be of great importance to other wind energy related issues, such as electrical grid balancing, and also to ocean wave energy applications. Moreover, the NCEP-GFS and NCEP-FNL analyses also showed interesting results, and can be considered as valid alternatives to ERA-Interim and NCEP-R2, in particular for cases where reliable forcing data is needed for real-time applications due to their fast availability.

Acknowledgements

D. Carvalho was supported by the Portuguese Foundation for Science and Technology (F.C.T.) Ph.D. Grant SFRH/BD/73070/2010. The authors would like to express their gratitude to all climate and meteorological institutions that we referred to in the text for providing the atmospheric data used in this work, particularly to Puertos del Estado Spanish Agency for providing the offshore wind measured data used in this study. This work was partially supported by Programa de Consolidación e Estruturação de Unidades de Investigación (Grupos de Referencia Competitiva, Xunta de Galicia) and funded by the European Regional Development Fund (FEDER).

References

- [1] Carvalho D, Rocha A, Gómez-Gesteira M, Silva Santos C. WRF wind simulation and wind energy production estimates forced by different reanalyses: comparison with observed data for Portugal. *Appl Energy* 2014;117:116–26.
- [2] Esteban M, Leary D. Current developments and future prospects of offshore wind and ocean energy. *Appl Energy* 2012;90(1):128–36.
- [3] Gil M, Gomis-Bellmunt O, Sumper A. Technical and economic assessment of offshore wind power plants based on variable frequency operation of clusters with a single power converter. *Appl Energy* 2014;125:218–29.
- [4] Snyder B, Kaiser M. A comparison of offshore wind power development in Europe and the US: patterns and drivers of development. *Appl Energy* 2009;86(10):1845–56.
- [5] Soukissian T. Use of multi-parameter distributions for offshore wind speed modeling: the Johnson SB distribution. *Appl Energy* 2013;111:982–1000.
- [6] Carvalho D, Rocha A, Silva Santos C, Pereira R. Wind resource modeling in complex terrain using different mesoscale-microscale coupling techniques. *Appl Energy* 2013;108:493–504.
- [7] Krajačić G, Duić N, Carvalho MG. How to achieve a 100% RES electricity supply for Portugal? *Appl Energy* 2011;88(2):508–17.
- [8] Carvalho D, Rocha A, Gómez-Gesteira M, Santos C. A sensitivity study of the WRF model in wind simulation for an area of high wind energy. *Environ Modell Softw* 2012;33:23–34.
- [9] Carvalho D, Rocha A, Gómez-Gesteira M. WRF model ocean surface wind simulation forced by different reanalysis: comparison with observed data along the Iberian Peninsula coast. *Ocean Model* 2012;56:31–42.
- [10] Carvalho D, Rocha A, Gómez-Gesteira M, Alvarez I, Silva Santos C. Comparison between CCMP, QuikSCAT and buoy winds along the Iberian Peninsula coast. *Remote Sens Environ* 2013;137:173–83.
- [11] Alvarez I, Gomez-Gesteira M, deCastro M, Carvalho D. Comparison of different wind products and buoy wind data with seasonality and interannual climate variability in the southern Bay of Biscay (2000–2009). *Deep-Sea Res Pt II* (in press).
- [12] Carvalho D, Rocha A, Gómez-Gesteira M, Silva Santos C. Comparison of reanalyzed, analyzed, satellite-retrieved and NWP modelled winds with buoy data along the Iberian Peninsula coast. *Remote Sens Environ* 2014;152:480–92.
- [13] Gallego C, Pinson P, Madsen H, Costa A, Cuerva A. Influence of local wind speed and direction on wind power dynamics – application to offshore very short-term forecasting. *Appl Energy* 2011;88(11):4087–96.
- [14] Berge E, Byrkjedal Ø, Ydersbond Y, Kindler D. Modelling of offshore wind resources. Comparison of a mesoscale model and measurements from FINO 1 and North Sea oil rigs. In: *Proceedings of EWEC 2009*, Marseille, France.
- [15] Jiménez B, Durante F, Lange B, Kreutzer T, Tambke J. Offshore wind resource assessment with WAsP and MM5: comparative study for the German Bight. *Wind Energy* 2007;10(2):121–34.
- [16] Ohsawa T, Hashimoto A, Shimada S, Yoshino J, De Paus T, Heinemann D, Lange B. Evaluation of Offshore Wind Simulations with MM5 in the Japanese and Danish Coastal Waters. In: *Proceedings of EWEC 2007*, Milan, Italy.
- [17] Penabad E, Alvarez I, Balseiro CF, deCastro M, Gomez B, Perez-Munuzuri V, et al. Comparative analysis between operational weather prediction models and QuikSCAT wind data near the Galician coast. *J Marine Syst* 2008;72:256–70.
- [18] Shimada S, Ohsawa T, Yatsu K. A study on the ability of mesoscale model MM5 for offshore wind resource assessment in Japanese coastal waters. In: *European Wind Energy Conference (EWEC) 2009*, Marseille.
- [19] Shimada S, Ohsawa T. Accuracy and characteristics of offshore wind speeds simulated by WRF. *SOLA* 2011;7:21–4.
- [20] Wallcraft AJ, Kara AB, Barron CN, Metzger EJ, Pauley RL, Bourassa MA. Comparisons of monthly mean 10 m wind speeds from satellites and NWP products over the global ocean. *J Geophys Res* 2009;114:16109–14.
- [21] Beaucage P, Glazer A, Choisnard J, Yu W, Bernier M, Benoit R, et al. Wind assessment in a coastal environment using synthetic aperture radar satellite imagery and a numerical weather prediction model. *Can J Remote Sens* 2006;33(5):368–77 (special section on OceanSAR 2006).
- [22] Cassola F, Burlando M. Wind speed and wind energy forecast through Kalman filtering of Numerical Weather Prediction model output. *Appl Energy* 2012;99:154–66.
- [23] Kanamitsu M et al. NCEP-DOE AMIP-II Reanalysis (R-2). *Bull Am Meteor Soc* 2002;83:1631–43.
- [24] Simmons A, et al. ERA-Interim: new ECMWF reanalysis products from 1989 onwards. *ECMWF Newsletter*, No. 110 2007, ECMWF, Reading, United Kingdom, 25–35.
- [25] Rienecker MM et al. MERRA: NASA's Modern-Era retrospective analysis for research and applications. *J Climate* 2011;24:3624–48.
- [26] Saha S et al. The NCEP climate forecast system reanalysis. *Bull Am Meteor Soc* 2010;91:1015–57.
- [27] Menéndez M et al. A methodology to evaluate regional-scale offshore wind energy resources. *OCEANS. IEEE*; 2011. p. 1–8.
- [28] Bao X, Fuqing Z. Evaluation of NCEP-CFSR, NCEP-NCAR, ERA-Interim, and ERA-40 reanalysis datasets against independent sounding observations over the Tibetan plateau. *J Climate* 2013;26:206–14.
- [29] Hodges KI et al. A comparison of extratropical cyclones in recent reanalyses ERA-Interim, NASA MERRA, NCEP CFSR, and JRA-25. *J Climate* 2011;24:4888–906.
- [30] Bromwich DH et al. An assessment of precipitation changes over Antarctica and the Southern Ocean since 1989 in contemporary global reanalyses. *J Climate* 2011;24:4189–209.
- [31] Liléo S, Petrik O. Investigation on the use of NCEP/NCAR, MERRA and NCEP/CFSR reanalysis data in wind resource analysis. In: *Proceedings of EWEC 2010*, Warsaw, Poland.
- [32] Tabata Y et al. Lower tropospheric horizontal wind over Indonesia: a comparison of wind profiler network observations with global reanalyses. *J Atmos Sol-Terr Phys* 2011;73(9):986–95.
- [33] Monin AS, Obukhov AM. Osnovnye zakonomernosti turbulentnogo peremeshivaniya v prizemnom sloye atmosfery (Basic Laws of Turbulent Mixing in the Atmosphere Near the Ground). *Trudy Geofiz Inst* 1954;AN SSSR 24(151):163–87.
- [34] Liu WT, Tang W. Equivalent neutral wind. *JPL Publication* 1996, Jet Propulsion Laboratory, California Institute of Technology, Pasadena, California.
- [35] Peixoto JP, Oort AH. *Physics of climate*. Woodbury (NY): American Institute of Physics; 1992.
- [36] Bourassa MA, Legler DM, O'Brian JJ, Smith SR. SeaWinds validation with research vessels. *J Geophys Res* 2003;108(3019):16.
- [37] Chelton DB, Freilich MH. Scatterometer-based assessment of 10-m wind analyses from the operational ECMWF and NCEP numerical weather prediction models. *Mon Weather Rev* 2005;133:409–29.
- [38] Kara AB, Wallcraft AJ, Bourassa MA. Air-sea stability effects on the 10 m winds over the global ocean: evaluations of air-sea flux algorithms. *J Geophys Res* 2008;113:4009–14.
- [39] Mears CA, Smith DK, Wentz FJ. Comparison of special sensor microwave imager and buoy-measured wind speeds from 1987 to 1997. *J Geophys Res* 2001;106(11):719–29.
- [40] Liu H, Xie L, Pietrafesa LJ, Bao S. Sensitivity of wind waves to hurricane wind characteristics. *Ocean Model* 2007;18(1):37–52.
- [41] Xu F, Perrie W, Toulany B, Smith PC. Wind-generated waves in Hurricane Juan. *Ocean Model* 2007;16(3–4):188–205.
- [42] Dee DP, Uppala S. Variational bias correction of satellite radiance data in the ERA-interim reanalysis. *Quart J Roy Meteorol Soc* 2009;135:1830–41.

Chapter 4 – Optimisation of the NWP model wind simulation: testing of PBL parameterizations options

This chapter focuses on the optimisation of the WRF model regarding which PBL physical parameterization schemes options provide wind power flux, wind speed and direction simulations closest to measured wind data, both for offshore and onshore areas. This chapter describes this research through one published research article, in which is detailed the methodology followed, state of the art area under study, parameterizations tested and observed data used to compare the several simulations. This article is available in the link:

<http://www.sciencedirect.com/science/article/pii/S0306261914008939>



Sensitivity of the WRF model wind simulation and wind energy production estimates to planetary boundary layer parameterizations for onshore and offshore areas in the Iberian Peninsula



D. Carvalho^{a,*}, A. Rocha^a, M. Gómez-Gesteira^b, C. Silva Santos^{c,d}

^a CESAM – Department of Physics, University of Aveiro, Campus Universitário de Santiago, 3810-193 Aveiro, Portugal

^b Ephyslab, Facultad de Ciencias, Universidad de Vigo, 32004 Ourense, Spain

^c CIDEM – Instituto Superior de Engenharia do Porto, Rua Dr. António Bernardino de Almeida 341, 4200-072 Porto, Portugal

^d MEGAJOULE Inovação, Rua Eng. Frederico Ulrich 2650, 4470-605 Moreira da Maia, Portugal

HIGHLIGHTS

- WRF model near surface wind simulation sensitivity to different PBL and SL parameterizations was assessed.
- Simulations were evaluated using onshore and offshore measured data in the Iberian Peninsula.
- ACM2-PX PBL–SL schemes provided the best overall results in terms of wind and wind energy flux simulation.
- QNSE–QNSE PBL–SL schemes presented the best energy flux estimates for offshore areas.
- This study provides valuable guidelines for future offshore and onshore wind energy assessment applications.

ARTICLE INFO

Article history:

Received 13 February 2014

Received in revised form 8 July 2014

Accepted 20 August 2014

Keywords:

WRF
Planetary boundary layer
Parameterizations
Wind energy
Offshore
Onshore

ABSTRACT

This work aims to assess the Weather and Research Forecasting (WRF) model wind simulation and wind energy production estimates sensitivity to different planetary boundary layer parameterization schemes. Five WRF simulations considering different sets of planetary boundary layer (PBL) and surface layer (SL) parameterization schemes were performed, and their results compared to measured wind data collected at five offshore buoys and thirteen onshore wind measuring stations located in the Iberian Peninsula. The objective is to determine which of these model configurations produces wind simulations and wind energy productions estimates closest to measured wind data and wind energy production estimates derived from measurements, aiming to provide guidelines for onshore and offshore wind energy assessment studies focused on areas where measured wind data is not available and numerical modelling is necessary. This work focuses on the Iberian Peninsula, an area with intensive wind energy penetration due to its favourable wind conditions, which combined with its large coastline makes this area a promising one for the future installation of offshore wind farms.

The results presented in this work show that, although no major differences are seen among the simulations in terms of wind speed and direction simulation accuracy, in terms of wind energy production estimates the differences are not negligible due to the high sensitivity of the wind energy production to the wind simulation accuracy. The PBL–SL parameterization set composed by the schemes ACM2-PX is the one with the lowest errors when compared to observed wind data, when considering all onshore and offshore sites together. The ACM2 PBL scheme combines features of local and non-local closure schemes and the PX LSM scheme provides a better parameterization of the surface meteorology, which proved to be important in the model performance. However, for offshore sites the PBL–SL parameterizations QNSE–QNSE produced the best wind energy production estimates.

Due to the close dependence of each PBL and SL scheme performance on the surrounding synoptic conditions and atmospheric stability, it is expected that for different geographical areas and/or temporal

* Corresponding author. Tel.: +351 234 370 356; fax: +351 234 378197.

E-mail addresses: david.carvalho@ua.pt (D. Carvalho), alfredo.rocha@ua.pt (A. Rocha), mgesteira@uvigo.es (M. Gómez-Gesteira), cmi@isep.ipp.pt, carlos.santos@megajoule.pt (C. Silva Santos).

periods these schemes may show different results. However, the fact that this study includes one complete year of simulation for a considerably wide geographical area, including the different synoptic conditions that typically occur in a annual cycle, provides a solid base of confidence that the conclusions drawn from this work may be applied to other periods and/or geographical areas.

© 2014 Elsevier Ltd. All rights reserved.

1. Introduction

The traditional energy sources based on fossil fuels are becoming scarce, economically and environmentally unsustainable [1,2]. Therefore, it is paramount to find valid renewable and environmentally-friendly alternatives to fossil fuels-based energy sources. This need has been increasingly recognized in public, political and economic frameworks, making the European Union a good example of the support and application of target-binding agreements and directives [3]. Wind-derived energy has been widely recognized as one of the most technologically mature and economically competitive renewable energy source, with a fast worldwide growing in terms of installed generating power in the last decades [4–10] and being presently one of the main electricity suppliers in European countries. In terms of installed onshore wind generating power, Portugal has been one of the leading countries: in 2012, Portugal ranked in 10th worldwide and 5th among European countries in terms of total installed capacity [11], and in the same year was able to achieve an 20% penetration of wind-derived energy in the total annual electricity consumption, surpassed only by Denmark in this parameter [12]. The Iberian Peninsula is presently one of the areas with the highest percentage of installed onshore wind power per capita worldwide due to its favourable wind conditions, making this area a promising one for the future installation of offshore wind farms due to its large coastal line and interesting wind energetic potential.

The global intensive growth of installed wind power witnessed in the last decade and the future expansion of the wind energy markets has increased the need to correctly identify the remaining most promising sites for wind energy exploitation [13]. Despite this quick proliferation of wind energy exploitation, the lack of reliable measured wind data in many areas of the world, especially in developing countries, is still hampering the development of new wind energy projects [14]: the potential wind energy resource of one area is typically assessed and quantified making use of wind measurements collected within that area, and to assess the wind resource of the area at least one year of wind measurements needs to be performed, to realistically characterize the local wind climatology. For onshore areas there is a considerable amount of measured wind data available, but the costs involved in the planning, installation and maintenance of wind measuring masts are considerably high and if the locally acquired wind data shows a low wind energetic potential of the area under consideration, a considerable amount of investment and time is irreversibly lost. For offshore areas the scenario is significantly worse, with a strong lack of measured wind data due to the fact that the costs and technological challenges involved in installing wind measurement masts are exponentially higher when compared to the onshore case. As a consequence, ocean wind data is traditionally obtained through buoys deployed on ocean areas, satellites, onboard ships and vessels. However, measured wind data from buoys and ships is normally collected inside a limited spatial and time window, while wind observations taken by satellites typically suffer from large amounts of missing/poor quality data and low spatial/temporal resolutions [15,16].

Considering these needs and limitations of measured wind data, reliable alternative sources of wind data specifically aimed to

assess the wind resource of a given area are currently a very valuable product. Numerical weather prediction (NWP) models, capable of derive high resolution wind data, are one of the most used alternative sources of wind data [17]. Despite the promising results obtained until now with NWP models, the modelling of the near-surface winds is still a major challenge to atmospheric researchers, mainly due to the strong interaction between these low-altitude atmospheric flows and the local topography. This interaction, which influences the flow circulation patterns particularly for near-surface winds, is described by the atmospheric planetary boundary layer (PBL) theory. Offshore winds, in particular coastal ones, normally present added difficulties for their modelling when compared to typical open sea and onshore winds due to the fact that they are strongly influenced by the local topography, discontinuities between land and sea roughness and by thermal gradients resulting from land-sea temperature differences.

Since both onshore and offshore wind energy are derived from near surface flows, the modelling results will strongly depend upon the ability of the NWP model to correctly represent and simulate the PBL processes. Usually the majority of these occur at spatial scales smaller than the model grid resolution, making them sub-grid processes (thus, unresolved explicitly by the model) that require an implicit treatment. This is done using physical parameterization schemes, which use physical assumptions and empirical approximations to represent these processes. The NWP mesoscale model used in this work is the WRF model (version 3.4.1), an extensively-used state-of-the-art NWP model. A detailed description of this model can be found in Skamarock et al. [18]. In this work, we focus on the PBL and surface layer (SL) parameterization schemes. These parameterizations are used to represent the heat, momentum and moisture transfers between the atmosphere and the surface and are closely interconnected, interacting non-linearly with each other and also with the dynamical core of the model. Therefore, identifying the best set of parameterization options becomes highly complex due to high-dimensional, multi-modal and mostly non-linear interactions that can occur [19]. Given this, in order to assess which is the best physical parameterization set to be used for a given model in a given area, a careful determination of the most appropriate model configuration is necessary by comparative evaluation of all the available options.

In the published literature, several studies can be found that assess the sensitivity of the WRF model to the use of different physical parameterization schemes in the near-surface winds simulation for different locations and time periods [20–28]. However, the performance of these physical parameterization schemes is highly dependent on the geographical area and time period under analysis, given that the results can be very different if the simulation is focused on a summer/winter period or on a specific meteorological episode due to the different atmospheric stability and synoptic conditions. Since this work is focused on a full-year period (covering a complete meteorological/weather annual cycle), findings drawn from those studies do not apply here. As far as the authors are aware, no study was found that analyzes WRF wind simulation sensitivity to the choice of PBL parameterizations schemes for the geographical area here considered that spans through at least one complete year. However, it is worth mentioning studies that tested the use of different PBL schemes considering

a complete year of simulation, although for different geographical areas: Menéndez et al. [29] assessed the WRF model sensitivity to the choice of several PBL and SL parameterizations schemes (ACM2-PX, YSU-MM5, MYJ-ETA, see Section 2.2 for the parameterization schemes naming conventions) for offshore wind simulation considering a complete year over the Mediterranean basin concluding that the YSU-MM5 schemes showed better results. Krogsaeter et al. [30] tested a broad range of PBL and SL physical parameterization schemes (ACM2-PX, YSU-MM5, MYJ-ETA, QNSE-QNSE, MYNN-2.5-MYNN) over a one-year simulation of offshore winds in the Southern North Sea, concluding that the best performances were provided by the MYJ-ETA and MYNN-2.5-MYNN schemes, and the worst results from the YSU-MM5 schemes. From these studies it is clear the performance of the parameterization schemes can vary from one site to another. Therefore, the best combination of physical parameterization schemes for one region may not necessarily be directly generalized to another. Thus, it becomes important to perform these sensitivity tests for the areas under study.

The aim of this paper, which builds on the previous studies of Carvalho et al. [31–33], is to compare the performance of the WRF model under the use of different physical parameterization sets related to atmospheric boundary layer processes, assessing which provides the most accurate simulation of offshore and onshore wind speed, direction and power flux density. This study can provide important information and guidelines for future onshore/offshore wind energy assessment studies focused on areas where measured wind data is not available (or is insufficient for the desired purposes) and NWP modelling is, therefore, unavoidable. This work focuses on the Iberian Peninsula, an area with intensive wind energy penetration due to its favourable wind conditions, which combined with its large coastline makes this area a promising one for the future installation of offshore wind farms.

2. Methodology and data

2.1. Measured wind data

Wind measurements collected at thirteen wind measuring stations distributed throughout the Portuguese territory, and offshore wind data collected by five buoys moored off the northern and western coasts of Galicia and the Gulf of Cádiz were used to evaluate the model simulations. The buoys are operated and maintained by the Spanish Agency Puertos del Estado, and their locations are depicted in Fig. 1. As for the onshore stations, they are mainly concentrated in four areas where several wind farms are currently in operation or planned to be built in the near future. All the wind measurements were performed before any wind farm was installed, being free from wake effects caused by nearby wind turbines in operation. The locations of the onshore stations are also depicted in Fig. 1, together with the terrain height extracted from the Shuttle Radar Topography Mission (SRTM) database [34]. Table 1 shows a brief description of each onshore and offshore site: name, terrain height, measurement height above ground level (a.g.l.) or above mean sea level (a.s.l.), distance to coast (for the offshore sites) and difference between the site real height a.g.l. and the site height a.g.l. in the WRF model simulation grid. This work uses data collected between January 1st and December 31st 2008.

Ocean surface wind is typically referred to 10 m above sea level (a.s.l.), and considering the fact that the buoys measure the wind at 3 m a.s.l., winds were extrapolated to 10 m a.s.l. Real winds are dependent on the surrounding atmospheric stability and, in order to perform a wind extrapolation that takes into account the atmospheric stability, methods like the Monin-Obukhov theory [35] should be applied. These methods require information regarding

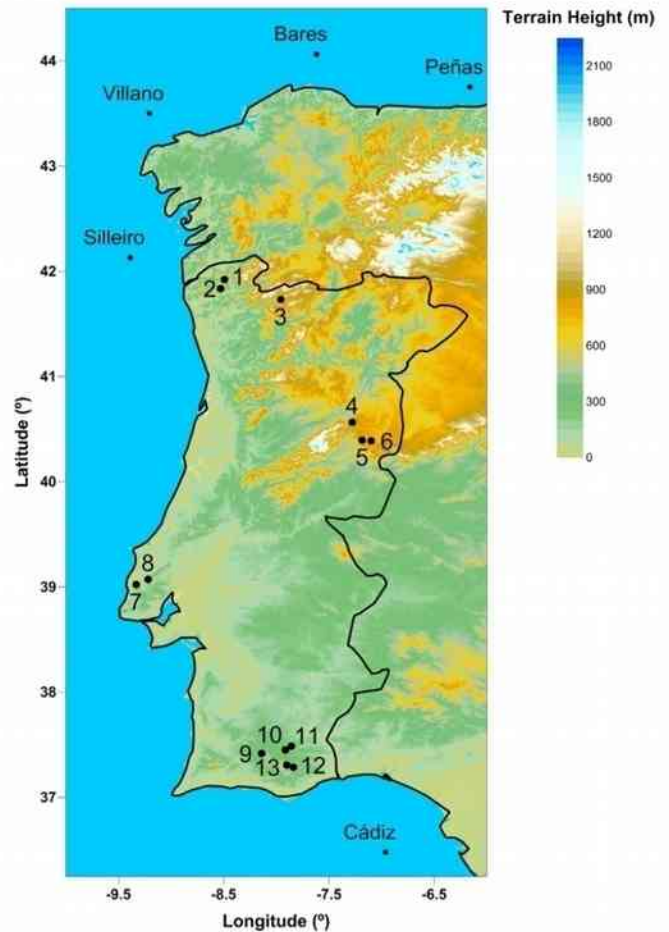


Fig. 1. Onshore and offshore sites.

the friction velocity, temperature and surface heat fluxes, which are not available for the buoys considered in this work. Therefore alternative methods, which do not take into account the atmospheric stability and assume a neutrally stable atmosphere, have to be considered. However, some of these alternative methods also require additional data such as air and sea surface temperatures, pressure and relative humidity (like the method described in Liu and Tang [36]) that are also unavailable for the buoys used here. In the absence of such data, the logarithmic wind profile expression (1) will be here employed to extrapolate the winds from 3 to 10 m a.s.l.:

$$U_z = (U_{z_m}) * \ln\left(\frac{z}{z_0}\right) / \ln\left(\frac{z_m}{z_0}\right) \quad (1)$$

This method assumes a neutrally stable atmosphere, where U_z is the wind speed at a height z , z_m is the measurement height, U_{z_m} is the wind speed at the measurement height and z_0 is the roughness length. A typical z_0 for the ocean surface can be assumed of 1.5×10^{-4} m [37]. Several authors [38–41] made detailed analyses on the differences between stability-dependant and equivalent neutral winds and concluded that differences between winds that assume a neutrally stable atmosphere and the real winds (stability-dependent) are typically low over the global ocean (in maximum 0.5 ms^{-1}). Moreover, the fact that this extrapolation is carried out for a relatively small difference of heights (from 3 to 10 m) over a surface with low roughness values, suggests that the difference between measured and extrapolated winds is negligible. Additionally, since this analysis covers a whole year of measurements it is expected that the average atmospheric stability will

Table 1
Information regarding the considered onshore and offshore sites.

Buoy	Height a.s.l. (m)	Measurement height (m)	Distance to coast
<i>Offshore sites</i>			
Peñas	0	3 (extrapolated to 10 m)	~20 km
Villano	0	3 (extrapolated to 10 m)	~30 km
Bares	0	3 (extrapolated to 10 m)	~32 km
Silleiro	0	3 (extrapolated to 10 m)	~40 km
Cádiz	0	3 (extrapolated to 10 m)	~55 km
Station	Height a.g.l. (m)	Measurement height (m)	Difference between real and WRF grid height (%)
<i>Onshore sites</i>			
1	676	60	-33
2	818	60	-56
3	1072	61	-23
4	979	60	-19
5	876	61	-9
6	876	61	-10
7	174	61	-55
8	162	60	-25
9	451	81	-12
10	325	82	-10
11	315	82	-16
12	501	61	-19
13	476	61	-16

be close to a neutral regime. However, and specifically for offshore wind energy applications, these measurements should be collected at typical hub heights (80–120 m a.s.l.) to avoid large extrapolations (from 3–10 to 80–120 m a.s.l.) and consequent introduction of non-negligible error sources in the measured data.

2.2. Model and simulations design

The WRF model contains several alternative schemes for the PBL processes parameterization. Although SL and PBL parameterizations schemes are treated separately by the model, they strongly interact with each other. Therefore, the choice of a given PBL parameterization scheme will determine the choice of the SL parameterization scheme [18]. 5 different combinations of PBL–SL schemes were tested, considering these restrictions and also avoiding the use of old, obsolete options, new schemes still at an experimental stage, and schemes specifically designed for particular applications (such as for large eddy simulations and urban canopy models).

The physical configuration of each simulation, summarized in Table 2, considered the following sets of PBL–SL parameterization schemes: the Yonsei University (YSU) PBL scheme [42] combined with the MM5 SL similarity scheme [43]; the Mellor–Yamada–Janjic (MYJ) PBL scheme [44] with the ETA SL similarity scheme [45]; the Asymmetric Convective Model version 2 (ACM2) PBL scheme [46,47] with the Pleim–Xiu (PX) SL scheme [48]; the Quasi-Normal Scale Elimination (QNSE) PBL scheme [49] in combination with the QNSE SL scheme [49,50] and the Mellor–Yamada Nakanishi and Niino level 2.5 (MYNN-2.5) PBL scheme [51] together with the Mellor–Yamada Nakanishi and Niino (MYNN) SL scheme [51,52]. As for

Table 2
Physical configuration of the simulations.

Simulation	YMN	MEN	APP	QQN	MMN
SL	MM5	ETA	PX	QNSE	MYNN
PBL	YSU	MYJ	ACM2	QNSE	MYNN-2.5
LSM	Noah		PX	Noah	
Long-wave radiation			RRTM		
Short-wave radiation			Dudhia		
Cumulus			Kain-Fritsch		
Microphysics			WSM6		

the remaining physical parameterizations, they were selected and used for all simulations as follows: the WRF Single-Moment 6-Class (WSM6) for the microphysics [53], the RRTM scheme for the long-wave radiation [54], the Dudhia parameterization for the short-wave radiation [55], the Kain-Fritsch scheme [56] for cumulus parameterization and the Noah LSM scheme [57]. The exception is when the PX SL together with the ACM2 PBL schemes are chosen: in this case, the PX LSM scheme [58] must be used.

The initial and boundary conditions data were selected according to the findings of Carvalho et al. [31–33], which tested the use of several reanalysis and analysis datasets in the simulation of near surface winds for the same areas under scope in this study and concluded that ERA-Interim reanalysis provide the best initial and boundary conditions for these sites. The innermost simulation domain (Fig. 2, darker grey) has a horizontal resolution of 5 km and the largest domain (Fig. 2, lighter grey) has a horizontal resolution of 25 km. 27 vertical levels were used in all domains.

Simulated wind time series for all sites, extracted at the same locations and measuring heights, were obtained by performing a horizontal and vertical bi-linear interpolation between the closest simulation grid points (of the 5 km resolution domain) to the wind measuring sites location.

2.3. Statistical metrics

The statistical metrics used to evaluate the simulations were the Root Mean Squared Error (RMSE), the bias, Standard Deviation of the Error (STDE) and the correlation coefficients (R^2) for the wind speed and direction.

Weibull probability density functions (PDFs) were used to characterize the local wind regimes (in terms of the wind speed distributions) and to assess which parameterization set produces Weibull PDFs closest to the ones derived from measured wind speed. The Weibull distribution has been extensively used to describe wind speed distributions, in particular for wind energy applications, due to its accurate fit to wind speed data. The mean and most probable wind speed, derived from the Weibull PDF, were also used as comparative metrics.

The wind power flux was computed for all sites using observed and simulated wind speeds. The power flux was calculated considering only wind speeds between 3.5 and 25 ms^{-1} , the typical wind turbines cut-in and cut-off speeds.

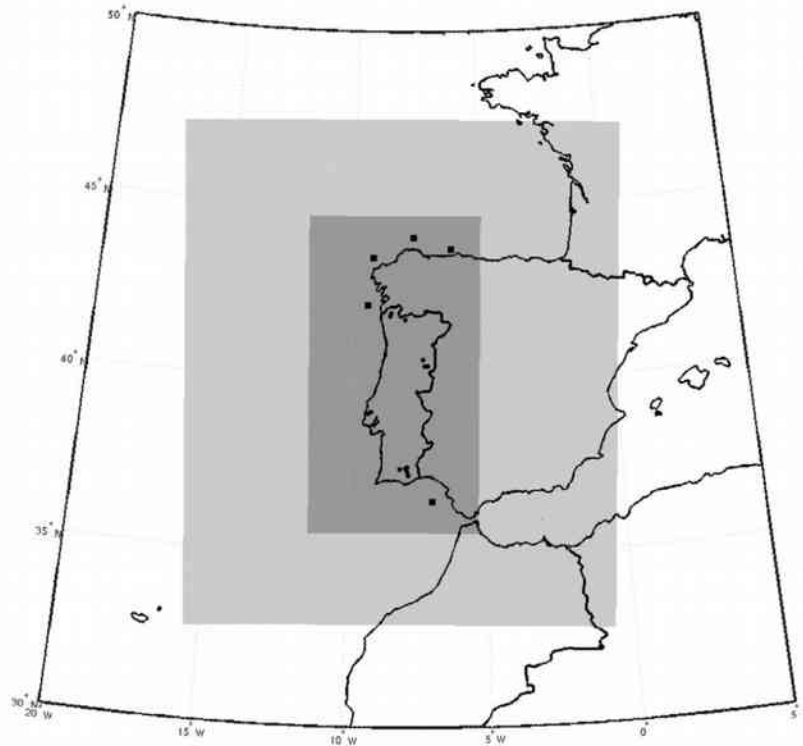


Fig. 2. Simulation domains.

3. Results and discussion

3.1. Statistical analysis

The RMSE, Bias, STDE and R between the measured and simulated wind data are presented in Table 3, considering the number of simultaneous and valid pairs of records between the simulations and the respective station. Due to the high number of stations, it was decided to divide Table 3 in three different sections: the weighted mean values (the mean for all sites weighted by the respective number of data records) for each statistical metric for the offshore sites; the weighted mean values for each statistical metric for the onshore sites; and finally the weighted mean values for each statistical metric considering all the sites together. In each one of these sections, the lower error scores for each statistical

error metric are highlighted in bold (for the offshore and onshore sections) and underlined (in the global weighted mean values), for a better interpretation.

Taking the weighted mean results considering both offshore and onshore sites (last section), simulation APP clearly appears as the one with the overall best performance. For the wind speed it shows the lowest RMSE, Bias and STDE, together with the highest correlation coefficients. For the wind direction simulation APP again shows the lowest Bias, although for the RMSE and STDE simulation YMN is the one with the best results but closely followed by simulation APP. For all simulations the weighted mean values of the wind speed bias are positive, indicating a tendency of the model to overestimate the wind speed.

Looking in more detail to the offshore group, in terms of the wind speed and direction, simulation APP is the one with the

Table 3
Statistics of the comparison between observed and simulated wind data.

Area	Simulation	RMSE		Bias		STDE		R	
		Speed (ms^{-1})	Direction ($^{\circ}$)	Speed (ms^{-1})	Direction ($^{\circ}$)	Speed (ms^{-1})	Direction ($^{\circ}$)	Speed (ms^{-1})	Direction ($^{\circ}$)
Offshore	YMN	1.85	38.59	0.48	3.41	1.78	38.36	0.88	0.83
	MEN	1.86	38.56	0.41	1.94	1.81	38.44	0.88	0.83
	APP	1.83	38.07	0.46	2.31	1.76	37.93	0.88	0.84
	QQN	1.86	38.19	0.35	1.81	1.82	38.01	0.87	0.83
	MMN	1.91	39.09	0.57	4.08	1.82	38.81	0.87	0.83
Onshore	YMN	2.10	35.02	0.34	-0.35	2.02	34.87	0.79	0.78
	MEN	2.03	35.55	0.11	-0.77	1.96	35.43	0.79	0.77
	APP	1.91	35.72	-0.17	-2.53	1.88	35.48	0.80	0.78
	QQN	2.19	37.68	0.26	-0.07	2.10	37.56	0.75	0.72
	MMN	2.02	35.53	0.18	0.03	1.96	35.39	0.79	0.77
All sites	YMN	1.97	36.81	0.41	1.53	1.90	36.61	0.83	0.81
	MEN	1.94	37.06	0.26	0.59	1.88	36.94	0.83	0.80
	APP	1.87	36.89	0.14	-0.11	1.82	36.71	0.84	0.81
	QQN	2.03	37.93	0.31	0.87	1.96	37.79	0.81	0.78
	MMN	1.97	37.31	0.38	2.05	1.89	37.10	0.83	0.80

highest R, lowest RMSE and STDE, while simulation QQN presents the lowest bias. The worst results are obtained with simulation MMN, also for the wind speed and direction. For all simulations at all buoys, the wind speed bias is positive, indicating a tendency of the model to overestimate the wind speed. For the wind direction, in all stations and simulations the obtained biases were positive, meaning that the model has a tendency to simulate the wind with a slight anti-clockwise wind rotation. Regarding the wind speed of the onshore group, simulation APP is the one with the best scores (highest R, lowest RMSE and STDE), while simulation MEN shows the lowest Bias (closely followed by simulations APP and MMN). All simulations show a tendency to overestimate the wind speed (positive bias for the wind speed) with simulation APP being the only exception, which shows an opposite tendency. For the wind direction, simulations YMN (RMSE, STDE and R) and MMN (Bias) show the best results. Given the negative biases for the wind direction, it can be seen that all simulations (except simulation MMN) depicted the wind direction with an anti-clockwise rotation, although these rotations are residual. The highest correlations for the wind speed are obtained with simulation APP, and for the wind direction with simulations YMN and APP (with simulation QQN standing out as the one with the worst correlation coefficient for the wind direction).

Considering the results presented in Table 3, it is noticeable that the different PBL–SL schemes lead to slightly different results, as a consequence of the different approaches to model the momentum, energy and moisture fluxes. One of the main differences between these five parameterizations sets is that some of the PBL schemes are based on non-local closure formulations (YSU), while other parameterizations sets use local closure approaches (MYJ, QNSE, MYNN-2.5). Although typically ACM2 is considered as a non-local scheme, this parameterization is in fact a mixed local and non-local scheme. Closure schemes are needed to calculate the turbulent fluxes from the mean variables: while local closure schemes estimate the turbulent flows at each model grid point from the mean atmospheric variables and/or their gradients at that point, non-local closure schemes estimate the same fluxes at a given point using the mean profiles over the entire domain of turbulent mixing [59]. Local closure schemes are more appropriate for stable atmospheric regimes [60,61]. Their assumption that fluxes only depend on the grid points values and gradients can lead to errors under unstable atmospheric conditions, when turbulent fluxes are dominated by large eddies that transport variables to longer distances [61–63]. By contrast, non-local closure schemes are more suitable for unstable boundary layers, due to the fact that this type of schemes account for larger eddies [61,64,65]. As reported by Muñoz-Esparza et al. [25,66] these kind of schemes fail in reproducing stable wind speed vertical profiles due to an excessive turbulent mixing near the surface, in particular during stable and stratified atmospheric conditions [67]. Therefore, non-local schemes, with the entrainment flux proportional to the surface flux, have their strength under unstable conditions, whereas in stable conditions the local closure schemes allow a better performance.

ACM2 includes characteristics both from local and non-local closure formulations: although it uses a non-local closure method (convective transport), it includes a first order eddy diffusion component to improve the vertical profiles simulation accuracy near the surface. This way, in the presence of stable or neutral atmospheric regimes, the ACM2 PBL scheme shuts off the non-local transport and uses local closure [59]. Basically, this scheme uses a non-local approach under unstable atmospheric regimes and a local one in the presence of stable/neutral conditions, which constitutes a clear advantage. Moreover, WRF's PBL schemes have a tendency to provide lower time variability due to the range of resolved scales and turbulence modeling, and explicit non-local mixing schemes like the ACM2 attenuates this effect [66]. Furthermore, none of

WRF's PBL schemes is able to accurately simulate the sudden increase in the wind speed following the convective initiation in the morning [61]. However, non-local closure schemes simulate more quickly the surface wind increase in the early stage of mixed-layer development than the local closure schemes. In addition, the LSM PX scheme (used together with ACM2) is able to provide more accurate near surface meteorology than the Noah LSM scheme [58,68] mainly due to its soil moisture nudging, which is one of the most sensitive parameters in simulating wind speeds [69]. LSM parameterizations interact with PBL and SL parameterizations due to the fact that they combine atmospheric information from the SL schemes with land surface properties to evaluate the vertical transport computed in the PBL schemes, which has a direct influence on the estimation of the PBL height [70]. This can have great impact in the near-surface wind simulation, due to the strong influence of the terrain characteristics (topography, land use, etc.) in the low altitude atmospheric flows. ACM2 PBL parameterization combines characteristics of local and non-local schemes and the PX LSM scheme is able to better represent the near-surface meteorology. These features of ACM2 and PX schemes can justify the better performance of this parameterization set in the simulation of near surface wind.

3.2. Geographical analysis of the simulations performance

All the onshore and offshore sites were divided into groups according to their geographical location and the same statistical analysis was performed for all the groups, in order to assess if the parameterization sets performance varies with the geographical area. To this end, and considering the spatial distribution of the offshore and onshore sites, these sites were divided into the following geographical areas: Area 1, which includes the offshore sites Peñas, Bares, Villano and Silleiro; Area 2, with the onshore sites 1, 2 and 3; Area 3 includes the onshore sites 4, 5 and 6; Area 4 with the onshore sites 7 and 8; Area 5 with the onshore sites 9–13; and Area 6 corresponding to the Cádiz offshore site. These areas are depicted in Fig. 3 and the weighted mean statistical scores for each area are presented in Table 4.

According to Table 4 it is visible that the RMSE and STDE for the wind speed has no significant geographical differences in terms of each simulation relative performance when compared to the remaining ones, this is, simulation APP shows the lowest wind speed RMSE and STDE for nearly all geographical groups. The exceptions are seen in area 2, where simulation MMN shows the best performance for the wind speed temporal variability (RMSE, STDE and R), and area 1 where the lowest RMSE is obtained by simulation QQN. But even in these areas simulation APP closely follows simulations QQN and MNN. As for the wind speed biases, simulation APP has the lowest values for all areas except group 1 and 2. For the wind direction the opposite is seen, with no simulation clearly standing out and appearing that for each group a different parameterization set produces the best results.

Although not shown in Table 4, it is worth mentioning that in all offshore simulations the worse results are seen in Peñas buoy. The simulations results for the Gulf of Cádiz site also show higher errors when compared to Bares, Silleiro and Villano. This is due to the strong dependence of these coastal winds with the surrounding topography and to high-resolution land-sea coastal interaction mechanisms (such as coastal breezes due to land-sea temperature gradients, terrain-induced wind circulations and abrupt roughness changes), and the limited resolution of the meso-scale model terrain data limits its accurate representation of these terrain-induced circulations. A more detailed analysis on this issue can be found in Carvalho et al. [32].

One intriguing fact shown in Tables 3 and 4 is that all simulations tend to overestimate the wind speed for onshore sites,

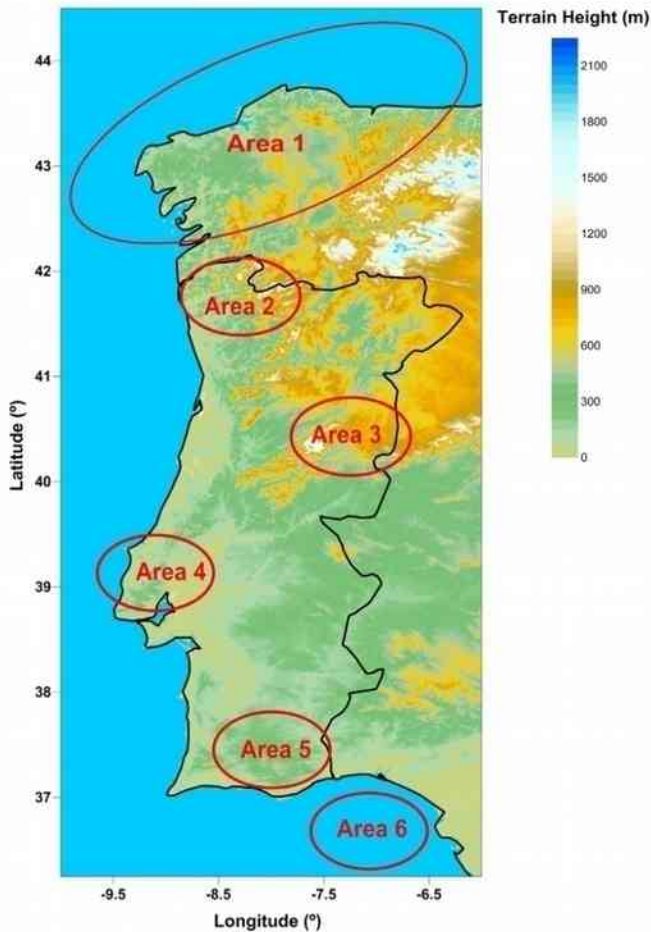


Fig. 3. Geographical areas.

considering the positive wind speed biases detected. This fact is not wholly surprising for offshore sites, since the WRF model considers the ocean as a constant and flat surface while the real ocean has higher roughness lengths (due to changes in the ocean surface heights), the simulated lower roughness lengths over the ocean produce winds with lower friction between atmosphere and ocean surface and, therefore, with higher speeds. In opposition, this wind speed overestimation can cause some surprise for onshore sites, because the application of mesoscale models for wind energy assessment studies typically shows wind speed underestimations at potential sites for installing wind farms (typically mountain ridges) [eg., 17, 21 and references therein]. Despite the fact that the aim of this study is not to analyze in detail the errors of the model but instead to determine which of the parameterization sets provides more accurate results, it should be noted that mesoscale near-surface wind simulation errors can have multiple sources (from model errors in representing atmospheric mesoscale features to incorrect representation of local terrain and roughness heights, leading to a misrepresentation of the local terrain complexity). Typically, this misrepresentation of the local terrain topography and complexity leads to underestimation of the wind speeds in mountain ridges, but other situations can occur that will cause the inverse behaviour. Carvalho et al. [31] reported the same tendency for the model to overestimate the wind speed in some of the stations used in this work. That study made a detailed analysis on the wind speed overestimation by WRF for these locations and concluded that this overestimation is often related to the fact that in those locations the smoothed topography in the model is not able to represent orographic blockages in dominant wind direction

sectors that occur in the real terrain. Also contributing to the overestimation of the wind speed by the model is the smoothing of the terrain complexity that can produce simulated winds: a flatter terrain means lower drag between the surface and the atmosphere, inducing higher surface flow speeds. Mass and Ovens [71] found that WRF modelled winds exhibit a high wind speed bias over land due to the exclusion of sub-grid orographic drag in the formulation of roughness lengths. Therefore, by formulating roughness length including these effects it was possible to significantly reduce the high wind speed bias in near surface winds. Moreover, there seems to be present a tendency for the model performance to be degraded in locations that show higher terrain complexity (quantified in the form of the ruggedness index, or RIX, factor) and, as a consequence, in stations where the difference between real and model mesh terrain height is higher (Table 1). This is the case for area 2, where the difference between real and model terrain height of the sites are higher, the local terrain complexities are also higher and the simulation errors are also higher when compared to the remaining geographical areas. This was to be expected and it is a feature common to almost any type of model, due to their low topography data resolution that cannot properly represent terrain-induced circulations. Considering also the results presented in Table 3, it is visible that the model tends to show a better performance for offshore sites, mainly in the wind speed simulation. This can be explained by the fact that, since in ocean areas these terrain topography/complexity model limitations do not apply, the model is able to attain a better performance.

3.3. Simulated wind speed performance variation with seasonality

In this section, the simulations and measured data are analyzed per season: Winter (December to February), Spring (March to May), Summer (June to August) and finally Autumn (September to November). For each season the wind speed RMSE and Bias of each simulation for all sites are presented in Table 5.

According to the results presented in Table 5, and considering the global results for all sites (last section of Table 5), simulation APP is the one with the best results for all seasons, both in terms of the wind speed temporal variability (RMSE) and in terms of the wind speed mean behaviour (Bias). The ACM2 PBL scheme it is systematically the one with the best results when considering all the sites statistics, which might be related to the fact that this PBL scheme combines features of local and non-local schemes as mentioned above. Analyzing these results for each geographical area, for practically all areas simulation APP is the one with the lowest errors for all seasons. Only for areas 1 and 2 local schemes seem to be the ones with the best results (simulation APP is the best only for Spring in area 2 and Summer in area 1). Also in area 4 the best results for Summer period are obtained with the MYNN2.5 PBL scheme.

An interesting fact is that all parameterization schemes seem to have worse performance in Winter and Autumn periods. This was somewhat expected for non-local schemes (simulation YMN, considering that simulation APP shares characteristics of both local and non-local schemes), due to the fact that particularly in Winter is more probable that stable atmospheric conditions can occur near the surface due to colder surface temperatures. Under these atmospheric conditions, non-local schemes can have worse performances. However, it would be expected that simulations MEN, QQN and MMN would show the best results in the Winter due to the local closure formulations of their PBL schemes. Nevertheless, it is visible that in Winter period the local schemes are the ones with the best performance after simulation APP, while for the Summer period these simulations show the worst overall results.

By performing simulations using different PBL–SL schemes under different atmospheric stability regimes, Draxl et al. [23]

Table 4
Statistics between observed and simulated wind data per geographical area.

Area	Simulation	RMSE		Bias		STDE		R	
		Speed (ms^{-1})	Direction ($^{\circ}$)	Speed (ms^{-1})	Direction ($^{\circ}$)	Speed (ms^{-1})	Direction ($^{\circ}$)	Speed (ms^{-1})	Direction ($^{\circ}$)
1	YMN	1.84	38.46	0.50	3.06	1.76	38.23	0.89	0.83
	MEN	1.84	38.52	0.40	1.68	1.79	38.40	0.88	0.83
	APP	1.84	37.70	0.49	2.21	1.76	37.55	0.89	0.84
	QQN	1.83	38.05	0.30	1.32	1.80	37.88	0.88	0.83
	MMN	1.87	38.75	0.56	3.88	1.78	38.47	0.88	0.83
2	YMN	2.34	43.37	-0.29	-1.83	2.28	43.18	0.76	0.65
	MEN	2.35	44.75	-0.63	-2.39	2.24	44.57	0.77	0.58
	APP	2.29	43.88	-0.43	-4.12	2.22	43.58	0.78	0.66
	QQN	2.42	46.33	-0.54	-3.57	2.35	46.06	0.75	0.39
	MMN	2.27	44.25	-0.47	-1.59	2.19	44.09	0.78	0.57
3	YMN	2.09	39.32	0.37	0.06	2.04	39.30	0.79	0.73
	MEN	2.05	39.85	0.24	0.42	2.02	39.83	0.78	0.72
	APP	1.89	39.02	-0.17	-1.23	1.87	38.99	0.80	0.72
	QQN	2.15	40.51	0.33	2.03	2.11	40.45	0.76	0.75
	MMN	2.09	39.46	0.37	1.08	2.04	39.43	0.79	0.73
4	YMN	2.08	26.84	0.57	2.53	2.00	26.72	0.79	0.88
	MEN	2.05	27.10	0.38	1.41	2.01	27.06	0.78	0.88
	APP	1.90	28.60	-0.17	0.80	1.89	28.58	0.78	0.87
	QQN	2.26	30.49	0.56	1.51	2.19	30.45	0.73	0.86
	MMN	2.01	26.80	0.43	3.11	1.97	26.62	0.78	0.88
5	YMN	1.97	30.70	0.60	-0.85	1.84	30.48	0.80	0.86
	MEN	1.82	30.85	0.36	-1.38	1.73	30.67	0.81	0.86
	APP	1.71	31.69	-0.02	-3.68	1.68	31.28	0.82	0.85
	QQN	2.06	33.67	0.58	0.14	1.92	33.57	0.76	0.85
	MMN	1.84	31.44	0.36	-0.86	1.77	31.27	0.81	0.86
6	YMN	1.87	39.07	0.41	4.64	1.83	38.79	0.86	0.84
	MEN	1.93	38.68	0.45	2.86	1.88	38.57	0.85	0.84
	APP	1.79	39.39	0.34	2.67	1.76	39.30	0.87	0.84
	QQN	1.96	38.66	0.54	3.55	1.88	38.50	0.85	0.85
	MMN	2.07	40.30	0.63	4.76	1.97	40.02	0.84	0.82

reported that for unstable conditions the YSU scheme showed the best performance, while for neutral and near-stable conditions the ACM2 PBL scheme was the best one and for stable and very stable conditions local schemes (such as the MYJ) outperformed the others. Considering that the use of a whole year of both measured and simulated data tends to average the atmospheric regime to a neutrally/slightly stable one, the results of this work corroborate what was concluded in that study. The fact that local schemes (simulations MEN, QQN and MMN for the present case) are the ones with the second best performance for the Winter period and the YSU non-local scheme the second best for the Summer period is also in accordance with those findings, assuming that in Winter the occurrence of stable atmospheric regimes are favoured (colder surface temperatures) and in Summer atmospheric instability is more likely to occur (surface warmer than the adjacent atmosphere). However, strong atmospheric stability typically occurs in hot Summer nights.

3.4. Simulations performance variation with measured wind speed and direction

In this section, the simulated wind speed/direction error variation with the measured wind speed/direction is analyzed. This can be important to understand if the model performance is sensitive to the magnitude of the wind speed or the direction of origin of the wind. To that end, the measured wind speed was binned into four categories and the simulated wind speed and direction errors (RMSE and Bias) were computed and analyzed. Table 6 shows the RMSE and Bias simulation scores divided into four measured wind

speed bins: wind speeds below 4 ms^{-1} , between 4 and 8 ms^{-1} , between 8 and 12 ms^{-1} and above 12 ms^{-1} .

According to Table 6, all simulations clearly show the highest errors in the presence of weak and strong wind speeds, both for the RMSE and the Bias. The best performances are seen for wind speeds between 4 and 12 ms^{-1} . The fact that the model shows worse performance for low wind speeds is not expected to bring any significant negative impact to wind energy assessment estimates, due to the fact that winds below 4 ms^{-1} do not contribute to wind energy production.

A striking feature is that all simulations tend to overestimate wind speeds below 8 ms^{-1} (with the exception of simulation APP) and underestimate wind speeds above this value. There appears to be a linear variation of the Bias with the measured wind speed: for low wind speeds the bias tends to be positive and high, gradually lowering its value with increasing measured wind speed and for strong wind speeds the biases are now negative and again high in magnitude. Similar behaviour of the model was detected in Carvalho et al. [31] for different initial and boundary conditions.

Furthermore, simulation APP provided the lowest errors for wind speeds below 8 ms^{-1} , whilst for higher wind speeds the best scores are obtained with the simulation MMN. This is a relevant finding if the purpose of the mesoscale simulation is to estimate maximum local wind speeds for site assessment purposes, for example. This feature might be related to the aforementioned fact that the local closure formulation of the MYNN PBL scheme used in simulation MMN can offer better performances in the presence of stable atmospheric regimes, while the non-local closure formulation of ACM2 PBL scheme used in simulation APP is more suitable for unstable atmospheric conditions: weak winds can be related to

Table 5
Statistics between observed and simulated wind speed per season.

Area		Winter		Spring		Summer		Autumn	
		RMSE (ms ⁻¹)	Bias (ms ⁻¹)	RMSE (ms ⁻¹)	Bias (ms ⁻¹)	RMSE (ms ⁻¹)	Bias (ms ⁻¹)	RMSE (ms ⁻¹)	Bias (ms ⁻¹)
1	YMN	1.53	0.53	1.42	0.37	1.27	0.24	1.50	0.45
	MEN	1.48	0.38	1.40	0.29	1.34	0.22	1.51	0.37
	APP	1.56	0.56	1.41	0.36	1.22	0.15	1.52	0.51
	QQN	1.51	0.23	1.42	0.24	1.27	0.17	1.49	0.30
	MMN	1.55	0.52	1.44	0.40	1.31	0.33	1.52	0.52
2	YMN	2.45	-0.77	2.25	-0.51	2.31	0.39	2.33	-0.29
	MEN	2.57	-1.11	2.35	-0.83	2.18	0.03	2.27	-0.63
	APP	2.48	-0.91	2.21	-0.53	2.19	0.20	2.27	-0.48
	QQN	2.64	-1.01	2.42	-0.86	2.29	0.15	2.34	-0.43
	MMN	2.43	-0.85	2.24	-0.72	2.16	0.10	2.24	-0.42
3	YMN	2.44	0.54	2.03	0.34	1.86	0.37	1.96	0.23
	MEN	2.40	0.49	2.02	0.18	1.82	0.20	1.91	0.10
	APP	2.13	-0.09	1.92	-0.03	1.65	-0.21	1.82	-0.34
	QQN	2.39	0.39	2.08	0.10	2.06	0.56	2.05	0.26
	MMN	2.42	0.52	2.03	0.38	1.86	0.31	1.99	0.27
4	YMN	2.21	0.83	1.99	0.41	1.47	0.12	2.53	0.92
	MEN	2.25	0.84	1.93	0.14	1.50	-0.14	2.42	0.71
	APP	2.04	0.25	1.81	-0.16	1.58	-0.70	2.13	-0.09
	QQN	2.60	1.02	2.08	0.32	1.61	-0.10	2.63	1.00
	MMN	2.19	0.75	1.90	0.11	1.45	0.01	2.41	0.84
5	YMN	2.07	0.53	2.02	0.64	1.79	0.56	1.99	0.66
	MEN	1.95	0.38	1.88	0.35	1.70	0.36	1.74	0.33
	APP	1.86	0.06	1.70	-0.02	1.56	-0.18	1.69	0.07
	QQN	2.07	0.46	2.11	0.50	2.13	0.86	1.89	0.49
	MMN	2.03	0.46	1.85	0.36	1.67	0.27	1.81	0.35
6	YMN	1.82	0.72	1.98	0.44	1.82	0.24	1.87	0.24
	MEN	1.80	0.57	2.01	0.56	1.96	0.47	1.95	0.22
	APP	1.69	0.56	1.90	0.41	1.75	0.20	1.81	0.21
	QQN	1.86	0.59	1.96	0.48	1.97	0.62	2.05	0.45
	MMN	1.89	0.74	2.19	0.71	2.17	0.77	2.00	0.28
All	YMN	2.13	0.49	1.96	0.37	1.76	0.35	2.02	0.44
	MEN	2.08	0.33	1.93	0.21	1.77	0.24	1.97	0.27
	APP	2.03	0.26	1.85	0.15	1.65	0.01	1.92	0.19
	QQN	2.16	0.28	2.00	0.21	1.87	0.39	2.04	0.35
	MMN	2.13	0.46	1.95	0.31	1.77	0.34	2.00	0.40

Table 6
Weighted-averaged wind speed RMSE and Bias per measured wind speed bin.

Simulation	<4 ms ⁻¹		4–8 ms ⁻¹		8–12 ms ⁻¹		>12 ms ⁻¹	
	RMSE (ms ⁻¹)	Bias (ms ⁻¹)	RMSE (ms ⁻¹)	Bias (ms ⁻¹)	RMSE (ms ⁻¹)	Bias (ms ⁻¹)	RMSE (ms ⁻¹)	Bias (ms ⁻¹)
YMN	2.09	1.02	1.88	0.34	1.88	0.06	2.44	-0.64
MEN	2.07	0.95	1.84	0.22	1.82	-0.18	2.49	-0.96
APP	1.96	0.87	1.74	0.09	1.83	-0.33	2.54	-1.00
QQN	2.21	1.10	1.93	0.31	1.86	-0.23	2.52	-1.16
MMN	2.12	1.03	1.89	0.31	1.83	0.02	2.36	-0.76

unstable atmospheric regimes, when convective turbulence is dominant over mechanical turbulence; oppositely, strong winds can be associated to stable atmospheric conditions in the absence of convective turbulence, when mechanical turbulence is dampened and there is little vertical mixing. Although the relation between strong/weak winds and stable/unstable atmospheric conditions is not straightforward and linear, there are indications that stronger (weaker) wind speeds are associated with stable (unstable) atmospheric conditions. Several atmospheric stability classifications schemes, such as the ones described in Pasquill [72] and the Pasquill–Gifford–Turner stability classifications [73] show that, under the same convective turbulence conditions, increasing wind speeds are associated to more stable atmospheric regimes. Therefore, the results depicted in Table 6 are in agreement with what would be expected due to the local or non-local formulations of each tested PBL scheme.

Table 7 shows the same comparison for the RMSE and Bias of the simulated wind direction.

Table 7 shows that non-local PBL schemes (simulation YMN and APP) provided the lowest wind direction simulation errors for wind speeds below 8 ms⁻¹, whilst for higher wind speeds the best scores are obtained by the MMN simulation. The most striking feature is that all simulations clearly show the highest RMSE in the presence of low wind speeds, and this error metric substantially decrease with increasing wind speed. This dependence of the wind direction error on the measured wind speed is explained by the fact that, in the presence of low wind speeds, the variation of the wind direction is obviously higher and its accurate measurement/simulation becomes affected. From the Bias values it is possible to see that the errors in wind direction are mainly anti-clockwise for intense wind speeds, while for low wind speeds they are clockwise.

Table 7

Weighted-averaged wind direction RMSE and Bias per measured wind speed bin.

Simulation	<4 ms ⁻¹		4–8 ms ⁻¹		8–12 ms ⁻¹		>12 ms ⁻¹	
	RMSE (°)	Bias (°)	RMSE (°)	Bias (°)	RMSE (°)	Bias (°)	RMSE (°)	Bias (°)
YMN	62.21	3.34	27.70	1.89	16.67	-0.15	15.34	-1.77
MEN	62.73	2.92	27.88	1.16	16.60	-1.63	15.67	-3.90
APP	62.10	1.39	27.84	-0.05	16.69	-1.18	15.52	-2.03
QQN	63.29	4.37	29.22	1.40	17.44	-2.13	16.43	-4.88
MMN	63.07	3.84	28.19	2.20	16.53	0.65	15.20	-0.88

Table 8

Weighted-averaged wind speed RMSE and Bias errors per measured wind direction bin for each simulation.

Simulation	North		East		South		West	
	RMSE (ms ⁻¹)	Bias (ms ⁻¹)	RMSE (ms ⁻¹)	Bias (ms ⁻¹)	RMSE (ms ⁻¹)	Bias (ms ⁻¹)	RMSE (ms ⁻¹)	Bias (ms ⁻¹)
YMN	1.85	0.25	2.14	0.48	2.06	0.44	1.92	0.51
MEN	1.80	0.06	2.13	0.40	2.07	0.32	1.89	0.36
APP	1.76	-0.06	1.95	0.21	1.98	0.23	1.86	0.32
QQN	1.88	0.14	2.23	0.45	2.13	0.43	1.95	0.37
MMN	1.82	0.17	2.14	0.48	2.09	0.45	1.91	0.50

Tables 8 and 9 show the wind speed and direction error variation as a function of the measured wind direction. The measured wind direction was binned into four main sectors: North (angles between 315° and 45°), East (between 45° and 135°), South (between 135° and 225°) and West (between 225° and 315°).

Analyzing Tables 8 and 9, the South sector shows the highest errors when compared to the other sectors, both to the wind speed and wind direction. This can be related to the fact that for this area of the Iberian Peninsula southerly winds are typically associated with atmospheric instability episodes with a weak synoptic forcing [74]. These episodes will enhance the influence of the terrain-induced circulations and produce winds with a high variability, which are not properly captured by mesoscale models due to their limited resolution. Another interesting fact is that all simulations, in terms of weighted mean values, seem to represent winds coming from North and East with an anti-clockwise wind rotation, and the inverse behaviour for winds coming from South and West.

From Tables 8 and 9 it is visible that the South and East sectors appear as the ones with overall higher errors, both for the simulated wind speed and direction. Looking at Fig. 1, it can be seen that the South sector represent winds coming from land in the offshore sites Peñas, Villano and Bares, and winds coming from the ocean for the onshore sites located in area 5. Furthermore, the East sector represents winds coming from the ocean at the Silleiro offshore site and winds coming from the ocean in all the remaining onshore near the coast. Therefore, it is possible that these results reflect a degradation of the model performance when the wind is coming from the land/ocean interface. To analyze this issue, the statistics of Tables 8 and 9 are now calculated for sites in which Southerly winds represent flows coming from the land/ocean interface (Peñas, Bares, Villano and onshore stations 9–13) and for sites

where Easterly winds represent winds coming from the land/ocean interface (Silleiro and onshore sites 1, 2, 7, 8).

From Table 10 it becomes clear that in sites where Southerly winds represent winds coming from land/ocean the simulation errors are substantially higher, both for the wind speed and direction.

Similarly to what was seen in Table 10, Table 11 shows that in sites where Easterly winds represent winds coming from land/ocean the simulation errors are substantially higher for the simulated wind speed and direction. The highest RMSE for the wind direction are still seen for the South sector, which is related to the southerly weak synoptic winds over the Iberian Peninsula. However, for the wind speed the highest RMSE values are clearly seen for the East sector. Therefore, results strongly suggest that the model has a higher difficulty in accurately represent sea-land circulations.

3.5. Weibull PDF comparison and potential wind energy production estimates

Weibull PDFs of the measured and simulated wind data are analyzed and depicted in Fig. 4. Due to the high number of sites considered and to the fact that the PDFs are similar in all sites, only differing in the fact that the model under- or overestimates the wind speed, only 2 sites are shown: one site where the model tends to overestimate the wind speed (as an example, onshore site 9 was chosen) and one site where the model tends to underestimate it (onshore site 2 was selected).

Bearing in mind that Weibull distributions, as with any statistical distribution, are merely cumulative and do not take into account the temporal simultaneity of the measured and simulated

Table 9

Weighted-averaged wind direction RMSE and Bias errors per measured wind direction bin for each simulation.

Simulation	North		East		South		West	
	RMSE (°)	Bias (°)	RMSE (°)	Bias (°)	RMSE (°)	Bias (°)	RMSE (°)	Bias (°)
YMN	31.51	-0.80	37.75	-2.64	49.03	7.53	33.64	4.03
MEN	32.25	-1.53	38.03	-2.93	47.49	5.64	34.61	2.97
APP	31.88	-2.49	37.18	-3.74	48.78	5.82	34.12	2.12
QQN	33.70	0.08	39.32	-2.38	47.16	5.36	35.44	1.49
MMN	32.22	-0.92	38.95	-2.08	49.15	9.30	33.56	4.59

Table 10

Weighted-averaged wind speed and direction RMSE per measured wind direction bin for each simulation in sites where Southerly winds represent winds coming from the land/ocean interface (Peñas, Bares, Villano and onshore stations 9–13). The highest errors are in bold and in italic for guidance.

Simulation	North		East		South		West	
	RMSE (ms ⁻¹)	RMSE (°)	RMSE (ms ⁻¹)	RMSE (°)	RMSE (ms ⁻¹)	RMSE (°)	RMSE (ms ⁻¹)	RMSE (°)
YMN	1.79	29.51	2.05	35.62	2.12	52.09	1.93	32.30
MEN	1.69	30.57	1.98	36.18	2.12	49.46	1.88	32.70
APP	1.64	30.06	1.82	34.21	2.09	52.07	1.84	32.67
QQN	1.81	33.99	2.12	38.49	2.28	46.58	1.94	32.30
MMN	1.72	30.33	1.95	37.03	2.17	51.00	1.90	31.56

Table 11

Weighted-averaged wind speed and direction RMSE per measured wind direction bin for each simulation in sites where Easterly winds represent winds coming from the land/ocean interface (Silleiro and onshore sites 1, 2, 7, 8). The highest errors are in bold and in italic for guidance.

Simulation	North		East		South		West	
	RMSE (ms ⁻¹)	RMSE (°)	RMSE (ms ⁻¹)	RMSE (°)	RMSE (ms ⁻¹)	RMSE (°)	RMSE (ms ⁻¹)	RMSE (°)
YMN	1.88	26.76	2.18	36.63	1.86	44.77	1.93	35.19
MEN	1.84	27.91	2.17	36.02	1.87	43.87	1.86	36.04
APP	1.87	27.73	1.95	36.71	1.78	45.23	1.90	36.51
QQN	1.89	29.78	2.37	38.71	1.91	44.42	1.89	37.48
MMN	1.81	26.79	2.20	38.96	1.84	46.68	1.88	34.77

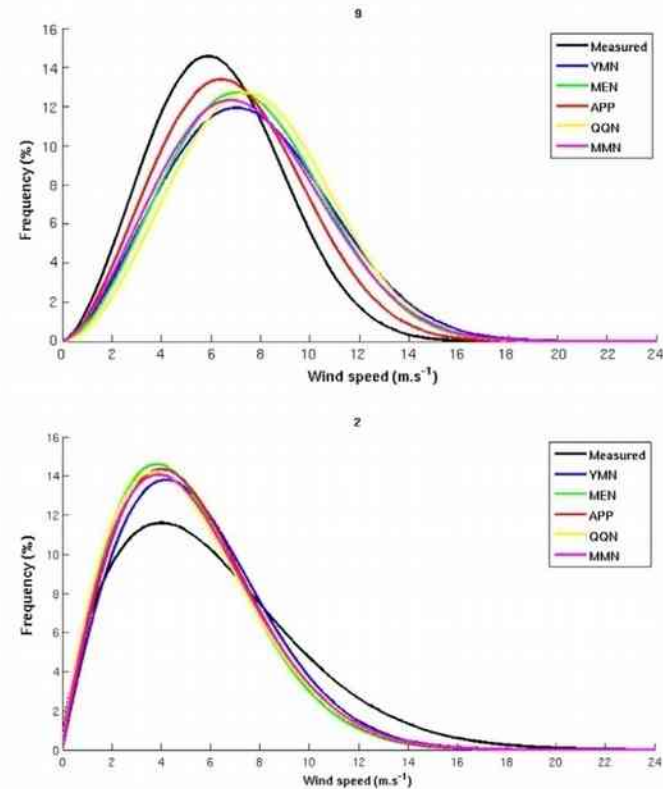


Fig. 4. Weibull PDF curves for onshore sites 9 (upper panel) and 2 (lower panel).

wind speed, the simulation with lower errors related to the mean state of the wind speed tends to show the Weibull PDF curve closest to the observed one. In all sites where the model overestimated the wind speed (shown as example station 9), there is a visible shift of the simulated PDFs to the right side of the wind speed axis relatively to the observed PDFs, meaning that low wind speed frequencies are underestimated by the model while strong wind speed frequencies are overestimated by the simulations. The combined effect of these inaccuracies produces the overall wind speed overestimation tendency. In sites where the model underestimated

Table 12

Weibull PDFs parameters, mean and most probable wind speed, wind energy flux deviations and wind speed bias averaged for all stations, using absolute values.

Area	Simulation	A (%)	k (%)	U _m (%)	U _{prob} (%)	P _{flux} (%)
Offshore	YMN	7.5	4.0	7.1	11.8	15.0
	MEN	6.4	2.9	6.2	9.7	13.4
	APP	7.1	2.8	6.8	10.1	15.5
	QQN	5.6	5.7	5.4	11.0	7.8
	MMN	8.8	5.3	8.6	14.1	16.6
Onshore	YMN	8.1	4.8	8.2	8.5	27.3
	MEN	6.8	4.8	7.0	7.1	21.4
	APP	4.9	5.2	4.9	5.0	13.1
	QQN	8.0	6.4	8.3	9.6	24.0
	MMN	7.0	4.3	7.1	7.3	22.6
All sites	YMN	7.8	4.8	7.7	10.3	21.2
	MEN	6.6	4.3	6.6	8.6	17.4
	APP	6.0	4.3	5.9	7.6	14.3
	QQN	6.8	6.1	6.8	10.4	15.9
	MMN	7.9	4.9	7.8	10.8	19.6

the wind speed, the opposite effect occurs: the model underestimates the frequency of strong wind speeds and overestimates the frequency of intermediate wind speeds, leading to an overall underestimation of the wind speed.

The Weibull PDFs A and k parameters, mean wind speed (U_m), most probable wind speed (U_{prob}) and wind energy power flux (P_{flux}) percentage deviations of each simulation when compared to observed data, are shown in Table 12 in the form of the average values (using absolute values for each simulation and each site).

According to Table 12, for the offshore group simulation QQN is the one with the A parameter, mean wind speed and wind power flux closest to the ones obtained from measured data, while simulation APP shows the lowest deviations in terms of the k parameter and simulation MEN the lowest most probable wind speed. For the onshore group, the lowest deviations of the A parameter, mean wind speed and wind power flux are obtained with simulation MEN, while the k parameter has its lowest deviation value for simulation MMN and simulation APP shows no deviations in terms of the most probable wind speed. However, the average deviations considering both onshore and offshore sites show that simulation APP is the one with the best performance for all parameters, including the wind power flux.

Combining the information presented in Tables 3 and 12 it can be concluded that simulation APP is, globally, the simulation with the lowest magnitude of errors. For the wind speed, it shows the lowest RMSE, STDE, Bias, Weibull parameters, mean and most probable wind speed and wind power flux deviations and higher correlation coefficients. The only exception is for offshore sites in what is related to the mean state of the wind speed and, consequently, for the wind power flux, where simulation QQN shows the lowest errors. The choice of the PBL–SL parameterization schemes in wind simulation applications can lead to significant differences in the near surface wind simulation results, particularly in terms of wind energy production estimates. The average results show improvements in the wind power flux estimates, and although not shown in Table 12, in some sites the choice of a given PBL parameterization scheme can reduce the deviations towards measured data from 30–40% to 5–10%, which is very significant for wind energy agents.

4. Conclusions

This work was conducted with the main goal of analyzing the WRF model wind simulation sensitivity to the use of different PBL and SL parameterization schemes, to identify which one of these PBL–SL parameterization sets is able to produce simulated winds closer to the observed ones. According to the results presented in this study, the choice of the PBL–SL schemes to use in wind simulation applications can lead to significant differences in the results, particularly in terms of wind energy production estimates. Although no major differences are seen between the simulations in terms of statistical analysis, in terms of potential wind energy production estimates the differences between the simulations are not negligible, and the choice of the PBL–SL scheme can greatly reduce the error in terms of wind power flux estimates. The expected energy production is highly sensitive to the local wind regimes and an increase in the wind speed and/or direction simulation accuracy, even if apparently not significant, can greatly improve the expected energy production estimates in assessment studies. In the particular case of offshore sites, wind direction is also of great importance in the wind energy production output as it will impact on the losses due to turbine wakes, which have a higher weight on overall production offshore than onshore, due to the reduced dissipation from lower offshore turbulence levels and bigger wind turbine dimensions.

Among the different PBL–SL parameterization sets tested, the simulation that used the ACM2–PX PBL and SL schemes showed, globally, the best statistical scores and wind characteristics closer to observed wind data, including the estimates of the wind power fluxes. The fact that the ACM2 PBL scheme combines features of local and non-local closure schemes and also the fact that the PX LSM scheme provides a better parameterization of the surface meteorology proved to be important in the model wind simulation performance. This parameterization set showed the best performance mainly in terms of the wind temporal variability accuracy (lower RMSE, STDE and higher correlation coefficients). Also for the wind mean state (Bias, Weibull parameters, mean wind speed and wind power flux) it was the one with the best error scores but here only for onshore sites. For offshore sites, the PBL parameterization scheme QNSE yielded the most accurate results for these statistical metrics.

Considering the lack of available studies that test the use of several PBL schemes in the near surface wind mesoscale simulation (both onshore and offshore) for the geographical areas here considered with at least one complete year of simulated wind datasets, the findings of this work can be very valuable for meteorological/oceanographic modelling studies that consider long term

simulations, especially if employed in areas located inside or in the vicinity of the area under scope. These findings are also particularly interesting for geographical areas where measured wind data are not available, or are insufficient for the desired purposes, and NWP modelling is, therefore, necessary to assess the wind energy resource of potential sites for the installation of wind farms. For offshore areas, this is precisely the case of Portugal, where presently no oceanic wind measurement campaigns are under operation and, therefore, no observed offshore wind data is available. Although it is expected that the close dependence of each PBL and SL scheme performance with the surrounding synoptic conditions and atmospheric stability can lead to different results, the fact that this focus on a complete meteorological/weather cycle, which includes all the different synoptic conditions, for a considerably wide geographical area offers a solid base of confidence that the conclusions drawn from this work can be considered to other periods and/or geographical areas.

Acknowledgements

D. Carvalho was supported by the Portuguese Foundation for Science and Technology (F.C.T.) Ph.D grant SFRH/BD/73070/2010. The authors would like to express their gratitude to all the climate and meteorological institutions referred in the text for providing the atmospheric data used in this work, and also to Megajoule S.A. for providing the onshore measured wind data.

References

- [1] Neill SP, Hashemi MR. Wave power variability over the northwest European shelf seas. *Appl Energy* 2013;106:31–46.
- [2] Akpınar A, Kömürçü Mİ. Assessment of wave energy resource of the Black Sea based on 15-year numerical hindcast data. *Appl Energy* 2013;101:502–12.
- [3] Krajačić G, Duić N, Carvalho MG. How to achieve a 100% RES electricity supply for Portugal? *Appl Energy* 2011;88(2):508–17.
- [4] Kou P, Gao F, Guan X. Sparse online warped Gaussian process for wind power probabilistic forecasting. *Appl Energy* 2013;108:410–28.
- [5] Morales JM, Mínguez R, Conejo AJ. A methodology to generate statistically dependent wind speed scenarios. *Appl Energy* 2010;87(3):843–55.
- [6] Chen K, Yu J. Short-term wind speed prediction using an unscented Kalman filter based state-space support vector regression approach. *Appl Energy* 2014;113:690–705.
- [7] Thiaw L, Sow G, Fall SS, Kasse M, Sylla E, Thioye S. A neural network based approach for wind resource and wind generators production assessment. *Appl Energy* 2010;87(5):1744–8.
- [8] Li G, Shi J. On comparing three artificial neural networks for wind speed forecasting. *Appl Energy* 2010;87(7):2313–20.
- [9] Fyrippis I, Axaopoulos PJ, Panayiotou G. Wind energy potential assessment in Naxos Island, Greece. *Appl Energy* 2010;87(2):577–86.
- [10] Poncela M, Poncela P, Perán JR. Automatic tuning of Kalman filters by maximum likelihood methods for wind energy forecasting. *Appl Energy* 2013;108:349–62.
- [11] Global Wind Energy Council. Global Wind Report, Annual market update 2012. <http://www.gwec.net/wp-content/uploads/2012/06/Annual_report_2012_LowRes.pdf>.
- [12] http://www.apren.pt/fotos/editor2/as_renovaveis_em_portugal_apren_abr2013.pdf.
- [13] Gallego C, Pinson P, Madsen H, Costa A, Cuerva A. Influence of local wind speed and direction on wind power dynamics – application to offshore very short-term forecasting. *Appl Energy* 2011;88(11):4087–96.
- [14] Ucar A, Balo F. Investigation of wind characteristics and assessment of wind-generation potentiality in Uludağ–Bursa, Turkey. *Appl Energy* 2009;86(3):333–9.
- [15] Carvalho D, Rocha A, Gómez-Gesteira M, Alvarez I, Silva Santos C. Comparison between CCMP, QuikSCAT and buoy winds along the Iberian Peninsula coast. *Remote Sens Environ* 2013;137:173–83.
- [16] Alvarez I, Gomez-Gesteira M, deCastro M, Carvalho D. Comparison of different wind products and buoy wind data with seasonality and interannual climate variability in the southern Bay of Biscay (2000–2009). *Deep-Sea Res Pt II* (in press). doi: <http://dx.doi.org/10.1016/j.dsr2.2013.09.028>.
- [17] Carvalho D, Rocha A, Silva Santos C, Pereira R. Wind resource modelling in complex terrain using different mesoscale-microscale coupling techniques. *Appl Energy* 2013;108:493–504.
- [18] Skamarock WC, et al. A Description of the advanced research WRF Version 3. NCAR Technical Note 2008, NCAR/TN-475+STR. p. 113.
- [19] Nossent J, Elsen P, Bauwens W. Sobol' sensitivity analysis of a complex environmental model. *Environ Modell Softw* 2011;26(12):1515–25.

- [20] Borge R et al. A comprehensive sensitivity analysis of the WRF model for air quality applications over the Iberian Peninsula. *Atmos Environ* 2008;42:8560–74.
- [21] Carvalho D, Rocha A, Gómez-Gesteira M, Santos C. A sensitivity study of the WRF model in wind simulation for an area of high wind energy. *Environ Modell Softw* 2012;33:23–34.
- [22] Challa VS, Indracanti J, Rabarison MK, Patrick C, Baham JM, Young J, et al. A simulation study of mesoscale coastal circulations in Mississippi Gulf coast. *Atmos Res* 2009;91:9–25.
- [23] Draxl C, Hahmann AN, Peña A, Giebel G. Evaluating winds and vertical wind shear from Weather Research and Forecasting model forecasts using seven planetary boundary layer schemes. *Wind Energy* 2014;17(1):39–55.
- [24] Krieger JR, Zhang J, Atkinson DE, Shulski MD, Zhang X. Sensitivity of WRF model forecasts to different physical parameterizations in the Beaufort Sea region. In: 8th conference on coastal atmospheric and oceanic prediction and processes; 2009.
- [25] Muñoz-Esparza D, van Beeck J, Cañadillas B. Impact of turbulence modeling on the performance of WRF model for offshore short-term wind energy applications. In: 13th international conference on wind engineering; 2011.
- [26] Shimada S, Ohsawa T. Accuracy and characteristics of offshore wind speeds simulated by WRF. *SOLA* 2011;7:21–4.
- [27] Wang C, Jin S, Hu, J, Zhang F, Feng S, Liu C. Comparing different boundary layer schemes of WRF by simulation the low-level wind over complex terrain. *Artificial Intelligence, Management Science and Electronic Commerce (AIMSEC)* 2011.
- [28] Wu WY, et al. Evaluation of planetary boundary layer parameterizations in WRF3.2. 11th Annual WRF users' workshop; 2010.
- [29] Menéndez M et al. A methodology to evaluate regional-scale offshore wind energy resources. *Oceans IEEE* 2011.
- [30] Krogsaeter O, Reuder J, Hauge G. WRF and the marine planetary boundary layer. 12th Annual WRF users workshop; 2011.
- [31] Carvalho D, Rocha A, Gómez-Gesteira M, Santos C. WRF wind simulation and wind energy production estimates forced by different reanalyses: comparison with observed data for Portugal. *Appl Energy* 2014;117:116–26.
- [32] Carvalho D, Rocha A, Gómez-Gesteira M. WRF model ocean surface wind simulation forced by different reanalysis: comparison with observed data along the Iberian Peninsula coast. *Ocean Model* 2012;56:31–42.
- [33] Carvalho D, Rocha A, Gómez-Gesteira M. Offshore wind energy resource simulation forced by different reanalyses: comparison with observed data in the Iberian Peninsula. *Appl Energy* 2014;134:57–64.
- [34] Farr TG, Rosen PA, Caro E, Crippen R, Duren R, Hensley S, et al. The shuttle radar topography mission. *Rev Geophys* 2007;45(2):1–33.
- [35] Monin AS, Obukhov AM. *Osnovnye zakonomernosti turbulentnogo peremeshivaniya v prizemnom sloe atmosfery (Basic Laws of Turbulent Mixing in the Atmosphere Near the Ground)*. Trudy geofiz inst 1954: AN SSSR 24(151): 163–187.
- [36] Liu WT, Tang W. *Equivalent neutral wind*. JPL Publication 1996, Jet Propulsion Laboratory, California Institute of Technology, Pasadena, California.
- [37] Peixoto JP, Oort AH. *Physics of climate*. Woodbury, N.Y.: American Institute of Physics; 1992.
- [38] Bourassa MA, Legler DM, O'Brian JJ, Smith SR. SeaWinds validation with research vessels. *J Geophys Res* 2003;108(3019):16.
- [39] Chelton DB, Freilich MH. Scatterometer-based assessment of 10-m wind analyses from the operational ECMWF and NCEP numerical weather prediction models. *Mon Weather Rev* 2005;133:409–29.
- [40] Kara AB, Wallcraft AJ, Bourassa MA. Air-sea stability effects on the 10 m winds over the global ocean: evaluations of air-sea flux algorithms. *J Geophys Res* 2008;113:4009–14.
- [41] Mears CA, Smith DK, Wentz FJ. Comparison of Special Sensor Microwave Imager and buoy-measured wind speeds from 1987 to 1997. *J Geophys Res* 2001;106(11):719–29.
- [42] Hong SY, Noh Y, Dudhia J. A new vertical diffusion package with an explicit treatment of entrainment processes. *Mon Weather Rev* 2006;134:2318–41.
- [43] Zhang D, Anthes RA. A high-resolution model of the planetary boundary layer-sensitivity tests and comparison with SESAME-79 data. *J Appl Meteorol* 1982;21:1594–609.
- [44] Janjic ZI. The step-mountain eta coordinate model: further developments of the convection, viscous sublayer and turbulence closure schemes. *Mon Weather Rev* 1994;122:927–45.
- [45] Janjic ZI. The step-mountain coordinate: physics package. *Mon Weather Rev* 1990;118:1429–43.
- [46] Pleim JE. A combined local and nonlocal closure model for the atmospheric boundary layer. Part I: Model description and testing. *J Appl Meteorol Clim* 2007;46:1383–95.
- [47] Pleim JE. A combined local and nonlocal closure model for the atmospheric boundary layer. Part II: Application and evaluation in a mesoscale meteorological model. *J Appl Meteorol Clim* 2007;46:1396–409.
- [48] Pleim JE. A simple, efficient solution of flux-profile relationships in the atmospheric surface layer. *J Appl Meteorol Clim* 2006;45:341–7.
- [49] Sukoriansky S, Galperin B, Perov V. Application of a new spectral theory of stable stratified turbulence to the atmospheric boundary layer over sea ice. *Bound-Lay Meteorol* 2005;117:231–57.
- [50] Galperin B, Sukoriansky S. Progress in turbulence parameterization for geophysical flows. In: 3rd international workshop on next-generation NWP models: bridging parameterization, explicit clouds, and large eddies; 2010.
- [51] Nakanishi M, Niino H. An improved Mellor-Yamada level-3 model; its numerical stability and application to a regional prediction of advection fog. *Bound-Lay Meteorol* 2006;119:397–407.
- [52] Nakanishi M, Niino H. An improved Mellor-Yamada level-3 model with condensation physics: its design and verification. *Bound-Lay Meteorol* 2004;112:1–31.
- [53] Hong SY, Lim JO. The WRF single-moment 6-class microphysics scheme (WSM6). *J Korean Meteor Soc* 2006;42:129–51.
- [54] Mlawer EJ, Taubman SJ, Brown PD, Iacono MJ, Clough SA. Radiative transfer for inhomogeneous atmosphere: RRTM, a validated correlated-k model for the longwave. *J Geophys Res* 1997;102:16663–82.
- [55] Dudhia J. Numerical study of convection observed during the winter monsoon experiment using a mesoscale two-dimensional model. *J Atmos Sci* 1989;46:3077–107.
- [56] Kain JS. The Kain-Fritsch convective parameterization: an update. *J Appl Meteorol* 2004;43:170–81.
- [57] Chen F, Dudhia J. Coupling an advanced land-surface/hydrology model with the Penn State/NCAR MM5 modeling system. Part I: Model description and implementation. *Mon Weather Rev* 2001;129:569–85.
- [58] Xiu A, Pleim JE. Development of a land surface model. Part I: Application in a mesoscale meteorological model. *J Appl Meteorol* 2001;40:192–209.
- [59] Hu XM, Nielsen-Gammon JW, Zhang F. Evaluation of three planetary boundary layer schemes in the WRF model. *J Appl Meteorol Clim* 2010;49:1831–44.
- [60] Mellor GL, Yamada T. Development of a turbulence closure model for geophysical fluid problems. *Rev Geophys* 1982;20:851–75.
- [61] Shin HH, Hong SY. Intercomparison of Planetary Boundary layer parameterizations in the WRF model for a single day from Cases 99. *Bound-Lay Meteorol* 2011;139:261–81.
- [62] Troen I, Mahrt L. A simple model of the atmospheric boundary layer: sensitivity to surface evaporation. *Bound-Lay Meteorol* 1986;37:129–48.
- [63] Stull RB. Transient turbulence theory. Part I: The concept of eddy-mixing across finite distances. *J Atmos Sci* 1984;41:3351–67.
- [64] Bright DR, Mullen SL. The sensitivity of the numerical simulation of the Southwest monsoon boundary layer to the choice of PBL turbulence parameterization in MM5. *Weather Forecast* 2002;17:99–114.
- [65] Misemis C, Zhang Y. An examination of sensitivity of WRF/Chem predictions to physical parameterizations, horizontal grid spacing, and nesting options. *Atmos Res* 2010;97(3):315–34.
- [66] Muñoz-Esparza D, van Beeck J. Forecasting the diabatic offshore wind profile at FINO1 with the WRF mesoscale model. *EWEA annual event*; 2011.
- [67] Hong SY, Kim SW. Stable boundary layer mixing in a vertical diffusion scheme. In: 9th WRF users' workshop proceedings; 2008.
- [68] Pleim JE, Xiu A, Finkelstein PL, Otte TL. A coupled land-surface and dry deposition model and comparison to field measurements of surface heat, moisture, and ozone fluxes. *Water Air Soil Poll* 2001;1(5–6):243–52.
- [69] Lundquist JK, Maxwell RM, Mirocha JD, Smith SG, Woodward CS, Thompson AFB. A coupled groundwater-atmospheric model for wind energy forecasting. In: 19th symposium on boundary layers and turbulence; 2010.
- [70] Han Z, Ueda H, An J. Evaluation and intercomparison of meteorological predictions by five MM5-PBL parameterizations in combination with three land-surface models. *Atmos Environ* 2008;42:233–49.
- [71] Mass CF, Owens D. Fixing WRF high speed wind bias: a new subgrid scale drag parameterization and the role of detailed verification. In: WRF users workshop; 2011.
- [72] Pasquill F. The estimation of the dispersion of windborne material. *Meteorol Mag* 1961;106:3–90.
- [73] Turner DB. *Workbook of atmospheric dispersion estimates*. Office of Air Program Publication N° AP-26, Environmental Protection Agency; 1970.
- [74] Penabad E et al. Comparative analysis between operational weather prediction models and QuikSCAT wind data near the Galician coast. *J Marine Syst* 2008;72:256–70.

Chapter 5 – Comparison of NWP modelled and satellite-derived offshore wind data with in situ offshore wind measurements

Unlike onshore wind measurements, which are invariably collected by wind measuring masts or meteorological stations, offshore winds are also measured by satellites orbiting the Earth. These offshore wind measurements derived from satellite observations have been widely used in the recent past in several meteorological, oceanographic and also offshore wind energy applications. However, it is recognized that these satellite derived offshore wind measurements are far from being as accurate and reliable as *in situ* measurements collected by wind measuring instruments, due to the fact that they show several and often significant error sources.

Having the WRF model optimised in what is related to the initial/boundary conditions and PBL parameterization options for the modelling of offshore winds, it becomes pertinent to assess if this optimised NWP model is able to surpass the performance of satellites in representing offshore winds. To this end, offshore wind simulations obtained from the WRF model, using its optimised configuration, are compared to offshore wind measurements collected by satellites.

5.1 – Determination of the best satellite offshore wind product

One of the most famous and widely used satellite derived offshore wind data sources for meteorological, oceanographic and wind energy applications is National Aeronautics and Space Administration (NASA) SeaWinds scatterometer installed aboard the QuikSCAT

satellite platform (henceforth simply referred to as QuikSCAT). This scatterometer was selected as source of satellite derived offshore wind data. Due to the fact that QuikSCAT wind data is available in several different products, which differ in the degree of data processing, it becomes important to first determine the QuikSCAT product with the best accuracy when compared to *in situ* measured offshore wind data. To this end, a comparison of the several official QuikSCAT products offered by NASA Physical Oceanography Distributed Active Archive Centre (PO.DAAC) was performed by comparing their data to *in situ* measured offshore winds. This research is presented in the following paper, in which is included the methodology followed, area under study, QuikSCAT products tested, observed data used to compare the simulations, introductory notes and state of the art. Although this paper also considers another offshore wind database (the Cross Calibrated Multi-Platform Ocean Surface Wind Vectors, CCMP) in the comparison, the most relevant finding of this article for the present thesis is which QuikSCAT product shows higher accuracy in representing offshore winds. This article can be consulted in the link:

<http://www.sciencedirect.com/science/article/pii/S0034425713001983>

In section 5.2 a wider selection of alternative sources of offshore wind data (including CCMP) is compared to measured offshore winds and with WRF modelled offshore winds (using its optimised configuration), in order to assess if WRF is able to surpass satellite-derived and also other alternative sources of offshore wind data.



Comparison between CCMP, QuikSCAT and buoy winds along the Iberian Peninsula coast



D. Carvalho^{a,*}, A. Rocha^a, M. Gómez-Gesteira^b, I. Alvarez^b, C. Silva Santos^c

^a CESAM — Department of Physics, University of Aveiro, Campus Universitário de Santiago, 3810–193 Aveiro, Portugal

^b EPHYSLAB — Environmental Physics Laboratory, Facultad de Ciencias, Universidad de Vigo, 32004 Ourense, Spain

^c Instituto Superior de Engenharia do Porto, Rua Dr. António Bernardino de Almeida 341, 4200–072 Porto, Portugal

ARTICLE INFO

Article history:

Received 18 March 2013

Received in revised form 29 May 2013

Accepted 3 June 2013

Available online 24 July 2013

Keywords:

Cross-Calibrated Multi-Platform Ocean Wind (CCMP)

QuikSCAT

Ocean surface wind

Offshore wind power

Iberian Peninsula

Galician coast

Gulf of Cádiz

ABSTRACT

Ocean surface wind data derived from several QuikSCAT products and the Cross-Calibrated Multi-Platform (CCMP) project were compared to wind speed and direction measurements, in order to assess which one of these databases has higher accuracy and ability to describe the local wind regime characteristics. For this, data from QuikSCAT (swath data from L2B 25 km and L2B 12.5 km slice composites, together with gridded L3) and CCMP were compared with measurements taken from five buoys located along the Iberian Peninsula coast.

The results presented in this work show that QuikSCAT products have their strength in representing the temporal variability of the wind speed (higher correlation coefficients and lower RMSE and STDE) and the mean state of the wind direction (lower biases). Although no major differences were detected among QuikSCAT products, the high-resolution database (12.5 km) was the one with the best overall scores. However, CCMP is able to bring significant improvements in terms of wind direction temporal variability and wind speed mean state. CCMP also showed its capability to partially mitigate some of QuikSCAT's known problems, mainly those related to QuikSCAT systematic tendency to overestimate the wind speed and land masking effects. In addition, CCMP consists in a gridded dataset with a higher temporal sampling and complete data availability when compared to QuikSCAT, allowing this database to be clearly the one with a better ability to characterize the wind regimes measured by the buoys in terms of wind speed frequency distributions.

These features can render CCMP an interesting ocean wind database for offshore wind energy assessment studies, where wind speed mean state accuracy plays the key role, and also for meteorological, oceanic and climate modelling applications where gridded wind data with good temporal sampling and data availability is vital to force numerical simulation models.

© 2013 Elsevier Inc. All rights reserved.

1. Introduction

The knowledge of the surface wind fields over the ocean is a key factor for a wide set of academic and industrial activities (Carvalho, Rocha, Gómez-Gesteira & Santos, 2012; Risien & Chelton, 2006). Ocean surface wind data (typically defined at 10 m above sea surface level) is crucial in climatic, meteorological and oceanographic studies in order to build ocean surface climatologies (Atlas, Ardizzone, & Hoffman, 2008; Atlas, Hoffman, Ardizzone, Leidner, & Jusem, 2009) and to run atmospheric/oceanic models, being one of the main parameters to realistically describe the oceanic forcing fields, air-sea interactions, and oceanic and atmospheric circulation regimes. Errors in the representation of the local wind field will distort the model forcing processes and can have a severe influence in the oceanic and atmospheric modelling results (Myers, Haines, & Josey, 1998; Ruti,

Marullo, D'Ortenzio, & Tremant, 2008). Furthermore, accurate ocean wind data is presently very valuable in the context of offshore wind energy resource assessment and offshore wind power production estimates, whose growth entered an exponential stage during the last decade and rely on an accurate knowledge of the local wind resource in terms of both wind speed and direction. Therefore, it is crucial to use accurate inputs of wind speed in wind resource assessment, as the predicted power is proportional to the cube of the wind speed.

Data regarding ocean surface wind typically comes in the form of observations (from buoys, ships, etc.), usually taken at a single point and/or in a limited time window. Due to their high spatial and temporal variability, these observations may not be representative of the wind regime over a medium/large spatial area and/or time span (Risien & Chelton, 2006). Moreover, these measurements are currently very sparse, both in time and space, and often suffer from long periods of missing and/or invalid data. Therefore, observational data is insufficient to accurately describe localized wind regimes in ocean areas. This lack of reliable, space and time consistent and representative ocean surface wind information, together with the growing need to have a preliminary knowledge of the ocean wind fields, raises the

* Corresponding author. Tel.: +351 234 370 356; fax: +351 234 378197.

E-mail addresses: david.carvalho@ua.pt (D. Carvalho), alfredo.rocha@ua.pt (A. Rocha), mggesteira@uvigo.es (M. Gómez-Gesteira), ialvarez@uvigo.es (I. Alvarez), cmi@isep.ipp.pt (C. Silva Santos).

importance of investigating alternative ocean surface wind databases. In the recent past, the development of satellite-derived wind data allowed for the first time the observation of the ocean surface wind field on a near-global scale showing their utility in the ocean surface wind assessment, both for climatic studies and offshore wind energy projects (Hasager et al., 2007). Until now, the best results have been obtained with scatterometers that consist in microwave radars that derive the sea surface wind field from sea surface roughness. Among the several existent scatterometers, the NASA SeaWinds scatterometer installed aboard the QuikSCAT satellite platform (henceforth simply referred to as QuikSCAT) is one of the most popular in terms of ocean wind data sources. A considerable number of studies have been performed aiming to assess the accuracy of QuikSCAT derived wind data, mainly in terms of comparison with measured winds (eg: Ebuchi, Graber, & Caruso, 2002; Moore, Pickart, & Renfrew, 2008; Penabad et al., 2008; Pensieri, Bozzano, & Schiano, 2010; Pickett, Tang, Rosenfeld, & Wash, 2003; Ruti et al., 2008; Sánchez et al., 2007; Satheesan, Sarkar, Parekh, Ramesh Kumar, & Kuroda, 2007; Tang, Liu, & Stiles, 2004). These studies concluded the success of QuikSCAT in achieving its mission requirements, proving its utility in climatic, meteorological, oceanographic and offshore wind resource assessment studies.

However, QuikSCAT performance is known to be highly affected by the presence of heavy rain (above $2.0 \text{ km.mm.hr}^{-1}$) that artificially increases the surface roughness (Portabella & Stoffelen, 2001), which disturbs the backscatter parameter resulting in a misrepresentation of the real wind vectors (overestimation of the surface winds and wind direction alignment across the swath). Moreover, the geophysical model function developed for NSCAT (Wentz & Smith, 1999) has been adjusted for SeaWinds (Lungu, 2001). The model function is the most accurate for wind speeds in the range $5\text{--}12 \text{ m.s}^{-1}$. Therefore, QuikSCAT data quality is highly diminished in the presence of low winds (below 5 m.s^{-1}), because low wind speeds produce little, or none at all, backscatter and under these conditions the ocean surface acts more like a smooth reflector than a scatterer, becoming difficult to accurately predict the wind vectors. Furthermore, strong winds (above 25 m.s^{-1}) are generally underestimated due to the ocean surface roughness threshold. In addition to these limitations, QuikSCAT shows a 25–30 km land masking effect that negatively affects the representation of the spatial and temporal variability of coastal winds (Furevik, Sempreviva, Cavaleri, Lefèvre, & ransericci, 2010). Finally, QuikSCAT mission ended in November 23, 2009 due to problems with the SeaWinds equipment. After this date, there is no ocean surface wind data available from QuikSCAT.

The recently released Cross-Calibrated Multi-Platform Ocean Surface Wind Vectors (CCMP) clearly appears as an interesting and promising alternative/complement to QuikSCAT (and other satellites) ocean surface wind data source. This database uses as background a first guess analysis of U and V gridded wind vectors and then assimilates multiple sources of observed data (satellites, ships, buoys, etc.), all combined in a 6-hourly globally gridded analysis of ocean surface winds. Due to the amount of data included in the CCMP grid, together with the quality control of all the assimilated data and a globally gridded first guess background, it is expected that CCMP can improve, at least to some extent, the abovementioned QuikSCAT limitations. However, as far as we know, there is no published literature that compares CCMP data, either with conventional measurements (buoy, ship, etc.) or with other sources of satellite-derived ocean wind data (namely QuikSCAT), nor literature that validates and explores CCMP data in terms of their quality and eventual limitations.

The aim of this paper is to assess and compare the performance of QuikSCAT and CCMP derived ocean surface wind data in terms of its accuracy, comparing them with ocean surface wind measurements collected by buoys located along the Iberian Peninsula coast (Galician coast and Gulf of Cádiz). This comparison will allow the assessment of which one of these ocean surface wind data sources describes more

accurately the local wind regime at the selected buoy locations. To achieve this goal, one complete year (in the present case, 2008) of wind measurements from four buoys located in the West and North Galician coast and one buoy placed at the Gulf of Cádiz will be compared to the same period of wind data from QuikSCAT and CCMP.

2. Data and methodology

2.1. Satellite wind data

2.1.1. QuikSCAT Ocean Surface Wind Vectors

The NASA SeaWinds scatterometer, aboard the QuikSCAT satellite platform, is an active microwave scatterometer that measures wind vectors at a height of 10 m above sea level (a.s.l.) at neutral air-sea stability conditions (Chelton & Freilich, 2005). Detailed description and information regarding these equipments can be found in Hoffman and Leidner (2005), and also in NASA's Jet Propulsion Laboratory Physical Oceanography Distributed Active Archive Centre (PO.DAAC) website (<http://podaac.jpl.nasa.gov/OceanWind/QuikSCAT>).

QuikSCAT wind products are available in three different levels that differ in the degree of data processing: Level 1B, Level 2A & 2B and Level 3. For a detailed description about the differences between these products, the reader is referred to Dunbar et al. (2006). The Level 2B (L2B) swath data and the Level 3 (L3) gridded data are the QuikSCAT products most often used by the scientific community. The L2B products are the most refined ones, while the L3 dataset is gridded, making it a standard product that can easily be used in many scientific applications, especially in oceanographic studies (Pensieri et al., 2010; Ruti et al., 2008). L2B products are made available by PO.DAAC in two different forms: the L2B ocean wind vectors in 25 Km swath, and the L2B ocean wind vectors in 12.5 km slice composites. For the latter, its increased sampling resolution enables users to obtain wind vectors 10 km closer to shore when compared to the L2B 25 km dataset, reducing the distance of valid measurements from the coastline and making this product of particular interest in studying near-shore ocean winds. In the published literature, only the study performed by Sharma and D'Sa (2008) compared the different QuikSCAT products used in this work (L2B 25 km, L2B 12.5 km and L3), concluding that the L2B products indicated a better accuracy than the L3. The QuikSCAT L2B 25 km data used in this work is described and available at (http://podaac.jpl.nasa.gov/dataset/QSCAT_LEVEL_2B_V2), the L2B 12.5 km at (http://podaac.jpl.nasa.gov/dataset/QSCAT_LEVEL_2B_COMP_12) and the L3 at (http://podaac.jpl.nasa.gov/dataset/QSCAT_LEVEL_3_V2). According to Hoffman and Leidner (2005), a careful quality control is vital mainly to what is related to data affected by rain and by ambiguity removal issues. As for ambiguity removal issues, the L2B products include two additional scientific datasets: the "wind speed selection" and the "wind dir selection", which contain the final output of the wind retrieval/ambiguity removal processing using the Direction Interval Retrieval with Threshold Nudging (DIRTH) algorithm. These two datasets were used in this study, and furthermore all QuikSCAT data marked with rain flags or as null/invalid were discarded.

2.1.2. CCMP Ocean Surface Wind Vectors

This dataset was derived under the CCMP project and provides a consistent, gap-free long-term time-series of ocean surface wind vector analysis fields from July 1987 through June 2011. It consists of a 6-hourly gridded ocean surface winds analysis, with a spatial resolution of $0.25 \times 0.25^\circ$ in latitude and longitude. CCMP uses as a starting estimate (or background) field the ECMWF Reanalysis (ERA-40) for July 1987 until December 1998, and the ECMWF Operational Analysis from January 1999 onward. CCMP includes cross-calibrated satellite winds obtained from TRMM TMI, QuikSCAT, QuikSCAT (SeaWinds), WindSat, SSM/I, SSMIS, AMSR-E and other satellites. All the considered wind data are referenced to a height of 10 m a.s.l. considering neutral

air-sea stability conditions. Detailed information about this dataset can be found on Atlas et al. (2011).

The CCMP Level 3 dataset used in this work, which has been extensively validated by the NASA's Ocean Vector Winds Science Team, is described and available at the NASA's Jet Propulsion Laboratory PO.DAAC website (http://podaac.jpl.nasa.gov/dataset/CCMP_MEASURES_ATLAS_L4_OW_L3_0_WIND_VECTORS_FLK). CCMP records include the 12 A.M., 6 A.M., 12 P.M. and 6 P.M. time instants.

2.2. Measured wind data

Measured wind data taken from five oceanographic buoys moored off the Galician northern and western coast and the Gulf of Cádiz were considered. These buoys, depicted in Fig. 1, are operated by the Puertos del Estado Spanish Agency and Table 1 presents their main characteristics. These five buoys measure hourly wind speed and direction at 3 m a.s.l. The datasets of the five considered buoys cover the period from January 1, 2008 to December 31, 2008.

Fig. 1 and Table 1 show that some of the buoys are placed in the vicinity of the satellite shadow area (25–30 km), being the Peñas buoy the only one located clearly inside this area while the remaining buoys are located outside this zone.

Table 1
Main characteristics of the considered buoys.

Station	Latitude	Longitude	Distance to coast
Peñas	43° 45' N	6° 9' 36" W	~20 km
Bares	44° 3' 54" N	7° 37' 5" W	~32 km
Villano	43° 30' N	9° 12' 36" W	~30 km
Silleiro	42° 7' 48" N	9° 23' 24" W	~40 km
Cádiz	36° 28' 37" N	36° 28' 37" N	~55 km

As pointed in Sections 2.1.1 and 2.1.2, QuikSCAT and CCMP winds consist in equivalent neutrally stable winds. These remotely retrieved winds are mainly from microwave sensors (radiometer, altimeter and scatterometer), which are sensitive to the ocean surface roughness than the wind speed due to atmospheric stratification. Therefore, these sensors are calibrated to an equivalent neutral wind at a reference height of 10 m above sea surface (Liu & Tang, 1996; Singh, Parekh, & Attada, 2013; Verschell, Bourassa, Weissman, & O'Brien, 1999). These equivalent neutral winds are the winds that would exist if the atmospheric boundary layer is neutrally stratified (Chelton, Schlax, Freilich, & Milliff, 2004), while the measured winds are collected at 3 m a.s.l. and they are stability-dependent. Therefore, to compare buoy measurements with QuikSCAT and CCMP, the buoy wind speeds need to be

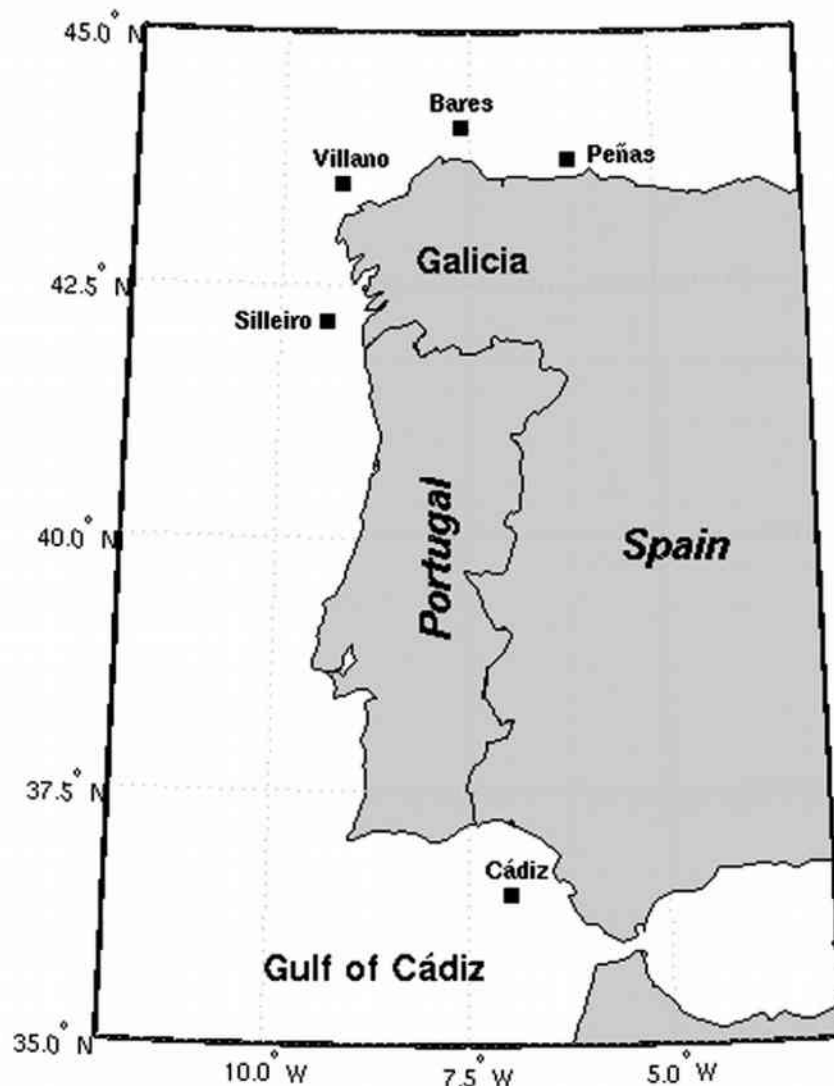


Fig. 1. Area under scope. The Iberian Peninsula with the position of the buoys.

converted to equivalent neutral winds at a height of 10 m a.s.l. To perform an extrapolation of real stability-dependant winds to equivalent neutral winds, one of the most accurate methods is the one proposed by Liu and Tang (1996), which takes into account the effects due to differences in the atmospheric stability. However, this requires the knowledge of air and sea surface temperatures, pressure and relative humidity. Since the whole of these data are not available for the buoys considered here, the logarithmic method proposed by Peixoto and Oort (1992) will be used to extrapolate the buoy winds from 3 to 10 m a.s.l. This method, which does not include effects due to differences in atmospheric stability, provides the wind speed at a height z following:

$$U_z = (U_{z_m}) * \ln\left(\frac{Z}{Z_0}\right) / \ln\left(\frac{Z_m}{Z_0}\right) \quad (1)$$

In this expression, U_z is the wind speed at a height z , z_m is the measurement height and z_0 is the roughness length. A typical oceanic value for z_0 of 1.52×10^{-4} m can be assumed, according to Peixoto and Oort (1992). In the impossibility of using the most accurate method to extrapolate the 3 m a.s.l. measured winds to 10 m a.s.l. equivalent neutrally stable ones (the method proposed by Liu & Tang, 1996), it becomes important to assess the possible differences between these two methods, which basically differ in if whether they account or not for the effects due to differences in atmospheric stability. Mears et al. (2001) made a comprehensive and detailed analysis on the differences in using the Liu and Tang (1996) or the logarithmic method in converting stability-dependant measured buoy winds from 3 m a.s.l. to equivalent neutrally stable winds at 10 m a.s.l., considering several buoys scattered around the world and several years. It was concluded in this study that the Liu and Tang (1996) correction is typically a few tenths of a meter per second higher (the study reports an average value of 0.12 m.s^{-1}) than the logarithmic correction. Under unstable conditions, the Liu and Tang (1996) corrected winds are higher than logarithmic corrected winds, and for stable conditions the opposite is seen. For neutral conditions, they are the same. Therefore, the positive mean difference of 0.12 m.s^{-1} of the Liu and Tang (1996) corrected winds relatively to the logarithmic corrected ones are due to the fact that over most of the global ocean there is a tendency for the atmospheric boundary layer to be neutral/slightly unstable. Also Ruti et al. (2008) made a more simple comparison between these two methods, concluding that the main difference between these two methods is observed only in the presence of strong winds (typically above 15 m.s^{-1}). Even in these conditions, the logarithmic wind extrapolation differs from the Liu and Tang (1996) one by less than 0.5 m.s^{-1} . Given this, it is then possible to assume that the application of the logarithmic method will not introduce significant errors. Considering the extrapolated winds to 10 m a.s.l., the local wind regimes described by each buoy for the year of 2008 are presented in Carvalho, Rocha and Gómez-Gesteira (2012). In this study, it is visible that these coastal winds tend to follow the local topography. These tendencies were reported for the Galician coast by Alvarez, Gomez-Gesteira, deCastro, and Dias (2008); Alvarez, Gomez-Gesteira, deCastro, Gomez-Gesteira, and Dias (2010) and Gómez-Gesteira, Moreira, Alvarez, and deCastro (2006), and for the Gulf of Cádiz by Jungclaus and Mellor (2000), and Peliz, Dubert, Marchesiolo, and Teles-Machado (2007).

2.3. Error statistical and comparative analysis

In the present study, two distinct kinds of comparisons were performed. First, a statistical analysis was conducted focusing on record-by-record accuracy of the several databases, considering only the simultaneous and valid records shared by all databases. QuikSCAT satellite follows a sun-synchronous orbit producing two records per day (corresponding to the ascending and descending passes, in UTC time reference), CCMP provides four records per day (corresponding to the hours UTC 0, 6, 12 and 18 of each day) and the buoys measure

the wind on an hourly basis (also using UTC reference). Analyzing QuikSCAT L2B and L3 valid wind data for the locations under study, it was seen that about 90% of their records correspond to 6 A.M. (ascending pass) and 6 P.M. (descending pass). Therefore, for this comparison only the 6 A.M and 6 P.M. records of the buoys, CCMP and QuikSCAT were selected, in order for all datasets will share the same temporal collocation and sampling rate. This analysis, presented in Sections 3.1 and 3.2, assesses the quality of the simultaneous records, both in terms of spatial and temporal accuracy. In Section 3.1, several statistical parameters were considered. The three most common statistical parameters were used to evaluate the wind data: the Root Mean Squared Error (RMSE),

$$RMSE = \left[\frac{1}{N} \sum_{i=1}^N (\theta_i')^2 \right]^{1/2} \quad (2)$$

where

$$\theta_i' = \theta_i^x - \theta_i^{obs} \quad (3)$$

represents the deviation between the QuikSCAT/CCMP wind speed (θ^x) and the respective observed wind speed in the buoy (θ^{obs}), being N the total number of pairs of simulation/observed records. For the wind direction, which is a circular variable and not a linear one, θ' takes a different expression because the absolute deviation of the wind direction cannot exceed 180° in module. For this case, θ' is given by

$$\theta_i' = (\theta_i^x - \theta_i^{obs}) * \left[1 - 360 / |\theta_i^x - \theta_i^{obs}| \right], \text{ if } |\theta_i^x - \theta_i^{obs}| > 180^\circ \quad (4)$$

The bias, defined as

$$Bias = \frac{1}{N} \sum_{i=1}^N \theta_i' \quad (5)$$

And the Standard Deviation of the Error (STDE), given by

$$STDE = \sigma(\theta_i') = \left[RMSE^2 - Bias^2 \right]^{1/2} \quad (6)$$

Furthermore, also the correlation coefficient (R^2) between QuikSCAT/CCMP data and observed records was used. While the RMSE, STDE and R^2 mainly assess if the QuikSCAT/CCMP data is able to represent the observed winds with temporal accuracy (this is, in accurately representing the temporal variability of the wind), the bias evaluates the data tendency and is more related to differences in the mean state of the wind field, this is, if QuikSCAT/CCMP data have a tendency to over/underestimate the measured wind speed/direction. In addition to the aforementioned statistical analysis, QuikSCAT and CCMP wind speed/direction error dependence with the observed wind speed/direction was also assessed. These results will be presented in Section 3.2, and the aim of this section is to conclude if the error associated to the satellite derived wind data is related to a particular wind speed/direction.

Second, in Section 3.3 a different analysis will be performed. This section aims to assess which one of the databases is able to offer a characterization of the buoys local wind regimes closer to reality. The closest characterization of the buoys local wind regimes is offered, obviously, by the buoy measurements. Not only because of the fact that the buoys measure the real wind, but also because the anemometers installed in the buoys measure the wind every hour. In order to assess which one of the databases (QuikSCAT or CCMP) provides the characterization of the local wind regimes closest to the real one (described by buoy measurements), all the valid data records of each one of the databases will be considered instead of just simultaneous records as in Sections 3.1 and 3.2. In order to evaluate QuikSCAT and CCMP ability to describe the buoy locations local wind regimes, in what is related to the wind speed

(U), Weibull probability density functions (PDF's) will be used. The use of Weibull PDF in QuikSCAT derived wind speed analysis was performed by, as an example, Liu, Tang, and Xie (2008). The Weibull PDF, $W_{(U)}$, is provided by (10), where A and k represent the Weibull PDF parameters:

$$W_{(U)} = \frac{k}{A} \left(\frac{U}{A}\right)^{k-1} e^{-\left(\frac{U}{A}\right)^k} \tag{7}$$

and the most probable value of U (U_{prob}) can be calculated from the first derivative of Eq. (7):

$$U_{prob} = A \left(\frac{k-1}{k}\right)^{1/k} \tag{8}$$

In this section, the temporal accuracy of the databases will not be reflected in the results, since they are presented in terms of a cumulative frequency distribution that does not reflect temporal coherence. A more detailed description about these equations and statistical methodology can be found on Carvalho et al. (2012).

The closest QuikSCAT L3 and CCMP grid points to the buoy locations were selected. For the L2B swath data, which do not consist in gridded data and each individual swath may or may not contain the buoy locations, it was also considered the closest point to the buoy locations at a maximum distance of 25 km, for the L2B 25 km database, and 12.5 km, for the L2B 12.5 km product.

3. Results and discussion

3.1. Statistical comparison

In this section, the RMSE, Bias, STDE and R^2 are computed between the buoys and the respective QuikSCAT and CCMP data. Table 2 displays the results, where N is the number of simultaneous and valid pairs of 6 A.M. and 6 P.M. records between QuikSCAT L2B 25 km (designated as QL2B-25), QuikSCAT L2B12.5 km (designated as QL2B-12.5), QuikSCAT L3 (designated as QL3), CCMP and the respective buoy.

Considering the average error values for all stations, weighted by the number of records at each station, it is visible that for the wind speed all QuikSCAT databases showed higher R^2 , lower RMSE and

STDE when compared to CCMP, which clearly showed the lowest bias. Among QuikSCAT databases, and although no major differences were found, the L2B-12.5 was the one with the best overall scores in terms of RMSE and STDE, being that the lowest bias was obtained with QL2B-25. For the wind direction, the opposite is seen: CCMP presents the highest R^2 , lowest RMSE and STDE, while QL2B-12.5 presented the lowest bias. These obtained values of RMSE and Bias for QuikSCAT databases are in line with the scores obtained in the studies referenced in Section 1 (Ebuchi et al., 2002; Moore et al., 2008; Penabad et al., 2008; Pensieri et al., 2010; Pickett et al., 2003; Ruti et al., 2008; Sánchez et al., 2007; Satheesan et al., 2007; Tang et al., 2004). According to these error scores, QuikSCAT products showed the lowest errors in what is related to the representation of the temporal variability of the wind speed (higher R^2 , lower RMSE and STDE) and the mean state of the wind direction (lower biases). However, CCMP clearly shows the best results in terms of wind direction temporal variability and wind speed mean state. CCMP uses as a first guess reanalysis and analysis fields with a resolution coarser than its own data (both the ERA-40 reanalysis and ECMWF operational analysis are available at a horizontal resolution of around 1°, both in latitude and longitude). This can introduce a kind of “phase lag” on CCMP data, due to eventual interpolation errors from the coarse first guess fields to the finer CCMP resolution (0.25° both in latitude and longitude).

For all QuikSCAT databases the weighted mean biases for the wind speed are positive, and even analyzing the wind speed bias scores for each buoy individually they are always positive, showing a tendency for QuikSCAT to overestimate the wind speed. For CCMP the weighted mean bias and the individual biases for each buoy are relatively small, but also with a positive signal. The exception is for Silleiro buoy, where CCMP shows a negative bias. For the wind direction, there is a tendency for the biases to be negative in the Northern Galician coast (Peñas, Bares and Villano) indicating an anti-clockwise deviation, and positive for the Western Galician coast (Silleiro) and Gulf of Cádiz, indicating a clockwise wind rotation. This feature for the wind direction is common to both QuikSCAT and CCMP databases.

One important aspect to report is that wind direction errors are significantly higher than the wind speed ones. Scatterometer wind vectors are relative to the local ocean current (e.g.: Cornillon & Park, 2001), whereas measured winds are earth-relative. Therefore, the

Table 2
Statistics of the comparison between QuikSCAT, CCMP and buoy wind data.

Station	Dataset	RMSE		Bias		STDE		R^2		N
		Speed (m.s ⁻¹)	Direction (°)							
Peñas	QL2B-12.5	2.42	54.86	1.21	-0.96	2.10	54.85	0.85	0.58	144
	QL2B-25	2.10	59.41	0.87	-8.49	1.91	58.80	0.88	0.60	
	QL3	2.10	59.83	0.88	-9.21	1.91	59.12	0.88	0.61	
	CCMP	2.05	51.06	0.04	-2.74	2.05	50.99	0.83	0.70	
Bares	QL2B-12.5	1.13	44.60	0.22	-12.93	1.11	42.68	0.96	0.73	138
	QL2B-25	1.29	37.50	0.34	-12.28	1.24	35.43	0.95	0.81	
	QL3	1.29	37.08	0.33	-12.01	1.25	35.08	0.95	0.79	
	CCMP	1.54	36.31	0.04	-8.35	1.54	35.34	0.92	0.82	
Villano	QL2B-12.5	1.40	44.87	0.50	2.79	1.31	44.78	0.94	0.84	178
	QL2B-25	1.41	40.30	0.60	-1.97	1.28	40.25	0.95	0.86	
	QL3	1.48	40.12	0.59	-0.79	1.36	40.11	0.94	0.86	
	CCMP	1.49	40.81	0.13	1.04	1.48	40.80	0.92	0.89	
Silleiro	QL2B-12.5	1.32	57.71	0.26	4.83	1.29	57.51	0.95	0.67	125
	QL2B-25	1.52	57.62	0.15	7.02	1.51	57.19	0.92	0.68	
	QL3	1.45	58.92	0.10	4.90	1.45	58.72	0.93	0.67	
	CCMP	1.41	47.36	-0.08	-1.65	1.41	47.33	0.93	0.78	
Cádiz	QL2B-12.5	1.13	54.80	0.32	1.32	1.08	54.78	0.96	0.63	118
	QL2B-25	1.31	49.35	0.35	9.08	1.26	48.51	0.95	0.73	
	QL3	1.34	49.13	0.59	8.45	1.20	48.40	0.95	0.74	
	CCMP	1.64	42.93	0.08	4.43	1.64	42.70	0.90	0.81	
Weighted average	QL2B-12.5	1.50	50.81	0.52	-0.95	1.39	50.37	0.93	0.70	-
	QL2B-25	1.53	48.26	0.48	-1.88	1.44	47.50	0.93	0.74	
	QL3	1.54	48.42	0.51	-2.15	1.44	47.72	0.93	0.74	
	CCMP	1.63	43.55	0.05	-1.49	1.62	43.29	0.90	0.80	

wind direction measured by the scatterometer can differ from the measured wind direction. For these reasons, the errors are expected to be larger in scatterometer estimates of wind direction than of wind speed (Chelton & Freilich, 2005). Also in QuikSCAT wind speed estimation this issue has a non negligible effect: for example, an 8 m.s^{-1} wind over a 1 m.s^{-1} ocean current, both flowing in the same direction, appears to the scatterometer as a 7 m.s^{-1} wind since it is the wind relative to the surface that generates the capillary waves (Hoffman & Leidner, 2005). However, considering that the ocean currents are typically much slower than surface winds, it is not expected that this issue will introduce large errors in the data.

One striking feature is that all the wind speed statistical scores (RMSE, Bias, STDE and R^2) are clearly worst for Peñas buoy. Note that this buoy is the one closest to the shore and the only one located inside QuikSCAT's coastal masking area, indicating that this can be related with the scatterometers known issues in representing coastal winds due to land contamination effects. The remaining buoys, which are located outside this zone, show significant lower wind speed errors when compared to Peñas. An interesting fact is that CCMP is able to partially mitigate these problems, mainly in what is related to the bias, since on this statistic this database shows clearly better results than QuikSCAT. Moreover, CCMP bias scores for Peñas are similar to the remaining buoys, which imply that land masking effects have less impact in CCMP. Focusing on QuikSCAT databases, it would be expected that the increased resolution of QL2B-12.5 could bring improvement to the results, in particular at those buoys closest to shore. Although this is true, due to the fact that QL2B-12.5 is the one with the lowest average errors among QuikSCAT databases for the wind speed (the only exceptions is for the bias), for the buoy closest to shore (Peñas), QL2B-12.5 is the database with the worst error scores for the wind speed.

3.2. Satellite-derived wind data error dependence on measured wind speed and direction

In this section, an analysis of the QuikSCAT and CCMP error variation with the wind speed bin and wind direction sector is presented, making use of two different comparisons. Firstly, an analysis of the

QuikSCAT and CCMP wind speed and direction RMSE and Bias variation with the buoy wind speed is performed. This comparison will show whether or not QuikSCAT and CCMP wind speed and direction errors vary with the measured wind speed. This approach is important to assess QuikSCAT performance in the presence of different wind speeds, and to observe if CCMP is able to overcome QuikSCAT limitations in the presence of low and strong winds. Secondly, a similar analysis is performed but now analyzing if QuikSCAT and CCMP wind speed and direction RMSE and Bias vary with the buoy wind direction. Tables 3 and 4 show the obtained results for the first described comparison, in which four buoy wind speed bins were considered: wind speeds below 4 m.s^{-1} , between 4 and 8 m.s^{-1} , between 8 and 12 m.s^{-1} and above 12 m.s^{-1} .

Taking into account the results displayed in Table 3, globally there is a tendency for QuikSCAT errors to be higher in the presence of low (below 4 m.s^{-1}) and strong (above 12 m.s^{-1}) wind speeds. This was expected, due to the scatterometers know problems in the presence of low and strong wind speeds. Moreover, the errors are significantly higher for strong wind speeds than for low wind speeds. CCMP shows the highest errors for strong wind speeds, while the lowest are seen for low wind speeds, mainly in terms of RMSE. The higher errors for strong wind speeds, present in both QuikSCAT and CCMP data, can also be related to the fact that this type of winds represents bad weather situations, which will cause buoy displacing and movements, associated to high ocean waves and also surface layer distortion (Ebuchi et al., 2002; Large, Morzel, & Crawford, 1995). For this reason not only satellite-derived wind data but also buoy measurements of strong wind speeds must be considered with caution.

Also visible in these results is QuikSCAT systematic wind speed overestimation, clear in the weighted average values of the bias for all wind speed bins, and especially for low and high wind speeds. QuikSCAT positive bias in low wind speeds was also observed in previous works in the Pacific (Ebuchi et al., 2002) and Indian Ocean (Satheesan et al., 2007) indicating that QuikSCAT performance is substantially degraded in the presence of low wind speeds, mainly due to QuikSCAT difficulty in accurately measure the small amount of backscatter produced by these weak winds. Contrarily to what is seen for QuikSCAT, CCMP does not show any clear over or underestimation

Table 3
Statistics of the comparison between QuikSCAT and CCMP wind speed error per buoy wind speed bin.

Wind speed bins		<4 m.s ⁻¹			4-8 m.s ⁻¹			8-12 m.s ⁻¹			>12 m.s ⁻¹		
Station	Database	RMSE (m.s ⁻¹)	Bias (m.s ⁻¹)	N	RMSE (m.s ⁻¹)	Bias (m.s ⁻¹)	N	RMSE (m.s ⁻¹)	Bias (m.s ⁻¹)	N	RMSE (m.s ⁻¹)	Bias (m.s ⁻¹)	N
Peñas	QL2B-12.5	2.64	1.91	53	2.21	1.08	53	1.67	0.00	28	3.66	1.59	10
	QL2B-25	2.07	1.22		2.14	0.97		1.50	-0.25		3.23	1.65	
	QL3	2.08	1.23		2.14	0.97		1.50	-0.27		3.19	1.70	
	CCMP	2.32	1.07		1.78	0.13		2.12	-1.61		1.64	-1.31	
Bares	QL2B-12.5	1.31	0.69	39	0.93	-0.01	44	0.97	0.02	42	1.60	0.21	13
	QL2B-25	1.29	0.43		1.37	0.25		1.10	0.24		1.52	0.73	
	QL3	1.29	0.44		1.37	0.25		1.12	0.20		1.53	0.73	
	CCMP	1.40	0.60		1.48	-0.06		1.15	-0.24		2.75	-0.40	
Villano	QL2B-12.5	1.39	0.80	53	1.33	0.38	56	1.35	0.22	49	1.71	0.72	20
	QL2B-25	1.39	0.83		1.19	0.31		1.48	0.52		1.77	1.03	
	QL3	1.52	0.90		1.21	0.29		1.58	0.46		1.75	0.90	
	CCMP	1.38	0.73		1.59	0.11		1.50	-0.40		1.48	-0.04	
Silleiro	QL2B-12.5	1.19	0.40	63	1.20	0.19	30	1.57	-0.20	23	1.83	0.71	9
	QL2B-25	1.43	0.41		1.62	0.24		1.44	-0.45		1.87	-0.38	
	QL3	1.44	0.40		1.31	0.07		1.43	-0.50		1.87	-0.36	
	CCMP	0.97	0.33		1.35	-0.11		1.76	-0.90		2.63	-0.74	
Cádiz	QL2B-12.5	1.05	0.49	48	1.08	0.22	39	1.29	0.01	22	1.35	0.63	9
	QL2B-25	1.02	0.27		1.15	0.28		1.92	0.33		1.43	1.09	
	QL3	1.22	0.70		1.35	0.53		1.52	0.35		1.44	0.80	
	CCMP	1.46	0.70		1.56	-0.14		2.03	-1.03		1.80	0.38	
Weighted average	QL2B-12.5	1.52	0.86	-	1.40	0.42	-	1.33	0.04	-	1.97	0.74	-
	QL2B-25	1.46	0.64		1.50	0.44		1.44	0.16		1.92	0.87	
	QL3	1.52	0.74		1.50	0.46		1.42	0.12		1.91	0.79	
	CCMP	1.49	0.68		1.58	0.01		1.62	-0.72		1.99	-0.37	

Table 4
Statistics of the comparison between QuikSCAT and CCMP wind direction error per buoy wind speed bin.

Wind speed bins		<4 m.s ⁻¹			4-8 m.s ⁻¹			8-12 m.s ⁻¹			>12 m.s ⁻¹		
Station	Database	RMSE (°)	Bias (°)	N	RMSE (°)	Bias (°)	N	RMSE (°)	Bias (°)	N	RMSE (°)	Bias (°)	N
Peñas	QL2B-12.5	78.75	1.00	53	40.40	0.94	53	21.75	-11.43	28	22.27	7.90	10
	QL2B-25	83.20	-14.83		42.23	-9.85		37.35	-2.07		27.90	14.30	
	QL3	84.07	-16.55		42.08	-9.94		37.38	-2.29		28.03	14.20	
	CCMP	71.44	-6.19		40.69	-0.36		16.52	-7.54		30.90	16.40	
Bares	QL2B-12.5	79.04	-32.33	39	20.98	-4.91	44	15.50	-6.76	42	10.52	-1.85	13
	QL2B-25	64.15	-22.05		20.85	-9.68		17.08	-8.79		12.84	-3.08	
	QL3	63.32	-20.28		20.84	-10.00		16.97	-9.17		12.83	-3.15	
	CCMP	62.44	-15.15		20.84	-5.84		13.98	-6.05		14.03	-3.85	
Villano	QL2B-12.5	72.38	6.53	53	34.21	3.80	56	15.46	-1.73	49	13.01	1.10	20
	QL2B-25	65.20	-8.17		29.02	1.98		15.53	-1.76		15.60	2.85	
	QL3	63.14	-2.83		31.63	1.30		16.94	-2.71		15.97	3.50	
	CCMP	65.76	4.17		30.78	-1.63		14.93	0.47		12.79	1.65	
Silleiro	QL2B-12.5	72.84	9.62	63	50.01	0.57	30	16.18	-3.04	23	10.50	5.67	9
	QL2B-25	68.58	8.30		60.48	12.93		16.65	-2.48		16.83	2.56	
	QL3	71.07	4.21		59.59	13.03		16.90	-2.87		16.73	2.44	
	CCMP	56.55	-4.06		49.12	3.20		15.31	-3.00		11.12	2.56	
Cádiz	QL2B-12.5	82.81	-3.04	48	22.86	4.69	39	13.57	3.59	22	9.56	4.44	9
	QL2B-25	69.72	11.00		35.13	12.54		15.91	2.41		6.11	0.22	
	QL3	68.89	10.33		36.04	11.95		16.53	2.14		6.20	-1.33	
	CCMP	61.48	5.54		26.69	5.36		18.48	3.23		9.00	-2.56	
Weighted average	QL2B-12.5	76.78	-1.57	-	33.21	1.11	-	16.39	-4.14	-	13.12	2.75	-
	QL2B-25	70.45	-4.02	-	35.88	0.18	-	19.86	-3.15	-	15.81	3.03	-
	QL3	70.53	-4.13	-	36.54	-0.17	-	20.38	-3.66	-	15.95	2.97	-
	CCMP	63.36	-2.69	-	32.94	-0.28	-	15.49	-2.68	-	15.22	2.41	-

tendency for the wind speed, but it appears to show a tendency to overestimate wind speeds below 4 m.s⁻¹ (positive biases) and to underestimate wind speeds above 8 m.s⁻¹ (negative biases).

Table 4 shows the same comparison as Table 3, but now for the satellite-derived wind direction error for each measured wind speed bin.

The most striking feature in Table 4 information is that, in terms of RMSE, wind direction errors are much higher for low wind speeds, but they significantly decrease with increasing wind speed. This is also a reported issue of QuikSCAT wind data retrievals (e.g., Chelton & Freilich, 2005; Hoffman & Leidner, 2005). Low winds have a very

poor directional skill, as a consequence of physical limitations of the instrument's measurement methodology.

Although the weighted average errors show that CCMP is the database with the best scores, it is clear that CCMP also suffers from this limitation and therefore is not able to overcome this deficiency in the wind direction retrieval.

Tables 5 and 6 depict the second described comparison. The four wind direction bins considered were North (angles between 315 and 45°), East (angles between 45 and 135°), South (angles between 135 and 225°) and West (angles between 225 and 315°).

Table 5
Statistics of the comparison between QuikSCAT and CCMP wind direction error per buoy wind direction bin.

Wind direction bins		North			East			South			West		
Station	Database	RMSE (°)	Bias (°)	N									
Peñas	QL2B-12.5	46.43	-18.28	25	61.29	7.21	53	74.38	-10.79	19	40.02	3.02	47
	QL2B-25	49.86	-22.68		65.13	-9.00		79.96	-15.47		46.09	2.45	
	QL3	49.88	-22.76		64.96	-9.15		80.06	-16.42		47.89	0.85	
	CCMP	37.23	-14.40		52.15	-4.26		66.46	11.16		48.97	-0.40	
Bares	QL2B-12.5	50.07	-18.35	34	40.65	-15.98	52	40.26	14.92	13	45.94	-13.44	39
	QL2B-25	37.09	-22.94		38.97	-16.08		34.24	-1.54		36.88	-1.51	
	QL3	37.12	-23.09		38.99	-16.21		36.86	0.85		34.41	-1.03	
	CCMP	37.80	-16.21		36.50	-18.06		33.19	4.46		35.70	7.18	
Villano	QL2B-12.5	46.67	-4.74	57	37.93	1.40	35	44.20	10.47	34	47.50	6.94	52
	QL2B-25	39.72	-8.86		37.23	-8.00		42.67	9.38		41.32	2.21	
	QL3	36.57	-10.42		37.26	-7.31		42.42	9.59		43.96	7.38	
	CCMP	40.83	-3.26		24.00	2.03		47.96	3.32		44.52	3.62	
Silleiro	QL2B-12.5	56.73	2.33	48	62.42	6.50	20	69.38	16.64	28	41.15	-3.59	29
	QL2B-25	60.04	3.79		50.43	-4.85		75.10	33.71		33.79	-5.24	
	QL3	63.32	-1.50		50.04	-5.65		75.01	33.75		34.14	-5.10	
	CCMP	43.99	2.65		58.41	-26.45		62.38	3.64		18.83	3.24	
Cádiz	QL2B-12.5	49.77	7.68	37	16.01	-3.82	33	92.36	-12.92	13	64.01	4.74	35
	QL2B-25	32.29	-3.43		32.02	-2.91		92.66	15.62		54.34	31.20	
	QL3	33.99	-4.11		35.13	-3.58		90.10	17.54		52.32	29.69	
	CCMP	30.89	-2.97		24.49	-6.48		85.40	-1.31		43.93	24.69	
Weighted average	QL2B-12.5	50.19	-4.75	-	43.87	-2.05	-	61.52	6.01	-	47.41	0.20	-
	QL2B-25	44.02	-8.94	-	45.84	-9.25	-	62.83	10.77	-	42.75	5.50	-
	QL3	44.23	-10.81	-	46.29	-9.40	-	62.75	11.20	-	43.07	6.31	-
	CCMP	38.79	-5.37	-	38.75	-9.52	-	57.77	4.37	-	40.06	6.97	-

Table 6
Statistics of the comparison between QuikSCAT and CCMP wind speed error per buoy wind direction bin.

Wind direction bins		North			East			South			West		
Station	Database	RMSE (m.s ⁻¹)	Bias (m.s ⁻¹)	N	RMSE (m.s ⁻¹)	Bias (m.s ⁻¹)	N	RMSE (m.s ⁻¹)	Bias (m.s ⁻¹)	N	RMSE (m.s ⁻¹)	Bias (m.s ⁻¹)	N
Peñas	QL2B-12.5	3.25	1.48	25	2.05	0.98	53	2.25	1.98	19	2.34	1.01	47
	QL2B-25	2.40	1.10		1.57	0.49		2.38	1.66		2.32	0.87	
	QL3	2.39	1.10		1.59	0.49		2.39	1.68		2.31	0.87	
	CCMP	1.74	0.34		1.67	-0.27		2.67	1.23		2.3	-0.26	
Bares	QL2B-12.5	1.16	0.45	34	1.19	0.20	52	1.11	0.71	13	1.03	-0.14	39
	QL2B-25	1.67	0.73		1.08	0.30		1.16	0.43		1.2	0.04	
	QL3	1.67	0.75		1.08	0.29		1.15	0.46		1.22	-0.01	
	CCMP	1.81	0.43		1.10	-0.10		1.35	0.82		1.81	-0.37	
Villano	QL2B-12.5	1.36	0.60	57	1.27	0.28	35	1.37	0.21	34	1.55	0.74	52
	QL2B-25	1.27	0.49		1.75	0.99		1.25	0.29		1.38	0.66	
	QL3	1.26	0.36		1.89	1.04		1.47	0.37		1.38	0.68	
	CCMP	1.40	0.00		1.35	-0.19		1.46	0.16		1.69	0.49	
Silleiro	QL2B-12.5	0.91	0.05	48	1.76	0.75	20	1.36	0.57	28	1.51	-0.03	29
	QL2B-25	1.55	-0.14		2.01	0.95		1.31	0.44		1.22	-0.18	
	QL3	1.33	-0.23		2.05	0.98		1.31	0.36		1.25	-0.19	
	CCMP	1.35	-0.41		2.01	-0.05		0.98	0.25		1.33	0.14	
Cádiz	QL2B-12.5	0.96	0.25	37	1.38	0.33	33	0.96	0.55	13	1.1	0.31	35
	QL2B-25	0.97	0.29		1.84	0.47		0.95	0.21		1.11	0.34	
	QL3	1.13	0.42		1.85	0.98		0.95	0.34		1.08	0.47	
	CCMP	1.58	-0.14		2.04	0.01		1.47	0.76		1.29	0.12	
Weighted average	QL2B-12.5	1.38	0.49	-	1.53	0.51	-	1.44	0.72	-	1.55	0.45	-
	QL2B-25	1.49	0.42		1.56	0.57		1.42	0.58		1.49	0.41	
	QL3	1.46	0.39		1.60	0.67		1.49	0.61		1.49	0.43	
	CCMP	1.53	-0.01		1.56	-0.14		1.54	0.53		1.73	0.04	

A particularly visible aspect is that the South sector presents substantially higher errors than the remaining sectors. In Peñas, Villano and Bares stations this could be due to the fact that this sector represents wind coming from land. As stated by Pensieri et al. (2010), oceanward winds are less accurately detected by satellites. Moreover, in this area southerly winds are typically associated with weak synoptic forcing events under unstable atmospheric conditions, which will produce very changeable winds. Thus, this kind of weather systems present usual difficulties in its forecasting. Additionally, if that is the case, the extrapolation of buoy measurements from 3 m to 10 m using a neutral wind profile may also contribute to the error.

Table 6 shows the same comparison as Table 5, but now for the satellite-derived wind speed error for each measured wind direction bin.

Table 6 shows that, for the wind speed at the buoys of Peñas, Silleiro and Cádiz, winds coming from land are associated to higher errors. Considering the information presented in Tables 5 and 6, it seems to be present a tendency for QuikSCAT and CCMP performance to be degraded when winds are coming from land.

3.3. Weibull distribution

The previous sections focused on a record-by-record analysis of simultaneous data, with particular attention to mean state and temporal variability accuracy. In this section, the goal is to assess which one of the databases is able to offer a characterization of the buoys wind regimes closer to reality. For this, Weibull PDF's will be used to evaluate QuikSCAT and CCMP ability to describe the buoy local wind regimes, in terms of the wind speed distribution frequency. The Weibull PDF's of the buoys, QuikSCAT and CCMP databases, are shown in Fig. 2. Table 7 depicts the Weibull PDF parameters (A and k) and the most probable wind speed (U_{prob}) values and respective errors. N represents the number of valid wind speed records of each one of the four databases and the respective buoy. It is worth to underline that, in this section, the temporal consistency of the databases will not be reflected in the results, since they are presented in terms of a frequency distribution that does not reflect temporal variability accuracy.

It is possible to see that CCMP Weibull PDF's are, in general, closer to the buoy ones for all stations when compared to QuikSCAT ones,

revealing a better ability to describe the wind speed frequency spectrum for all buoys. All QuikSCAT databases present similar results, except for Silleiro and Cádiz buoys. Fig. 2 shows also some interesting facts.

Firstly, that QuikSCAT databases systematically overestimate the frequencies of wind speeds above 6–8 m.s⁻¹ and underestimate the frequencies of wind speeds below 5–6 m.s⁻¹, making QuikSCAT Weibull curves clearly shifted to the right side of the wind speed axis in all stations, relatively to the buoy ones. The exceptions are for QL2B-12.5 in Silleiro and Cádiz buoys, and QL2B-25 for Cádiz. This shifting reveals that QuikSCAT data presents higher frequencies of strong winds and lower frequencies of weak winds than in reality. The underestimation of low winds and overestimation of strong winds probably reflects the worst performance of QuikSCAT for low and strong winds speeds observed in Section 3.2. The conjugation of the overestimation of strong winds frequencies and the underestimation of low winds frequencies originates the overall wind speed overestimation tendency detected in all the results presented in this work.

Secondly, that CCMP tends to introduce a lower variability in the wind speed distribution. This is visible in its overestimation of the frequency of the observed most frequent wind speeds and consequent underestimation of frequency of the observed wind speeds with lower frequencies: CCMP PDF's show a slight overestimation tendency of the frequency of winds between 4 and 8 m.s⁻¹ together with a slight underestimation of wind frequencies above 10 m.s⁻¹. Nevertheless, CCMP accurately represents the shape and position of the Weibull PDF curves, without any clear shifting tendency.

Analysing Table 7, it is clear that CCMP presents the best results, showing a lower weighted average deviation for all the Weibull parameters (including the estimation of the most probable wind speed). CCMP better performance is particularly visible in the scale parameter (A) error scores, which is related to (but not equal) to the mean wind speed. Among QuikSCAT databases, QL2B-25 is the one with the lowest errors for the scale parameter and most probable wind speed, whilst for the shape parameter (k) QL3 is the one with the best overall performance. It is again clear that QuikSCAT presents worse overall results in Peñas, due to its location inside the satellite land contamination area. CCMP seems to be able to attenuate this QuikSCAT limitation.

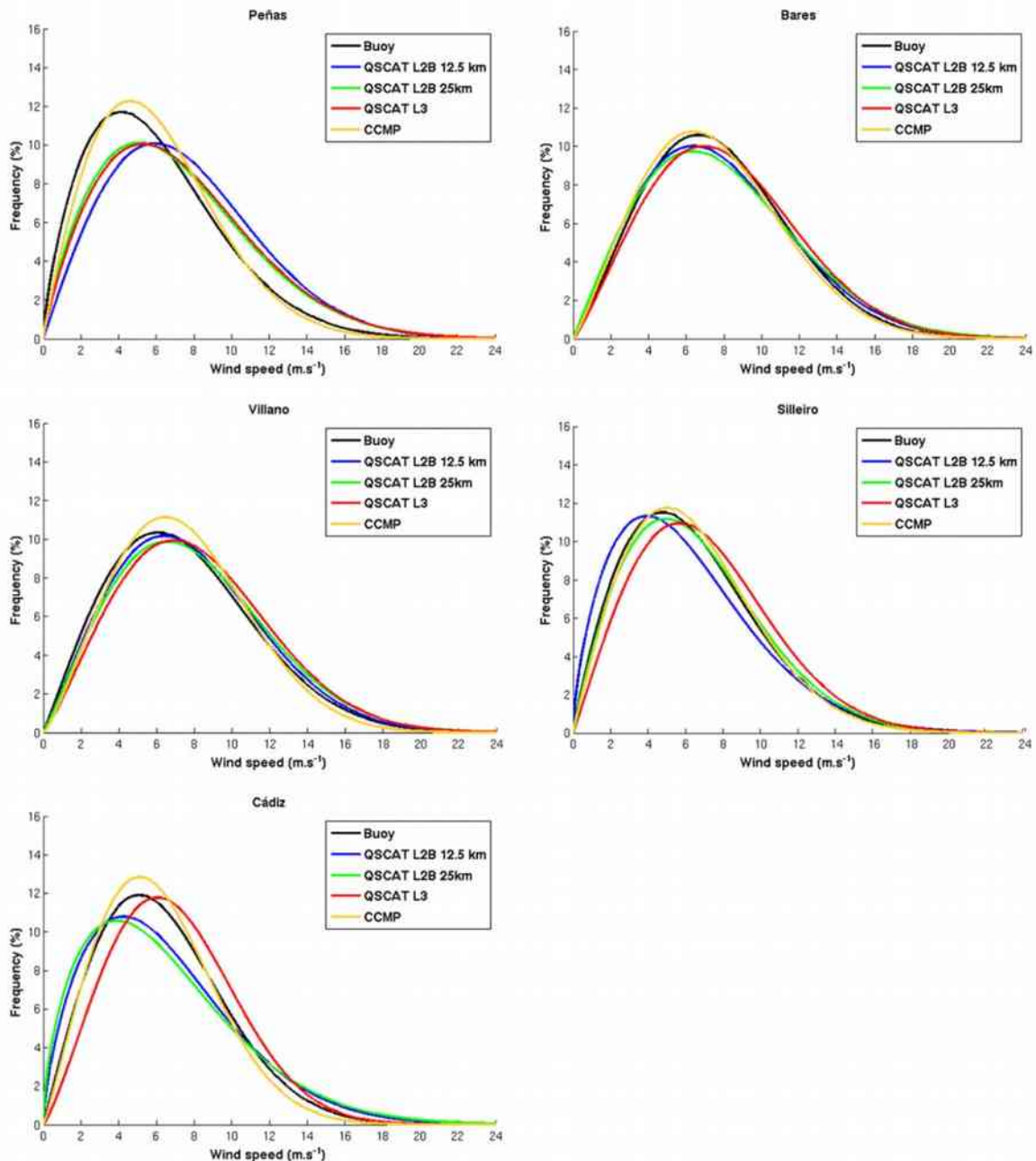


Fig. 2. Buoy, QuikSCAT and CCMP Weibull PDFs for all buoys.

These results were expected, since this analysis based on a frequency distribution does not reflect errors due to inaccuracies in the temporal variability representation. Although QuikSCAT databases showed better performance for the wind speed temporal variability (RMSE, STDE and R^2), CCMP lower errors in the estimation of the wind speed frequency distribution are related to its lower biases for the wind speed. Moreover, the fact that CCMP includes four records per day and all of these records are valid, also improves its ability to accurately describe the local wind regimes. Taking into account the full available valid records for each database, and not only the simultaneous, it is possible to see that QL2B-12.5 km is able to provide higher number of records for locations inside QuikSCAT's land masking area. For Peñas, the buoy closest to shore, QL2B-12.5 km accounts for almost more 40% of valid data records when compared to QL2B-25 km, due to its increased resolution. Obviously, due to the fact that CCMP includes four valid records per day, this database is able to offer much more data than QuikSCAT.

Besides the results presented and analyzed in this study, it should be borne in mind that, as stated by Sánchez et al. (2007), winds measured by anemometers (like the ones considered here) and satellite-derived wind data can be very different due to the fact that scatterometer winds tend to represent synoptic winds (Austin & Pierson, 1999). Although QuikSCAT is able to detect mesoscale features (e.g.: Atlas et al., 1999, 2001), this detection is somewhat limited and distorted due to its low spatial resolution and temporal sampling. These mesoscale features include land-sea breezes, orography and tidal effects that if not present in the satellite-derived winds, can lead to large differences between this type of wind data and the ones measured in situ, which take into account these mesoscale effects. Furthermore, and as stated by Pensieri et al. (2010), satellite winds represent a spatial average of instantaneous moments, while anemometer wind data is closer to a temporal average of instantaneous measurements taken at a specific and fixed location. Moreover, Carvalho et al. (2012) proved that these buoy winds are very correlated with the surrounding

Table 7
Deviations of the Weibull PDF parameters (A and k) and most probable wind speed (U_{prob}) for all databases. Note that the weighted mean errors are calculated using absolute values.

Station	Database	A ($\text{m}\cdot\text{s}^{-1}$)	Error	K (–)	Error	U_{prob} ($\text{m}\cdot\text{s}^{-1}$)	Error	N
Peñas	Buoy	6.76	-	1.74	-	3.65	-	7 048
	QL2B-12.5	8.46	25.1%	1.98	13.7%	5.88	61.1%	587
	QL2B-25	7.97	17.8%	1.80	3.6%	4.62	26.7%	424
	QL3	8.11	20.0%	1.84	5.6%	4.89	34.0%	321
	CCMP	6.80	0.5%	1.91	9.7%	4.42	21.0%	1 464
Bares	Buoy	8.70	-	2.22	-	7.41	-	7 470
	QL2B-12.5	8.77	0.7%	2.07	-6.6%	6.62	-10.7%	425
	QL2B-25	8.89	2.1%	2.03	-8.7%	6.43	-13.2%	448
	QL3	9.14	5.0%	2.20	-1.0%	7.65	3.1%	506
	CCMP	8.46	-2.9%	2.18	-1.8%	6.98	-5.9%	1 464
Villano	Buoy	8.43	-	2.05	-	6.22	-	8 745
	QL2B-12.5	8.73	3.5%	2.10	2.7%	6.76	8.6%	435
	QL2B-25	8.95	6.2%	2.09	2.0%	6.85	10.0%	484
	QL3	9.17	8.8%	2.18	6.5%	7.58	21.8%	496
	CCMP	8.39	-0.5%	2.26	10.3%	7.36	18.3%	1 464
Silleiro	Buoy	7.16	-	1.88	-	4.48	-	7 754
	QL2B-12.5	6.84	-4.5%	1.66	-11.3%	3.34	-25.4%	255
	QL2B-25	7.40	3.4%	1.89	0.5%	4.68	4.4%	408
	QL3	7.92	10.7%	2.03	8.4%	5.77	28.8%	575
	CCMP	7.22	0.8%	1.97	4.8%	4.94	10.2%	1 464
Cádiz	Buoy	7.21	-	2.00	-	5.10	-	8 770
	QL2B-12.5	7.22	0.2%	1.69	-15.5%	3.65	-28.3%	237
	QL2B-25	7.20	-0.1%	1.60	-20.1%	3.21	-37.0%	202
	QL3	7.88	9.4%	2.24	12.0%	6.82	33.7%	534
	CCMP	6.93	-3.8%	2.11	5.6%	5.41	6.1%	1 464
Weighted average	QL2B-12.5	-	6.8%	-	9.8%	-	26.4%	-
	QL2B-25	-	5.9%	-	6.8%	-	17.8%	-
	QL3	-	10.7%	-	6.6%	-	23.9%	-
	CCMP	-	1.7%	-	6.4%	-	12.3%	-

ography and, according to Sánchez et al. (2007), the comparison between these types of winds with satellite-derived wind data can produce large errors associated to spatial heterogeneities of the wind field and small-scale wind variability. Despite these limitations, together with the ones shown in this study, satellite-derived data have their strength in their high spatial frequency over the ocean where it could make up for the usual lack of observations, contributing then to a better description of the surface wind field within the data assimilation process.

4. Conclusions

The present work analyses and compares the performance of three QuikSCAT and the recently released CCMP ocean surface wind databases, with the objective of determining which database offers the best representation of the surface ocean wind when compared to measured wind. One year of wind data from CCMP, QuikSCAT L2B (12.5 and 25 km resolution), QuikSCAT L3 and measurements from five buoys located along the Iberian Peninsula shore (Galician coast and Gulf of Cádiz) were selected for this comparison.

Different types of comparison were performed. First, a thorough statistical analysis was conducted focusing on the record-per-record accuracy of the several databases. For this comparison, the main conclusions can be summarised as follows:

- For the wind speed, QuikSCAT databases showed the best results in terms of accuracy in representing the wind magnitude temporal variability, with the high-resolution QuikSCAT product showing the highest R^2 and lowest RMSE and STDE. Oppositely, CCMP clearly showed the best performance in depicting the mean wind state due to the lowest biases. QuikSCAT databases showed clearly higher errors for low and strong wind speeds and significant better performances for intermediate wind speeds (between 4 and $12 \text{ m}\cdot\text{s}^{-1}$), while CCMP performance is better for low and intermediate wind speeds. All QuikSCAT databases showed a systematic tendency to

overestimate the wind speed, with this overestimation being higher in the presence of low (below $4 \text{ m}\cdot\text{s}^{-1}$) and strong winds (above $12 \text{ m}\cdot\text{s}^{-1}$). CCMP also shows a tendency to overestimate the wind speed in the presence of low winds, but oppositely has a tendency to underestimate wind speeds above $8 \text{ m}\cdot\text{s}^{-1}$.

- For the wind direction, CCMP showed the best results in representing the temporal variability (in average, highest R^2 , lowest RMSE and STDE) and the high-resolution QuikSCAT product presented the lowest average bias. All databases presented a slight anti-clockwise rotation for the Northern Galician coast and a clockwise rotation for the Western Galician coast and Gulf of Cádiz. All products showed the highest wind direction errors in the presence of low wind speeds and a clear improvement when the wind speed increases. Moreover, the wind direction errors are significantly higher than the wind speed ones.
- All QuikSCAT products presented worse results for Peñas buoy. This is related to the fact that this buoy is the only one positioned inside the satellite land contaminated area, indicating that satellite-derived data shows limitations in representing coastal winds. CCMP showed ability to improve these results, but not to mitigate this issue completely. Although the high-resolution QuikSCAT L2B product is the one with the best overall results for all the near-shore buoys considered in this work, it was not able to show any significant improvement for the one closest to shore (Peñas).

For the second comparison, which aims to assess which database is able to offer the wind regime characterization closest to reality, the main conclusion is that CCMP is clearly the database with the best ability to characterize the local wind regimes. The fact that CCMP has higher temporal sampling (four records per day), complete data availability (it does not contain invalid records) and the lowest wind speed biases can explain this performance.

The results presented in this work show that QuikSCAT products have their strength in representing the temporal variability of the wind speed and the mean state of the wind direction. Although no major differences

were detected among QuikSCAT products, the high-resolution product was the one with the best overall scores. However, CCMP is able to bring significant improvements in terms of wind direction temporal variability and wind speed mean state. Moreover, CCMP is able to partially overcome some of QuikSCAT's known problems, mainly those related to QuikSCAT systematic tendency to overestimate the wind speed and land masking effects. Furthermore, is a gridded dataset with a higher temporal sampling and complete data availability when compared to QuikSCAT. These features, all together, can make of CCMP an interesting and valuable database for offshore wind energy assessment studies, where the accuracy in representing the wind speed mean state plays a key role, and also for meteorological, oceanic and climate modelling applications where gridded wind data with good temporal sampling and data availability is vital to force numerical simulation models.

Acknowledgements

D. Carvalho was supported by the Portuguese Foundation for Science and Technology (F.C.T.) Ph.D grant SFRH/BD/73070/2010. The authors would like to express their gratitude to all the climate and meteorological institutions referred in the text, for providing the data used in this work. I. Alvarez was supported by the Ramón y Cajal Program. This work was also partially supported by Xunta de Galicia under Programa de Consolidación e Estruturación de Unidades de Investigación (Grupos de Referencia Competitiva) funded by European Regional Development Fund (FEDER).

References

- Alvarez, I., Gomez-Gesteira, M., deCastro, M., & Dias, J. M. (2008). Spatio-temporal evolution of upwelling regime along the western coast of the Iberian Peninsula. *Journal of Geophysical Research*, 113, C07020.
- Alvarez, I., Gomez-Gesteira, M., deCastro, M., Gomez-Gesteira, J. L., & Dias, J. M. (2010). Summer upwelling frequency along the western Cantabrian coast from 1967 to 2008. *Journal of Marine Systems*, 79, 218–226.
- Atlas, R., Ardizzone, J., & Hoffman, R. N. (2008). Application of satellite surface wind data to ocean wind analysis. *Proceedings of the Society of Photographic Instrumentation Engineers*, 7087, 70870B.
- Atlas, R., Bloom, S. C., Hoffman, R. N., Brin, E., Ardizzone, J., Terry, J., et al. (1999). Geophysical validation of NSCAT winds using atmospheric data and analyses. *Journal of Geophysical Research*, 104, 11405–11424.
- Atlas, R., Hoffman, R. N., Ardizzone, J., Leidner, S. M., & Jusem, J. C. (2009). Development of a new cross-calibrated, multiplatform (CCMP) ocean surface wind product. *AMS 13th Conference on Integrated Observing and Assimilation Systems for Atmosphere, Oceans, and Land Surface (IOAS-AOLS)*, Phoenix, Arizona.
- Atlas, R., Hoffman, R. N., Ardizzone, J., Leidner, S. M., Jusem, J. C., Smith, D. K., et al. (2011). A cross-calibrated, multiplatform ocean surface wind velocity product for meteorological and oceanographic applications. *Bulletin of the American Meteorological Society*, 92, 157–174.
- Atlas, R., Hoffman, R. N., Leidner, S. M., Sienkiewicz, J., Yu, T. -W., Bloom, S. C., et al. (2001). The effects of marine winds from scatterometer data on weather analysis and forecasting. *Bulletin of the American Meteorological Society*, 82, 1965–1990.
- Austin, S., & Pierson, W. J. (1999). Mesoscale and synoptic-scale effects on the validation of NSCAT winds by means of data buoy reports. *Journal of Geophysical Research*, 104(C5), 11437–11447.
- Carvalho, D., Rocha, A., & Gómez-Gesteira, M. (2012b). WRF model ocean surface wind simulation forced by different reanalysis: comparison with observed data along the Iberian Peninsula coast. *Ocean Modelling*, 56, 31–42.
- Carvalho, D., Rocha, A., Gómez-Gesteira, M., & Santos, C. (2012a). A sensitivity study of the WRF model in wind simulation for an area of high wind energy. *Environmental Modelling and Software*, 33, 23–34.
- Chelton, D. B., & Freilich, M. H. (2005). Scatterometer-based assessment of 10-m wind analyses from the operational ECMWF and NCEP numerical weather prediction models. *Monthly Weather Review*, 133, 409–429.
- Chelton, D. B., Schlax, M. G., Freilich, M. H., & Milliff, R. F. (2004). Satellite measurements reveal persistent small-scale features in ocean winds. *Science*, 303, 978–983.
- Cornillon, P., & Park, K. -A. (2001). Warm core ring velocities inferred from NSCAT. *Geophysical Research Letters*, 28, 575–578.
- Dunbar, R. S., Lungu, T., Weiss, B., Stiles, B., Huddleston, J., Callahan, P. S., et al. (2006). QuikSCAT Science Data Product User Manual, Version 3.0, JPL Document D-18053 - Rev A. Pasadena, CA: Jet Propulsion Laboratory.
- Ebuchi, N., Graber, H. C., & Caruso, M. J. (2002). Evaluation of wind vectors observed by QuikSCAT/SeaWinds using ocean buoy data. *Journal of Atmospheric and Oceanic Technology*, 19, 2049–2062.
- Furevik, B. R., Sempreviva, A. M., Cavaleri, L., Lefèvre, J. M., & ranserici, C. (2010). Eight years of wind measurements from scatterometer for wind resource mapping in the Mediterranean Sea. *Wind Energy*, 14(3), 355–372.
- Gómez-Gesteira, M., Moreira, C., Alvarez, I., & deCastro, M. (2006). Ekman transport along the Galician coast (NW, Spain) calculated from forecasted winds. *Journal of Geophysical Research*, 111, C10005.
- Hasager, C. B., Astrup, P., Nielsen, M., Christiansen, M. B., Badger, J., Nielsen, P., et al. (2007). SAT-WIND project. *Final report. Risø-R-1586(EN)* (pp. 131). Roskilde, Denmark: Risø National Laboratory, Technical University of Denmark.
- Hoffman, R. N., & Leidner, S. M. (2005). An Introduction to the Near-Real-Time QuikSCAT Data. *Weather and Forecasting*, 20, 476–493.
- Jungclaus, J. H., & Mellor, G. L. (2000). A three-dimensional model study of the Mediterranean outflow. *Journal of Marine Systems*, 24, 41–66.
- Large, W. G., Morzel, J., & Crawford, G. B. (1995). Accounting for surface wave distortion of the marine wind profile in low-level ocean storms wind measurements. *Journal of Physical Oceanography*, 25, 2959–2971.
- Liu, W. T., & Tang, W. (1996). Equivalent Neutral Wind. *JPL Publication*, 96–17. Pasadena, California: Jet Propulsion Laboratory, California Institute of Technology.
- Liu, W. T., Tang, W., & Xie, X. (2008). Windpower distribution over global ocean. *Geophysical Research Letters*, 35, L13808.
- Lungu, T. (2001). QuikSCAT science data product user's manual, overview and geophysical data products. *Technical Report D-18053*. NASA Jet Propulsion Laboratory.
- Mears, C. A., Smith, D. K., & Wentz, F. J. (2001). Comparison of Special Sensor Microwave Imager and buoy-measured wind speeds from 1987 to 1997. *Journal of Geophysical Research*, 106(11), 719–729.
- Moore, G. W. K., Pickart, R. S., & Renfrew, I. A. (2008). Buoy observations from the windiest location in the world ocean, Cape Farewell, Greenland. *Geophysical Research Letters*, 35, 5.
- Myers, P. G., Haines, K., & Josey, S. (1998). On the importance of the choice of wind stress forcing to the modeling of the Mediterranean Sea circulation. *Journal of Geophysical Research*, 103(15), 729–749.
- Peixoto, J. P., & Oort, A. H. (1992). *Physics of Climate*. Woodbury, N.Y.: American Institute of Physics.
- Peliz, A., Dubert, J., Marchesio, P., & Teles-Machado, A. (2007). Surface circulation in the Gulf of Cadiz: model and mean flow structure. *Journal of Geophysical Research*, 112, C11015.
- Penabad, E., Alvarez, I., Balseiro, C. F., deCastro, M., Gomez, B., Perez-Munuzuri, V., et al. (2008). Comparative analysis between operational weather prediction models and QuikSCAT wind data near the Galician coast. *Journal of Marine Systems*, 72, 256–270.
- Pensieri, S., Bozzano, R., & Schiano, M. E. (2010). Comparison between QuikSCAT and buoy wind data in the Ligurian Sea. *Journal of Marine Systems*, 81, 286–296.
- Pickett, M. H., Tang, W., Rosenfeld, L. K., & Wash, C. H. (2003). QuikSCAT satellite comparisons with nearshore buoy wind data off the U.S. west coast. *Journal of Atmospheric and Oceanic Technology*, 20, 1869–1979.
- Portabella, M., & Stoffelen, A. (2001). Rain Detection and Quality Control of SeaWinds. *Journal of Atmospheric and Oceanic Technology*, 18(7), 1171–1183.
- Risien, C. M., & Chelton, D. B. (2006). A satellite-derived climatology of global ocean winds. *Remote Sensing of Environment*, 105(3), 221–236.
- Ruti, P. M., Marullo, S., D'Ortenzio, F., & Tremant, M. (2008). Comparison of analyzed and measured wind speeds in the perspective of oceanic simulations over the Mediterranean basin: Analyses, QuikSCAT and buoy data. *Journal of Marine Systems*, 70(1/2), 33–48.
- Sánchez, R., Relvas, P., & Pires, H. O. (2007). Comparison of ocean scatterometer and anemometer winds off the southwestern Iberian Peninsula. *Continental Shelf Research*, 27, 155–175.
- Satheesan, K., Sarkar, A., Parekh, A., Ramesh Kumar, M. R., & Kuroda, Y. (2007). Comparison of wind data from QuikSCAT and buoys in the Indian Ocean. *International Journal of Remote Sensing*, 10, 2375–2382.
- Sharma, N., & D'Sa, E. (2008). Assessment and Analysis of QuikSCAT Vector Wind Products for the Gulf of Mexico: A Long-Term and Hurricane Analysis. *Sensors*, 8, 1927–1949.
- Singh, P., Parekh, A., & Attada, R. (2013). Comparison of a simple logarithmic and equivalent neutral wind approaches for converting buoy-measured wind speed to the standard height: special emphasis to North Indian Ocean. *Theoretical and Applied Climatology*, 111, 455–463.
- Tang, W., Liu, W. T., & Stiles, B. W. (2004). Evaluation of high-resolution ocean surface vector winds measured by QuikSCAT scatterometer in coastal regions. *IEEE Transactions on Geoscience and Remote Sensing*, 42(8), 1762–1769.
- Verschell, M. A., Bourassa, M. A., Weissman, D. E., & O'Brien, J. J. (1999). Model validation of the NASA scatterometer winds. *Journal of Geophysical Research*, 104, 11359–11374.
- Wentz, F. J., & Smith, D. K. (1999). A model function for the ocean-normalized radar cross section at 14 GHz derived from NSCAT observations. *Journal of Geophysical Research*, 104, 11499–11514.

5.2 – Is the optimised WRF offshore wind simulation able to surpass satellite-derived and other alternative sources of offshore wind data?

After the selection of the best official QuikSCAT product, this database and other alternative sources of offshore wind data are compared to *in situ* measured offshore winds and with offshore winds simulated by WRF using its optimised configuration, aiming to assess if WRF is able to surpass satellite (QuikSCAT) derived and also other alternative sources of offshore wind data. These other alternative sources of offshore wind data include unofficial QuikSCAT data processed by other agencies besides NASA (blended QuikSCAT products that may or not use other data sources in its processing), CCMP Ocean Surface Wind Vectors, reanalyses and analyses datasets.

This research is presented in the following paper, in which is included the methodology followed, area under study, offshore wind data sources tested, observed data used to compare the simulations, introductory notes and state of the art. This article can be found on the link: <http://www.sciencedirect.com/science/article/pii/S003442571400265X>



Comparison of reanalyzed, analyzed, satellite-retrieved and NWP modelled winds with buoy data along the Iberian Peninsula coast



D. Carvalho^{a,*}, A. Rocha^a, M. Gómez-Gesteira^b, C. Silva Santos^c

^a CESAM, Department of Physics, University of Aveiro, Campus Universitário de Santiago, 3810-193 Aveiro, Portugal

^b EPHYSLAB – Environmental Physics Laboratory, Facultad de Ciencias, Universidad de Vigo, 32004 Ourense, Spain

^c Instituto Superior de Engenharia do Porto, Rua Dr. António Bernardino de Almeida 341, 4200-072 Porto, Portugal

ARTICLE INFO

Article history:

Received 14 April 2014

Received in revised form 26 June 2014

Accepted 19 July 2014

Available online xxx

Keywords:

Cross-Calibrated Multi-Platform Ocean Wind (CCMP)

QuikSCAT

WRF

Wind simulation

NCEP-R2

ERA-Interim

NCEP-CFSR

NASA-MERRA

GFS

NCEP-FNL

Reanalysis

Analysis

Ocean surface wind

Offshore wind energy

Iberian Peninsula

Portugal

Spain

ABSTRACT

Offshore wind data derived from satellite measurements (CCMP, QuikSCAT, NCDC Blended Sea Winds and IFREMER Blended Wind Fields), reanalyses (NCEP-CFSR, ERA-Interim, NASA-MERRA and NCEP-R2), analyses (NCEP-FNL and NCEP-GFS) and WRF modelled offshore winds were compared to in situ measurements, in order to assess which one of these products is the best alternative to in situ offshore measured wind data. Wind speed and direction from these products were compared to measurements collected at five buoys moored along the Iberian Peninsula Atlantic coast.

Results show that WRF modelled offshore winds are the best alternative to in situ measured offshore wind data, showing the highest temporal accuracy (the ability in representing the wind speed and direction at a given time instant) and lowest errors in terms of offshore wind power flux estimations. However, offshore wind data taken from CCMP shows the lowest errors in terms of the mean wind speeds and, together with IFREMER-BWF, the best wind temporal accuracy after WRF simulation. Therefore, in general CCMP and IFREMER-BWF can be considered as the best alternatives to WRF high resolution modelled offshore winds, if the latter is not available. Specifically for offshore wind energy resource assessment, NCEP-CFSR reanalysis or NCEP-GFS analysis data can also be used with confidence as an alternative to WRF modelled data, showing better wind power flux estimates than CCMP and IFREMER-BWF.

Despite the best performances of WRF high resolution offshore winds, such modelling tasks require considerable computational resources and time to obtain quality results. Therefore, the value of satellite-derived wind data should not be disregarded. These remotely sensed offshore wind measurements should be seriously considered when searching for alternative sources of wind information for ocean areas, in particular for open ocean areas where they have their strength.

© 2014 Elsevier Inc. All rights reserved.

1. Introduction

Climatic, atmospheric and oceanic modelling applications require accurate oceanic surface wind data to, realistically, represent the oceanic forcing fields and interactions between air and sea. Moreover, data regarding ocean winds is very valuable in the context of offshore wind energy, which is expected to constitute a significant part of the future wind-derived energy as a whole (Carvalho, Rocha, Gómez-Gesteira, & Santos, 2012; Carvalho, Rocha, Santos, & Pereira, 2013). However, it is known that ocean areas suffer from a strong lack of measured wind data, mainly due to the high costs and technological challenges involved in the installation of wind measuring masts at such sites. Even when in situ data exists (collected on board ships, vessels, moored buoys, etc.)

their availability is highly variable both in space and time and cannot be considered as representative of local wind regimes (Risien & Chelton, 2006). Especially for offshore wind resource assessment applications, accurate wind data is a key factor because energetic production is proportional to the wind speed cubed (Bruun, Koch, Horstmann, Hasager, & Nielsen, 2006), making that apparent small inaccuracies in the wind velocity can originate large discrepancies in the expected wind-derived energy production.

Thus, it becomes paramount to search and validate alternative data sources to in situ measured wind data over ocean areas. These alternative sources of offshore wind data consist, basically, in satellite-derived measurements, data simulated by numerical weather prediction (NWP) models and products that combine observed and NWP simulated data (mainly reanalysis and analysis datasets). While satellite-derived wind data is available at a near-global scale and in a time-continuous way, they are indirect measurements (that is, they are derived from other measurements and processed using complex geophysical models) and

* Corresponding author. Tel.: +351 234 370 356; fax: +351 234 378197.
E-mail addresses: david.carvalho@ua.pt (D. Carvalho), alfredo.rocha@ua.pt (A. Rocha), mggesteira@uvigo.es (M. Gómez-Gesteira), cmi@isep.ipp.pt (C. Silva Santos).

often suffer from low spatial and/or temporal resolutions, together with large missing/erroneous data gaps (data records affected by rain, malfunction of instruments, etc.). NWP models, in particular regional circulation models (RCMs, also known as mesoscale models), are able to produce meteorological data at high spatial and temporal resolutions for any area of the globe, and in a relatively fast way (depending on the available computational resources, NWP model configuration, desired resolutions and spatial/time coverage). In the recent past, NWP modelling has found a number of applications focused on deriving wind information to study meteorological and climatic events, drive oceanic models and in the preliminary search and identification of potential sites for wind energy exploitation. However, NWP modelled wind data usually shows non-negligible deviations when compared to observed data, mainly due to their inability in accurately resolving medium- to small scale meteorological processes (Carvalho, Rocha, Gómez-Gesteira, & Silva Santos, 2014). Reanalysis and analysis products combine data simulated by global circulation models (GCMs) with large amounts of meteorological measurements, providing a complete and homogeneous synthesis of the available global observations assimilated into a continuous and coherent physical structure (Trenberth et al., 2010). However, these kinds of products are usually available at low spatial resolutions (250 to 50 km), insufficient to accurately characterize local wind regimes and adequately represent medium and small scale meteorological features.

The aim of this study is to evaluate and compare several alternative sources of offshore wind data with in situ ocean surface wind measurements, with the main objective of determining which of these alternative offshore wind sources best describe the local wind regimes at the selected buoy locations and, thus, can be considered as the best alternative to in situ measured offshore wind data. For this, one complete year of satellite-derived wind data, NWP modeled and reanalysis/analysis products are compared with in situ offshore wind measurements collected by five buoys moored offshore the Iberian Peninsula Atlantic coast (Gulf of Cádiz, West and North Galician coast). The NWP chosen to run the offshore wind simulation for the area under study is the Weather Research and Forecasting (WRF) mesoscale model. The sources of satellite-derived offshore wind data used in this study are: NASA's SeaWinds scatterometer installed onboard the QuikSCAT satellite platform (henceforth referred to as QuikSCAT); the National Climatic Data Center Blended Sea Winds (NCDC-BSW); the French Research Institute for Exploitation of the Sea Blended Wind Fields (IFREMER-BWF); and the Cross-Calibrated Multi-Platform Ocean Surface Wind Vectors (CCMP). The reanalyses and analyses considered in this study are: the National Centres for Environmental Prediction Reanalysis 2 (NCEP-R2); the European Centre for Medium-Range Weather Forecasts (ECMWF) Interim reanalysis (ERA-Interim); the National Centre for Environmental Prediction Climate Forecast System Reanalysis (NCEP-CFSR); NASA's Modern Era Retrospective Analysis for Research and Applications (NASA-MERRA);

the National Centre for Environmental Prediction Global Forecast System (NCEP-GFS) and the National Centre for Environmental Prediction Final Analysis (NCEP-FNL). The main characteristics of all these sources of offshore wind data are presented in Table 1, and in Sections 2.1, 2.2 and 2.3 additional information about these datasets are presented.

The published literature includes several studies that compare NWP offshore wind simulations with observations (eg.: Berge, Byrkjedal, Ydersbond, & Kindler, 2009; Carvalho, Rocha, & Gómez-Gesteira, 2012; Carvalho, Rocha, Gómez-Gesteira, & Silva Santos, in press-a,b; Jiménez, Durante, Lange, Kreutzer, & Tambke, 2007; Ohsawa et al., 2007; Shimada & Ohsawa, 2011; Shimada, Ohsawa, & Yatsu, 2009), or that compare satellite-derived offshore winds with buoy measurements (eg.: Ebuchi, Graber, & Caruso, 2002; Moore, Pickart, & Renfrew, 2008; Pensieri, Bozzano, & Schiano, 2010; Pickett, Tang, Rosenfeld, & Wash, 2003; Sánchez et al., 2007; Satheesan, Sarkar, Parekh, Ramesh Kumar, & Kuroda, 2007; Tang, Liu, & Stiles, 2004). Also studies that compare satellite-derived, reanalyses, and/or blended satellite-derived offshore winds with measurements are available (eg.: Kent, Fangohr, & Berry, 2013; Li et al., 2013; Ruti, Marullo, D'Ortenzio, & Tremant, 2008), as well as studies that focus on the comparison of NWP and satellite-derived offshore winds with observations (eg.: Accadia, Zecchetto, Lavagnini, & Speranza, 2007; Karagali et al., 2013; Wallcraft et al., 2009). From these studies there are evidences that products that combine satellite and NWP data, and in particular CCMP, can offer improvements when compared to individual satellite records. However, satellite-derived records are usually more accurate than reanalyses/analyses. Furthermore, NWP-derived data, in particular the ones obtained with mesoscale NWP models, seems to show better performance in terms of wind variability but higher biases when compared to satellite-derived winds. In particular for the area here under study, the following studies should be highlighted: Penabad et al. (2008) compared 4 years (2002–2005) of QuikSCAT and two NWP (MM5 and ARPS) modelled winds with measured wind data collected offshore the Galician Coast, concluding that no significant differences between models and satellite data were found. Otero and Ruiz-Vilarreal (2008) evaluated the reliability of different meteorological models through the comparison with observed winds around the north-west and north Iberia during autumn 2002 showing significant differences among modeled wind data products. Carvalho, Rocha, Gómez-Gesteira, Alvarez, and Silva Santos (2013) compared 3 different QuikSCAT products (gridded L3 and swath L2B with 25 and 12.5 km) and CCMP with measured winds collected in the same buoys considered in this study, for the same time period (2008), concluding that the high resolution QuikSCAT L2B product showed the best results for the wind speed variability and wind direction means, while CCMP showed the best results for wind speed means and wind direction variability. Alvarez, Gomez-Gesteira, deCastro, and Carvalho (2013) compared 10 years (2000–2009) of wind data from six databases (NCEP-R2, ERA-Interim, NASA-MERRA, NCEP-CFSR, QuikSCAT and

Table 1
Main characteristics of the considered offshore wind datasets.

Dataset	Type of dataset	Spatial resolution	Temporal resolution	Processing level	Included data sources	Time coverage
WRF	NWP	5 km	Hourly	–	Forcing data from reanalyses	–
QuikSCAT	Satellite (Swath)	12.5 km	2 times/day	L2B	QuikSCAT	1999–2009
NCDC-BSW	Satellites (Gridded) ^a	0.25° lat/lon	4 times/day	L3	QuikSCAT, SSM/I, TMI, AMSR-E	1987–Present
IFREMER-BWF	Satellites + analysis	0.25° lat/lon	4 times/day	L4	QuikSCAT, SSM/I, ECMWF Analyses	1999–2009
CCMP	Satellites + analysis	0.25° lat/lon	4 times/day	L4	QuikSCAT, SSM/I, SSMIS, AMSR-E, WindSat, ECMWF Analyses	1987–2011
NCEP-R2	Reanalysis	2.5° lat/lon	4 times/day	–	NWP and observations	1979–Present
ERA-Interim	Reanalysis	0.75° lat/lon	4 times/day	–	NWP and observations	1979–Present
NCEP-CFSR	Reanalysis	0.5° lat/lon	Hourly	–	NWP and observations	1979–Present
NASA-MERRA	Reanalysis	0.5° lat–2/3 lon	Hourly	–	NWP and observations	1979–Present
NCEP-FNL	Analysis	1° lat/lon	4 times/day	–	NWP and observations	1999–Present
NCEP-GFS	Analysis	0.5° lat/lon	4 times/day	–	NWP and observations	2004–Present

^a The NCDC-BSW uses NCEP-R2 wind direction data, but does not blend reanalysis or analysis wind fields with remotely sensed data.

CCMP) with wind measurements collected by four buoys moored in the southern limit of the Bay of Biscay, concluding that the wind products with finer spatial resolution provide the best results, especially in near-shore areas. Sousa, Alvarez, Vaz, Gomez-Gesteira, and Dias (2013) evaluated 1 year of QuikSCAT and WRF modelled winds with in situ measurements collected by three buoys moored offshore the Galician coast, reporting that the wind speeds derived from QuikSCAT and WRF do not show significant differences along the coast. Despite all of this research, no study was found that makes a joint comparison of all these sources of offshore wind data, objectively assessing through an integrated comparison which one of these products is the best alternative to in situ offshore wind measurements, nor for the area here under study nor for any other areas of the globe. Such findings can be of great value for areas where no in situ offshore measured data are available (or the available data is insufficient and/or inadequate for the desired purposes) and, therefore, valid alternatives have to be found. This is the case for the area under study, since the Iberian Peninsula is presently one of the areas with the highest percentage of installed onshore wind power per capita worldwide due to its attractive wind conditions. This asset, combined with its large coastal line, makes this area a promising one for future installation of offshore wind farms.

2. Data and methodology

2.1. Satellite wind data

NASA's SeaWinds instrument, onboard the QuikSCAT satellite launched in 1999, consists of a microwave scatterometer that retrieves wind fields by measuring the ocean surface backscatter, with a spatial resolution of 0.25° in latitude and longitude and collecting two measurements per day (corresponding approximately to 6 A.M. for the ascending pass and 6 P.M. for the descending pass). More details are available in Hoffman and Leidner (2005) and in NASA's Jet Propulsion Laboratory Physical Oceanography Distributed Active Archive Centre (JPL-PO.DAAC) website (<http://podaac.jpl.nasa.gov/OceanWind/QuikSCAT>). QuikSCAT wind data is available in three different products, according to their processing level (Dunbar et al., 2006). Carvalho, Rocha, Gómez-Gesteira, et al. (2013) compared all QuikSCAT different products (the official and original QuikSCAT data provided by JPL-PO.DAAC only) for the area here under study and concluded that the L2B processing-level high resolution (12.5 km) QuikSCAT product showed higher accuracy when compared to measured data. Therefore, this L2B high resolution QuikSCAT database was selected to use in the present work. Despite the good results obtained with QuikSCAT, making it one of the most famous and used sources of satellite-retrieved offshore wind data, it shows strong limitations in retrieving quality wind records in the presence of rain (that artificially increases the ocean surface roughness and, consequently, the measured backscatter), originating an overestimation of the ocean surface wind speed and misalignments of the wind direction. Additionally, in the presence of either low (below $5 \text{ m}\cdot\text{s}^{-1}$) or strong winds (above $15 \text{ m}\cdot\text{s}^{-1}$), QuikSCAT data is known to be affected. Moreover, for coastal areas located less than 25–30 km from the coast QuikSCAT is not able to accurately represent the spatial and temporal variability of the wind fields due to land masking effects. Finally, QuikSCAT instruments permanently failed in November 2009 ending its 10-year mission.

The NCDC Blended Sea Winds database consists of a 6-hourly (0, 6, 12 and 18 h) gridded global dataset of ocean surface wind vectors, with a spatial resolution of 0.25° in latitude and longitude. Wind speeds are produced by blending observations from multiple satellites: the several SSM/I missions (SSM/I F08, F10, F11, F13, F14, F15 and F17), QuikSCAT, the Tropical Rainfall Measuring Mission Microwave Imager (TRMM-TMI), and the Advanced Microwave Scanning Radiometer Earth Observing System (AMSR-E). Wind direction data is extracted from NCEP-R2 and ECMWF operational analysis, being interpolated to the blended wind speed grid. By blending multiple satellite

observations, it is possible to fill in the data gaps of each satellite individual measuring missions, both in time and space, allowing the construction of an ocean surface wind database that spans from 1987 to the present time in near real-time. Detailed description about this dataset can be found in Zhang, Reynolds, and Bates (2006).

The IFREMER Blended Wind Fields gridded product blends wind data from the same satellites as NCDC-BSW (QuikSCAT and SSM/I radiometers available at Météo France at near real-time), with the same spatial and temporal resolution (6-hourly for a 0.25° latitude/longitude grid). The main difference between this product and NCDC-BSW is that IFREMER-BWF also blends the ECMWF analysis wind speed and direction data onto its grid, instead of simply adding wind direction records to its grid as NCDC-BSW does. Furthermore, this product spans from 1999 to 2009, not being available after this date. This dataset was obtained from the Centre de Recherche et d'Exploitation Satellitaire (CERSAT), at IFREMER, Plouzané (France), and more details can be found at the CERSAT-IFREMER website (<http://cersat.ifremer.fr/>).

The CCMP is a long-term (presently from 1987 to 2011), gap-free 6-hourly gridded database of global ocean surface wind vectors, with a spatial resolution of 0.25° both in latitude and longitude. CCMP also uses, as first-guess background fields, NWP reanalysis/analysis: the ECMWF ERA-40 reanalysis from mid-1987 to the end of 1998, and the ECMWF operational analysis from 1999 onward. CCMP assimilates into these background field satellite wind measurements from the TRMM-TMI, QuikSCAT, WindSat, SSM/I, SSMIS, AMSR-E and other satellites, and also data from in situ measurements (ships, buoys, etc.). More details about this product can be found in Atlas, Hoffman, Ardizzone, Leidner, and Jusem (2009).

All these satellite-derived wind data are retrieved mainly by microwave sensors (radiometer, altimeter and/or scatterometer), which are more sensitive to the ocean surface roughness (from which the wind fields are derived through geophysical models) rather than the wind speed due to atmospheric stratification. Thus, this kind of sensors is calibrated to an equivalent neutrally stable wind at a reference height of 10 m above sea level (a.s.l.) (Chelton, Schlax, Freilich, & Milliff, 2004; Liu & Tang, 1996; Singh, Parekh, & Attada, 2013; Verschell, Bourassa, Weissman, & O'Brien, 1999). Furthermore, for all satellite-derived data, a thorough quality control was performed and all records flagged with poor quality were disregarded.

2.2. Reanalysis and analysis datasets

The NCEP-R2 (Kanamitsu et al., 2002) reanalysis belongs to the first generation of reanalysis produced and publicly released. It is still operational and updated in near real-time, a unique feature among the first generation reanalyses, and still widely used. However, this product has a very coarse spatial resolution (approximately 2.5° in latitude and longitude) and the amount of satellite-derived meteorological data assimilated is very limited.

In recent years, a newer generation of reanalysis datasets has been produced: the ERA-Interim (Simmons et al., 2007) represents the state-of-the-art reanalysis produced in Europe, with unique assets such as the four dimensional variational analysis assimilation methods for observed data (4D-var). The NCEP-CFSR (Saha et al., 2010) also offers exclusive features, such as the highest spatial resolution of all reanalyses and the use of a coupled atmosphere-land-ocean-sea ice model. Both ERA-Interim and NCEP-CFSR employ a variational bias correction that offers clear improvement in satellite radiance biases. The reanalysis produced by NASA, NASA-MERRA (Rienecker et al., 2011) introduced an innovation by implementing an incremental analysis update, a nudging technique that offers smoother transitions from the model towards the observations.

The NCEP-FNL and NCEP-GFS analysis, although not reanalysis products, have a substantial record in wind energy applications, mainly due to the advantage of being available and released in real-time (within a day or less). This fast availability is related to the fact that these

analyzed datasets only assimilate operational observations (i.e., that are part of the global operational measurements network and are quickly available for model assimilation). However, and as consequence of this fast availability, these analyzed products do not assimilate as much observed data as reanalysis products do. Although these two NCEP analyses share the same GCM model, characteristics and configuration details, NCEP-FNL assimilates a higher amount of measurements but NCEP-GFS has a much finer spatial resolution.

2.3. WRF mesoscale model simulation

The NWP simulation of the near surface ocean winds was performed with the WRF mesoscale model, version 3.4.1, a widely used state-of-the-art NWP modelling code developed by NCEP and the National Center for Atmospheric Research (NCAR), among other institutions that collaborated in the developing, testing and validation of this model. Details regarding this code are available in Skamarock et al. (2008). The configuration and design of the ocean surface wind fields simulation are based on the findings of Carvalho, Rocha, and Gómez-Gesteira (2012), Carvalho et al. (in press-a,b) which evaluated and optimized this mesoscale model for the area under study. The simulation domains followed a two-way nesting strategy, with the innermost domain (with 5 km horizontal resolution) nested on a parent domain with 25 km horizontal resolution. Fig. 1 depicts the simulation domains.

2.4. Offshore measured wind data

The observed offshore wind data used in this study was collected by five buoys moored off the Galician northern and western coasts and the Gulf of Cádiz, which are operated and maintained by the Puertos del Estado Spanish Agency. Summarized information regarding these buoys is presented in Table 2, and Fig. 1 depicts their locations.

The buoys collect their wind measurements at 3 m a.s.l., while all the alternative offshore wind data sources under study refer their wind data to 10 m a.s.l. (including the WRF simulation, to match the other databases). Moreover, winds measured by buoys and simulated by NWP models (reanalyses, analyses and WRF simulation for the present case) are dependent on the surrounding atmospheric stability while, as aforementioned, all satellite-retrieved data considers equivalent neutrally stable winds. Since the aim of this study is to assess which of the alternative sources of offshore wind data is closer to “real” winds (stability-dependent), data from buoys and NWP models were not converted to equivalent neutrally stable winds. However, it is necessary to extrapolate the buoy data to 10 m a.s.l. Ideally, this extrapolation should be done with methods that account for the atmospheric stability, such as the Monin–Obukhov theory (Monin & Obukhov, 1954). However, to apply this method measurements of temperature, heat fluxes and friction velocity are necessary, and the buoys considered here do not collect such data. Thus, methods to extrapolate the wind that assume a neutral atmosphere, and that can be employed with the available buoy measurements (wind speed and direction only), were chosen. The logarithmic wind profile was used to extrapolate the measured winds:

$$U_z = (U_{z_m}) * \ln\left(\frac{z}{z_0}\right) / \ln\left(\frac{z_m}{z_0}\right) \quad (1)$$

In this expression, U_z is the wind speed at the desired measurement height z , z_m is the reference measurement height, U_{z_m} is the wind speed at the reference measurement height and z_0 is the site roughness length. Peixoto and Oort (1992) suggested a value of 1.52×10^{-4} m for the global ocean roughness length. There is evidence that differences between real winds and neutrally stable winds are low over the global ocean, rarely exceeding $0.5 \text{ m}\cdot\text{s}^{-1}$ in the wind speed (Bourassa,

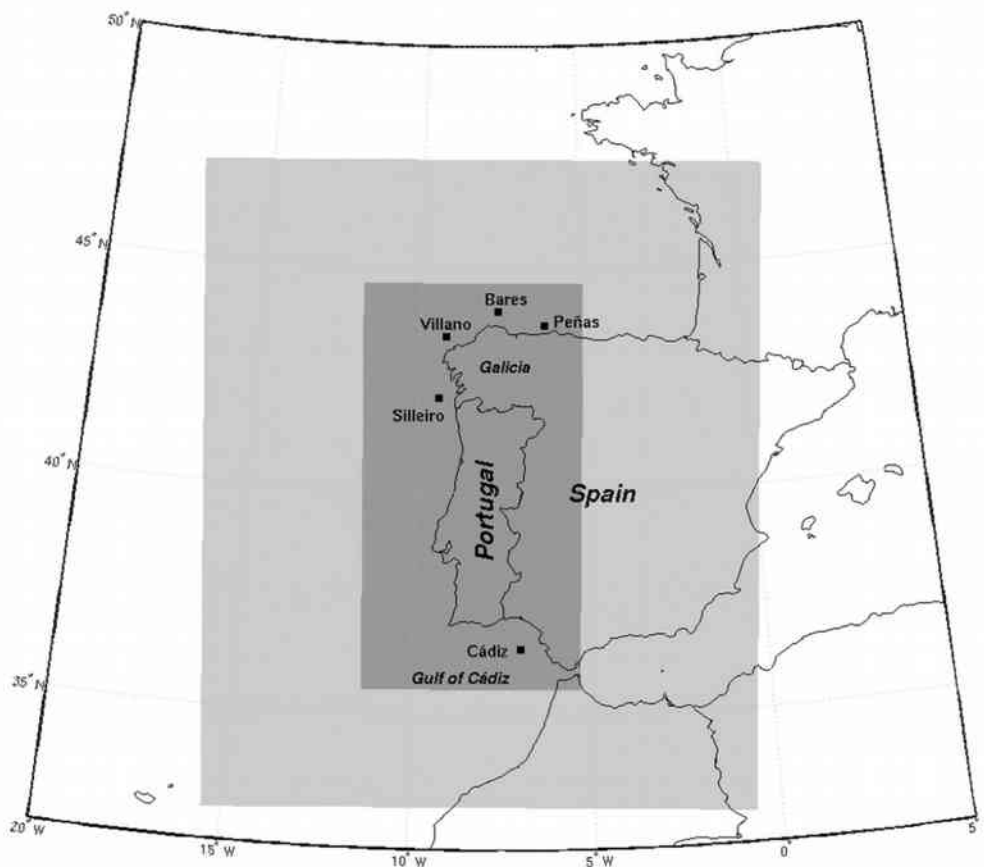


Fig. 1. Buoy locations and simulation domains.

Table 2
Main characteristics of the considered buoys.

Buoy	Latitude	Longitude	Distance to the coast
Peñas	43° 45' N	6° 9' 36" W	–20 km
Bares	44° 3' 54" N	7° 37' 5" W	–32 km
Villano	43° 30' N	9° 12' 36" W	–30 km
Silleiro	42° 7' 48" N	9° 23' 24" W	–40 km
Cádiz	36° 28' 37" N	6° 57' 47" W	–55 km

Legler, O'Brian, & Smith, 2003; Chelton & Freilich, 2005; Kara, Wallcraft, & Bourassa, 2008; Mears, Smith, & Wentz, 2001). Moreover, this extrapolation is done for a small height difference (from 3 to 10 m a.s.l.) over a surface with low roughness lengths, suggesting that eventual differences between measured and extrapolated winds will be small. Furthermore, this analysis spans through a complete year of wind data, whereby it is reasonable to suppose that the average atmospheric stratification is close to neutral.

Considering the 10 m a.s.l. winds obtained with the abovementioned methodology, the local wind regimes of each buoy in 2008 are depicted in Fig. 2. The wind roses show the sector-wise percentage of wind direction occurrence and, for each sector, the relative frequency of wind speed bins, at $3 \text{ m}\cdot\text{s}^{-1}$ intervals.

It is visible that these coastal winds tend to follow the local topography. These tendencies were previously reported for the Galician coast by Alvarez, Gomez-Gesteira, deCastro, and Dias (2008), Alvarez, Gomez-Gesteira, deCastro, Gomez-Gesteira, and Dias (2010), Gómez-Gesteira, Moreira, Alvarez, and deCastro (2006), and for the Gulf of Cádiz by Jungclaus and Mellor (2008) and Peliz, Dubert, Marchesielo, and Teles-Machado (2007). At Peñas buoy, the wind regime is dominated by the West–east axis with a higher percentage of occurrences for the West and adjacent sectors, and speeds reach $15 \text{ m}\cdot\text{s}^{-1}$ in these prevailing sectors. At Bares the wind regime is similar to the one observed in Peñas, but here the West–Southwest sector is the dominant one with a high frequency of strong winds (above $9 \text{ m}\cdot\text{s}^{-1}$). In Villano, the wind regime is characterized by strong (above $9 \text{ m}\cdot\text{s}^{-1}$) Northeast winds. At Silleiro buoy, it is possible to see a clear prevalence of intense (above $9 \text{ m}\cdot\text{s}^{-1}$) northerly winds, while in Cádiz the North–Northwest sector is the dominant one with moderate winds (ranging from 6 to $9 \text{ m}\cdot\text{s}^{-1}$), while the strongest winds arise from the East–Southeast sector.

It is important to mention that these measured winds were not assimilated into any of the reanalysis and analysis datasets here considered (at least in an operational and constant way, in what is related to the reanalysis and analysis datasets), nor in the WRF modelled winds, making this measured winds an independent database for validation of all these tested wind products.

2.5. Statistical evaluation of the wind data

To compare the alternative sources of offshore wind data with the measurements, the following statistical error metrics were used: the Root Mean Squared Error (RMSE), the bias, Standard Deviation of the Error (STDE) and the correlation coefficients (R^2) for the wind speed and direction. The buoys, WRF simulation, NASA-MERRA and NCEP-CFSR have hourly records, while CCMP, NCDC-BSW, IFREMER-BWF, ERA-Interim, NCEP-FNL and NCEP-GFS offer four records per day (00, 06, 12 and 18 h) and QuikSCAT only has two records per day (06 and 18 h for the ascending and descending passes, respectively). For these error metrics, only the simultaneous and valid wind speed and direction data records among all databases were considered, in order to analyze the record-by-record accuracy of the several databases and thus assess the performance of each wind product to represent the measured wind speed and direction at a given time instant. In addition, the Weibull probability density functions (PDFs) were used to characterize the local wind regimes in terms of wind speed distribution frequency

and to compare which database offers the Weibull PDF closer to the one derived from measured data. The Weibull distribution has been widely used to describe wind speed distributions, in particular for wind energy applications, due to its accurate fit to wind speed data. The most probable and mean wind speed, derived from the Weibull wind speed distribution, were also used as comparative metrics. To compute the Weibull PDFs, all the valid data records of each database were considered, instead of just the simultaneous records. In this way, the hypothetical advantage of a given wind data source having higher temporal sampling is preserved in the analysis. Also, the available wind power flux at each site, derived from measurements and from alternative data sources, was computed and used as a comparative metric, considering only wind speed data between 3.5 and $25 \text{ m}\cdot\text{s}^{-1}$ (to comply with typical wind turbine cut-in and cut-off speeds).

For all the gridded offshore wind databases, the closest grid points to the buoy locations were selected for comparison. As for QuikSCAT data, the closest swath point to the buoy locations (at a maximum distance of 12.5 km to the buoy) was selected.

3. Results and discussion

3.1. Statistical analysis

Table 3 shows the RMSE, bias, STDE and R^2 computed between the buoys and the alternative offshore wind data sources. The last section of Table 3 correspond to the mean values of each error metric for all buoys, weighted by the number of valid and simultaneous records shared by all databases (N). The bias weighted means were computed using the absolute values of the individual bias values, in order to assess the magnitude of the biases avoiding mutual cancellations effects, due to the positive and negative values that this error metric can assume. For guidance, for each error metric weighted mean the best value is in bold and underlined.

Considering the overall (weighted mean) errors, Table 3 shows that WRF modelled winds present the lowest errors in terms of RMSE and STDE and the highest correlations, both for the wind speed and direction (for the wind direction, although it does not show the best score its R^2 is very close to the highest one). Still for these error metrics, CCMP-derived wind data showed the best results after WRF (showing even the highest R^2 for the wind direction, together with NCEP-CFSR and NCEP-GFS), with the exception of the wind speed STDE, where IFREMER-BWF has the lowest value after WRF simulated winds. These results translate the fact that WRF simulated winds are the best ones in terms of temporal accuracy. For the wind speed biases, CCMP was the one with the best performance, although closely followed by WRF and NCEP-CFSR wind speed data. For the wind direction biases, the NCEP-GFS is the one with the lowest value, with CCMP showing the second best weighted mean bias. Looking at all the error metric weighted means, WRF and CCMP clearly stand out when compared to the other databases, generally showing winds closest to the measurements.

If analysis is restricted to satellite-derived winds, CCMP is clearly the one with the most accurate wind data, being the only exception the wind direction STDE and wind speed correlation coefficient where IFREMER-BWF shows the best scores. Even for the remaining error metrics, IFREMER-BWF is the satellite-derived database with the lowest errors after CCMP. QuikSCAT is in general the one with the highest errors among the satellite-derived wind data sources, and only in the wind speed bias it does not show the highest errors (NCDC-BSW showed the highest wind speed weighted mean bias among the satellite-derived wind data). These better performances of blended satellite products over QuikSCAT are in accordance with the findings of Ruti et al. (2008).

If analysis is now restricted to several reanalyses and analyses, NCEP-CFSR shows the lowest overall errors. The fact that this reanalysis is the only one that includes an ocean model in its architecture is clearly contributing to this good performance in terms of offshore wind

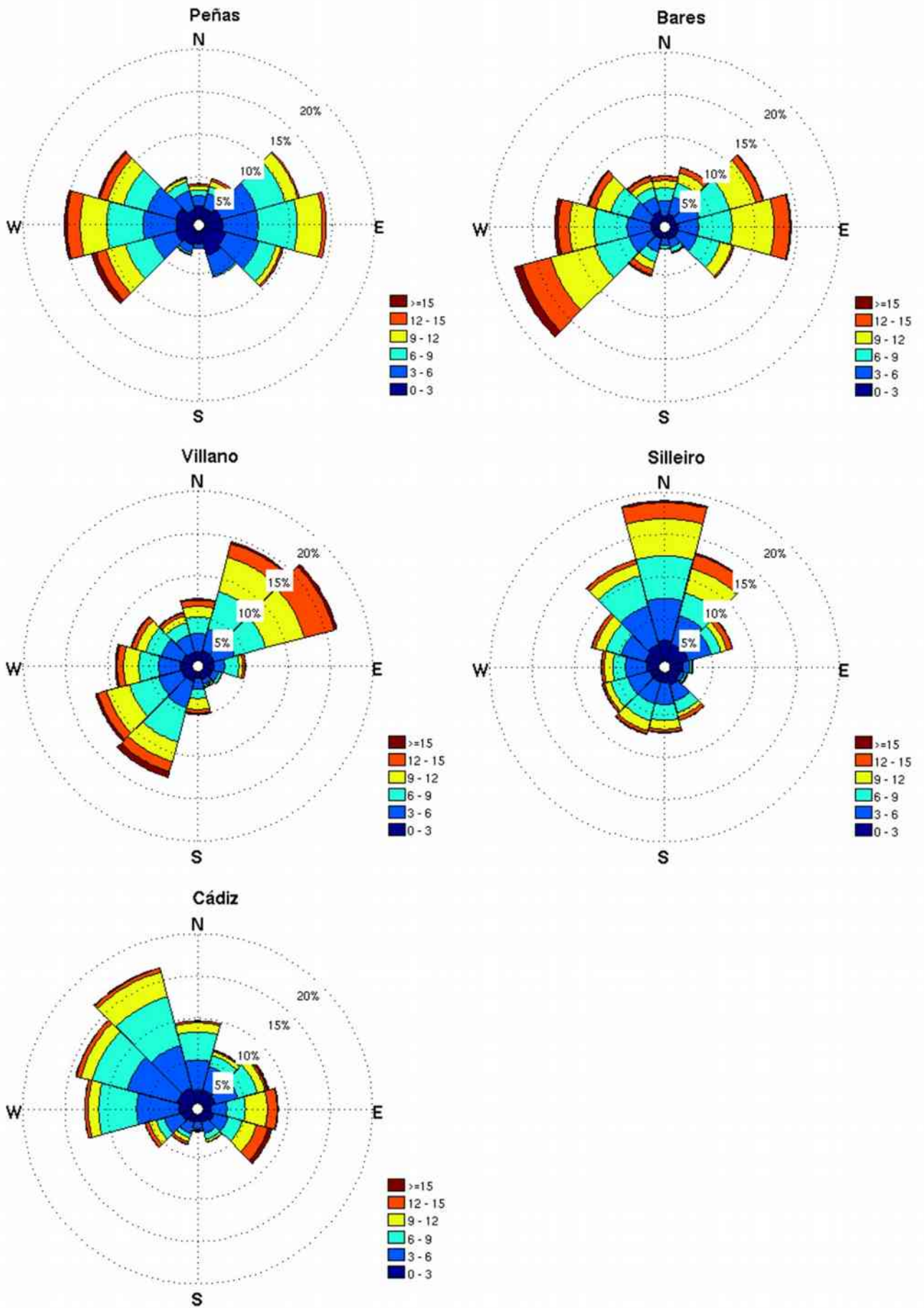


Fig. 2. Wind regimes at the buoys.

Table 3
Statistics of the comparison between alternative sources of offshore wind data and buoy wind measurements. The bold and underlined values correspond to the lowest errors for each statistical metric, for guidance.

Buoy	Database	RMSE		Bias		STDE		R ²		N
		Speed	Direction	Speed	Direction	Speed	Direction	Speed	Direction	
Peñas	WRF	1.93	47.54	0.26	4.21	1.91	47.35	0.86	0.69	412
	QuikSCAT	2.71	57.79	1.18	−3.03	2.44	57.71	0.80	0.63	
	CCMP	2.16	52.40	0.02	0.34	2.16	52.40	0.81	0.64	
	NCDC-BSW	2.63	58.69	1.25	0.63	2.32	58.69	0.81	0.63	
	IFREMER-BWF	2.42	52.48	0.89	−0.54	2.26	52.48	0.82	0.65	
	NCEP-CFSR	2.07	45.08	0.16	3.40	2.06	44.95	0.84	0.74	
	ERA-Interim	2.59	61.99	0.93	2.14	2.42	61.95	0.76	0.65	
	NASA-MERRA	2.14	51.37	0.03	0.86	2.14	51.36	0.81	0.67	
	NCEP-RII	3.97	60.84	1.57	10.15	3.64	59.99	0.59	0.57	
	NCEP-FNL	2.33	48.82	0.70	−1.21	2.22	48.81	0.81	0.69	
	NCEP-GFS	2.26	48.77	0.40	−0.11	2.22	48.77	0.81	0.69	
	Bares	WRF	1.60	30.82	0.06	−4.06	1.60	30.55	0.91	
QuikSCAT		1.70	40.56	0.41	−11.50	1.65	38.89	0.91	0.81	
CCMP		1.56	31.07	0.15	−7.73	1.55	30.10	0.92	0.91	
NCDC-BSW		1.70	46.74	0.55	−10.20	1.61	45.61	0.91	0.72	
IFREMER-BWF		1.44	33.28	0.22	−7.47	1.42	32.43	0.93	0.89	
NCEP-CFSR		1.81	34.59	−0.28	−6.83	1.79	33.91	0.89	0.84	
ERA-Interim		2.27	45.82	0.19	−5.51	2.26	45.49	0.80	0.90	
NASA-MERRA		1.94	36.08	−0.98	−6.44	1.67	35.50	0.90	0.89	
NCEP-RII		3.27	50.82	0.75	−3.28	3.18	50.72	0.72	0.62	
NCEP-FNL		1.82	33.85	0.46	−6.04	1.76	33.30	0.89	0.84	
NCEP-GFS		1.84	36.61	−0.19	−5.86	1.83	36.14	0.88	0.84	
Villano		WRF	1.60	32.43	0.24	3.20	1.59	32.28	0.91	0.91
	QuikSCAT	1.61	40.18	0.55	2.82	1.51	40.09	0.92	0.87	
	CCMP	1.56	34.96	0.16	1.63	1.55	34.93	0.91	0.91	
	NCDC-BSW	1.59	48.14	0.78	2.75	1.38	48.06	0.93	0.73	
	IFREMER-BWF	1.49	32.32	0.34	3.34	1.45	32.15	0.93	0.90	
	NCEP-CFSR	1.76	37.88	−0.13	0.96	1.75	37.86	0.89	0.88	
	ERA-Interim	2.42	41.20	0.61	9.44	2.34	40.10	0.80	0.91	
	NASA-MERRA	1.62	37.63	−0.46	5.12	1.55	37.28	0.92	0.90	
	NCEP-RII	2.81	51.27	0.23	8.69	2.80	50.53	0.73	0.70	
	NCEP-FNL	2.30	38.40	1.27	1.78	1.92	38.36	0.87	0.88	
	NCEP-GFS	1.72	35.91	0.13	0.80	1.71	35.90	0.90	0.90	
	Silleiro	WRF	1.64	47.44	0.17	3.57	1.63	47.30	0.91	0.70
QuikSCAT		1.31	53.52	0.18	5.09	1.30	53.28	0.94	0.73	
CCMP		1.39	43.32	−0.04	−1.34	1.38	43.30	0.93	0.85	
NCDC-BSW		1.78	55.21	0.65	6.87	1.66	54.78	0.90	0.56	
IFREMER-BWF		1.44	41.97	−0.06	2.55	1.43	41.89	0.93	0.84	
NCEP-CFSR		1.62	49.26	−0.03	0.55	1.62	49.26	0.91	0.80	
ERA-Interim		2.46	57.24	0.98	9.78	2.25	56.39	0.82	0.82	
NASA-MERRA		1.89	48.53	−0.58	3.65	1.80	48.39	0.89	0.80	
NCEP-RII		3.92	65.32	1.30	9.81	3.70	64.57	0.54	0.37	
NCEP-FNL		3.07	48.86	−2.02	−1.68	2.31	48.83	0.84	0.76	
NCEP-GFS		1.65	47.29	−0.15	−0.77	1.64	47.28	0.90	0.78	
Cádiz		WRF	1.57	43.89	−0.03	−0.13	1.57	43.89	0.90	0.81
	QuikSCAT	1.51	48.63	0.27	3.71	1.48	48.49	0.93	0.69	
	CCMP	1.68	39.17	−0.12	3.56	1.67	39.01	0.89	0.79	
	NCDC-BSW	1.57	55.02	0.63	0.71	1.43	55.02	0.92	0.76	
	IFREMER-BWF	1.61	44.23	0.05	6.19	1.61	43.79	0.90	0.75	
	NCEP-CFSR	1.85	40.09	0.17	5.54	1.84	39.70	0.87	0.82	
	ERA-Interim	2.46	55.84	−0.03	5.65	2.46	55.56	0.73	0.79	
	NASA-MERRA	2.08	47.31	−0.85	3.19	1.90	47.20	0.85	0.79	
	NCEP-RII	3.20	69.83	−0.36	2.85	3.18	69.77	0.54	0.44	
	NCEP-FNL	2.26	49.03	0.90	11.14	2.08	47.75	0.84	0.69	
	NCEP-GFS	1.74	36.52	0.12	3.86	1.74	36.31	0.89	0.85	
	Weighted mean	WRF	1.69	39.85	0.17	3.29	1.68	39.69	0.90	0.80
QuikSCAT		1.89	48.09	0.61	5.10	1.77	47.65	0.89	0.75	
CCMP		1.72	40.72	0.10	2.77	1.72	40.48	0.88	0.81	
NCDC-BSW		1.93	52.68	0.83	3.95	1.74	52.37	0.89	0.68	
IFREMER-BWF		1.75	41.08	0.39	3.71	1.69	40.79	0.90	0.80	
NCEP-CFSR		1.85	40.98	0.16	3.45	1.84	40.74	0.87	0.81	
ERA-Interim		2.45	52.09	0.58	6.08	2.35	51.60	0.78	0.80	
NASA-MERRA		1.93	43.91	0.52	3.74	1.82	43.67	0.87	0.80	
NCEP-RII		3.43	58.23	0.87	7.31	3.28	57.68	0.64	0.57	
NCEP-FNL		2.30	43.19	0.98	3.79	2.04	42.88	0.85	0.78	
NCEP-GFS		1.89	41.21	0.22	2.08	1.88	41.08	0.87	0.81	

simulation. NCEP-GFS also shows good performance, surpassing the other reanalysis products. Analysis products, unlike reanalysis, make use of the most recent and up-to-date NWP operational model configuration, bug fixes, updates and improvements in the measured data

assimilation systems. Although this fact can cause some inconsistencies in their data homogeneity over time (Carvalho et al., 2014), it may also produce better results. Furthermore, NCEP-CFSR and NCEP-GFS are the reanalysis/analysis products with finer resolution, which can also be

related to their good performances. Oppositely, NCEP-RII is clearly the database with the highest errors among all the databases considered here, mainly in terms of temporal accuracy (RMSE, STDE and R^2). This is certainly related to the fact that this reanalysis is the database with the coarsest spatial resolution, which results in the fact that the closest NCEP-RII point to each buoy is about 100 km distant and, obviously, higher errors are to be expected.

There seems to be present a tendency for WRF, QuikSCAT, NCDC-BWF, IFREMER-BWF, ERA-Interim, NCEP-RII and NCEP-FNL to overestimate the wind speed, since in all buoys these databases show positive wind speed biases. Only in Silleiro (CCMP, IFREMER-BWF, NCEP-FNL) and Cádiz (WRF, CCMP, RII and ERA-Interim) an underestimation of the wind speed by some of these databases is present. QuikSCAT tendency to overestimate the wind speed was previously reported for the Pacific (Ebuchi et al., 2002) and Indian Ocean (Satheesan et al., 2007), and also for the Iberian Peninsula Atlantic coast (Alvarez et al., 2013; Carvalho, Rocha, Gómez-Gesteira, et al., 2013). As for NWP models, this offshore wind speed overestimation might be explained by the fact that normally NWP models do not include an ocean model in their code (only NCEP-CFSR does), representing the ocean as a constant flat surface. Obviously, real ocean tides and swells produce variations in the ocean surface height, meaning higher and variable roughness lengths. Therefore, NWP models will consider ocean areas with lower roughness values, meaning lower friction between atmosphere and ocean surface that produces higher surface wind speeds. Oppositely, NASA-MERRA reanalysis show a tendency to underestimate the wind speed, with negative biases for all buoys except in Peñas. CCMP, NCEP-CFSR and NCEP-GFS do not seem to have any tendency to bias the data.

Moreover, the spatial resolution of the databases seems to influence their performance, with the finest resolution products (WRF and satellite-derived databases) showing better results than the coarser databases (NCEP-RII, NCEP-FNL and ERA-Interim). From the results presented in Table 3 all databases show poorer performance for Peñas buoy, which is the closest to the coast. The difference between the error figures for Peñas and the remaining buoys is more pronounced for all satellite-derived products, especially for QuikSCAT. This issue is related to land masking limitations, which are typical of satellite-derived wind data. Since CCMP and IFREMER-BWF blend data from several satellites with NWP output (NCDC-BSW only considers wind direction data from NWP, not blending any NWP wind data), they are able to attenuate these land masking effects for areas near the coast. However, NWP-derived winds also show worse results for this location, albeit less markedly than satellite-derived winds for the remaining buoys. Although NWP modelled data does not suffer from land masking limitations, these coastal winds are very dependent on the surrounding topography (Fig. 2). As the Cape of Peñas is close to a mountain range with very complex orography, NWP models are unable to accurately simulate these terrain-induced wind flows, mainly because of their limited resolution. Moreover, coastal areas are characterized by land-sea gradients and discontinuities (land use, topography, temperature, etc.) that are not easily captured by NWP models. Since WRF is the modelled dataset with the finest spatial resolution here considered, it is able to better resolve these coastal wind circulations, partially mitigating these issues and producing the best results to this, and the others, buoys locations. These better performances of high resolution NWP modelled offshore wind data over satellite-derived data were previously reported by Penabad et al. (2008).

Looking at the number of available simultaneous and valid data records (N) considered on the statistical results depicted in Table 3 and to the temporal sampling of each dataset, QuikSCAT is the one that limits the number of available records due to its lower temporal sampling and also large amount of discarded (missing/poor quality) data. NWP-derived winds do not suffer from missing/erroneous records, and the satellite data blended products show only few data gaps. Therefore, it becomes interesting to repeat the results of Table 3 but

without considering QuikSCAT. This way, it is possible to obtain much more data records for this comparison: an increase on averaged N for all buoys from about 300 to nearly 1300, meaning almost 100% availability (remembering that discarding QuikSCAT all other databases offer at least 4 records per day). These results are presented in Table 4, where only the weighted mean results are shown.

By considering a higher number of compared records, it becomes possible to see that WRF is still the database with the overall best results but now mainly for the wind speed. IFREMER-BWF is now the database with the best performance for the wind direction, and also for the wind speed after WRF. Although CCMP and IFREMER-BWF show similar results, by considering a higher number of wind data the latter is able to surpass CCMP, except for the wind speed biases where CCMP is still the best.

3.2. Error dependence on measured wind speed

In this section it will be assessed if the wind speed and direction data derived from the alternative wind data sources show any variation or dependence with the measured speed (i.e., if the satellite-derived and/or NWP modelled winds show a better or worse performance in the presence of weak or strong winds). To this end, the wind speed RMSE and bias are computed for four different bins: when measured winds are below $4 \text{ m}\cdot\text{s}^{-1}$; between 4 and $8 \text{ m}\cdot\text{s}^{-1}$; between 8 and $12 \text{ m}\cdot\text{s}^{-1}$ and above $12 \text{ m}\cdot\text{s}^{-1}$. Table 5 shows these results in terms of the weighted mean of all buoys.

All databases show higher errors in the presence of low and strong wind speeds, and consequently better performances for intermediate ones (between 4 and $12 \text{ m}\cdot\text{s}^{-1}$). IFREMER-BWF seems to show the worst performance only for low wind speeds, improving their accuracy with increasing wind speeds. Conversely, NCEP-CFSR and NASA-MERRA show the best results for low wind speeds, with its errors increasing for wind speeds above $8 \text{ m}\cdot\text{s}^{-1}$ (mainly in terms of RMSE). This behaviour was expected for scatterometer-derived data such as QuikSCAT, since this kind of instrument has known limitations in the presence of low and strong wind speeds. Weak winds produce very low (or none) amounts of backscatter, which scatterometers have difficulties in measuring. Strong winds can only produce proportional backscatter in the ocean surface until a certain threshold, after which no more backscatter is produced even if the wind speed keeps increasing.

A remarkable issue is that all databases show positive high biases for low wind speeds, which decrease in magnitude and pass from positive to negative with increasing wind speed. For the strongest wind speed bin, these biases are now negative (except QuikSCAT) but high in magnitude again. The only exception is QuikSCAT, which systematically shows positive biases. This reflects the fact that all databases have a tendency to overestimate weak winds and underestimate strong winds, with the over/underestimation tendencies being minimized in the presence of intermediate wind speeds. Li et al. (2013) also confirmed this behaviour.

3.3. Weibull PDFs

In this section, the wind speed PDFs assuming a Weibull distribution are computed for measured and alternative sources derived wind data. Through these PDFs, it is possible to assess which of the alternative sources of offshore wind data offers a more accurate characterization of the local wind speed distribution. Assessing the wind speed distribution accuracy of each database is of particular importance for offshore wind energy assessment applications, which traditionally fit wind speed data to Weibull distributions in order to quantify the average wind energetic potential of a given area. It should be taken into account that these PDFs translate the wind speed frequency distributions, meaning that the temporal accuracy of each database will not be reflected in the PDFs. The Weibull PDFs for all offshore wind data sources are depicted in Fig. 3.

Table 4
Statistics of the comparison between alternative sources of offshore wind data and buoy wind measurements excluding QuikSCAT. The bold and underlined values correspond to the lowest errors for each statistical metric, for guidance.

Buoy	Database	RMSE		Bias		STDE		R ²		N
		Speed	Direction	Speed	Direction	Speed	Direction	Speed	Direction	
Weighted mean	WRF	1.72	37.35	0.17	2.56	1.71	37.26	0.88	0.85	-
	CCMP	1.78	36.70	0.15	2.74	1.77	36.56	<u>0.87</u>	0.85	
	NCDC-BSW	2.05	49.57	0.73	3.61	1.91	49.38	0.85	0.72	
	IFREMER-BWF	1.76	36.69	0.25	3.19	1.73	36.51	0.88	0.85	
	NCEP-CFSR	1.85	<u>37.92</u>	0.24	2.88	1.83	<u>37.80</u>	<u>0.86</u>	0.85	
	ERA-Interim	2.50	48.95	0.50	5.16	2.41	48.48	0.75	0.84	
	NASA-MERRA	2.03	39.90	0.67	4.16	1.88	39.65	0.85	0.83	
	NCEP-RII	3.53	55.74	0.84	6.78	3.39	55.29	0.59	0.62	
	NCEP-FNL	2.47	40.01	1.07	3.02	2.15	39.80	0.82	0.83	
	NCEP-GFS	1.96	38.20	0.23	2.30	1.94	38.11	0.85	0.85	

In general, WRF modelled winds present the best results, with PDFs very close to the ones derived from measured data. CCMP seems to be the best database after WRF. In Bares and Villano all databases show similar PDFs with the exception of NASA-MERRA (in both) and NCEP-RII (in Bares), which show distinct PDF shapes when compared with the remaining databases and, especially, when compared to the PDFs derived from measurements. For the remaining buoys, the PDFs show higher disagreements between themselves, especially in Peñas and Cádiz. At Silleiro, NCEP-FNL clearly fails to represent the wind speed distribution frequency, which might be related to the fact this database has a coarse spatial resolution (1° lat/lon). Moreover, its nearest grid point to Silleiro buoy is located close to the coast, which can induce higher errors in its representation of coastal circulations.

It is visible that all databases show higher errors in representing the wind speed distribution in Peñas and Cádiz sites, and it is also on these buoys that it is seen the highest discrepancies among the several databases PDFs. As aforementioned, satellites show limitations in collecting accurate wind measurements in Peñas due to land masking effects, while NWP modelled data has difficulties in resolving land-sea discontinuities and small scale terrain-induced atmospheric flows (that are likely to occur in this complex area in terms of topography) due to their coarse resolution. Even WRF 5 km spatial resolution is unable to resolve accurately these flows, although it shows far better results than the other databases. As for Cádiz, and although this buoy is considerably distant from the coast (around 55 km), it is located inside the Gulf of Cádiz, surrounded by land in almost all directions, which can also originate land masking issues in satellites. Moreover, the Gulf of Cádiz is also characterized by a complex orography that favours terrain-induced flows, where NWP models show weaknesses due to their coarse spatial resolution. Here, WRF finer resolution seems able to partially resolve these coastal flows, showing a PDF that practically matches the observed one.

Table 6 shows the wind power flux (P_{flux}), the mean (U_m) and most probable wind speed (U_{prob}) values for each database, together with the respective errors in terms of percentual deviations from the values derived from measurements. N represents the number of valid wind speed records of each one of the databases. The weighted mean errors are calculated using absolute values.

Table 6 confirms the results depicted in Fig. 3. WRF and CCMP generally show the Weibull distribution parameters closest to the ones derived from measured data, with NCEP-CFSR, IFREMER-BWF and NCEP-GFS showing also good results. These reanalyses/analyses are the ones with the finest resolution, which is certainly related to their good performances. CCMP shows the lowest deviations when compared to measured winds in terms of the Weibull A parameter, mean most probable wind speed. WRF modelled winds show the best results after CCMP for these deviations. For the k parameter, NCEP-CFSR shows the lowest deviations, closely followed by WRF. As for the wind power flux, WRF has the best performance with only 4.5% of average deviations when compared with the wind power fluxes derived from observed data. Although NCEP-CFSR and NCEP-GFS show the lowest wind power flux deviations after WRF, CCMP is also able to produce good estimations of the wind power flux.

As seen for the statistical analysis of Section 3.1, WRF, QuikSCAT, NCDC-BWF, IFREMER-BWF, ERA-Interim, NCEP-RII and NCEP-FNL show a tendency to overestimate the wind speed and, consequently, the wind power flux estimations. NASA-MERRA shows the opposite behaviour, systematically underestimating the mean wind speed and wind power fluxes. The remaining databases do not seem to have any tendency to over- or underestimate wind speeds and power fluxes. However, for the wind power fluxes CCMP always underestimates its values. Although CCMP does not reveal any over/underestimation tendency of the wind speed, since the wind power fluxes vary with the cube of the wind velocities, small underestimations can be enhanced.

Table 5
Wind speed RMSE and Bias per buoy wind speed bin. The bold and underlined values correspond to the lowest errors for each statistical metric, for guidance.

Buoy	Database	<4 m·s ⁻¹		4–8 m·s ⁻¹		8–12 m·s ⁻¹		>12 m·s ⁻¹	
		RMSE	Bias	RMSE	Bias	RMSE	Bias	RMSE	Bias
Weighted mean	WRF	1.87	0.80	1.61	0.06	1.58	-0.27	1.64	-0.30
	QuikSCAT	1.90	1.07	1.75	0.47	1.89	0.22	2.12	0.76
	CCMP	1.73	0.79	1.65	0.05	1.63	-0.60	1.97	-0.49
	NCDC-BSW	2.13	1.43	1.90	0.79	1.73	0.24	1.77	0.64
	IFREMER-BWF	1.87	0.84	1.74	0.40	1.66	-0.06	1.49	0.03
	NCEP-CFSR	1.82	0.88	1.79	-0.16	1.86	<u>-0.69</u>	2.07	-0.59
	ERA-Interim	2.80	2.01	2.19	0.52	2.16	-0.38	2.67	-1.18
	NASA-MERRA	1.74	0.80	1.72	-0.47	2.05	-1.46	2.53	-2.08
	NCEP-RII	3.63	2.42	3.14	0.61	3.17	-0.44	4.12	-0.57
	NCEP-FNL	2.30	1.26	2.18	0.49	2.15	-0.21	2.40	-0.27
NCEP-GFS	1.94	0.90	1.80	0.03	1.82	-0.49	2.09	-0.57	

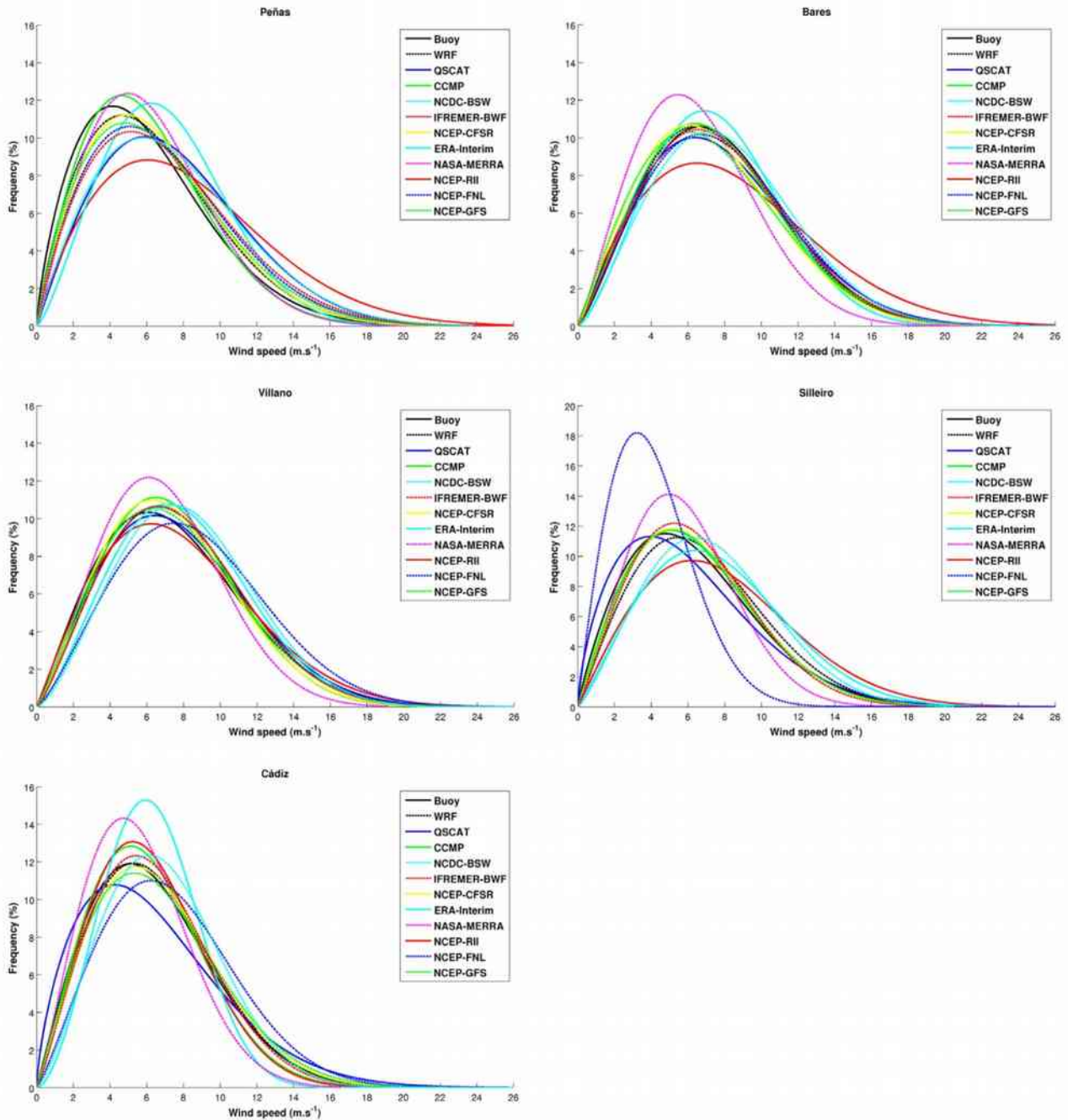


Fig. 3. Weibull PDFs for all offshore wind databases in all buoys.

Again visible in Table 6 is the worst performances off all databases for Peñas and Cádiz, due to the aforementioned reasons. One remarkable fact is that the temporal resolution is not a determinant factor to accurately represent the wind speed distribution at a given site. Although WRF and NCEP-CFSR have the highest temporal samplings (hourly data) and show good performances, NASA-MERRA shares their temporal resolution and is not able to depict the wind speed distributions so accurately. The 6-hourly records of CCMP seem to be sufficient to successfully depict the wind speed frequency distribution.

4. Conclusions

This study evaluates and compares offshore wind data derived from satellites (Cross-Calibrated Multi-Platform ocean wind vectors, QuikSCAT scatterometer, NCDC Blended Sea Winds and IFREMER

Blended Wind Fields), reanalyses (NCEP-CFSR, ERA-Interim, NASA-MERRA and NCEP-RII), analyses (NCEP-FNL and NCEP-GFS) and WRF modelled offshore winds, aiming to determine which one of these databases offers the offshore wind data closest to measurements collected by buoys moored offshore the Iberian Peninsula Atlantic coast. The findings presented here can be of great value for climate, oceanic, meteorological and offshore wind energy resource assessment applications that focus on ocean areas where in situ measured wind data is either not available or is insufficient and, therefore, alternative sources of offshore wind data have to be considered.

The results presented in this study show that WRF offshore wind simulation is the best alternative source to in situ measured offshore wind data, showing the highest temporal accuracy (RMSE, STDE and correlation coefficients) and offshore wind power flux estimations. However, offshore wind data taken from CCMP database shows the

Table 6
Wind power flux, mean and most probable wind speed for all databases and respective errors. The bold and underlined values correspond to the lowest errors for each statistical metric, for guidance.

Buoy	Database	A	Error	k	Error	U_m	Error	U_{prob}	Error	P_{flux}	Error	N	
		(–)		(–)		($m \cdot s^{-1}$)		($m \cdot s^{-1}$)		($W \cdot m^{-2}$)			
Peñas	Buoy	6.76	–	1.74	–	6.03	–	4.14	–	404	–	7048	
	WRF	7.22	6.7%	1.82	4.3%	6.41	6.3%	4.65	12.2%	452	11.9%	8784	
	QuikSCAT	8.46	25.1%	1.98	13.7%	7.46	23.7%	5.93	43.2%	604	49.4%	587	
	CCMP	6.80	0.5%	1.91	9.7%	6.03	0.0%	4.62	11.4%	345	–14.5%	1464	
	NCDC-BSW	8.40	24.1%	1.94	11.2%	7.43	23.2%	5.77	39.3%	560	38.6%	1388	
	IFREMER-BWF	7.88	16.5%	1.84	5.6%	7.01	16.2%	5.14	24.1%	538	33.2%	1440	
	NCEP-CFSR	7.36	8.8%	1.88	8.1%	6.52	8.1%	4.92	18.8%	449	11.1%	8784	
	ERA-Interim	7.99	18.1%	2.30	31.9%	7.08	17.3%	6.23	50.3%	421	4.1%	1464	
	NASA-MERRA	6.98	3.2%	2.02	15.9%	6.18	2.6%	4.97	20.0%	350	–13.4%	8784	
	NCEP-RII	9.24	36.6%	1.85	5.9%	8.21	36.1%	6.05	46.1%	817	102.2%	1464	
	NCEP-FNL	7.71	14.0%	1.85	6.4%	6.85	13.5%	5.07	22.4%	504	24.7%	1464	
	NCEP-GFS	7.48	10.6%	1.81	4.2%	6.65	10.3%	4.81	16.1%	491	21.6%	1435	
	Bares	Buoy	8.70	–	2.22	–	7.74	–	6.65	–	551	–	7470
		WRF	8.55	–1.8%	2.18	–2.0%	7.57	–2.2%	6.44	–3.1%	544	–1.3%	8784
		QuikSCAT	8.77	0.7%	2.07	–6.6%	7.75	0.1%	6.38	–4.0%	628	14.0%	425
CCMP		8.46	–2.9%	2.18	–1.8%	7.50	–3.1%	6.38	–4.0%	514	–6.6%	1464	
NCDC-BSW		9.13	4.9%	2.29	3.0%	8.08	4.4%	7.10	6.8%	603	9.5%	1461	
IFREMER-BWF		8.71	0.0%	2.17	–2.0%	7.72	–0.2%	6.56	–1.3%	567	2.9%	1440	
NCEP-CFSR		8.25	–5.2%	2.08	–6.1%	7.31	–5.6%	6.03	–9.2%	514	–6.7%	8784	
ERA-Interim		8.58	–1.4%	2.41	8.6%	7.60	–1.7%	6.87	3.4%	490	–11.1%	1464	
NASA-MERRA		7.32	–15.9%	2.15	–3.4%	6.48	–16.3%	5.46	–17.9%	361	–34.4%	8784	
NCEP-RII		9.60	10.3%	1.90	–14.3%	8.51	10.0%	6.49	–2.4%	871	58.1%	1464	
NCEP-FNL		8.90	2.3%	2.17	–2.4%	7.89	1.9%	6.69	0.7%	600	8.9%	1464	
NCEP-GFS		8.35	–4.0%	2.02	–9.2%	7.40	–4.3%	5.95	–10.5%	553	0.5%	1435	
Villano		Buoy	8.43	–	2.05	–	7.49	–	6.08	–	556	–	8745
		WRF	8.66	2.7%	2.22	8.2%	7.68	2.5%	6.60	8.7%	546	–1.6%	8784
		QuikSCAT	8.73	3.5%	2.10	2.7%	7.71	2.8%	6.42	5.7%	606	9.1%	435
	CCMP	8.39	–0.5%	2.26	10.3%	7.44	–0.8%	6.48	6.6%	492	–11.5%	1464	
	NCDC-BSW	9.25	9.7%	2.44	19.3%	8.19	9.3%	7.46	22.7%	587	5.7%	1461	
	IFREMER-BWF	8.66	2.7%	2.22	8.7%	7.68	2.4%	6.62	9.0%	549	–1.1%	1440	
	NCEP-CFSR	8.29	–1.6%	2.19	6.8%	7.34	–2.0%	6.27	3.2%	495	–10.8%	8784	
	ERA-Interim	8.97	6.5%	2.37	15.6%	7.95	6.1%	7.12	17.1%	560	0.9%	1464	
	NASA-MERRA	7.79	–7.6%	2.31	12.8%	6.91	–7.8%	6.09	0.3%	395	–28.8%	8784	
	NCEP-RII	8.82	4.6%	2.00	–2.4%	7.82	4.3%	6.23	2.5%	631	13.5%	1464	
	NCEP-FNL	9.65	14.4%	2.28	11.5%	8.55	14.0%	7.50	23.4%	705	26.9%	1464	
	NCEP-GFS	8.49	0.8%	2.13	4.2%	7.52	0.4%	6.31	3.9%	547	–1.5%	1435	
	Silleiro	Buoy	7.16	–	1.88	–	6.35	–	4.77	–	421	–	7754
		WRF	7.66	7.0%	2.01	7.4%	6.78	6.9%	5.45	14.2%	452	7.3%	8784
		QuikSCAT	6.84	–4.5%	1.66	–11.3%	6.08	–4.3%	3.94	–17.4%	505	20.0%	255
CCMP		7.22	0.8%	1.97	4.8%	6.40	0.7%	5.03	5.4%	402	–4.4%	1464	
NCDC-BSW		8.29	15.8%	2.25	19.9%	7.33	15.4%	6.38	33.8%	475	12.9%	1461	
IFREMER-BWF		7.21	0.7%	2.08	10.7%	6.38	0.5%	5.26	10.2%	370	–12.0%	1440	
NCEP-CFSR		7.26	1.5%	2.00	6.7%	6.43	1.3%	5.14	7.8%	393	–6.6%	8784	
ERA-Interim		8.62	20.4%	2.13	13.7%	7.63	20.2%	6.41	34.3%	568	35.0%	1464	
NASA-MERRA		6.51	–9.0%	2.21	17.8%	5.77	–9.1%	4.96	4.0%	261	–38.0%	8784	
NCEP-RII		8.82	23.1%	2.00	6.5%	7.82	23.1%	6.23	30.6%	631	49.9%	1464	
NCEP-FNL		4.64	–35.1%	1.95	4.2%	4.11	–35.2%	3.22	–32.5%	147	–65.0%	1464	
NCEP-GFS		7.27	1.6%	1.99	6.0%	6.44	1.4%	5.12	7.3%	401	–4.7%	1435	
Cádiz		Buoy	7.21	–	2.00	–	6.39	–	5.10	–	384	–	8770
		WRF	7.32	1.6%	2.06	2.8%	6.48	1.4%	5.29	3.9%	383	–0.1%	8784
		QuikSCAT	7.22	0.2%	1.69	–15.5%	6.42	0.5%	4.25	–16.6%	579	51.0%	237
	CCMP	6.93	–3.8%	2.11	5.6%	6.13	–4.1%	5.12	0.4%	325	–15.3%	1464	
	NCDC-BSW	7.79	8.1%	2.35	17.5%	6.89	7.8%	6.15	20.7%	377	–1.7%	1458	
	IFREMER-BWF	7.27	0.8%	2.13	6.6%	6.42	0.5%	5.40	5.9%	359	–6.5%	1440	
	NCEP-CFSR	7.46	3.5%	2.06	3.1%	6.61	3.4%	5.40	6.0%	398	3.8%	8784	
	ERA-Interim	7.04	–2.3%	2.70	35.2%	6.28	–1.8%	5.93	16.4%	256	–33.2%	1464	
	NASA-MERRA	6.30	–12.5%	2.16	7.8%	5.59	–12.5%	4.72	–7.4%	243	–36.7%	8784	
	NCEP-RII	6.95	–3.6%	2.17	8.7%	6.16	–3.6%	5.23	2.6%	307	–20.0%	1464	
	NCEP-FNL	8.27	14.7%	2.18	9.0%	7.31	14.4%	6.24	22.4%	486	26.6%	1464	
	NCEP-GFS	7.52	4.4%	2.00	0.0%	6.66	4.3%	5.32	4.4%	424	10.6%	1435	
	Weighted mean	WRF	–	3.9%	–	4.9%	–	3.8%	–	8.4%	–	4.5%	–
		QuikSCAT	–	6.8%	–	10.0%	–	6.3%	–	17.4%	–	28.7%	–
		CCMP	–	1.7%	–	6.4%	–	1.7%	–	5.5%	–	10.5%	–
NCDC-BSW		–	12.5%	–	14.2%	–	12.0%	–	24.7%	–	13.7%	–	
IFREMER-BWF		–	4.2%	–	6.7%	–	4.0%	–	10.1%	–	11.1%	–	
NCEP-CFSR		–	4.1%	–	6.2%	–	4.1%	–	9.0%	–	7.8%	–	
ERA-Interim		–	9.7%	–	21.0%	–	9.4%	–	24.3%	–	16.9%	–	
NASA-MERRA		–	9.7%	–	11.5%	–	9.7%	–	9.9%	–	30.3%	–	
NCEP-RII		–	15.7%	–	7.6%	–	15.4%	–	16.8%	–	48.7%	–	
NCEP-FNL		–	16.1%	–	6.7%	–	15.8%	–	20.3%	–	30.4%	–	
NCEP-GFS	–	4.3%	–	4.7%	–	4.2%	–	8.4%	–	7.8%	–		

lowest errors in terms of the mean wind speeds (biases and mean wind speed) and, together with IFREMER-BWF, a temporal accuracy similar to the WRF simulation. Therefore, in general CCMP and IFREMER-BWF can be seen as the best alternatives to WRF high resolution modelled offshore winds, if such results are unavailable. Specifically for offshore wind energy resource assessment, NCEP-CFSR reanalysis and NCEP-GFS analysis data can also be used with confidence as alternative to WRF modelled data, with better performances than CCMP and IFREMER-BWF.

While WRF, QuikSCAT, NCDC-BWF, IFREMER-BWF, ERA-Interim, NCEP-RII and NCEP-FNL show a tendency to overestimate the wind speeds and wind power fluxes estimates, NASA-MERRA shows an opposite tendency. CCMP, NCEP-CFSR and NCEP-GFS do not seem to have any tendency to over/underestimate wind velocities and wind power fluxes estimates (except CCMP, which seems to systematically underestimate the wind power fluxes). A common feature to all databases is that all of them overestimate low wind speeds and underestimate strong winds (except QuikSCAT, which shows an overestimation tendency transversal to all wind velocities magnitudes). The best performances are usually obtained in the presence of intermediate wind speeds ($4\text{--}12\text{ m}\cdot\text{s}^{-1}$).

Spatial resolution seems to have an important impact on the databases accuracy. The ones with finer spatial resolution are typically the ones with the best results (with some exceptions such as NASA-MERRA and NCDC-BSW). Since the in situ data here used is strongly influenced by the neighbouring topography, terrain characteristics and land-sea discontinuities, products with finer spatial resolutions are more likely to attain better performances. Although satellite-derived winds have finer spatial resolutions when compared to reanalysis and analysis products, they suffer from land masking issues that limit their accuracy in retrieving coastal winds. Temporal sampling rate does not seem to have such an impact, at least in what is related to the ability to represent local wind speed distributions (although it is advisable to use databases with at least 6-hourly records). However, temporal resolution of the wind products is an important characteristic in terms of the ability to accurately represent local wind circulation patterns.

Although the advantages in using mesoscale NWP models for high resolution offshore wind modelling are shown in this study, such tasks require considerable computational resources and time to obtain quality results. Moreover, it is known that satellite-derived wind data has its strength in open ocean areas. Therefore, the value of satellite-derived wind data cannot be disregarded, and these kinds of offshore wind data sources have to be seriously considered when searching for alternative sources of wind information in particular for wide ocean areas. Since the buoys considered in this study are distributed through a wide geographical area, where each buoy shows its own local wind micro-climate, the conclusions and findings provided in this study can be considered with confidence for other areas, in particular coastal ones.

Acknowledgements

D. Carvalho was supported by the Portuguese Foundation for Science and Technology (F.C.T.) Ph.D grant SFRH/BD/73070/2010. This work was partially financed by Xunta de Galicia under the project "Programa de Consolidación e Estructuración de Unidades de Investigación Competitivas (Grupos de Referencia Competitiva)", co-funded by the European Regional Development Fund (FEDER). The authors would like to express their gratitude to all the climate, meteorological and oceanographic institutions referred in the text, for providing the data used in this work.

References

- Accadia, C., Zecchetto, S., Lavagnini, A., & Speranza, A. (2007). Comparison of 10-m wind forecasts from a regional area model and QuikSCAT scatterometer wind observations over the Mediterranean sea. *Monthly Weather Reviews*, *135*, 1945–1960.
- Alvarez, I., Gomez-Gesteira, M. M., deCastro, M., & Carvalho, D. (2013). Comparison of different wind products and buoy wind data with seasonality and interannual climate variability in the southern Bay of Biscay (2000–2009). *Deep-Sea Research Part II: Topical Studies in Oceanography*. <http://dx.doi.org/10.1016/j.dsr2.2013.09.028>.
- Alvarez, I., Gomez-Gesteira, M., deCastro, M., & Dias, J. M. (2008). Spatio-temporal evolution of upwelling regime along the western coast of the Iberian Peninsula. *Journal of Geophysical Research*, *113*, C07020.
- Alvarez, I., Gomez-Gesteira, M., deCastro, M., Gomez-Gesteira, J. L., & Dias, J. M. (2010). Summer upwelling frequency along the western Cantabrian coast from 1967 to 2008. *Journal of Marine Systems*, *79*, 218–226.
- Atlas, R., Hoffman, R. N., Ardizzone, J., Leidner, S. M., & Jusem, J. C. (2009). Development of a new cross-calibrated, multiplatform (CCMP) ocean surface wind product. *AMS 13th Conference on Integrated Observing and Assimilation Systems for Atmosphere, Oceans, and Land Surface (IOAS-AOLS)*, Phoenix, Arizona.
- Berge, E., Byrkjedal, Ø., Ydersbond, Y., & Kindler, D. (2009). Modelling of offshore wind resources. *Comparison of a mesoscale model and measurements from FINO 1 and North Sea oil rigs. Proceedings of EWEC 2009, Marseille, France*.
- Bourassa, M. A., Legler, D. M., O'Brian, J. J., & Smith, S. R. (2003). SeaWinds validation with research vessels. *Journal of Geophysical Research*, *108*(3019), 16.
- Bruun, M., Koch, W., Horstmann, J., Hasager, C., & Nielsen, M. (2006). Wind resource assessment from C-band SAR. *Remote Sensing of Environment*, *105*(1), 68–81.
- Carvalho, D., Rocha, A., & Gómez-Gesteira, M. (2012). WRF model ocean surface wind simulation forced by different reanalysis: Comparison with observed data along the Iberian Peninsula coast. *Ocean Modelling*, *56*, 31–42.
- Carvalho, D., Rocha, A., Gómez-Gesteira, M., Alvarez, I., & Silva Santos, C. (2013). Comparison between CCMP, QuikSCAT and buoy winds along the Iberian Peninsula coast. *Remote Sensing of Environment*, *137*, 173–183.
- Carvalho, D., Rocha, A., Gómez-Gesteira, M., & Santos, C. (2012). A sensitivity study of the WRF model in wind simulation for an area of high wind energy. *Environmental Modelling and Software*, *33*, 23–34.
- Carvalho, D., Rocha, A., Gómez-Gesteira, M., & Silva Santos, C. (2014). WRF wind simulation and wind energy production estimates forced by different reanalyses: Comparison with observed data for Portugal. *Applied Energy*, *117*, 116–126.
- Carvalho, D., Rocha, A., Gómez-Gesteira, M., & Silva Santos, C. (2014a). WRF offshore wind simulation and wind energy production estimates forced by different reanalyses – Comparison with observed data in the Iberian Peninsula. *Applied Energy* (in press).
- Carvalho, D., Rocha, A., Gómez-Gesteira, M., & Silva Santos, C. (2014b). Sensitivity of the WRF model wind simulation and wind energy production estimates to planetary boundary layer parameterizations for onshore and offshore areas in the Iberian Peninsula. *Applied Energy* (in press).
- Carvalho, D., Rocha, A., Santos, C. S., & Pereira, R. (2013). Wind resource modelling in complex terrain using different mesoscale-microscale coupling techniques. *Applied Energy*, *108*, 493–504.
- Chelton, D. B., & Freilich, M. H. (2005). Scatterometer-based assessment of 10-m wind analyses from the operational ECMWF and NCEP numerical weather prediction models. *Monthly Weather Reviews*, *133*, 409–429.
- Chelton, D. B., Schlax, M. G., Freilich, M. H., & Milliff, R. F. (2004). Satellite measurements reveal persistent small-scale features in ocean winds. *Science*, *303*, 978–983.
- Dunbar, R. S., Lungu, T., Weiss, B., Stiles, B., Huddleston, J., Callahan, P. S., et al. (2006). *QuikSCAT science data product user manual, version 3.0, JPL Document D-18053 – Rev A*. Pasadena, CA: Jet Propulsion Laboratory.
- Ebuchi, N., Graber, H. C., & Caruso, M. J. (2002). Evaluation of wind vectors observed by QuikSCAT/SeaWinds using ocean buoy data. *Journal of Atmospheric and Oceanic Technology*, *19*, 2049–2062.
- Gómez-Gesteira, M., Moreira, C., Alvarez, I., & deCastro, M. (2006). Ekman transport along the Galician coast (NW, Spain) calculated from forecasted winds. *Journal of Geophysical Research*, *111*, C10005–C10012.
- Hoffman, R. N., & Leidner, S. M. (2005). An introduction to the near-real-time QuikSCAT data. *Weather Forecasting*, *20*, 476–493.
- Jiménez, B., Durante, F., Lange, B., Kreutzer, T., & Tambke, J. (2007). Offshore wind resource assessment with WAsP and MM5: Comparative study for the German Bight. *Wind Energy*, *10*(2), 121–134.
- Jungclaus, J. H., & Mellor, G. L. (2008). A three-dimensional model study of the Mediterranean outflow. *Journal of Marine Systems*, *24*, 41–66.
- Kanamitsu, M., Ebisuzaki, W., Woollen, J., Yang, S.-K., Hnilo, J. J., Fiorino, M., et al. (2002). NCEP-DOE AMIP-II Reanalysis (R-2). *Bulletin of the American Meteorological Society*, *83*, 1631–1643.
- Kara, A. B., Wallcraft, A. J., & Bourassa, M. A. (2008). Air-sea stability effects on the 10 m winds over the global ocean: Evaluations of air-sea flux algorithms. *Journal of Geophysical Research*, *113*, 4009–4014.
- Karagali, I., Badger, M., Hahmann, A. N., Peña, A., Hasager, C. B., & Sempreviva, A. M. (2013). Spatial and temporal variability of winds in the Northern European Seas. *Renewable Energy*, *57*, 200–210.
- Kent, E. C., Fangohr, S., & Berry, D. I. (2013). A comparative assessment of monthly mean wind speed products over the global ocean. *International Journal of Climatology*, *33*(11), 2520–2541.
- Li, M., Liu, J., Wang, Z., Wang, H., Zhang, Z., Zhang, L., et al. (2013). Assessment of sea surface wind from NWP reanalyses and satellites in the Southern Ocean. *Journal of Atmospheric and Oceanic Technology*, *30*, 1842–1853.
- Liu, W. T., & Tang, W. (1996). *Equivalent neutral wind*. JPL Publication, 96–17, Pasadena, California: Jet Propulsion Laboratory, California Institute of Technology.
- Mears, C. A., Smith, D. K., & Wentz, F. J. (2001). Comparison of special sensor microwave imager and buoy-measured wind speeds from 1987 to 1997. *Journal of Geophysical Research*, *106*(11), 719–729.
- Monin, A. S., & Obukhov, A. M. (1954). Osnovnye zakonomernosti turbulentnogo peremeshivaniya v prizemnom sloye atmosfery (Basic laws of turbulent mixing in the atmosphere near the ground). *Trudy Geofizicheskogo Instituta, Akademiya Nauk SSSR*, *24*(151), 163–187.

- Moore, G. W. K., Pickart, R. S., & Renfrew, I. A. (2008). Buoy observations from the windiest location in the world ocean, Cape Farewell, Greenland. *Geophysical Research Letters*, 35, 5.
- Ohsawa, T., Hashimoto, A., Shimada, S., Yoshino, J., De Paus, T., Heinemann, D., et al. (2007). Evaluation of Offshore Wind Simulations with MM5 in the Japanese and Danish Coastal Waters. *Proceedings of EWEC 2007, Milan, Italy*.
- Otero, P., & Ruiz-Villarreal, M. (2008). Wind forcing of the coastal circulation off north and northwest Iberia: Comparison of atmospheric models. *Journal of Geophysical Research*, 113, C10019.
- Peixoto, J. P., & Oort, A. H. (1992). *Physics of climate*. Woodbury, N.Y.: American Institute of Physics.
- Peliz, A., Dubert, J., Marchesiello, P., & Teles-Machado, A. (2007). Surface circulation in the Gulf of Cadiz: Model and mean flow structure. *Journal of Geophysical Research*, 112, C11015–C11020.
- Penabad, E., Alvarez, I., Balseiro, C. F., deCastro, M., Gomez, B., Perez-Munuzuri, V., et al. (2008). Comparative analysis between operational weather prediction models and QuikSCAT wind data near the Galician coast. *Journal of Marine Systems*, 72, 256–270.
- Pensieri, S., Bozzano, R., & Schiano, M. E. (2010). Comparison between QuikSCAT and buoy wind data in the Ligurian Sea. *Journal of Marine Systems*, 81, 286–296.
- Pickett, M. H., Tang, W., Rosenfeld, L. K., & Wash, C. H. (2003). QuikSCAT satellite comparisons with nearshore buoy wind data off the U.S. west coast. *Journal of Atmospheric and Oceanic Technology*, 20, 1869–1979.
- Rienecker, M. M., Suarez, M. J., Gelaro, R., Todling, R., Bacmeister, J., Liu, E., et al. (2011). MERRA: NASA's modern-era retrospective analysis for research and applications. *Journal of Climate*, 24, 3624–3648.
- Risien, C. M., & Chelton, D. B. (2006). A satellite-derived climatology of global ocean winds. *Remote Sensing of Environment*, 105(3), 221–236.
- Ruti, P. M., Marullo, S., D'Ortenzio, F., & Tremant, M. (2008). Comparison of analyzed and measured wind speeds in the perspective of oceanic simulations over the Mediterranean basin: Analyses, QuikSCAT and buoy data. *Journal of Marine Systems*, 70(1/2), 33–48.
- Saha, S., Moorthi, S., Pan, H. -L., Wu, X., Wang, J., Nadiga, S., et al. (2010). The NCEP climate forecast system reanalysis. *Bulletin of the American Meteorological Society*, 91, 1015–1057.
- Sánchez, R., Relvas, P., & Pires, H. O. (2007). Comparison of ocean scatterometer and anemometer winds off the southwestern Iberian Peninsula. *Continental Shelf Research*, 27, 155–175.
- Satheesan, K., Sarkar, A., Parekh, A., Ramesh Kumar, M. R., & Kuroda, Y. (2007). Comparison of wind data from QuikSCAT and buoys in the Indian Ocean. *International Journal of Remote Sensing*, 10, 2375–2382.
- Shimada, S., & Ohsawa, T. (2011). Accuracy and characteristics of offshore wind speeds simulated by WRF. *SOJA*, 7, 21–24.
- Shimada, S., Ohsawa, T., & Yatsu, K. (2009). A study on the ability of mesoscale model MM5 for offshore wind resource assessment in Japanese coastal waters. *European Wind Energy Conference (EWEC) 2009, Marseille*.
- Simmons, A., Uppala, S., Dee, D., & Kobayashi, S. (2007). ERA-Interim: New ECMWF reanalysis products from 1989 onwards. *ECMWF Newsletter*, No. 110 (pp. 25–35). Reading, United Kingdom: ECMWF.
- Singh, P., Parekh, A., & Attada, R. (2013). Comparison of a simple logarithmic and equivalent neutral wind approaches for converting buoy-measured wind speed to the standard height: Special emphasis to North Indian Ocean. *Theoretical and Applied Climatology*, 111, 455–463.
- Skamarock, W. C., Klemp, J. B., Dudhia, J., Gill, D. O., Barker, D. M., Duda, M., et al. (2008). A description of the advanced research WRF version 3. *NCAR Technical Note, NCAR/TN-475 + STR* (pp. 113).
- Sousa, M. C., Alvarez, I., Vaz, N., Gomez-Gesteira, M., & Dias, J. M. (2013). Assessment of wind patterns accuracy from the QuikSCAT satellite and the WRF model along the Galician coast (NW Iberian Peninsula). *Monthly Weather Review*, 141(2), 742–753.
- Tang, W., Liu, W. T., & Stiles, B. W. (2004). Evaluation of high-resolution ocean surface vector winds measured by QuikSCAT scatterometer in coastal regions. *IEEE Transactions on Geoscience and Remote Sensing*, 42(8), 1762–1769.
- Trenberth, K. E., Dole, R., Xue, Y., Onogi, K., Dee, R., Balmaseda, M., et al. (2010). Atmospheric reanalyses: A major resource for ocean product development and modeling. In J. Hall, D. E. Harrison, & D. Stammer (Eds.), *Proc. "OceanObs'09: Sustained Ocean Observations and Information for Society" Conference, Venice, Italy, 21-25 September 2009*. Vol. 2, ESA Publication WPP-306.
- Verschell, M. A., Bourassa, M. A., Weissman, D. E., & O'Brien, J. J. (1999). Model validation of the NASA scatterometer winds. *Journal of Geophysical Research*, 104, 11359–11374.
- Wallcraft, A. J., Kara, A. B., Barron, C. N., Metzger, E. J., Pauley, R. L., & Bourassa, M. A. (2009). Comparisons of monthly mean 10 m wind speeds from satellites and NWP products over the global ocean. *Journal of Geophysical Research*, 114, 16109–16114.
- Zhang, H. -M., Reynolds, R. W., & Bates, J. J. (2006). Blended and gridded high resolution global sea surface wind speed and climatology from multiple satellites: 1987–Present. *American Meteorological Society 2006 Annual Meeting, Paper #P2.23, Atlanta, GA, January 29 - February 2, 2006*.

Chapter 6 – Climate change impacts on future wind energy resource over Europe

This chapter presents the investigation about whether climate changes due to anthropogenic activities will impact the future wind energy resource in Europe. This research is presented in the form of an article presently submitted to an international peer-reviewed scientific journal. Due to the fact that this article is presently under review, the submitted version of this article is presented below in its original submitted form. In this article is included the methodology followed, area under study, CMIP5 present and future climate wind data used, complete and detailed introductory notes and state of the art.

1 **Potential impacts of climate change on European**
2 **wind energy resource under the CMIP5 future**
3 **climate projections**

4

5 Carvalho, D. ^(a), Rocha, A. ^(b), Gómez-Gesteira, M., ^(c) Silva Santos, C. ^(d)

6 ^(a) *CESAM - Department of Physics, University of Aveiro, Campus Universitário de Santiago, 3810-193*
7 *Aveiro, Portugal.* e-mail: david.carvalho@ua.pt

8 ^(b) *CESAM - Department of Physics, University of Aveiro, Campus Universitário de Santiago, 3810-193*
9 *Aveiro, Portugal.* e-mail: alfredo.rocha@ua.pt

10 ^(c) *EPHYSLAB - Environmental Physics Laboratory. Facultad de Ciencias. Universidad de Vigo, 32004*
11 *Ourense, Spain.* e-mail: mggesteira@uvigo.es

12 ^(d) *Instituto Superior de Engenharia do Porto, Rua Dr. António Bernardino de Almeida 341, 4200-072*
13 *Porto, Portugal.* e-mail: cmi@isep.ipp.pt

14

15 Corresponding author: David Carvalho

16 *CESAM - Department of Physics, University of Aveiro, Campus Universitário de Santiago, 3810-193*
17 *Aveiro, Portugal*

18 E-mail: david.carvalho@ua.pt

19 Tel: 00351 234 370 356

20 Fax: 00351 234 378197

21

22 **Abstract**

23 This work focused on possible impacts of climate changes on future European wind energy resource,
24 using the latest IPCC future climate projections derived from the CMIP5 project. Although wind energy
25 plays a key role in the goal of replacing fossil fuels by renewable energy sources, and thus minimize
26 future climate changes, it is also sensitive to climate change itself due to hypothetical changes in the
27 future atmospheric flow patterns. This study focuses on Europe, one of the main areas in terms of
28 installed wind-derived electricity generating capacity in the world. This work comprised two stages:
29 first, to assess the CMIP5 GCMs that best reproduce contemporary near surface wind speeds over
30 Europe. The validation of these CMIP5 GCMs wind data for the contemporary period serves as a solid
31 and important background for the upcoming CMIP5 GCMs downscaling initiatives to regional and local
32 scales. Secondly, data from the best GCMs was used to quantify and assess future changes in the
33 wind energetic resource and their geographical distributions over Europe, together with its intra- and
34 inter-annual variability. Research about the GCMs wind climate future projections provides an
35 important preliminary picture of changes in large-scale wind energetic resource over Europe.

36 The results presented show that, although the CMIP5 global models are still not able to represent
37 satisfactorily the contemporary wind speed climatology over Europe, the models HadGEM2-ES,
38 HadGEM2-CC, ACCESS 1.3 and ACCESS 1.0 showed the best ability to represent the contemporary
39 near surface wind speed climatology over Europe. Using data from these models, the future European
40 wind energy resource tends to be lower than the one presently available, due to a decreasing
41 tendency of the large-scale wind speeds over the current century, especially in the end of the current
42 century and under scenarios of stronger radiative forcing. Some exceptions to this decreasing
43 tendency of future wind speeds are detected in Central/Northern Europe, Turkey and in the Iberian
44 Peninsula, where the wind energy resource can slightly increase in future. Changes can be expected
45 in the intra-annual variability due to wind speeds decrease in cold seasons and increase in warmer
46 seasons, particularly at the end of the current century and under scenarios of stronger radiative
47 forcing. Oppositely, no significant changes in the inter-annual variability are expected over Europe
48 during the current century.

49 The validation results of this study showed the poor ability of the CMIP5 global models to represent
50 realistically the past-present European wind speed climatology, and the use of such coarse models

51 can be considered as somewhat over-simplistic and insufficiently detailed for the desired purposes.
52 Notwithstanding, the findings presented herein can serve as an important background for future
53 downscaling initiatives of CMIP5 data to regional and local scales, and should be seen as a
54 preliminary warning that a continuous increase of greenhouse gases emissions can jeopardize our
55 ability to mitigate such emissions, at least in what is related to the role and contribution of wind energy.
56 However, it needs to be borne in mind the significant uncertainty associated to global models future
57 climate projections. Thus, the information provided by these models should be seen as a preliminary
58 picture of the large scale future tendencies of the wind energy resource, and further research focused
59 on these themes should be performed by downscaling CMIP5 GCMs output to regional and local
60 scales in order to better represent the topography and land use and thus better simulate near surface
61 winds.

62 *Keywords: Wind energy, Climate change; CMIP5; IPCC; Global models; Europe*

63

64 **1 – Introduction**

65 The Intergovernmental Panel on Climate Change (IPCC) Assessment Report 5 (IPCC AR5,
66 2013) includes the latest existent knowledge about the scientific, technical and socio-
67 economic aspects of climate change. According to this report, the 1983-2012 period was
68 likely the warmest 30-year period of the last 1400 years in the Northern Hemisphere. The
69 World Meteorological Organization (WMO) also confirmed this global warming trend: based
70 on measured temperatures since 1850, 13 of the 14 warmest years were observed in the 21st
71 century. IPCC AR5 projects that global temperatures can rise 1 to 5°C over the next 100
72 years, depending on the amounts of greenhouse gases (GHG) emitted and the sensitivity of
73 the climate system. As for sea-level changes, the same report foresees a rise comprised
74 between 28 and 98 cm by the end of the current century, and to more than 3 meters by 2300.
75 If no GHG emission mitigation strategies are employed, the Arctic Ocean will likely become
76 virtually ice-free in summer before the middle of the current century (IPCC AR5, 2013). This
77 report also confirms that it is virtually certain (>95%) that human activity has been the main
78 cause of the observed increasing temperatures since the mid-20th century. Other possible
79 factors, such as natural internal variability of the climate system and natural external forcings
80 (variation of solar activity, activity of volcanoes, etc.), are considered to have a marginal
81 contribution to global warming. These human-induced climate changes are mainly forced by
82 the continuously increasing emissions of GHG (mainly CO₂) to the atmosphere, being well
83 established that one of the main emission sources of GHG is the electricity generation from
84 fossil fuels combustion (IPCC AR4, 2007; IPCC AR5, 2013).

85 Renewable energies are a cornerstone in the reduction of GHG emissions and consequent
86 mitigation of changes in the global climatic system. Of all the renewable energy sources
87 presently used for electricity generation, wind is one of the leaders in terms of installed
88 generating capacity, fastest growth and technological maturity, being the second leading
89 renewable energy source worldwide only exceeded in terms of installed capacity by
90 hydropower (Santos et al., 2015). Europe has been leading the efforts in expanding the

91 contribution of renewable energy sources to the overall electricity production and
92 consumption, setting a binding target of 20% of energy obtained from renewable sources to
93 achieve by 2020 (Carvalho et al., 2013a; Pryor and Barthelmie, 2010). Wind can provide up
94 to one third of this target value and, considering the current wind-derived energy growth rate.
95 It is projected that its electrical generating installed capacity can increase up to fivefold in the
96 upcoming decade (de Vries, 2008a and 2008b).

97 Although wind energy growth is part of the solution to reduce GHG emissions and
98 consequently mitigate future climate change, this renewable energy source is sensitive to
99 climate change itself, due to hypothetical changes in the future atmospheric flow patterns.
100 Since the wind energetic potential varies with the wind speed cubed, even apparently small
101 variations in future wind circulation patterns and characteristics can strongly impact future
102 wind energy production (Carvalho et al., 2012b). Variations in the future mean wind speeds
103 and their geographical distribution will change the wind resource of a given region, while
104 changes in its future inter- and intra-annual variability can affect the reliability of the produced
105 wind-derived electricity (Pryor and Barthelmie, 2010). The higher the intra-annual variability
106 (this is, the variability within a year-period), the more variable will be the injection of the
107 produced energy into the electrical grid, causing supply-demand balancing problems and
108 enhancing the need to perform short-term wind energy production forecasts. Inter-annual
109 variability (the variability between different years) is a key issue for the economic feasibility of
110 a wind farm. The typical lifetime of wind farms currently in operation is typically 20 to 30
111 years, and the question of whether the wind farm expected energy yield will significantly vary
112 during its lifetime can determine the success or failure of the wind farm project as a whole.

113 IPCC AR5 relies on the World Climate Research Programme (WCRP) Fifth Coupled Model
114 Intercomparison Project (CMIP5), a globally coordinated set of global coupled atmosphere-
115 ocean general circulation models (AOGCMs) simulations (for more details see Taylor et al.,
116 2012). CMIP5 output, the latest available data regarding future climate change projections,
117 allows the evaluation of how the models realistically simulate the recent past and present,

118 and provides projections of future climate changes from the present date up to 2100 (and
119 beyond, for some models and experiments). CMIP5 is the successor of the CMIP3, which
120 served as basis of the IPCC fourth assessment report (IPCC AR4, 2007). When compared to
121 the older generation models used in CMIP3, the new state-of-the-art models used in CMIP5
122 offer higher spatial resolutions, improved physical process descriptions, improvements in the
123 representation of external forcings and interaction between the atmosphere, land use and
124 vegetation. Moreover, CMIP5 introduced a new breed of AOGCMs: the Earth System Models
125 (ESMs). ESMs are currently the state-of-the-art models, expanding on AOGCMs by including
126 additional earth system components such as atmospheric chemistry, biogeochemical cycles,
127 aerosols, ozone, sulphur and carbon cycles (Taylor et al., 2012; Brands et al., 2013). ESMs
128 constitute the most comprehensive tools presently available for simulating the climate system
129 future response to external forcings, in which biogeochemical feedbacks play a key role
130 (IPCC AR5).

131 CMIP5 future climate projections, called Representative Concentration Pathways (RCPs),
132 describe hypothetical future climate scenarios based on the emissions rate of GHG (more
133 details are available in Moss et al., 2010). These RCPs make use of a broad range of
134 anthropogenic climate forcings, such as aerosols, GHG, land use and chemically active
135 gases (Bracegirdle et al., 2013; Meinshausen et al., 2011). When compared to their
136 predecessors - the IPCC AR4/CMIP3 Special Reports on Emissions Scenarios (SRES) -
137 RCPs consider new and larger amounts of data such as socio-economic aspects, emerging
138 technologies, land use and land cover changes (Moss et al., 2010).

139 This work aims to assess and quantify the impacts of the latest CMIP5 future climate
140 projections on the wind energetic resource in Europe, one of the main areas in terms of
141 installed wind-derived electricity generating capacity and one of the main boosters of further
142 growth and penetration of wind-derived energy in the world. To this end, data from CMIP5
143 project is used to build future projections of near surface wind speed and energy density
144 geographical distributions over Europe, and to quantify how different from the past-present

145 are the future scenarios for wind energy production. As far as the authors are aware, there is
146 still no published literature that addresses this issue in light of the new CMIP5 future climate
147 projections for the European continent as a whole. However, the study of Sterl et al. (2014)
148 focused on possible impacts of climate changes on future large-scale wind climate over the
149 Netherlands by downscaling CMIP5 future climate projections, concluding that climate
150 changes will not likely change Netherlands and the North Sea wind climate beyond the range
151 of the typical natural climate variability. As for other areas of the globe, the study of Kulkarni
152 and Huang (2014) considers CMIP5 data on the evaluation of possible changes in surface
153 wind speeds over North American territory. This work concludes that the projected future
154 changes in surface wind speeds are moderate and no significant changes in North American
155 wind power potential are to be expected in the future due to GHG induced climate changes.
156 Also the study of Chen et al. (2013) uses CMIP5 data to investigate the impact of climate
157 change on wind speeds, but now for the Chinese territory, concluding that geographical
158 distributions of wind speed over China at the end of the 21st century do not show significant
159 differences when compared to those of the last 35 years. Considering earlier IPCC
160 assessment reports and future climate projections such as the IPCC AR4/CMIP3, and also
161 downscaling initiatives that followed them such as the PRUDENCE (Christensen and
162 Christensen, 2007) and ENSEMBLES (ENSEMBLES, 2006) projects, there is a good
163 background in published studies focusing on climate changes impacts in wind power
164 resource over Europe. Pryor and Barthelmie (2010) reviewed the published literature
165 regarding climate change impacts on wind energy. According to this review, by the end of the
166 current century the mean wind resource in Europe can suffer small magnitude changes, with
167 indications that wind energy density and annual mean wind speeds in winter can increase in
168 northern Europe and decrease in the south of the continent (Pryor et al., 2005a; Bloom et al.,
169 2008; Walter et al., 2006). Santos et al. (2015) analyzed changes in future wind energy
170 potential over the Iberian Peninsula considering the A1B IPCC AR4/CMIP3 SRES scenario,
171 downscaled by a regional circulation models (RCM), and concluded that these climate
172 change projections show significant decreases in the future wind energy production potential

173 over most of the Iberian Peninsula. Pryor et al. (2005b) performed a statistical downscaling
174 of one global circulation model (GCM) on the Baltic States and projected a decrease of the
175 wind speed and energy density by 2071-2100. Cradden et al. (2012) assessed if climate
176 changes could affect wind energy development in the UK, considering three different IPCC
177 AR4/CMIP3 SRES scenarios. The authors concluded that the typical UK wind speed intra-
178 annual variability (higher in winter and lower in summer) could be larger in the future due to
179 climate changes, but did not find any conclusive evidence of a marked future change in wind
180 energy resource in any area of the UK. To sum up, until the present moment there is in the
181 published research a consensus that no significant changes in future European wind climate
182 are to be expected due to climate warming. Instead, natural variability seems to be the main
183 reason for changes in global decadal and centurial wind climatology, and this will likely
184 continue to be in the upcoming century. Nevertheless, and although significant uncertainty
185 still remains on how future wind climatologies will change over Europe, several recent
186 studies have reported a decline tendency in observed near-surface wind speeds and in
187 indices based on wind power generation during the past decades in Europe (Bakker et al.,
188 2013; Brázdil et al., 2009; Pirazzoli and Tomasin, 2003; Smits et al., 2012; Vautard et al.,
189 2010).

190 The significant uncertainty of these projected climate changes should be borne in mind.
191 GCMs show strong limitations in realistically represent past and present wind climates
192 (mainly related to their coarse spatial resolution), whilst RCMs downscaling of these GCMs
193 output show high inter-model variability and uncertainty regarding the climate change signal
194 (Pryor and Barthelmie, 2010). Nevertheless, the continuous effort devoted to the evolution of
195 GCMs (AOGCMs and ESMs included), RCMs and their input data poses the challenge to
196 continuously investigate their latest future climate projections. Several CMIP5 data
197 downscaling projects are currently under progress, namely the CORDEX project (<http://wcrp-cordex.ipsl.jussieu.fr/>) and, more specifically, the EURO-CORDEX branch of the CORDEX
198 project that downscales CMIP5 data for Europe (<http://www.euro-cordex.net/>). Thus, it
199 becomes relevant to compare and assess the performance of the several GCMs, in order to
200

201 select the one(s) with the best performance(s) as candidate(s) for downscaling applications.
202 This work also aims to assess the performance of CMIP5 GCMs in what is related to their
203 ability to realistically represent past and present near surface wind climatology in Europe.
204 This validation is expected to be of great value to downscaling initiatives focused on climate
205 change impact on wind energy, since no information is presently available regarding the
206 individual performance of each CMIP5 GCM in representing contemporary near surface
207 winds. Brands et al. (2013) highlighted the importance of GCM validation for downscaling
208 applications, assessing which CMIP5 GCMs show better ability to reproduce present climate
209 conditions in Europe and Africa and, therefore, can be seen as the best candidate(s) for use
210 in downscaling applications. The authors concluded that the CMIP5 ESM models HadGEM2-
211 ES and MPI-ESM-LR outperform the other models along the lateral boundaries of the several
212 CORDEX regional domains.

213 Thus, the present work comprises two main stages. First, near surface wind speed data from
214 21 CMIP5 GCMs are compared against a reanalysis dataset, in order to identify the GCM(s)
215 that best reproduce contemporary near surface wind speeds over Europe. After, data from
216 these GCMs is used to preliminarily quantify and assess future changes in the large-scale
217 wind energetic resource and their geographical distributions over Europe, together with its
218 intra- and inter-annual variability. While the validation of CMIP5 GCMs wind data for the
219 contemporary period will serve as a solid and important background for the upcoming CMIP5
220 GCMs downscaling initiatives to regional and local scales focused on wind energy, research
221 about the GCMs future wind speed projections will provide an important preliminary picture of
222 potential changes in large-scale wind energy resource over Europe.

223 **2 – Data and methodology**

224 **2.1 – CMIP5 data and experiments**

225 CMIP5 GCMs near surface wind data regarding the past-present period and two RCPs future
226 climate projections were considered in this work. This near surface wind data reports to 10 m

227 above ground/mean sea level, while typical wind turbines are placed at 80-120 m above
228 ground/mean sea level. Since the CMIP5 GCMs do not provide output regarding winds at
229 these heights, this near surface 10 m wind data was considered as the best estimator of the
230 wind at typical wind turbines height. Although near surface winds are lower than the ones at
231 80-120 m, both are highly correlated (Kulkarni and Huang, 2014). Since the aim of this work
232 is to compare past-present with future winds and not to quantify them, it can be expected that
233 changes between past-present and future near surface winds are of similar magnitude to the
234 ones expected at higher heights.

235 Past-present near surface wind data was extracted from the historical run, performed to
236 characterize the contemporary period (1986-2005). This run was forced by observed
237 atmospheric composition changes, both from anthropogenic and natural sources, and time-
238 evolving land cover (Taylor et al., 2012). Future wind data was obtained from future climate
239 projections of two RCPs. One somewhat pessimistic, although realistic, which basically
240 assumes that no GHG mitigation actions will be employed in the upcoming decades and
241 GHG emission rates will continue to grow at the rates witnessed in the last decades (the
242 RCP 8.5); and a more optimistic scenario, which foresees a reduction of GHG emissions, the
243 RCP 4.5.

244 RCP 8.5 is a "business as usual" emission scenario, characterized by escalating GHG
245 emissions and high concentration levels of these gases in the atmosphere. RCP 8.5 can be
246 seen as the projection of future GHG concentration and radiative forcing if no emissions
247 mitigation strategies are employed until the end of the 21st century. The numerical value
248 assigned to a RCP translates its radiative forcing present in 2100. Thus, RCP 8.5 radiative
249 forcing (CO₂ equivalent emissions) peaks at 2100 with a value of 8.5 W.m⁻², approximately
250 1370 ppm of CO₂ equivalent concentration. The RCP 4.5 is a midrange stabilization
251 scenario, where GHG emissions are mitigated by policy actions, strategies and technologies,
252 employed to achieve emission targets before 2100 (Taylor et al., 2012). In this scenario, the
253 radiative forcing and GHG emissions peak around 2070-2080 with a value of 8.5 W.m⁻²

254 (approx. 650 ppm of CO₂ equivalent concentration) and stabilizes further on, remaining
 255 constant beyond this peak.

256 For both RCPs, the following time windows were considered: near future, ranging from 2016
 257 to 2035; medium-term future, from 2046 to 2065; and long term future, from 2081 to 2100.

258 The spatial domain considered in this work was based on the EURO-CORDEX one, but
 259 slightly expanded in order to include the Portuguese Azores and Madeira archipelagos, and
 260 the Spanish Canary islands.

261 **2.2 – Validation of CMIP5 models**

262 For the assessment of which CMIP5 GCMs best describe the contemporary wind resource
 263 over Europe, all CMIP5 models with available daily average near surface wind speed data for
 264 the historical and the two RCPs here considered were selected. The models that fulfilled
 265 these requisites are listed in Table 1.

266 **Table 1** – Main characteristics of the considered CMIP5 models

Model	Modelling Center	Type of GCM	Horizontal resolution (lat/lon)
ACCESS 1.0	CSIRO-BOM (Australia)	ESM	1.25° / 1.875°
ACCESS 1.3	CSIRO-BOM (Australia)	ESM	1.25° / 1.875°
BNU-ESM	GCESS (China)	ESM	2.8° / 2.8°
CanESM2	CCCma (Canada)	ESM	2.8° / 2.8°
CMCC-CMS	CMCC (Italy)	AOGCM	2° / 2°
CNRM-CM5	CNRM-CERFACS (France)	AOGCM	1.4° / 1.4°
CSIRO-Mk 3.6.0	CSIRO-QCCCE (Australia)	AOGCM	1.9° / 1.9°
GFDL-CM3	NOAA GFDL (USA)	AOGCM	2° / 2.5°
GFDL-ESM2G	NOAA GFDL (USA)	ESM	2° / 2.5°
GFDL-ESM2M	NOAA GFDL (USA)	ESM	2° / 2.5°
HadGEM2-CC	MOHC (UK)	ESM	1.25° / 1.875°
HadGEM2-ES	MOHC (UK)	ESM	1.25° / 1.875°
IPSL-CM5A-LR	IPSL (France)	ESM	1.875° / 3.75°
IPSL-CM5A-MR	IPSL (France)	ESM	1.25° / 2.5°
IPSL-CM5B-LR	IPSL (France)	ESM	1.875° / 3.75°
MIROC-ESM	MIROC (Japan)	ESM	2.8° / 2.8°
MIROC-ESM-CHEM	MIROC (Japan)	ESM	2.8° / 2.8°
MIROC5	MIROC (Japan)	AOGCM	1.4° / 1.4°

MPI-ESM-LR	MPI-M (Germany)	ESM	1.9 ^o / 1.875 ^o
MPI-ESM-MR	MPI-M (Germany)	ESM	1.9 ^o / 1.875 ^o
MRI-CGCM3	MRI (Japan)	AOGCM	1.125 ^o / 1.125 ^o

267 The validation of these models was performed as follows. First, and due to the fact that these
268 21 models have different native horizontal resolutions (Table 1), all models historical near
269 surface wind speed grids were remapped to a regular 1.5^o lat/lon grid (an intermediate
270 resolution given the native resolutions of all models). Afterwards, 20-year historical wind
271 speed medians (instead of the mean, in order to avoid normality fitting restrictions and outlier
272 contamination) were computed from the daily near surface wind speed time series for all
273 models and grid points, and each model historical wind speed median grid was compared
274 with ERA-Interim wind speed 20-year median grid. ERA-Interim reanalysis were selected as
275 “real wind” data source, not only because they are widely recognized as a superior quality
276 reanalysis product (especially for the European territory), but also because it is the official
277 validation dataset used for the CORDEX CMIP5 dynamical downscaling initiatives (Brands et
278 al., 2013). The most important aspect to assess in terms of validation is if the wind speed
279 data from the CMIP5 GCMs and from ERA-Interim come from the same continuous
280 distribution. Since wind speeds are generally not normally distributed, the non-parameteric
281 two-sample Kolmogorov-Smirnov (KS) test (Gibbons and Chakraborti, 2011) was applied to
282 the CMIP5 GCMs and ERA-Interim wind speed datasets for each grid point, with a 5%
283 significance level. The KS test tests the null hypothesis that two samples belong to the same
284 continuous distributions (with the same shape and location), against the alternative
285 hypothesis that they are from different distributions (different in shape and/or location). The
286 CMIP5 GCMs with the highest number of grid points where the KS test shows that their wind
287 speed data is from the same distribution as ERA-Interim were considered the ones that
288 better represent the contemporary (historical) period wind climatology over Europe and,
289 consequently, those used to assess climate change impacts on wind energy.

290 For the following sections, data from these selected GCMs was organized in a multi-model
291 ensemble (MME) strategy where, for each time period and RCP, data from the selected

292 GCMs was concatenated into one multi-model ensemble. This multi-model ensemble
293 strategy is a way to minimize the individual model biases, since it is expected that the multi-
294 model ensemble mean (or median) shows lower uncertainties and better results than each
295 individual model (Pires et al., 2014). This fact is supported by several studies that compared
296 individual models and multi-model ensemble means with observed data (Raisanen and
297 Palmer, 2001; Pierce et al., 2009; Annan and Hargreaves, 2010).

298 **2.3 – Impacts of climate change on future wind energy resource**

299 MME data was used to evaluate climate change impacts on future wind energetic resource
300 over Europe. These impacts were quantified and assessed in three different categories: (i)
301 future changes in the wind speed and energy density medians; (ii) intra- and (iii) inter-annual
302 variability of the wind speed and energy density.

303 ***2.3.1 – Climate change impacts in future wind energetic resource***

304 The main and most direct mechanism from which climate change can affect future wind
305 energetic resource is by altering the average wind speed (and consequently the available
306 wind energy density) of a given area. To assess possible changes in future wind speed and
307 wind energy density in Europe (and their respective geographical distributions) due to climate
308 changes, MME historical daily wind speed and energy density data was compared to future
309 daily wind speed and energy density data, for the two RCPs and three future time windows
310 considered. The wind energy density (also called wind power flux) is derived from equation 1,
311 where U is the wind speed and ρ is the air density (the standard value of $1.225 \text{ kg}\cdot\text{m}^{-3}$ was
312 assumed).

$$313 \quad P_{flux} = \frac{1}{2} * \rho * U^3 \quad (1)$$

314 Changes in future wind energetic resource were evaluated by comparing, for each grid point,
315 the wind speed and energy density historical and future 20-year MME medians, for all RCPs
316 and time windows. The existence of statistically significant differences between the historical

317 and future medians is evaluated by applying the Mann-Whitney (or Wilcoxon rank sum) non-
318 parametric test (Gibbons and Chakraborti, 2011), with a 5% significance level. The Mann-
319 Whitney test tests the null hypothesis of two data samples belonging to continuous
320 distributions with equal medians, against the alternative that they do not.

321 To further detail future changes in the wind energetic resource, the aforementioned
322 methodology was repeated but now in a seasonal perspective. For this purpose, all data and
323 analysis were divided into seasons: Winter, comprising the months of December, January
324 and February; Spring, with the months of March, April and May; Summer, corresponding the
325 months of June, July and August: and Autumn, between September and November.

326 Changes in future wind energetic resource were evaluated by comparing, for each grid point,
327 the wind speed and energy density historical and future MME medians of the four seasons,
328 for all RCP's and time windows. The Mann-Whitney test for the difference of medians was
329 again used to assess the statistical significance of differences in the seasonal medians.

330 ***2.3.2 – Climate change impacts in future wind energy intra-annual variability***

331 In order to analyze future changes in the wind energetic resource intra-annual variability,
332 annual median absolute deviations (MAD) were computed for the historical and future wind
333 speed and energy density MME data. MAD (Sachs, 1984) is a non-parametric measure of
334 the sample variability around its median, and is given by the following equation:

$$335 \quad \quad \quad MAD = \text{median} [|X_i - \text{median}(X)|] \quad (1)$$

336 MAD can be considered as a non-parametric equivalent of the standard deviation or
337 variance. It is a very robust scale estimator, with the best possible breakdown point (50%,
338 the double of the interquartile range) and its influence function has the sharpest bound
339 among all scale estimators (Rousseeuw and Croux, 1993).

340 Annual MAD data series were computed for each historical and future 20-year periods,
341 resulting in three-dimensional grids where the temporal dimension has 20 elements (20

342 years). Each one of these temporal element is an annual MAD, the median absolute
343 deviation regarding that year. After, the median of these annual MADs was computed for
344 each grid point, in order to produce an estimate of the average intra-annual variability of each
345 20-year period (the historical and future 20-year periods). Differences between the historical
346 and future annual MAD medians were quantified and analyzed. For each grid point,
347 differences between historical and future wind speed and energy density annual MAD
348 medians can be seen as indicators of changes in wind speed and energy density intra-
349 annual variability. The statistical significance of these annual MAD median differences was
350 evaluated with the Mann-Whitney test, with a significance level of 5%.

351 ***2.3.3 – Climate change impacts in future wind speed and wind energy density inter-*** 352 ***annual variability***

353 To assess hypothetical changes in future inter-annual variability, all daily wind speed and
354 energy density MME data was averaged to annual wind speed and energy density records.
355 Although wind speeds are not usually normally distributed, annual mean wind speeds can be
356 realistically characterized by a normal distribution (European Wind Energy Association,
357 2009). These annual mean wind speed and energy density data series were computed for
358 each historical and future 20-year periods, resulting in three-dimensional grids where the
359 temporal dimension has 20 elements (20 years). Each one of these temporal element is the
360 annual mean wind speed and energy density regarding that year. The standard deviation of
361 each one of these annual means data series will quantify their inter-annual variability. Thus,
362 differences between the standard deviations of two annual means data series will quantify
363 changes in the inter-annual variability.

364 For each grid point, the differences between historical and future standard deviations were
365 analyzed and the respective statistical significance of such differences computed. Statistical
366 significance of standard deviation differences was evaluated using the F-test with a
367 significance level of 5% assuming, as previously mentioned, that wind speed and energy
368 density annual means data series can be fitted to a normal distribution. The F-test asses the

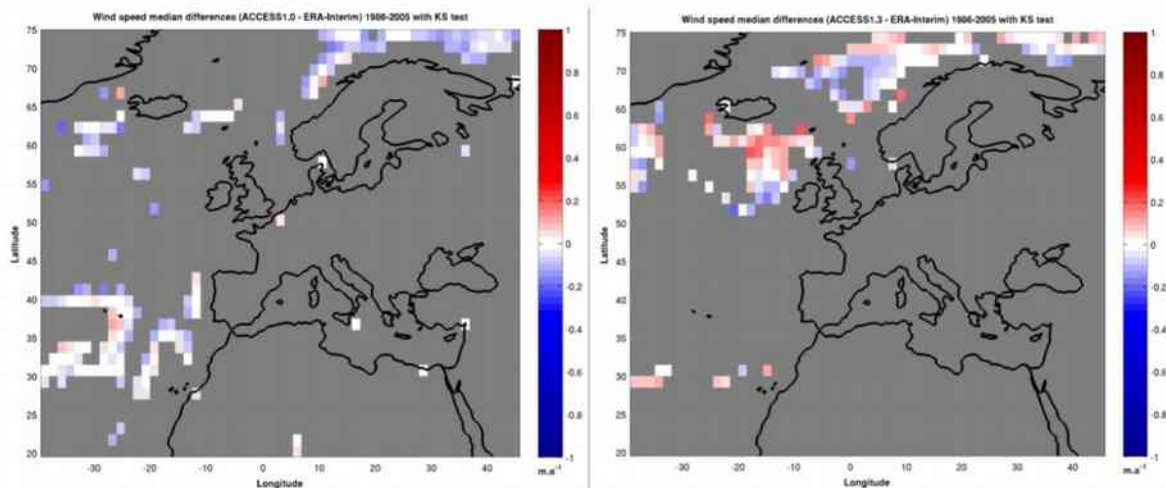
369 null hypothesis that the data in two samples comes from normal distributions with the same
370 variance, against the alternative hypothesis that they come from normal distributions with
371 different variances.

372 **3 – Results and discussion**

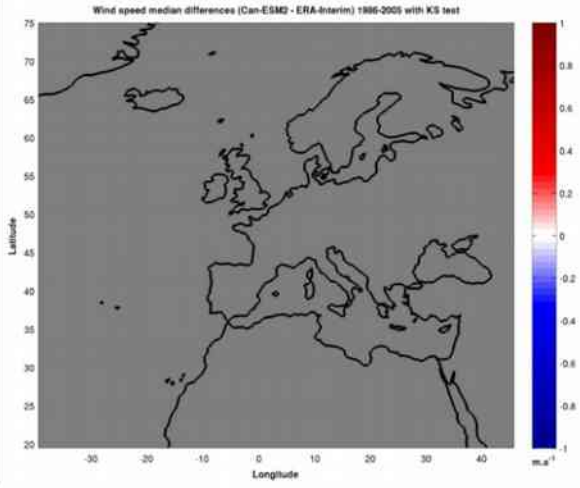
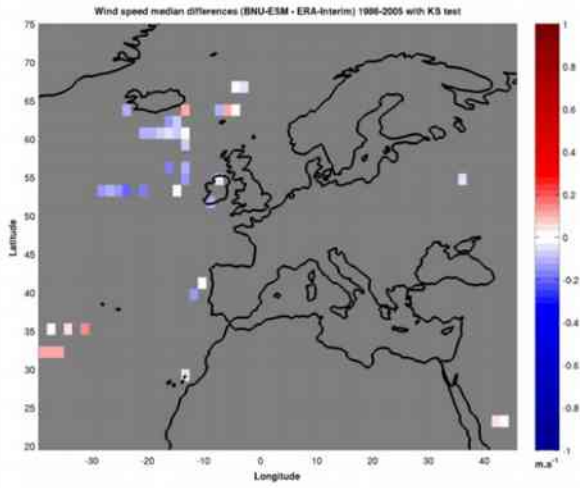
373 **3.1 – Validation of CMIP5 models**

374 The validation results of the 21 CMIP5 models are presented here. Figure 1 shows the
375 differences between ERA-Interim and each model historical wind speed medians, together
376 with the KS test output. For grid cells where the KS test shows statistically significant
377 differences, the grid cell is coloured in grey. For grid cells where the KS test does not show
378 statistically significant differences (this is, the model grid cell is in accordance with ERA-
379 Interim), the grid cell is coloured according to the ERA-Interim and CMIP5 model wind speed
380 median difference for that grid cell.

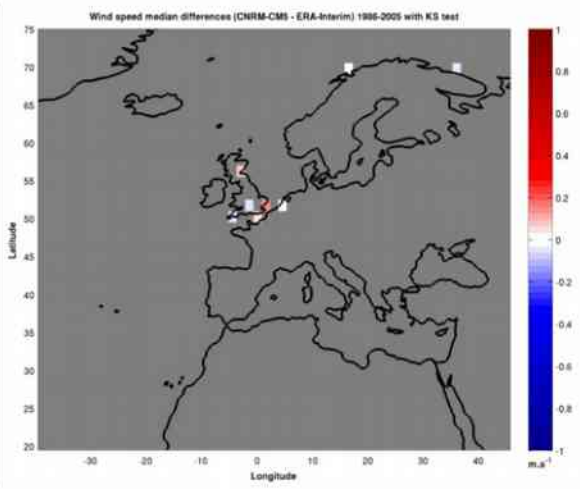
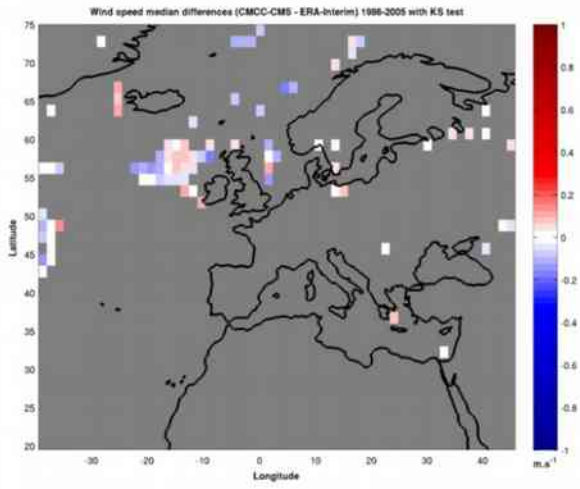
381



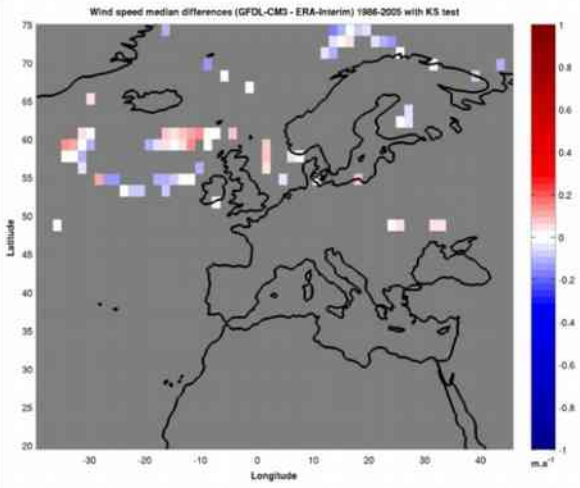
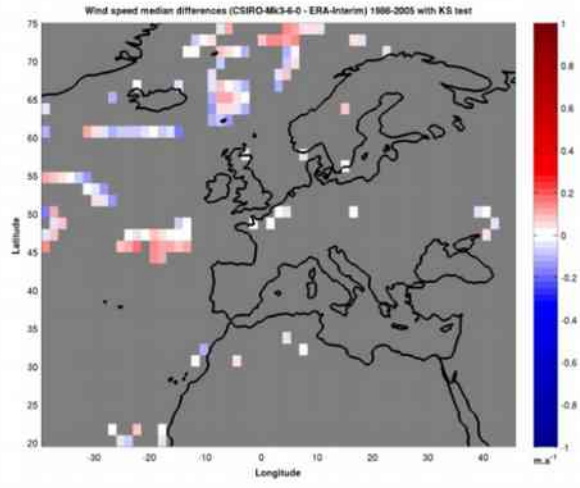
382

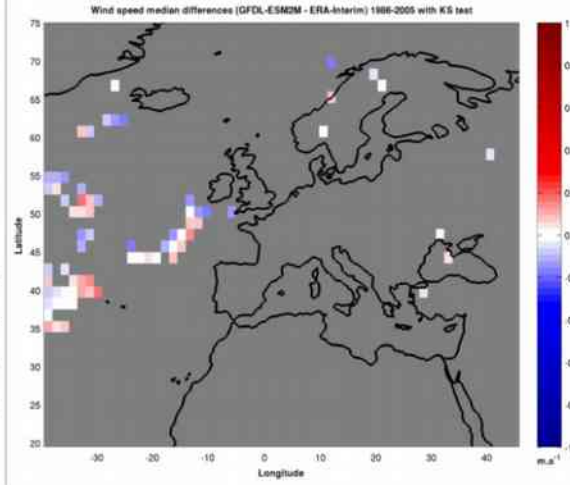
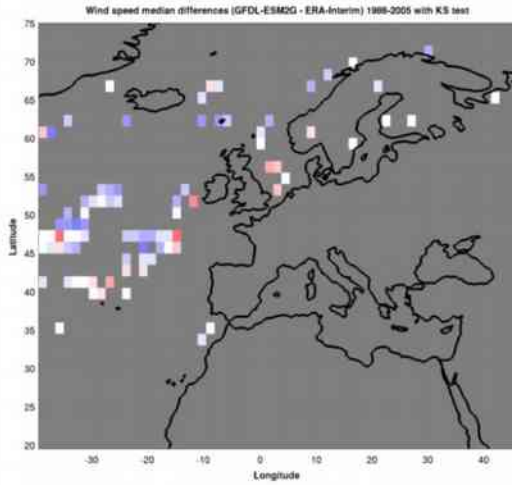


383

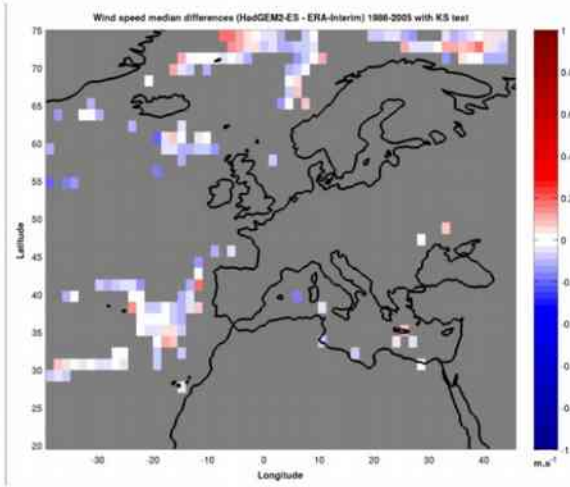
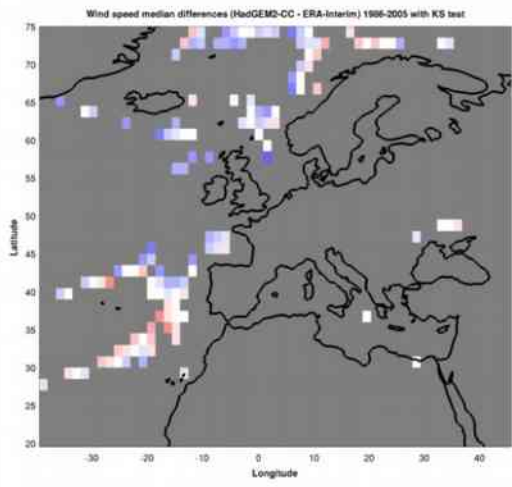


384

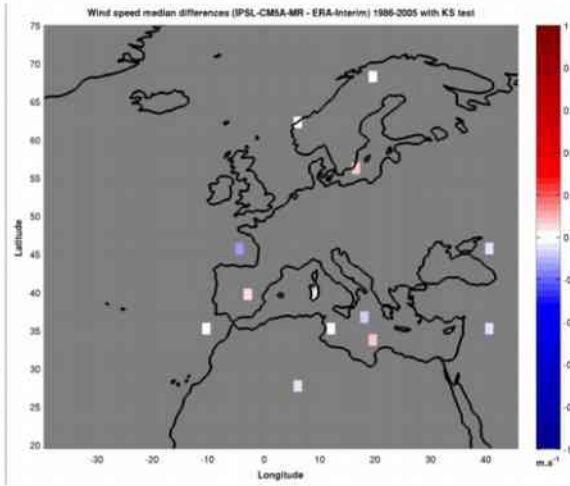
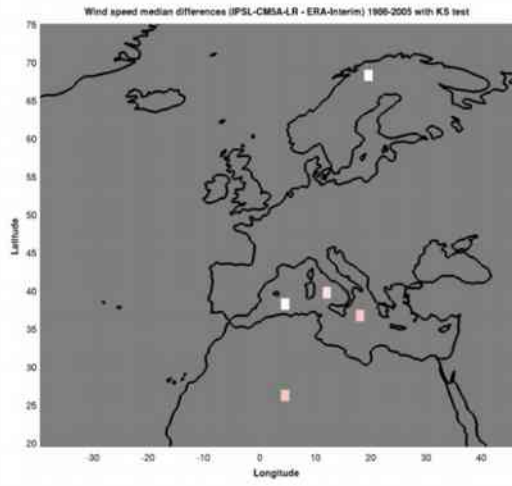




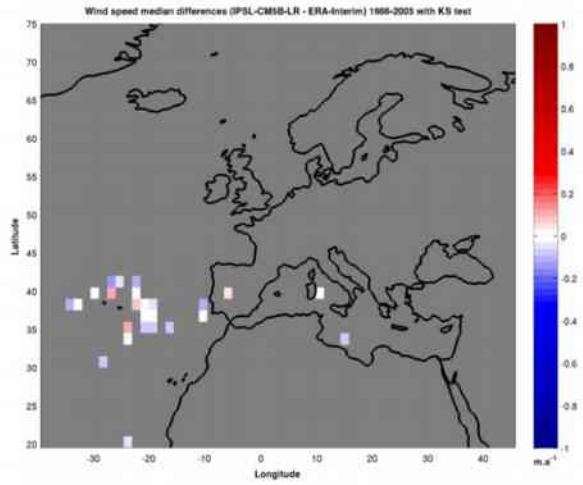
385



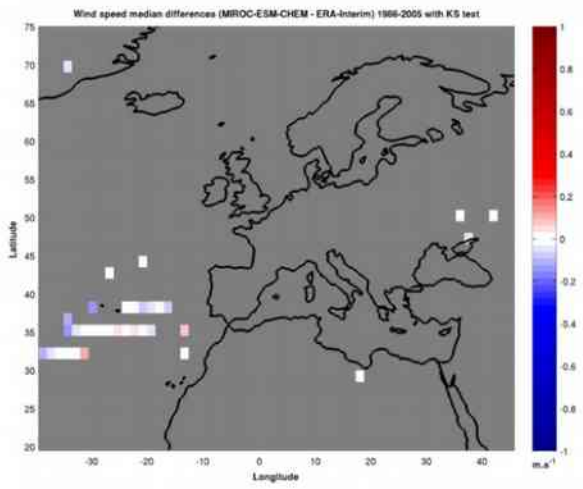
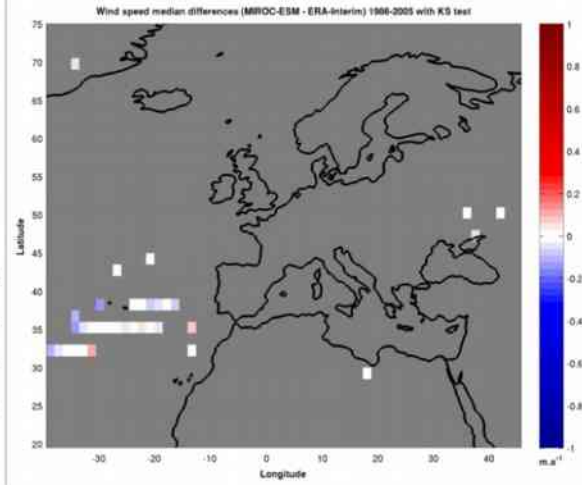
386



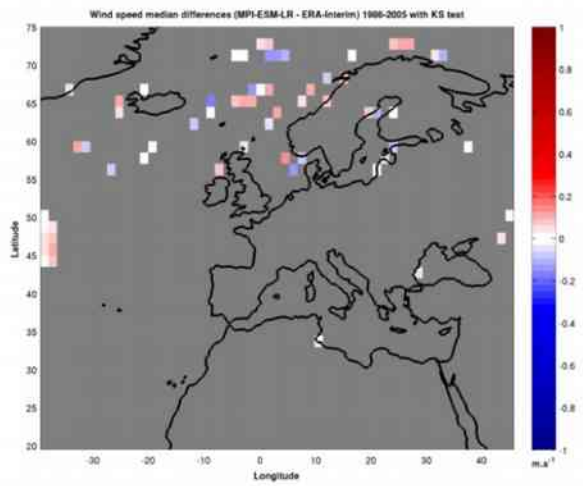
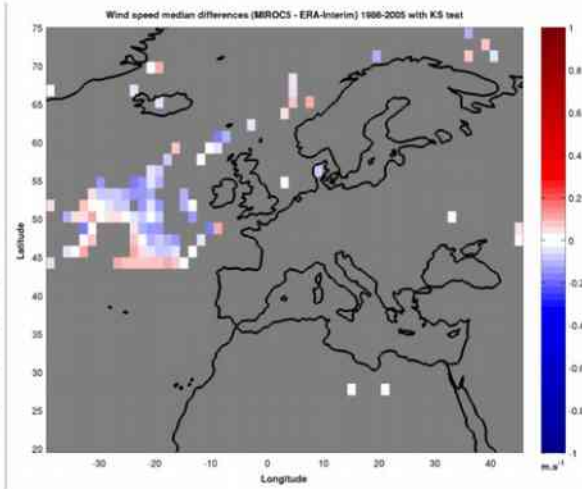
387



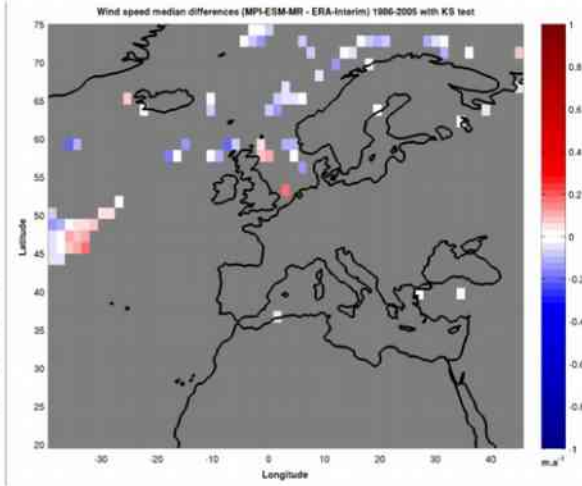
388

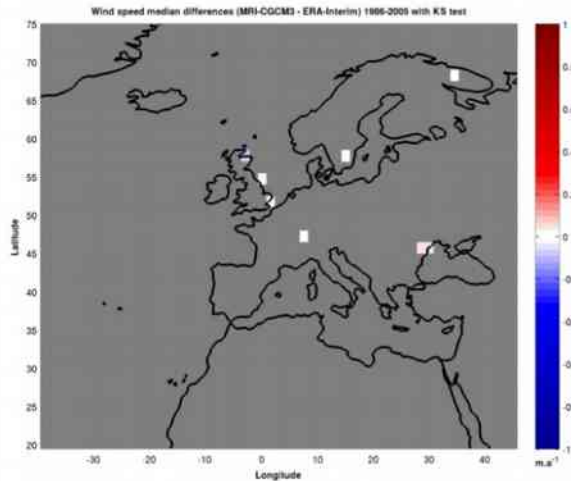


389



390





391

392 **Figure 1** – Wind speed median differences (CMIP5 model minus ERA-Interim) with a KS test (5% of significance level)

393 Figure 1 shows that, in general, none of the CMIP5 GCMs is able to satisfactorily represent
 394 the wind speed distributions over Europe. In all models, the majority of the grid points show
 395 different wind speed distributions from those from ERA-Interim. These results, although not
 396 encouraging, are not wholly surprising and it was previously reported that GCMs are not
 397 typically able to accurately reproduce contemporary wind climates or historical trends (Pryor
 398 and Barthelmie, 2010). The typical GCMs coarse resolution does not allow an accurate
 399 representation of near surface meteorological variables such as near surface winds, due to a
 400 weak representation of the Earth's surface. Near surface winds depend strongly on the
 401 surrounding terrain characteristics, mainly topography and land use (which determines the
 402 surface roughness). Thus, a limited representation of the terrain characteristics will lead to
 403 substantial errors in the representation of near surface atmospheric flows (Carvalho et al.,
 404 2012a; 2013b; 2014a; 2014b; 2014c; 2014d; Alvarez et al., 2013). Chen et al. (2012)
 405 investigated possible causes of the differences between nine CMIP5 GCMs near surface
 406 wind fields and reanalysis output, by examining the differences between geopotential height
 407 gradients from the GCMs and the reanalysis, reporting that the upper air pressure gradients
 408 characteristics are considerably better captured by the GCMs than the near-surface wind
 409 speeds. This finding supports the hypothesis that the GCMs topography and land use weak
 410 representation may be one of the major error sources in the simulation of near-surface wind
 411 speeds, not properly simulating the atmosphere-surface coupling and interaction. Not

412 surprisingly, the CMIP5 GCMs grid points that are in accordance to ERA-Interim are mostly
413 located in ocean areas, where limitations in the representation of surface characteristics are
414 obviously attenuated. McInnes et al. (2011) also reported that a 19 CMIP3 AOGCMs
415 ensemble exhibit lower skills over land areas, by comparing this multi-model ensemble winds
416 with reanalysis winds for the period 1981-2000. The interaction between the surface and
417 adjacent atmosphere will ultimately result in medium- to small-scale atmospheric circulations.
418 Thus, this type of global models has their strength in representing large-scale meteorological
419 and climatic trends. Albeit reanalysis products, such as ERA-Interim, usually have similar
420 resolutions and suffer from the same terrain representation limitations, they incorporate and
421 assimilate significant amounts of observed meteorological data. Therefore, unlike pure GCM
422 output, reanalysis products may be able, at least to some extent, to depict medium-scale
423 wind circulations and this fact can explain the differences detected between CMIP5 GCMs
424 and ERA-Interim reanalysis.

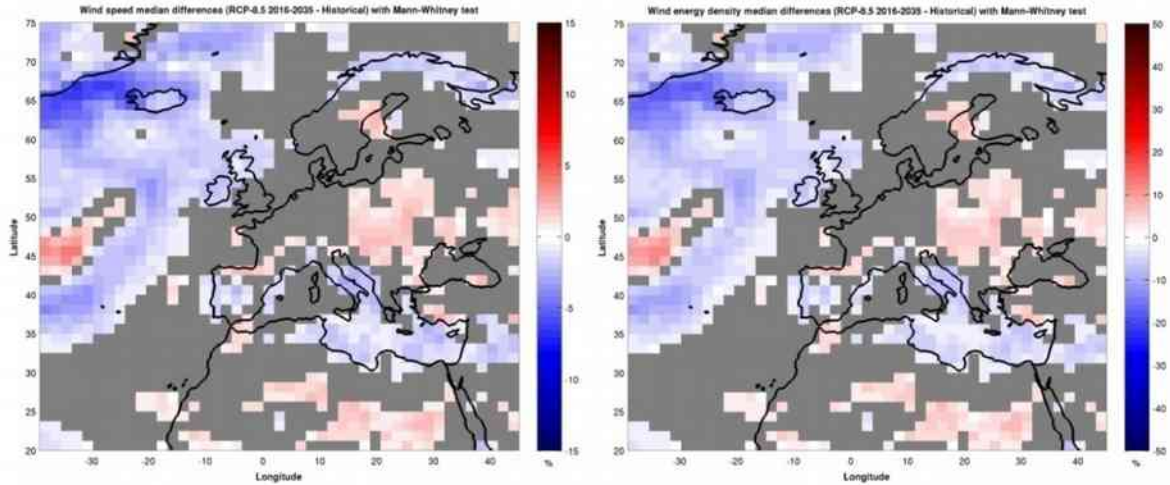
425 Nevertheless, from Figure 1 four GCMs stand out with the highest number of grid points
426 similar to ERA-Interim in terms of wind speed distributions: HadGEM2-ES (180 valid grid
427 points), ACCESS 1.3 (177 valid grid points), ACCESS 1.0 (174 valid grid points) and
428 HadGEM2-CC (137 valid points). Also for these models, the differences between their wind
429 speed medians and ERA-Interim ones is relatively small. Oppositely, CanESM2 (with no
430 valid grid points), IPSL-CM5A-LR (5 valid grid points), MRI-CGCM3 and CNRM-CM5 (both
431 with only 8 valid grid points) are the models with worst performance. Therefore, the
432 HadGEM2-ES, HadGEM2-CC, ACCESS 1.0 and ACCESS 1.3 GCMs were chosen as the
433 models that best represent contemporary wind speed climatology and the ones that may
434 have the best performance in simulating future wind climate due to climate change. Thus,
435 data from these four models was used to build the MME dataset. The overall superiority of
436 HadGEM2-ES model (as well as its earlier CMIP3 version, the HadGEM2) was previously
437 reported in other studies such as Brands et al. (2013) and Brands et al. (2011). These
438 differences among the several CMIP5 GCMs performances in representing contemporary
439 wind climates should be seriously considered in dynamical downscaling applications focused

440 on wind energy, given the typical equiprobable treatment of the driving models in these
441 dynamical downscaling studies (Brands et al., 2013). Only the models with the best
442 performances should be used as source of initial and boundary data in dynamical
443 downscaling applications, in order to minimize RCM (or RCMs ensemble) simulations errors.

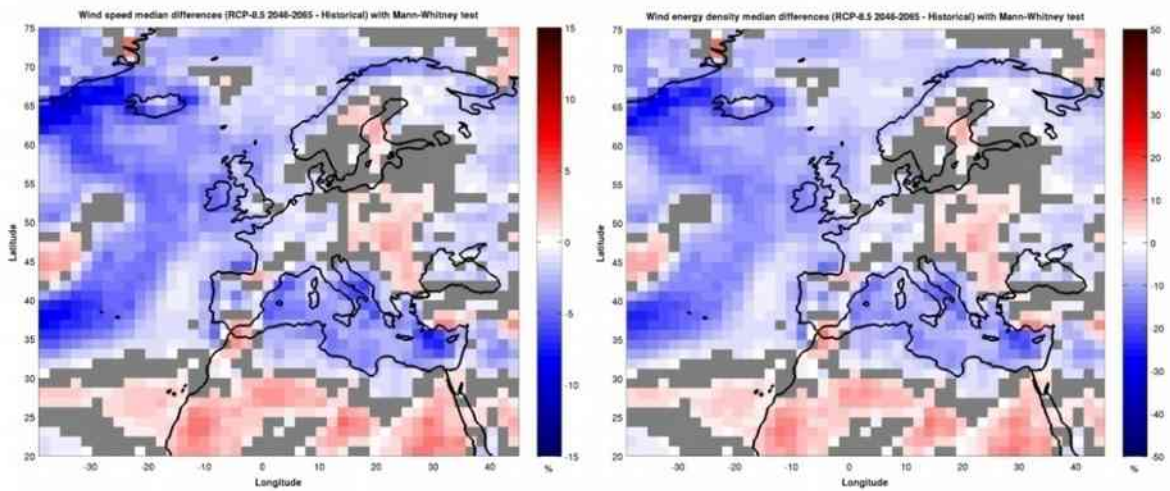
444 Thus, the use of GCM models such as the ones here tested can be considered as somewhat
445 over-simplistic and insufficiently detailed to analyze these issues, due to their inherent
446 limitations and uncertainties. Adding to this fact, these results revealed the inability of the
447 CMIP5 global models here considered to realistically represent the past-present European
448 wind speed climatology. Nevertheless, it is expected that information from GCMs can
449 provide, at least, a preliminary picture of future changes in the large-scale European wind
450 speed climatology.

451 **3.2 – Climate change impacts in future wind energetic resource**

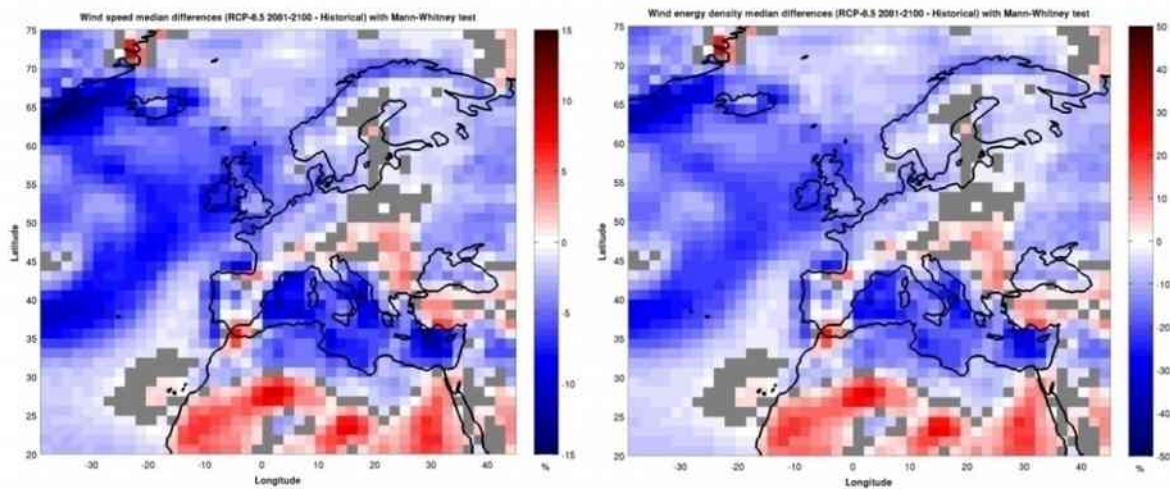
452 Climate change impacts on future wind energy resource and their respective geographical
453 distributions in Europe are analyzed in this section. To this end, MME wind speed and
454 energy density historical and future 20-year medians are compared and the statistical
455 significance of such differences assessed. Figures 2 and 3 show wind speed (left column)
456 and energy density (right column) median differences (future vs. historical) for RCP 8.5. Grey
457 colour represents areas with no median differences according to the Mann-Whitney test (5%
458 significance level). The first, second and third lines are for the short-term, medium-term and
459 long-term future, respectively.



460



461



462

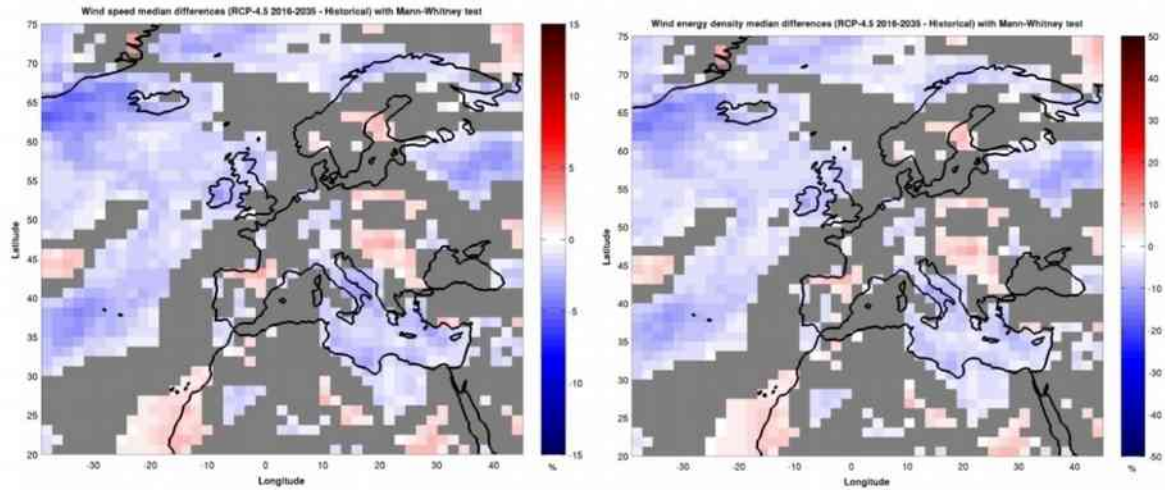
463 **Figure 2** – Wind speed (left column) and energy density (right column) median differences (future minus historical) with Mann-Whitney test - RCP 8.5. The grey colour represents areas without median differences according to a Mann-Whitney test (5% significance level). The first, second and third lines are for the short-term, medium-term and long-term future, respectively.

466 According to Figure 2, if no GHG emissions mitigation strategies are employed (RCP 8.5),
 467 there is a tendency for a cutback in future wind speed and energy density in Europe. The

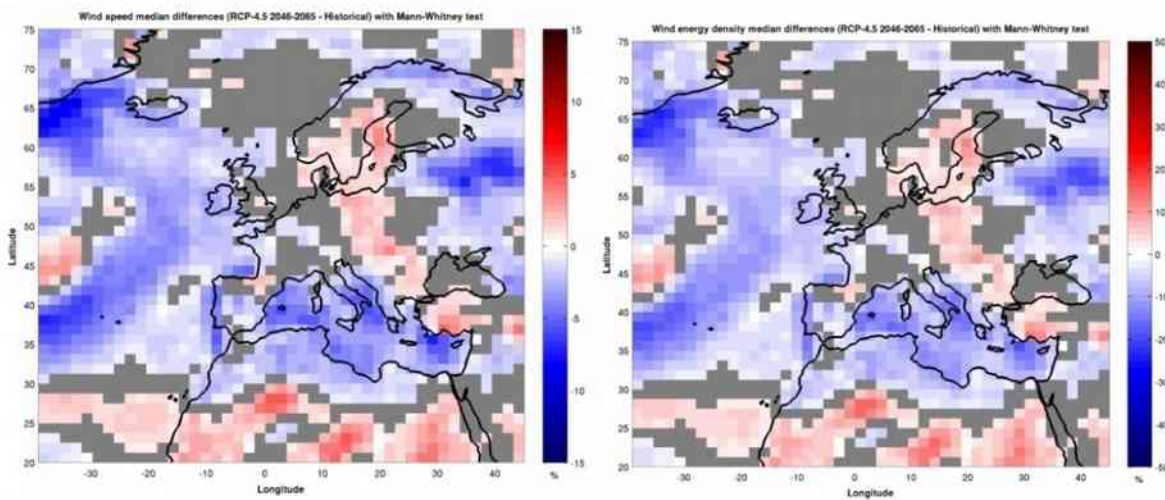
468 exceptions are some areas located in Central Europe (reaching up to Northern Europe),
469 Turkey, offshore areas adjacent to Madeira and Canary archipelagos and in the southern
470 and northern tips of the Iberian Peninsula, where the wind power resource can slightly
471 increase in the future. This reduction is clearly stronger in offshore areas than in onshore
472 ones.

473 These differences, together with increasing number of grid points statistically different from
474 the historical period, are clearly more marked for the medium and long-term future. For the
475 short-term future (2016-2035), the majority of the grid points do not show statistically
476 significant changes from the past-present period and, even when there are statistically
477 significant changes, they are relatively small in magnitude (typically lower than 5% for the
478 wind speed and than 10% for the energy density). For the medium-term future (2046-2065),
479 the number of grid points statistically different from the past-present winds increase together
480 with the magnitude of changes, although lower than 7-10% for the wind speed and 15-20%
481 for the energy density. By the end of the century (2081-2100), practically all the grid points
482 show statistically meaningful differences from the past-present period and the magnitude of
483 changes is clearly higher, reaching up to 10-15% in terms of wind speed and 30-40% for the
484 energy density. In this period, the areas that show a modest increase in the average wind
485 speed and energy density are fewer, and the decrease of the wind energetic potential is
486 more pronounced.

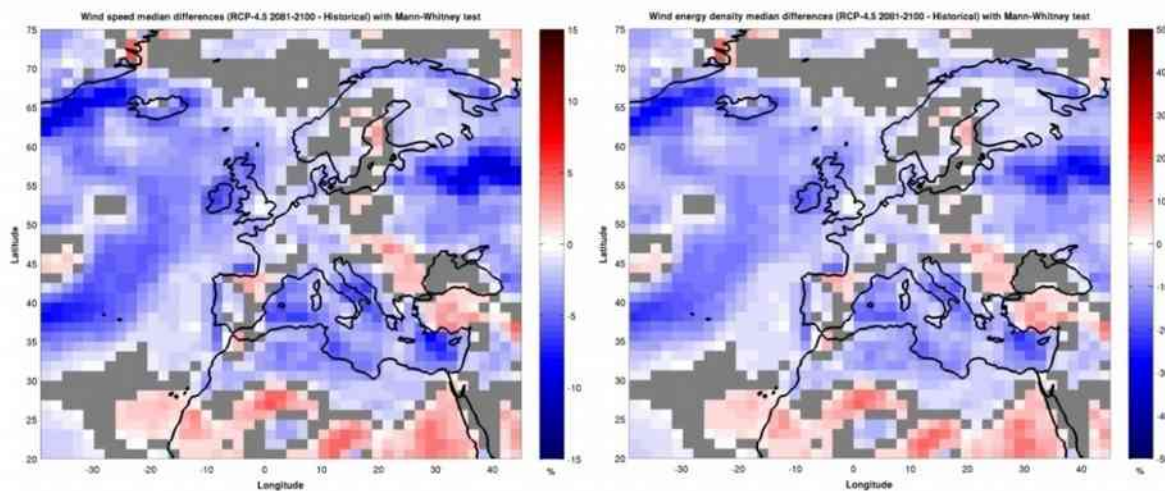
487 It should be noted that, since the energy density varies with the wind speed cubed, the
488 percentual differences shown in Figure 2 are similar for the wind speed and energy density
489 grids due to the colour scale chosen, where the energy density scale limits are about three
490 times higher than the wind speed ones. Next, Figure 3 shows the same analysis but
491 considering now the RCP 4.5 medium mitigation scenario.



492



493

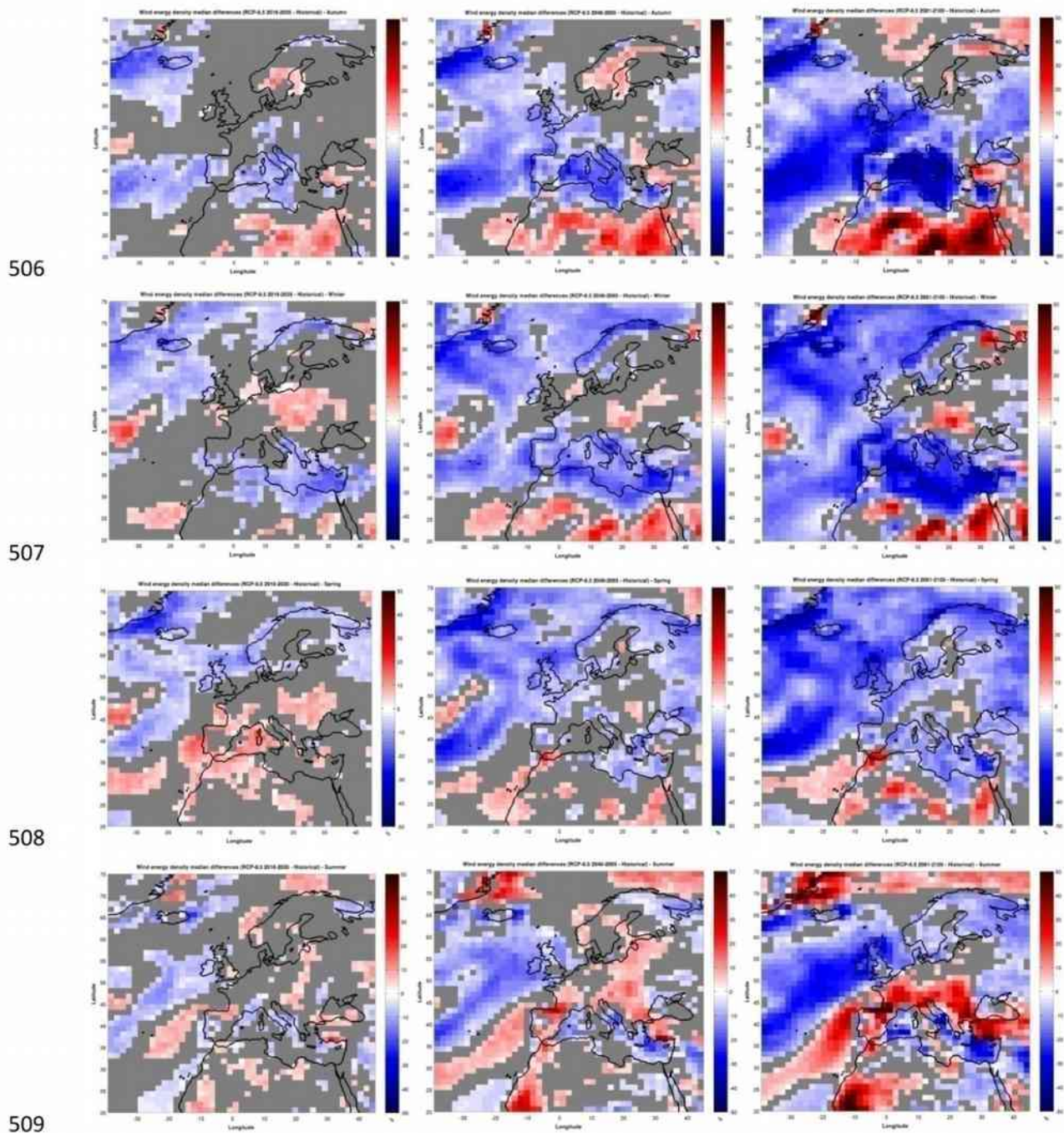


494

495 **Figure 3** – Wind speed (left column) and energy density (right column) median differences (future minus historical) with Mann-
 496 Whitney test - RCP 4.5. The grey colour represents areas without median differences according to a Mann-Whitney test (5%
 497 significance level). The first, second and third lines are for the short-term, medium-term and long-term future, respectively.

498 The future outlook and geographical variation of the wind energy resource under this
 499 scenario, which considers GHG emissions mitigation actions, is similar to the one described

500 by the RCP 8.5 scenario (Figure 2). However, under this scenario the differences between
501 past-present and future wind energetic resource are considerably lower (both in terms of
502 increase/decrease of the wind energetic resource) than the ones witnessed under the RCP
503 8.5, particularly for end of the century. To further analyze and detail the future tendencies of
504 wind energetic resource over Europe, Figures 4 and 5 show the same analysis of Figures 2
505 and 3 for the wind energy density, but now divided by seasons.



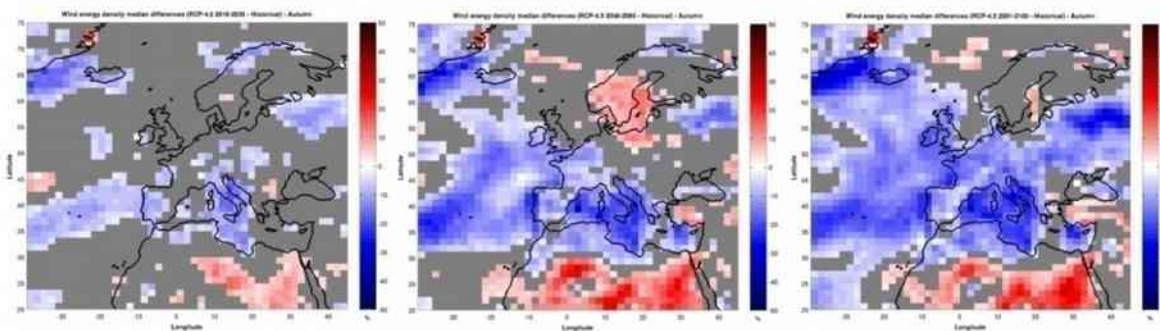
510 **Figure 4** – Seasonal RCP 8.5 wind energy density median differences (future minus historical) with Mann-Whitney test. The
511 grey colour represents areas without median differences according to a Mann-Whitney test (5% significance level). The first,
512 second, third and fourth lines are for Autumn, Winter, Spring and Summer periods, respectively.

513 According to Figure 4 there is some seasonality in the changes of the wind energy density.
514 Although in almost all seasons there is a general tendency for the future wind energy density
515 to be lower than in the contemporary period (specially in Autumn and Spring for the medium
516 and long term future), in Summer periods almost all Europe (with the exception of the
517 Scandinavian Peninsula and Eastern Europe) can see its wind energetic resource increase.
518 All of these tendencies show increasing magnitudes with time.

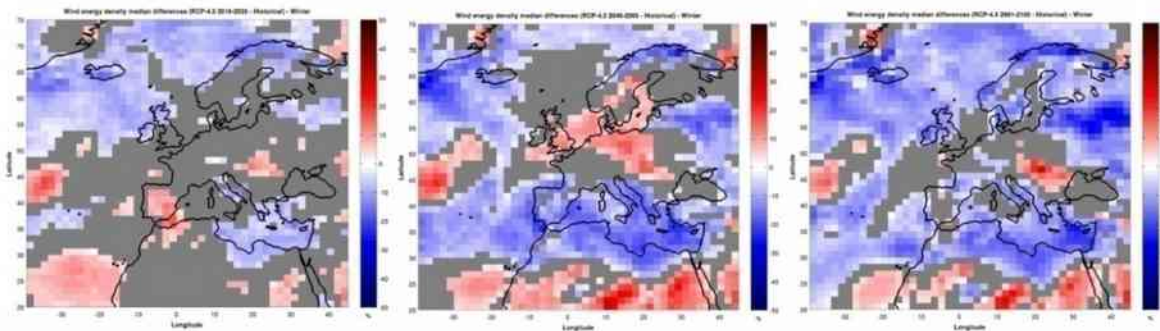
519 In Autumn, practically all Europe shows a generalized tendency for a cutback in the wind
520 power resource, with a strong decrease of the wind energy densities in the Mediterranean
521 area. The exceptions are seen in some areas located in Northern and Central Europe (short
522 and medium-term futures), in Turkey (medium and long-term futures) and in the offshore
523 areas adjacent to the Canary and Madeira archipelagos. Winter periods show similar trends
524 and patterns to the Autumn ones, but here the exceptions for the reduction of the wind
525 energy densities are more localized in Central Europe and in offshore areas around the
526 Madeira and Canary archipelagos (with the exception of the long term future projections). In
527 Spring periods, although the near-term future projections show a generalized increase in the
528 wind energy density across Europe (with the exception of Northern areas), the medium and
529 long-term future projections show opposite tendency. For these periods, practically all
530 European territory shows a decrease in the wind energy density, the only exceptions being
531 the southernmost tip of the Iberian Peninsula and the offshore areas adjacent to the Madeira
532 and Canary archipelagos. In Summer, while the Scandinavian Peninsula and eastern areas
533 of Europe show lower future wind energy densities, central and southern Europe shows a
534 strong increase of the wind energetic resource. This is particularly visible for the long-term
535 future.

536 Figure 5 shows the same information as Figure 4 but now for the RCP 4.5.

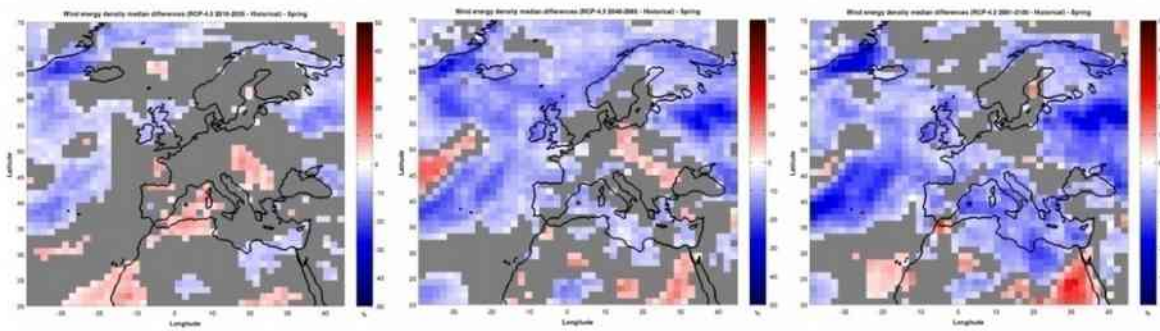
537



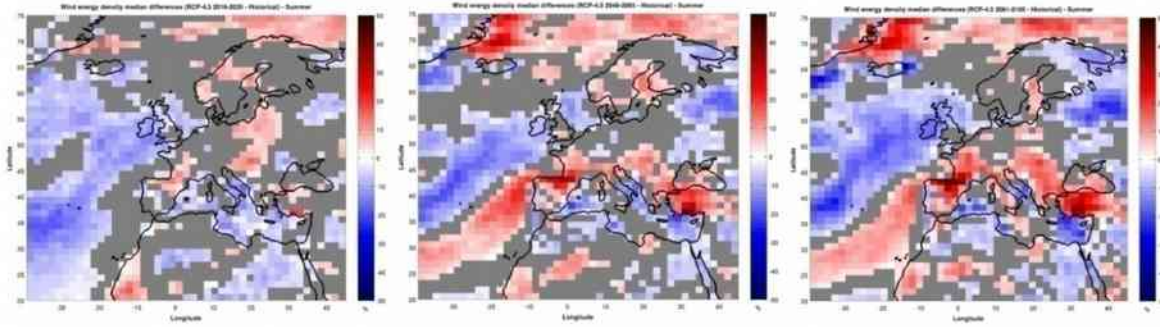
538



539



540



541 **Figure 5** – Seasonal RCP 4.5 wind energy density median differences (future minus historical) with Mann-Whitney test. The
 542 grey colour represents areas without median differences according to a Mann-Whitney test (5% significance level). The first,
 543 second, third and fourth lines are for Autumn, Winter, Spring and Summer periods, respectively.

544 Figure 5 shows that in, similarly to what was seen in Figures 2 and 3, the major difference
 545 between RCP 8.5 and RCP 4.5 is that the latter shows lower differences between
 546 contemporary and future wind energy resource. This is also true when this analysis is divided
 547 into seasons. Nevertheless, these seasonal differences between contemporary and future

548 wind energy density are still present, albeit somewhat smoothed under this mid-range GHG
549 emission scenario.

550 From Figures 2 and 3, a general tendency for a decrease of future wind speeds and energy
551 densities over Europe becomes noticeable. Although some areas show an opposite
552 tendency (some areas located in Central Europe reaching up to Northern Europe, Turkey
553 and the southern and northern tips of the Iberian Peninsula), with a modest increase in future
554 wind energetic resource, the negative trends are clearly dominant both in magnitude and
555 geographical distribution. These tendencies magnify in time, since the variations of the wind
556 energetic resource are lower for the near-term future and higher in the end of the current
557 century. Furthermore, it is clear that these changes and tendencies are higher under
558 scenarios of stronger radiative forcing. When analyzing the future variation of the wind
559 energetic resource in a seasonal perspective (Figures 4 and 5), it is detectable a seasonality
560 in the variation of the wind energy density. While in Autumn and Spring there is a tendency
561 for the future wind energy density to be lower than in the contemporary period (with some
562 localized exceptions in Central/Northern Europe), in Summer almost all Europe (with the
563 exception of the Scandinavian Peninsula and Eastern Europe) shows an opposite tendency,
564 with an increase in its wind energetic resource. All of these tendencies show increasing
565 magnitudes with time and under stronger emission scenarios.

566 Although it is not straightforward to find a direct and objective cause for these tendencies due
567 to the non-linear dependence of near-surface winds with a wide range of meteorological and
568 terrain features, some studies that investigated CMIP5 data reported findings that can be
569 related to this issue: decreasing trends in cyclone number and frequency in most of the North
570 Atlantic and Europe (Eichler et al., 2013; Zappa et al., 2013); decrease of extreme cyclones
571 events and in storm track activity in the Northern Hemisphere (Chang et al., 2012); and an
572 increased frequency of the negative phase of the North-Atlantic Oscillation (NAO) under
573 future warming (Cattiaux et al., 2013). A negative phase of the NAO is related to a
574 weakening of its two pressure centres (Azores high and Iceland low), leading to lower zonal

575 winds (mainly westerlies), together with fewer and weaker cyclones (Pryor et al., 2005a).
576 Thus, a future decrease in the storm activity, number and intensity of cyclones in Europe and
577 a tendency for the NAO to be more negative can explain the tendency for future lower wind
578 speeds across Europe.

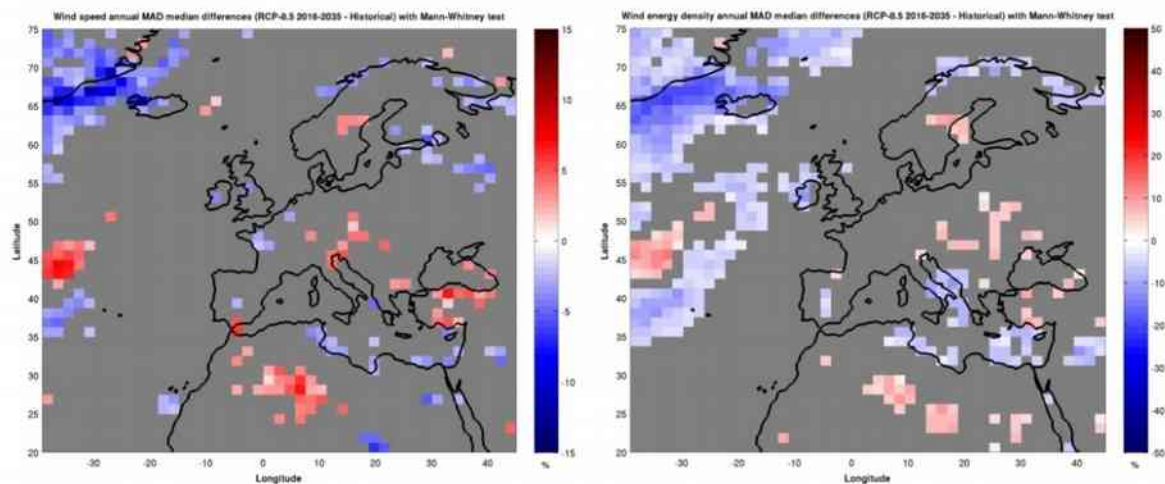
579 It becomes pertinent to discuss the obvious differences between the future tendencies of
580 wind speeds over Europe projected by CMIP5 and its predecessor, CMIP3. The latter
581 projected that by the end of the current century the wind energy density and annual mean
582 wind speeds can increase in northern Europe and decrease in the south of the continent,
583 especially in Winter (Pryor et al., 2005a; Bloom et al., 2008; Walter et al., 2006). Several
584 authors (Pryor and Barthelmie, 2010, and references therein) reported that such findings are
585 consistent with a tendency present in CMIP3 future climate projections toward a positive
586 phase of the NAO (Rauthe et al., 2004), a poleward displacement of the storm track (Pryor
587 and Barthelmie, 2003) and an increase of midlatitude cyclones intensity over the North
588 Atlantic, particularly in Winter (Nolan et al., 2011). Ergo, it becomes clear that CMIP5 and
589 CMIP3 modelling results show different trends and future wind climatology projections over
590 Europe and its driving mechanisms. This fact is not surprising given the aforementioned
591 differences in the GCMs used in CMIP3 and CMIP5. One of the differences between these
592 two generations of GCMs that can have a strong impact in realistically simulating future near-
593 surface winds is that CMIP5 GCMs are able to incorporate land use and land cover changes
594 that are frequent over time (Moss et al., 2010). CMIP3 GCMs may not realistically update
595 these changes over their simulations in their boundary conditions, as reported by Vautard et
596 al. (2010). Aside differences in the GCMs design, Cattiaux and Cassou (2013) studied the
597 differences between CMIP5 and CMIP3 trends in the wintertime Northern Annular Mode
598 (NAM, also known as the Arctic Oscillation). The NAM directly influence European climate
599 through changes in its regional feature, the NAO (Ambaum et al., 2001). Cattiaux and
600 Cassou (2013) reported that CMIP3 future projections showed a positive NAM trend, while
601 CMIP5 revealed an opposite (negative) trend, and these differences are mostly related to the
602 CMIP5 faster sea ice depletion in early winter and stronger warming in the western tropical

603 Pacific in late winter, which will remotely influence the NAM through teleconnection
604 mechanisms. Also, Cattiaux et al. (2013) found that CMIP5 models, oppositely to CMIP3
605 ones, project a stronger winter North-Atlantic jet stream than observed, suggesting an
606 increased frequency of the NAO negative phase under future warming. Furthermore, Chang
607 et al. (2012) reported that CMIP5 models project a larger decrease in the Northern
608 Hemisphere (NH) storm track activity than CMIP3 models. Thus, it appears that CMIP5 and
609 CMIP3 projected opposite trends in future NAO phases, and CMIP5 models foresee a larger
610 decrease in NH storm activity when compared to CMIP3 results. These findings can be
611 related to CMIP5 and CMIP3 different projections of future near-surface winds over Europe.

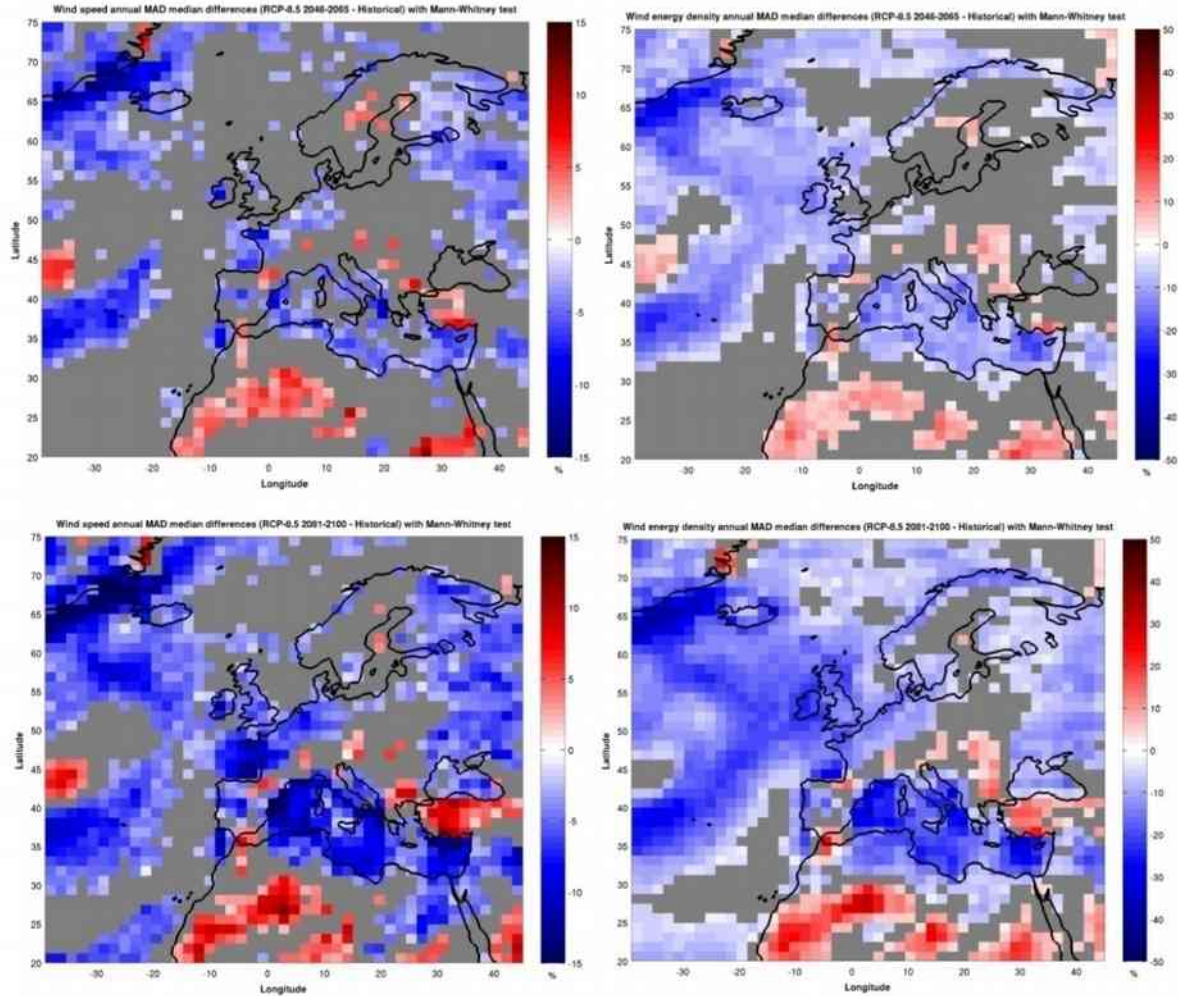
612 3.3 – Climate change impacts in future wind energy intra-annual variability

613 To assess climate change impacts on future wind energetic resource intra-annual variability,
614 historical and future MME wind speed and energy density annual MAD medians are
615 compared and the statistical significance of such differences assessed. These results are
616 presented in Figures 6 and 7.

617



618



619

620

621

622

Figure 6 – Wind speed (left column) and energy density (right column) MAD median differences (future minus historical) with Mann-Whitney test - RCP 8.5. The grey colour represents areas without median differences according to a Mann-Whitney test (5% significance level). The first, second and third lines are for the short-term, medium-term and long-term future, respectively.

623

624

625

626

627

628

629

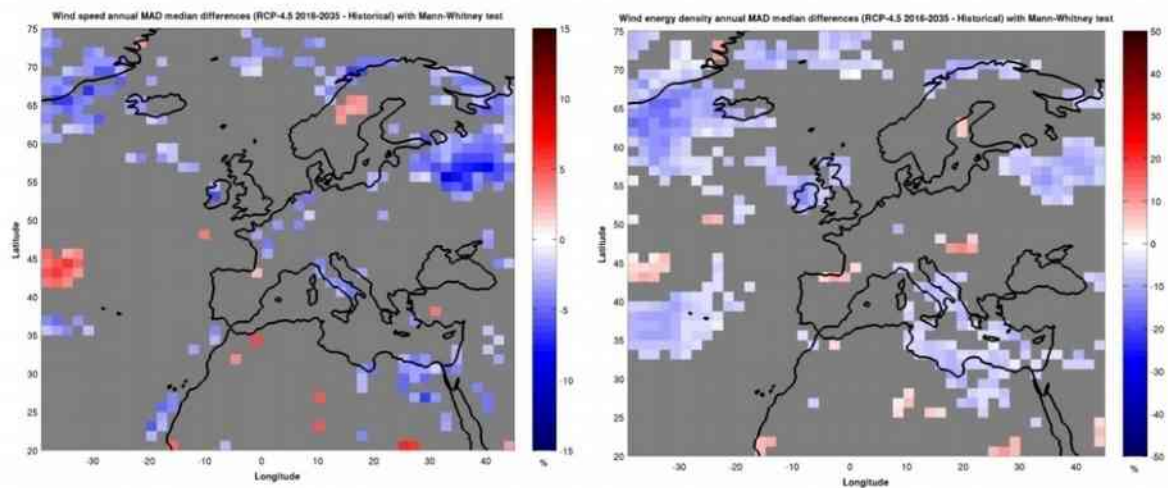
630

631

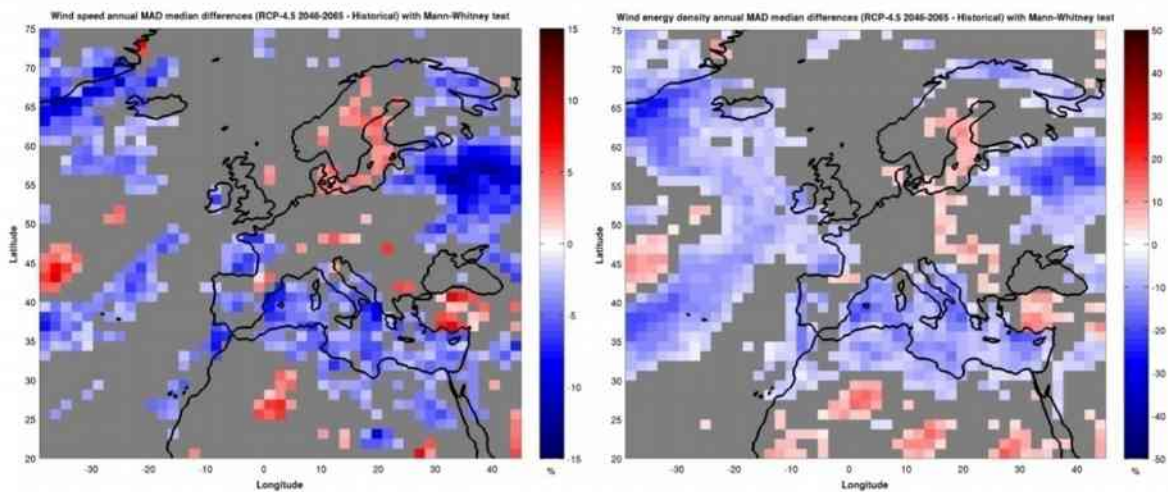
632

According to Figure 6, in the short-term future (2016-2035) no significant changes in the wind speed and energy density intra-annual variability are to be expected, since only a small number of grid points show statistically significant MAD median differences between the contemporary and short-term future. Although the differences are more significant for the wind energy density than for the wind speed, in European mainland almost all grid points show statistically negligible differences. However, for the medium and long-term future the panorama is considerably different. For these periods, the wind speed and energy density intra-annual variability are expected to be significantly lower, especially in the end of the current century. In the medium-term future (2046-2065), the wind speed and energy density intra-annual variability trends are somewhat homogeneous in Europe, decreasing around 2-

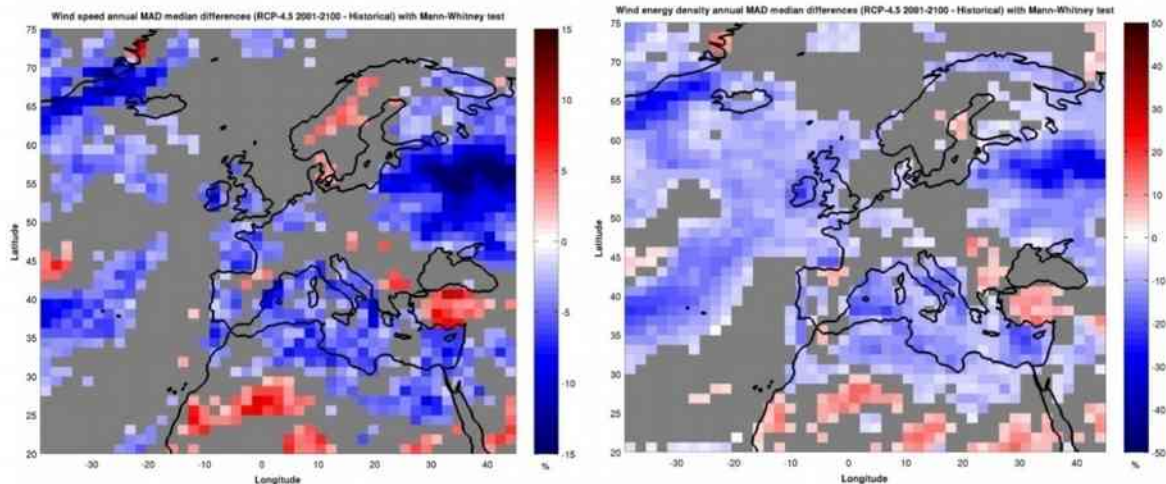
633 10% in terms of wind speed, corresponding to about 10-30% in terms of wind energy density.
 634 This tendency is present practically in all European territory, with the exceptions of some
 635 localized areas in the Iberian and Scandinavian Peninsula, Turkey and in central Europe.
 636 The long-term future shows similar geographical patterns and signal for the wind speed and
 637 energy density intra-annual variability changes, but with intensified magnitudes: the wind
 638 speed intra-annual variability can decrease up to 8-15%, while the wind energy density intra-
 639 annual variability can be reduced in about 15-40%. This negative trend of the wind speed
 640 and energy density intra-annual variability is more pronounced in the Mediterranean area,
 641 whereas some areas located in Turkey and Central Europe can see the intra-annual
 642 variability increase. Figure 7 shows the same information but now considering RCP 4.5 data.



643



644



645
 646 **Figure 7** – Wind speed (left column) and energy density (right column) MAD median differences (future minus historical) with
 647 Mann-Whitney test - RCP 4.5. The grey colour represents areas without median differences according to a Mann-Whitney test
 648 (5% significance level). The first, second and third lines are for the short-term, medium-term and long-term future, respectively.

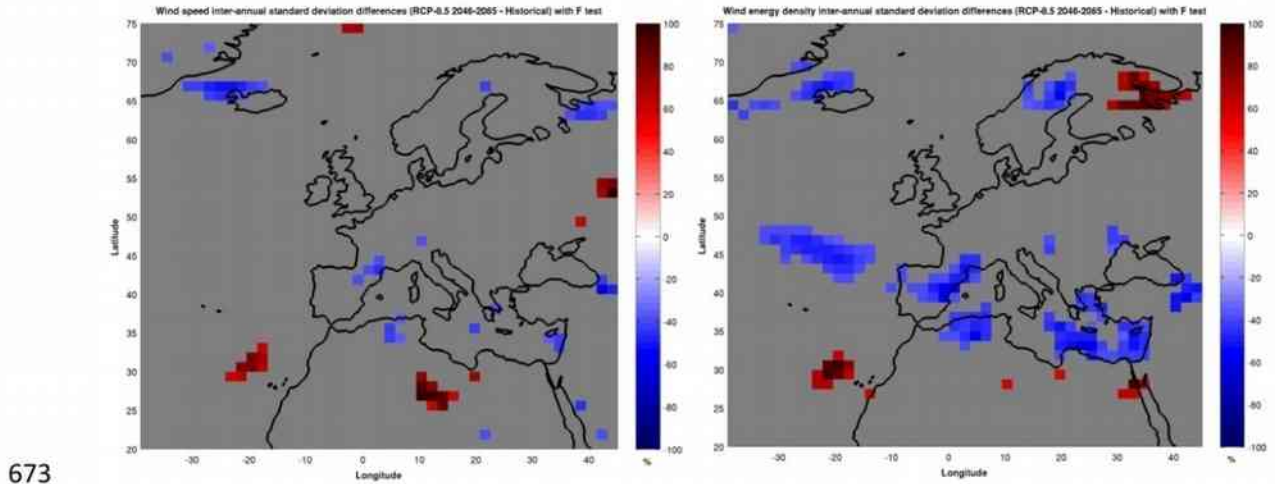
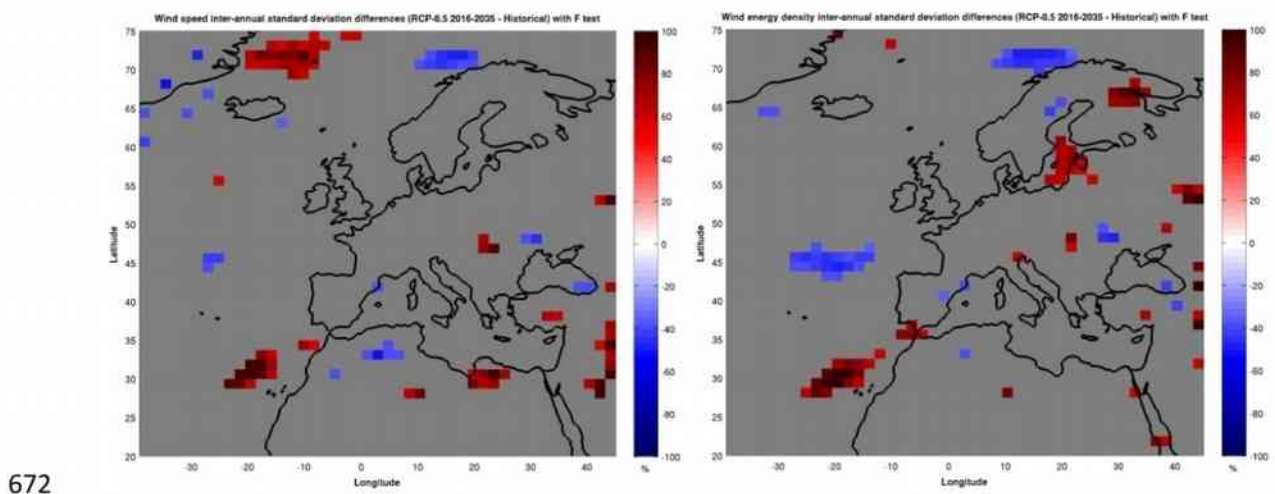
649 The expected changes in the wind speed and energy density intra-annual variability
 650 considering RCP 4.5 data are very similar to the ones expected with RCP 8.5, although with
 651 lower magnitudes. Similarly to what was seen for RCP 8.5, RCP 4.5 foresees a generalized
 652 decrease in the wind speed and energy density intra-annual variability all over European
 653 territory, more marked in the medium and long-term futures. The exceptions are again seen
 654 in Turkey and in some localized areas in Central/Northern Europe.

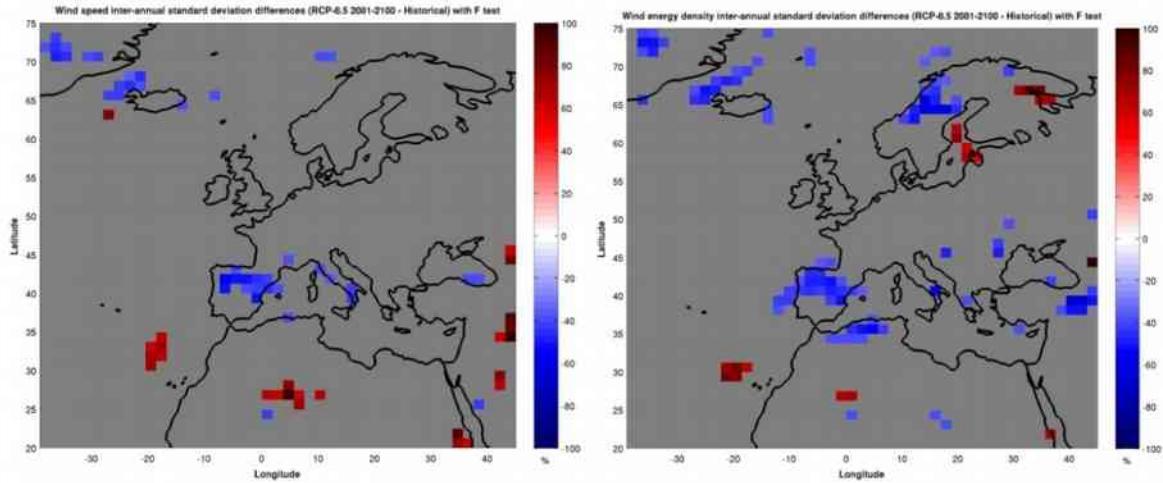
655 Bearing in mind that, typically, average wind speeds tend to be higher in cold seasons and
 656 lower in warmer ones, the results presented in the previous section (Figures 4 and 5) are
 657 consistent with the general decrease in the wind speed and energy density intra-annual
 658 variability here detected: if in Winter the wind speed and energy density tend to be lower and
 659 in Summer they tend to be higher, the difference between Winter-Summer wind energetic
 660 resource will be lower and, hence, lower will its intra-annual variability be (the typical
 661 variation the wind speed and energy density within a year). This reduction of the wind energy
 662 density intra-annual variability, particularly if it reaches 30-40% of its current value, is of great
 663 interest for the electrical grid operators, since the offer-demand grid balance can be easier to
 664 maintain with a less variable wind-derived electricity injection.

665 **3.4 – Climate change impacts in future wind speed and wind energy density**
666 **inter-annual variability**

667 In order to assess climate change impacts in future wind speed and wind energy density
668 inter-annual variability (this is, the variability between different years), differences in the
669 standard deviation between historical and future wind speed and energy density annual
670 means data series are computed and their statistical significance assessed with the F-test.

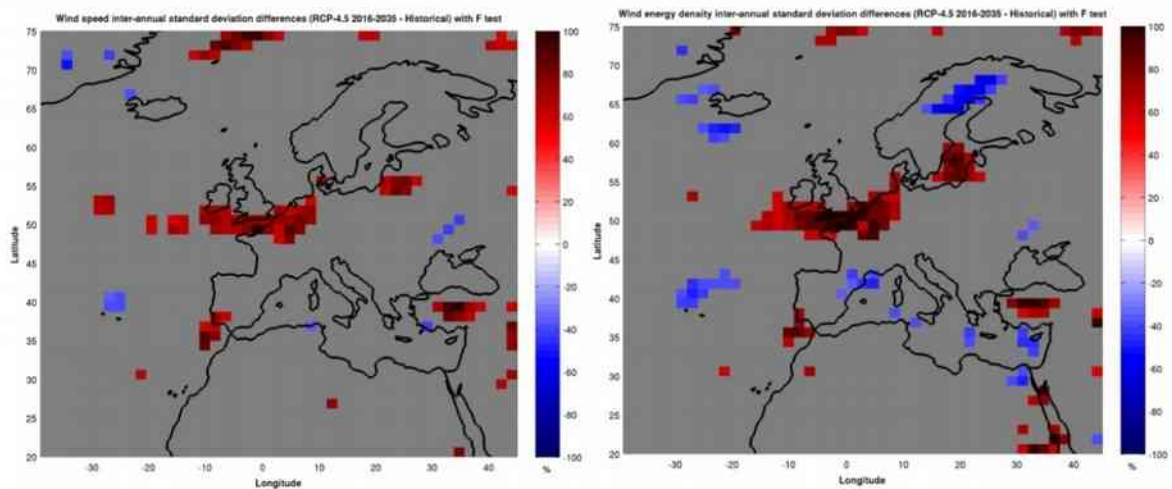
671 These results are shown in Figures 8 and 9.



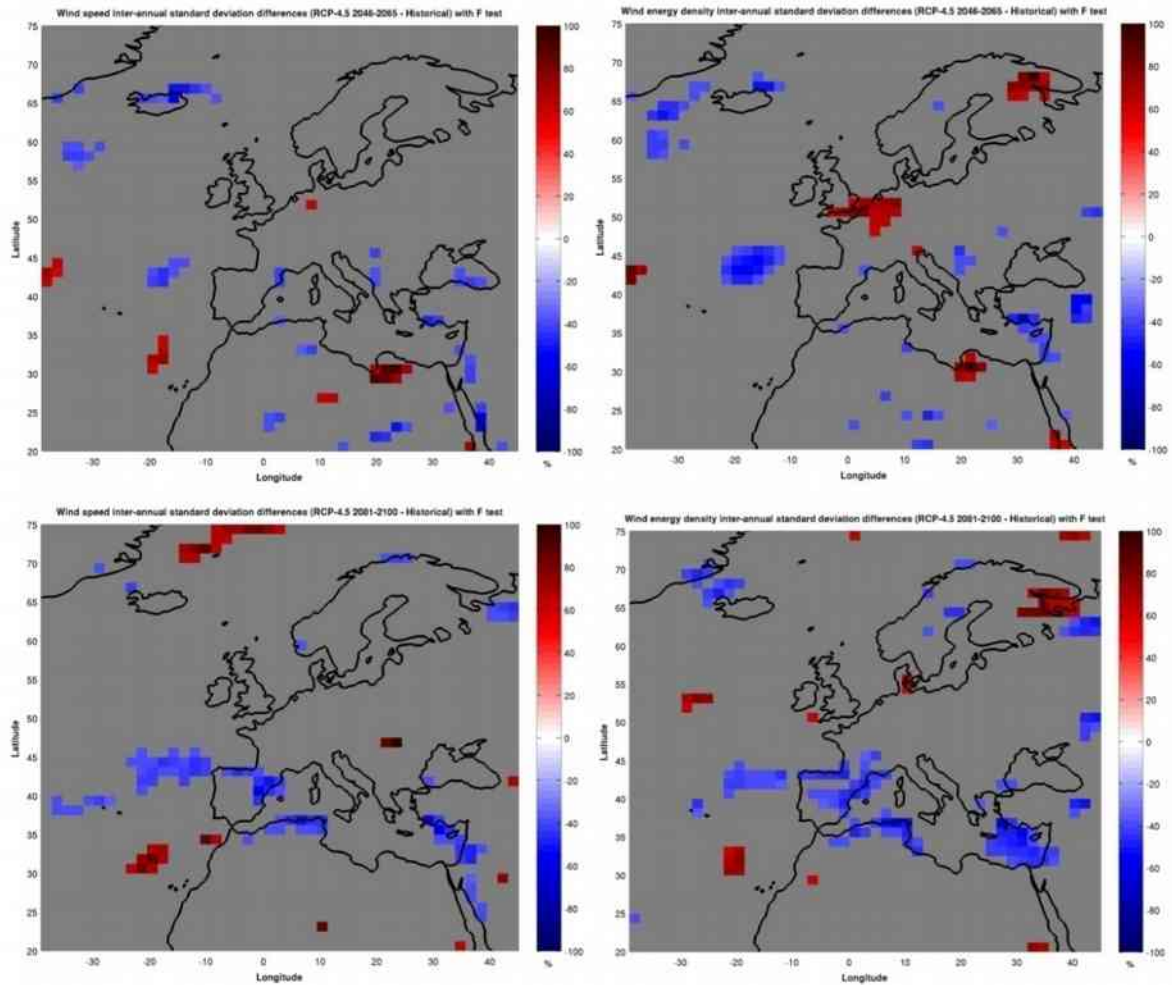


674
 675 **Figure 8** – Wind speed (left column) and energy density (right column) standard deviation differences (future minus historical)
 676 with the F-test - RCP 8.5. The grey colour represents areas without median differences according to a F-test (5% significance
 677 level). The first, second and third lines are for the short-term, medium-term and long-term future, respectively.

678 According to Figure 8, no significant changes are to be expected in the inter-annual
 679 variability for the wind speed and energy density over Europe until the end of the current
 680 century. For all future periods, the great majority of the grid points show statistically not
 681 significant differences when compared to the contemporary period inter-annual variability.
 682 Although when such differences are statistically significant they are high in magnitude
 683 (reaching up to an increase of 100% a decrease of 60-70%), these statistically significant
 684 grid points are scattered and no conclusive trend, geographical or temporal, is detectable.
 685 Figure 9 shows the same analysis but now considering RCP 4.5 data.



686



687

688

689 **Figure 9** – Wind speed (left column) and energy density (right column) standard deviation differences (future minus historical)
 690 with the F-test - RCP 4.5. The grey colour represents areas without median differences according to a F-test (5% significance
 691 level). The first, second and third lines are for the short-term, medium-term and long-term future, respectively.

692

693

694

695

696

697

698

Figure 9 shows similar geographical and temporal changes of the wind speed and energy density inter-annual variability of Figure 8. Thus, also when considering future climate projections of RCP 4.5 scenario no significant changes are to be expected in the inter-annual variability for the wind speed and energy density. Considering the information presented in Figures 8 and 9, it is advisable to adopt a conservative point of view in this issue and consider that no significant changes are to be expected in the inter-annual variability for the wind speed and energy density over Europe until the end of the current century.

699 **4 – Conclusions**

700 This work aimed to provide a large-scale picture of future changes in European wind
701 resource due to climate changes, using the latest IPCC future climate projections derived
702 from the CMIP5 project. This work comprised two stages: first, to assess the GCMs that best
703 reproduce contemporary near surface wind speeds over Europe. Secondly, data from the
704 best GCMs was used to quantify and assess future changes in the large-scale wind
705 energetic resource and their geographical distributions over Europe, together with its intra-
706 and inter-annual variability. The main conclusions of this work can be summarized as follows:

- 707 ➤ The CMIP5 GCMs HadGEM2-ES, HadGEM2-CC, ACCESS 1.3 and ACCESS 1.0
708 are the models that showed the best ability to represent the European contemporary
709 near surface wind speed climatology over Europe described by the ERA-Interim
710 reanalysis. Near surface wind speed data from these models was used to assess
711 future projections of wind speed climatology over Europe. However, it should be
712 highlighted that all tested CMIP5 GCMs showed poor results in accurately
713 representing past-present European wind climatology. Additional efforts should be
714 employed to improve the performance of these models.
715
- 716 ➤ The future European wind energetic resource is predicted to be lower than the one
717 available at present, due to a decreasing tendency of the large-scale wind speeds
718 over the current century. Although some areas (located in Central Europe reaching
719 up to Northern Europe, Turkey and the southern and northern tips of the Iberian
720 Peninsula) can show a modest increase in future wind energy resource, negative
721 trends are clearly dominant both in magnitude and geographical distribution. These
722 tendencies increase in time, since the variations of the wind energy resource are
723 lower for the upcoming decades and higher by the end of the current century. They
724 are also higher under scenarios of stronger radiative forcing. Although in the
725 upcoming decades (2016-2035) no alarming changes in the wind energetic resource

726 are to be expected (lower than 10% for the “business as usual” scenario and below
727 5% for the midrange GHG emission mitigation RCP), the panorama drastically
728 changes for the last decades of the current century (2081-2100), where the reduction
729 in the wind energetic resource over Europe can reach an alarming 30-40% (when
730 considering RCP 8.5).

731

732 ➤ Seasonality is also patent in the variation and changes in the future wind energy
733 resource. While in Autumn and Spring there is a tendency for the future wind
734 energetic resource to be lower than in the contemporary period (with some localized
735 exceptions in Central/Northern Europe), in Summer almost all Europe shows an
736 opposite tendency (with the exception of the Scandinavian Peninsula and Eastern
737 Europe), with an increase in its wind energetic resource. Again, these tendencies
738 magnify in time and they are higher under scenarios of stronger radiative forcing that
739 consider less GHG emission mitigation actions.

740

741 ➤ No significant changes in the wind speed and energy density intra-annual variability
742 are to be expected in the period 2016-2035. However, for the medium (2046-2065)
743 and long-term (2081-2100) future the panorama is considerably different. For these
744 periods, the wind speed and energy density intra-annual variability are expected to
745 be significantly lower (except in Turkey and in some localized areas in
746 Central/Northern Europe), especially in the end of the current century (around 15-
747 40%). These tendencies are also higher under scenarios of stronger radiative forcing.

748

749 ➤ In terms of inter-annual variability, no significant changes are to be expected over
750 Europe during the current century. The statistical analysis revealed that the
751 differences between past-present and future inter-annual variability, although
752 sometimes high in magnitude, are not statistically significant. Thus, no conclusive
753 trends, geographical or temporal, are detectable.

754 Although the validation results of this study showed the inability of the CMIP5 global models
755 to realistically represent the past-present European wind speed climatology, and the use of
756 such coarse models can be considered as somewhat over-simplistic and insufficiently
757 detailed for the desired purposes, the findings of this work can serve as an important
758 background for future downscaling initiatives of CMIP5 data to regional and local scales and
759 should be seen as a preliminary warning that a continuous increase of greenhouse gases
760 emissions can jeopardize our ability to mitigate such emissions, at least in what concerns the
761 role and contribution of wind energy. By negatively affecting future wind energy resource,
762 climatic changes can weaken wind power active and vital contribute to reduce greenhouse
763 gases emissions. However, it needs to be strongly emphasised that there is significant
764 uncertainty associated to global models future climate projections that, together with the poor
765 ability of the CMIP5 global models to accurately represent the past-present wind climate over
766 Europe due to their intrinsic limitations, provides limited confidence to the future outlook of
767 the European wind energy resource projected by these models. Thus, the information
768 provided by these models should be seen as a preliminary picture of the large scale future
769 tendencies of the wind energy resource, and further research focused on these themes
770 should be performed by downscaling CMIP5 GCMs output to regional and local scales in
771 order to better represent the topography and land use and thus better simulate near surface
772 winds.

773 **Acknowledgements**

774 D. Carvalho was supported by the Portuguese Foundation for Science and Technology
775 (FCT) Ph.D grant SFRH/BD/73070/2010. This work was partially financed by Xunta de
776 Galicia under the project "Programa de Consolidación e Estructuración de Unidades de
777 Investigación Competitivas (Grupos de Referencia Competitiva)", co-funded by the European
778 Regional Development Fund (FEDER). The authors would like to express their gratitude to
779 all the CMIP5 community and institutions involved for providing the GCM data used in this

780 work. This work was also supported by the project CLICURB - Urban atmospheric quality,
781 climate change and resilience (EXCL/AAG-MAA/0383/2012), funded by FCT.

782 **References**

783 Alvarez I., Gomez-Gesteira M.M, deCastro M, Carvalho D. (2013). Comparison of different wind
784 products and buoy wind data with seasonality and interannual climate variability in the southern Bay of
785 Biscay (2000-2009). *Deep-Sea Res Pt II*, 106, 38-48

786 Ambaum M, Hoskins B, Stephenson D (2001). Arctic Oscillation or North Atlantic Oscillation? *J Clim*,
787 14, 3495-3507

788 Annan JD, Hargreaves JC (2010). Reliability of the CMIP3 ensemble. *Geophys Res Lett*, 37, L02703.

789 Bakker AMR, van den Hurk BJJM, Coelingh JP (2013). Decomposition of the windiness index in the
790 Netherlands for the assessment of future long-term wind supply. *Wind Energy*, 16, 927-936

791 Bloom A, Kotroni V, Lagouvardos K. (2008). Climate change impact of wind energy availability in the
792 Eastern Mediterranean using the regional climate model PRECIS. *Nat Hazards Earth Sys*, 8(6),1249-
793 57

794 Bracegirdle TJ, et al. (2013). Assessment of surface winds over the Atlantic, Indian, and Pacific Ocean
795 sectors of the Southern Ocean in CMIP5 models: historical bias, forcing response, and state
796 dependence. *J Geophys Res Atmos*, 118, 547–562

797 Brands S, Herrera S, San-Martin D, Gutierrez JM (2011). Validation of the ENSEMBLES global
798 climate models over southwestern Europe using probability density functions, from a downscaling
799 perspective. *Climate Res*, 48(2-3),145–161

800 Brands S, Herrera S, Fernández J, Gutiérrez JM (2013). How well do CMIP5 Earth System Models
801 simulate present climate conditions in Europe and Africa? *Clim Dynam*, 41(3-4), 803-817

802 Brázdil R, Chroma K, Dobrovolny P, Tolasz R (2009). Climate fluctuations in the Czech Republic
803 during the period 1961-2005. *Int J Climatol*, 29, 223-22

804 Carvalho D, Rocha A, Gómez-Gesteira M, Santos C (2012a). A sensitivity study of the WRF model in
805 wind simulation for an area of high wind energy. *Environ Modell Softw*, 33, 23-34.

806 Carvalho D, Rocha A, Gómez-Gesteira M (2012b). WRF model ocean surface wind simulation forced
807 by different reanalysis: comparison with observed data along the Iberian Peninsula coast. *Ocean*
808 *Model*, 56, 31-42

809 Carvalho D, Rocha A, Santos CS, Pereira R (2013a). Wind resource modelling in complex terrain
810 using different mesoscale-microscale coupling techniques. *Appl Energ*. 108, 493-504.

811 Carvalho D, Rocha A, Gómez-Gesteira M, Alvarez I, Silva Santos C (2013b). Comparison between
812 CCMP, QuikSCAT and buoy winds along the Iberian Peninsula coast. *Remote Sens Environ* 137, 173-
813 183

814 Carvalho D, Rocha A, Gómez-Gesteira M, Silva Santos C (2014a). WRF wind simulation and wind
815 energy production estimates forced by different reanalyses: Comparison with observed data for
816 Portugal. *Appl Energ*, 117, 116–126

817 Carvalho D, Rocha A, Gómez-Gesteira M, Silva Santos C (2014b). Offshore wind energy resource
818 simulation forced by different reanalyses: Comparison with observed data in the Iberian Peninsula.
819 *Appl Energ*, 134, 57-64

820 Carvalho D, Rocha A, Gómez-Gesteira M, Silva Santos C (2014c). Sensitivity of the WRF model wind
821 simulation and wind energy production estimates to planetary boundary layer parameterizations for
822 onshore and offshore areas in the Iberian Peninsula. *Appl Energ*, 135, 234-246

823 Carvalho D, Rocha A, Gómez-Gesteira M, Silva Santos C (2014d). Comparison of reanalyzed,
824 analyzed, satellite-retrieved and NWP modelled winds with buoy data along the Iberian Peninsula
825 coast. *Remote Sens Environ* 152, 480-492

826 Cattiaux J, Douville H, Peings Y (2013). European temperatures in CMIP5: origins of present-day
827 biases and future uncertainties. *Clim Dynam*, 41:11-12, 2889-2907

828 Cattiaux J, Cassou C (2013). Opposite CMIP3/CMIP5 trends in the wintertime Northern Annular Mode
829 explained by combined local sea ice and remote tropical influences. *Geophys Res Lett*, 40, 3682–
830 3687

831 Chang EKM, Guo Y, Xia X (2012). CMIP5 multimodel ensemble projection of storm track change
832 under global warming. *Journal of Geophysical Research: Atmospheres*, Volume 117, Issue D23, 16

833 Chen L., Pryor SC, Li D (2013). Assessing the performance of IPCC AR5 Climate Models in simulating
834 and projecting wind speeds over China. *J Geophys Res Atmos*, 117(D24):24102

835 Christensen JH, Christensen OB (2007). A summary of the PRUDENCE model projections of changes
836 in European climate by the end of this century. *Clim Change*, 81, 7-30

837 Cradden LC, Harrison GP, Chick JP (2012). Will climate change impact on wind power development in
838 the UK? *Clim Change*, 115, 837–852.

839 de Vries E (2008a). 40,000 MW by 2020: building offshore wind in Europe. *Renewable Energy World*,
840 36-47

841 de Vries E (2008b). The DEWI report: wind energy study 2008. *Renewable Energy World*, 93-101

842 Eichler TP, Gaggini N, Pan Z (2013). Impacts of global warming in Northern Hemisphere winter storm
843 tracks in the CMIP5 model suite. *J Geophys Res*, 118, 3919-3932

844 ENSEMBLES (2006). Ensemble-based prediction of climate changes and their impacts.
845 <http://ensembles-eu.metoffice.com/index.html>.

846 European Wind Energy Association (2009). Wind energy. The facts. A guide to the technology,
847 economics and future of wind power. Earthscan, London

848 Gibbons JD, Chakraborti S (2011). Nonparametric Statistical Inference, 5th Ed., Boca Raton, FL:
849 Chapman & Hall/CRC Press, Taylor & Francis Group.

850 Kulkarni S, Huang H-P (2014). Changes in Surface Wind Speed over North America from CMIP5
851 Model Projections and Implications for Wind Energy. *Advances in Meteorology*, 292768

852 IPCC AR5 (2013). Climate Change 2013: The Physical Science Basis. Contribution of Working Group
853 I to the Fifth Assessment Report of the Intergovernmental Panel on Climate Change [Stocker, T.F., D.
854 Qin, G.-K. Plattner, M. Tignor, S.K. Allen, J. Boschung, A. Nauels, Y. Xia, V. Bex and P.M. Midgley
855 (eds.)]. Cambridge University Press, Cambridge, United Kingdom and New York, NY, USA, 1535 pp.

856 IPCC AR4 (2007). Climate Change 2007: The Physical Science Basis. Contribution of Working Group
857 I to the Fourth Assessment Report of the Intergovernmental Panel on Climate Change [Solomon, S.,
858 D. Qin, M. Manning, Z. Chen, M. Marquis, K.B. Averyt, M. Tignor and H.L. Miller (eds.)]. Cambridge
859 University Press, Cambridge, United Kingdom and New York, NY, USA, 996 pp.

860 McInnes KL, Erwin TA, Bathols JM (2011). Global climate model projected changes in 10 m wind
861 speed and direction due to anthropogenic climate change. *Atmos Sci Lett*, 12, 325–333

862 Meinshausen M, et al. (2011). The RCP Greenhouse Gas Concentrations and their Extension from
863 1765 to 2300. *Clim Change*, 109(1:2), 213-241

864 Moss RH, et al. (2010). The next generation of scenarios for climate change research and
865 assessment. *Nature*, 463, 747-756

866 Nolan P, Lynch P, McGrath R, Semmler T, Wang S (2011). Simulating climate change and its effects
867 on the wind energy resource of Ireland. *Wind Energy*, 15(4), 593–608

868 Pierce DW, Barnett TP, Santer BD, Gleckler PJ (2009). Selecting global climate models for regional
869 climate change studies. *Proc Natl Acad Sci*, 106(21):8441–8446

870 Pirazzoli PA, Tomasin A (2003). Recent near-surface wind changes in the central Mediterranean and
871 Adriatic areas. *Int J Climatol*, 23, 963-973

872 Pires AC, Nolasco R, Rocha A, Ramos AM, Dubert J (2014). Global climate models as forcing for
873 regional ocean modeling: a sensitivity study in the Iberian Basin (Eastern North Atlantic). *Clim Dynam*,
874 43:3-4, 1083-1102

875 Pryor SC, Barthelmie RJ (2003). Long term trends in near surface flow over the Baltic. *Int J Climatol*,
876 23, 271–289

877 Pryor SC, Barthelmie RJ, Kjellström E (2005a). Potential climate change impact on wind energy
878 resources in northern Europe: analyses using a regional climate model. *Clim Dynam*, 25(7-8), 815-
879 835

880 Pryor SC, Schoof JT, Barthelmie RJ (2005b). Empirical downscaling of wind speed probability
881 distribution. *J Geophys Res*, 110, D19

882 Pryor SC, Barthelmie RJ (2010). Climate change impacts on wind energy: A review. *Renew Sust*
883 *Energ Rev*, 14(1), 430-437

884 Räisänen J, Palmer TN. (2001). A probability and decision-model analysis of a multimodel
885 ensemble of climate change simulations. *J Clim* 14:3212-3226

886 Rauthe M, Hense A, Paeth H (2004). A model intercomparison study of climate change-signals in
887 extratropical circulation. *Int J Climatol*, 24:5, 643–662

888 Rousseeuw PJ, Croux C (1993). Alternatives to the Median Absolute Deviation. *J Am Stat Assoc* 88,
889 424

890 Sachs L (1984). *Applied Statistics: A Handbook of Techniques*. New York: Springer-Verlag

891 Santos JA, Rochinha C, Liberato MLR, Reyers M, Pinto JG (2015). Projected changes in wind energy
892 potentials over Iberia. *Renew Energ*, 75, 68-80

893 Smits A, Klein Tank AMG, Konnen GP (2005). Trends in storminess over the Netherlands, 1962-2002.
894 *Int J Climatol*, 25, 1331-1344

895 Sterl, A, Bakker A, van den Brink H, Haarsma R, Stepek A, Wijnant IL, de Winter RC (2014). Large-
896 scale winds in the KNMI'14 climate change scenarios. *Environ Res Lett* (in press).

897 Taylor KE, Stouffer RJ, Meehl GA (2012). An overview of CMIP5 and the experiment design. *Bull Am*
898 *Meteorol Soc* 93(4):485–498

899 Vautard R, Cattiaux J, Yiou P, Thépaut JN, Ciais P (2010), Northern Hemisphere atmospheric stilling
900 partly attributed to an increase in surface roughness. *Nat Geosci*, 3, 756-761

901 Walter A, et al. (2006). A high resolution reference data set of German wind velocity 1951–2001 and
902 comparison with regional climate model results. *Meteorol Z*, 15(6), 585-96

903 Zappa G, Shaffrey LC, Hodges KI, Samson PG, Stephenson DB (2013). A multimodel assessment of
904 future projections of North Atlantic and European extratropical cyclones in the CMIP5 climate models.
905 *J Clim*, 26, 5846-5862

Chapter 7 – Main conclusions

In this chapter the main findings of all the research presented in this thesis are presented in an integrated approach. Thus, the main conclusions to be drawn from the previous chapters can be summarized as follows:

- The choice of the initial and boundary data used to force the WRF model is of paramount importance to obtain accurate modelled winds and wind energy production estimates. ERA-Interim reanalysis is the initial and boundary dataset that provides the most accurate forcing data to drive the WRF model wind simulation and wind energy production estimates, both for Portuguese onshore and adjacent Spanish offshore areas. Among other features, the fact that ERA-Interim reanalysis makes use of a four-dimensional variational analysis method to assimilate observed data, oppositely to the three variational data assimilation methods used by the other reanalyses, proved to be determinant in obtaining accurate modelling results. The NCEP-FNL and NCEP-GFS analyses can be seen as the best alternatives to ERA-Interim, particularly for cases where reliable NWP forcing data is needed for real-time applications due to their fast availability.
- The accuracy of the simulated winds and wind energy production estimates is also very dependent on the choice of the planetary boundary layer parameterization schemes. The parameterizations set composed by the ACM2-PX PBL and SL schemes was proven to be the best choice in terms of planetary boundary layer parameterization schemes for the wind simulation and wind energy production estimates for mainland Portugal and adjacent Spanish offshore areas, for a complete year simulation period. The fact that the ACM2 PBL scheme combines features of local and non-local closure schemes and also the fact that the PX LSM scheme provides a better parameterization of the surface meteorology proved to be important in the model near-surface wind simulation performance for a period that includes the different synoptic/atmospheric stability conditions that typically occur

in a annual cycle. However, if considering shorter simulation periods (days, weeks, months), it is necessary to assess the performance of the several PBL-SL parameterization schemes due to their close dependence with the local atmospheric stability/stratification conditions and synoptic situation.

- The optimisation of the WRF model here presented allowed a significant decrease of the model errors in simulating wind and wind energy production estimates for the area under study. Although NWP models can already be successfully seen as reliable alternatives to *in situ* measured winds for wind energy resource spatial mapping and preliminary production estimates, particularly if using its optimal configuration, the same cannot be said for wind farm projects in a more advanced stage (that require highly accurate wind data) due to errors that NWP models still show when compared with *in situ* wind measurements. The main caveats of the WRF model performance in near surface wind simulation detected in this work were: a systematic tendency to overestimate offshore wind speeds; worse performance in simulating atmospheric flows over complex terrain and areas located close to the coast due to limitations in representing the terrain characteristics; in simulating low (below 4 m.s⁻¹) and high (above 12 m.s⁻¹) wind speeds, showing better performance in simulating intermediate winds; a systematic overestimation of low wind speeds and underestimation of high wind speeds, revealing a tendency to remain close to the mean wind speed state. Despite these limitations, NWP models (particularly the WRF model) are being continuously improved and new configuration options being added to their already wide panoply of available choices, which are expected to improve their performances. Therefore, it is vital to continuously test and optimise NWP models in order to attain their fullest capacities and accuracy, aiming to minimize the errors and shorten the path to NWP models being able to substitute *in situ* measurements for accurate wind energy production estimates.
- Notwithstanding, and specifically for offshore areas, the optimal WRF configuration obtained in this work allowed a simulation of offshore winds and wind energy production estimates closer to measured values than offshore wind measurements collected by satellites (QuikSCAT, CCMP and NWP/QuikSCAT

blended datasets) for the offshore areas under study. This outcome is of particular relevance given that, according to the literature published until the present moment, never a NWP was able to surpass the accuracy of these satellite offshore wind observations, which are often used to assess offshore wind energy production potential. Moreover, NWP models have additional advantages such as offering higher spatial/temporal resolutions and full data availability when compared to satellite-derived offshore wind data, and are able to offer wind data for any geographical area and temporal period. However, the offshore areas under study are coastal and it is known that satellites have their strength in open ocean areas, showing strong limitations in collecting measurements over areas near the coast due to their limited resolution. Thus, it is expected that satellites can show better performances in measuring open ocean offshore winds. Nevertheless, considering that currently typical offshore wind farms are located in coastal areas and that satellites are unable to accurately depict winds over such areas, together with the fact that the NWP modelling results showed better performance than satellite measurements in these coastal areas over the Iberian Peninsula, an optimised NWP model may be the best alternative to in situ offshore wind measurements in coastal areas. Yet, new generations of satellites that measure offshore winds are continuously being developed and deployed in orbit. Thus, it becomes vital to conduct a parallel effort that, on the one hand, continuously performs NWP optimisation studies in order to attain their fullest capacities and accuracy and, on the other hand, continuously compares optimised NWP modelled winds to the latest satellite-derived offshore wind data to choose the best alternative to in situ offshore wind measurements.

- According to the IPCC latest future climate projections under anthropogenic-induced climate changes, the future panorama for the large-scale wind energy resource over Europe does not seem promising. The future European wind energy production potential tends to be lower than the one presently available, due to a decreasing tendency of the large-scale wind speeds over the current century, especially by the end of the current century and under scenarios of stronger radiative forcing. Some exceptions to this decreasing tendency of future wind speeds are detected in Central/Northern Europe, Turkey and in the Iberian

Peninsula. In these areas, the wind energy resource can slightly increase in future times, especially by the end of the current century and under scenarios of stronger radiative forcing. In terms of the wind energy resource intra-annual variability, it tends to be lower in the future due to wind speeds decrease in cold seasons and increase in warmer seasons, particularly in the end of the current century and under scenarios of stronger radiative forcing. Oppositely, no significant changes in the inter-annual variability are expected over Europe during the current century. These findings should be seen as a preliminary warning that a continuous increase of greenhouse gases emissions can jeopardize our ability to mitigate such emissions, at least in what is related to the role and contribution of wind energy. By negatively affecting future wind energetic resource, climatic changes can weaken wind power active and vital contribute to reduce greenhouse gases emissions. Therefore, the climate change itself can inherently diminish our ability to fight it, in a kind of “snow ball” effect, at least in what is related to the wind energy role in of greenhouse gases emissions mitigation. However, it needs to be highlighted and seriously borne in mind the significant uncertainty associated to global models future climate projections that, together with the limited ability of the IPCC CMIP5 global models to accurately represent the past-present wind climate over Europe due to their intrinsic limitations, provides limited confidence to the future panorama of the European wind energy resource projected by these models. Thus, the information provided by these models should be seen primarily as a preliminary picture of the large scale future tendencies of the wind energy resource and further research focused on these themes should be performed by downscaling CMIP5 GCMs output to regional and local scales, in order to better represent the topography and land use and thus better simulate near surface winds.

Chapter 8 – Future work

Although the work presented in this thesis encompassed several different approaches to optimise the WRF model, aiming to improve its wind simulations and wind energy estimates, and focused on the anthropogenic-induced climate changes impacts on future wind energy resource over Europe, it also revealed that these are continuous efforts with a lot of work left to be done. This chapter aims to shed some light in “where do we go from here” in the issues focused in this work: what can be done to further optimise the WRF model, improving its wind simulations and wind energy production estimates, namely in what is related to its initial/boundary conditions and configuration options? Even if these improvements are achieved, will NWP offshore wind modelling be able to keep up with the developments and progress in satellite offshore wind measurements, providing more accurate offshore wind data than satellites? As for the future panorama of wind energy resource, what can be done to add certainty and detail to future climate projections?

As aforementioned, the WRF model is being continuously improved and new configuration options being added to its already wide panoply of available choices in each new release of this model. In order to continue to use its optimal configuration and thus obtain the best wind modelling results, it is necessary to continuously test its latest configuration options assessing if they can improve the wind modelling accuracy. In what is more directly related to near-surface wind modelling, it is necessary to test the new PBL parameterization schemes added to the latest WRF model versions released. Besides PBL parameterization schemes, the latest WRF versions include new options that are expected to refine the WRF performance in near-surface wind modelling. For onshore sites, an updated version of the topographic correction of surface winds to represent extra drag from sub-grid topography and enhanced atmospheric flow at hill tops (option `topo_wind`, described in Jimenez and Dudhia, 2012) appears as a promising tool to minimize the WRF model near-surface wind errors caused by its limitations in accurately representing the terrain topography and land use/roughness. As reported in this work, one of the main limitations and sources of error of WRFs onshore wind modelling performance is its

limited ability to resolve the local topography and terrain roughness, which will strongly impact the simulation of near-surface winds, particularly in sites located in complex terrain. Thus, it becomes clear the need to test this new option for onshore areas, particularly for sites located in complex terrain. For offshore sites, the new 3D ocean model added to WRF (detailed in Price et al., 1994) seems able to offer improvements in near-surface ocean wind modelling. This model predicts horizontal advection, pressure gradient force, as well as mixed layer processes. From the work presented in this thesis it was seen that the WRF model tends to overestimate near-surface ocean winds, most likely due (but not only) to the fact the WRF model does not include an ocean model, thus considering the ocean as a constant flat surface while the real ocean has higher and variable roughness lengths as a consequence of variations in the ocean surface height (tides, swells, etc.). Therefore, the lower roughness lengths simulated by the model over the ocean will originate higher winds, due to the lower friction between atmosphere and ocean surface. Therefore, this new 3D ocean model may be able to offer significant improvements in the simulation of near-surface ocean winds.

As for further improve the initial and boundary data to drive NWP wind modelling, given that in this work practically all reanalyses and analyses currently available were tested, the next step will be to assimilate wind measurements directly to the initial and boundary fields. Given that wind measurements collected in wind farm measuring campaigns and in offshore buoys moored offshore the Iberian Peninsula are not assimilated in any of the reanalyses and analyses datasets currently available, it is expected that the assimilation of this wind data on the NWP model initial and boundary fields can bring significant improvements to wind modelling results. For this, the WRF model Data Assimilation System (both the 3D-Var, 4D-Var and the observational nudging) can be used to assimilate wind measurements onto the WRF model initial and boundary fields and further improve the wind modelling results. To further improve the wind modelling results the NWP spatial resolution can also be increased, depending on the available computational resources. Having the NWP model optimized, further improvements in the wind modelling results can be achieved by using Model Output Statistics and Neural Networks in the post-processing of the NWP output. Furthermore, the NWP output can be downscaled from the meso- to the micro-scale by using CFD (Computational Fluid Dynamics) models. CFD models are

capable of modelling wind flows at very fine spatial resolutions (50-10 m), and also able to represent the terrain topography and land-use at these fine resolutions. Thus, the use of CFD models to downscale mesoscale output from NWP models is expected to bring significant improvements in the wind modelling performance, as it has been witnessed in the recent past.

In parallel with these efforts to further optimise the WRF model wind modelling, it also necessary to focus on the new generation of satellites that remotely measure offshore near-surface winds (for example, the ASCAT, OSCAT and RAPIDSCAT scatterometers). Besides the pertinent issue of comparing these new offshore wind datasets with the best WRF offshore wind simulations, aiming to assess what is the best alternative to directly *in situ* measured offshore wind data, if any of these satellite-derived offshore wind data shows higher accuracy than the optimised WRF offshore wind simulations when compared to *in situ* measurements, it will also be pertinent to assimilate this remotely sensed data into WRFs initial and boundary fields, which can be of particular importance when no *in situ* offshore wind data is available for assimilation.

As for the future panorama of wind energy resource under climate change scenarios, the obvious next step is to analyse the EURO-CORDEX downscaling project data. This project, in which are involved the main European research institutes connected to climatology and climate changes, downscales the CMIP5 GCM data to Europe making use of several RCMs. Due to the aforementioned GCMs limitations in accurately representing the terrain characteristics (topography and land use/roughness) caused by its limited spatial resolution and, consequently, also the near-surface atmospheric circulations that are strongly influenced by these factors, it is expected that the downscaling of GCM data with RCMs can bring significant improvements in terms of detail, confidence and reliability of the future climate projections. Another approach that can be followed is to use the optimised WRF configuration to downscale CMIP5 GCM data to regional and local scales.

References

APREN (2013):

http://www.apren.pt/fotos/editor2/as_renovaveis_em_portugal_apren_abr2013.pdf

APREN (2014):

http://www.apren.pt/fotos/noticias/2014_02_35_do_consumo_nacional_de_eletricidade_de_origem_eolica_em_janeiro_1392637959.wmv

Carvalho D, Rocha A, Gómez-Gesteira M, Santos C (2012). A sensitivity study of the WRF model in wind simulation for an area of high wind energy. *Environmental Modelling & Software*, Vol. 33, pp. 23-34

Carvalho D, Rocha A, Santos CS, Pereira R (2013). Wind resource modelling in complex terrain using different mesoscale-microscale coupling techniques. *Applied Energy*. Vol. 108, pp. 493-504

de Vries E (2008a). 40,000 MW by 2020: building offshore wind in Europe. *Renewable Energy World 2008*, pp. 36-47

de Vries E (2008b). The DEWI report: wind energy study 2008. *Renewable Energy World 2008*, pp. 93–101

Global Wind Energy Council (2010). *Global Wind Energy Report of the Global Wind Energy Council 2010*.

http://www.gwec.net/fileadmin/images/Publications/GWEC_annual_market_update_2010_-_2nd_edition_April_2011.pdf

Global Wind Energy Council (2011). *Global Wind Report of the Global Wind Energy Council, Annual market update 2011*.

http://www.gwec.net/fileadmin/documents/NewsDocuments/Annual_report_2011_lowres.pdf

Global Wind Energy Council (2012). Global Wind Report of the Global Wind Energy Council, Annual market update 2012

http://www.gwec.net/wp-content/uploads/2012/06/Annual_report_2012_LowRes.pdf

IPCC (2013). Climate Change 2013: The Physical Science Basis. Contribution of Working Group I to the Fifth Assessment Report of the Intergovernmental Panel on Climate Change [Stocker, T.F., D. Qin, G.-K. Plattner, M. Tignor, S.K. Allen, J. Boschung, A. Nauels, Y. Xia, V. Bex and P.M. Midgley (eds.)]. Cambridge University Press, Cambridge, United Kingdom and New York, NY, USA, 1535 pp.

IPCC (2007). Climate Change 2007: The Physical Science Basis. Contribution of Working Group I to the Fourth Assessment Report of the Intergovernmental Panel on Climate Change [Solomon, S., D. Qin, M. Manning, Z. Chen, M. Marquis, K.B. Averyt, M. Tignor and H.L. Miller (eds.)]. Cambridge University Press, Cambridge, United Kingdom and New York, NY, USA, 996 pp.

Jiménez PA, Dudhia J (2012). Improving the Representation of Resolved and Unresolved Topographic Effects on Surface Wind in the WRF Model. *Journal of Applied Meteorology and Climatology*, Vol. 51, pp. 300–316

Lorenz E (1996). *The Essence of Chaos*, University of Washington Press, 1996

NCAR (2012). *ARW Version 3 Modeling System's User's Guide*, NCAR, Boulder, Colorado, USA

Pryor SC, Barthelmie RJ (2010). Climate change impacts on wind energy: A review, *Renewable and Sustainable Energy Reviews*, Vol. 14, Issue 1, pp. 430-437

Price JF, Sanford TB, Forristall GZ (1994). Forced Stage Response to a Moving Hurricane. *Journal of Physical Oceanography*, Vol. 24, pp. 233–260

Trenberth K, et al. (2010). Atmospheric Reanalyses: A Major Resource for Ocean Product Development and Modeling. *Proceedings of OceanObs'09: Sustained Ocean Observations and Information for Society*, Vol. 2, Venice, Italy.

Skamarock WC, Klemp JB, Dudhia J, Gill DO, Barker DM, Huang XY, et al. (2008). A Description of the Advanced Research WRF Version 3. NCAR Technical Note, Mesoscale and Microscale Meteorology Division of NCAR.

URL 1:http://ec.europa.eu/clima/policies/package/index_en.htm